US Army Corps of Engineers
Waterways Experiment
Station

AD-A275 975

SUPERTANK Laboratory Data Collection Project

Volume I: Main Text

*by Nicholas C. Kraus, Jane McKee Smith
Coastal Engineering Research Center*

DTIC
ELECTE
FEB 24 1994
S E D

Approved For Public Release; Distribution Is Unlimited

94-05762

DTIC QUALITY INSPECTED 1

94 2 23 011

Prepared for Headquarters, U.S. Army Corps of Engineers

Best
Available
Copy

The contents of this report are not to be used for advertising, publication, or promotional purposes. Citation of trade names does not constitute an official endorsement or approval of the use of such commercial products.

SUPERTANK Laboratory Data Collection Project

Volume I: Main Text

by Nicholas C. Kraus, Jane McKee Smith

Coastal Engineering Research Center

U.S. Army Corps of Engineers
Waterways Experiment Station
3909 Halls Ferry Road
Vicksburg, MS   39180-6199

Accesion For	
NTIS CRA&I	☒
DTIC TAB	☐
Unannounced	☐
Justification	
By	
Distribution /	
Availability Codes	
Dist	Avail and / or Special
A-1	

Final report

Approved for public release; distribution is unlimited

**US Army Corps
of Engineers**
Waterways Experiment
Station

N

INFORMATION
TECHNOLOGY
LABORATORY

GEOTECHNICAL
LABORATORY

HEADQUARTERS
BUILDING

COASTAL ENGINEERING
RESEARCH CENTER

HYDRAULICS
LABORATORY

MAIN
ENTRANCE

ENVIRONMENTAL
LABORATORY

STRUCTURES
LABORATORY

FOR INFORMATION CONTACT :
**PUBLIC AFFAIRS OFFICE
U. S. ARMY ENGINEER
WATERWAYS EXPERIMENT STATION
3909 HALLS FERRY ROAD
VICKSBURG, MISSISSIPPI 39180-6199
PHONE : (601)634-2502**

SCALE

500   0   500 m

AREA OF RESERVATION = 2.7 sq km

Contents

Preface

This study was conducted as a joint effort of the Coastal Engineering Research and Development Program (CERDP) and the Dredging Research Program (DRP) authorized by Headquarters, U.S. Army Corps of Engineers (HQUSACE) through research work units administered at the U.S. Army Engineer Waterways Experiment Station (WES), Coastal Engineering Research Center (CERC). The CERDP portion of the study was conducted under the Calculation of Cross-Shore Sediment Transport and Beach Profile Change Work Unit 32530 and the Nearshore Waves and Currents Work Unit 31672. The DRP portion of the study was conducted under the Calculation of Boundary Layer Properties (Noncohesive Sediments) Work Unit 32463 and the Open Water Disposal Site Planning Management and Design Work Unit 32489. HQUSACE Technical Monitors were Messrs. John H. Lockhart, Jr., John G. Housley, Barry W. Holliday, and David A. Roellig for the CERDP, and Messrs. Robert H. Campbell, John H. Lockhart, Jr., and David B. Mathis for the DRP. Ms. Carolyn M. Holmes (CERC) was CERDP Program Manager (PM), and Mr. E. Clark McNair, Jr., (CERC) and Dr. Lyndell Z. Hales (CERC) were DRP PM and Assistant PM, respectively.
Dr. Nicholas C. Kraus, Senior Scientist (CERC), was DRP Technical Area 1 (TA1) Manager for Work Unit 32463, and Mr. Thomas W. Richardson (CERC) was DRP TA5 Manager for Work Unit 32489.

This two-volume report provides information and data documenting a coastal processes data collection project called the SUPERTANK Data Collection Project performed at the O.H. Hinsdale Wave Research Laboratory, Oregon State University, over the period 29 July to 20 September 1991. The project was conducted as a multidisciplinary and multi-institutional cooperative effort in which the investigators shared instrumentation and expertise. Volume I of this report contains narrative and example results of major data collection activities and is presented in independent chapters written by the investigators who participated in the project. Chapter 1 of Volume I provides an overview of the project and the activities of all investigators. Volume II contains appendices summarizing properties of the data sets collected and was also prepared by the individual investigators.

Technical editors for this report were Dr. Nicholas C. Kraus, Senior Scientist (CERC), and Ms. Jane McKee Smith, Research Hydraulic Engineer, Coastal Processes Branch (CPB), Research Division (RD), CERC, who were

Conversion Factors, Non-SI to SI Units of Measurements

Non-SI units of measurement used in this report can be converted to SI units as follows

Multiply	By	To Obtain
feet	0.3048	meters
inches	0.0254	meters

1 Introduction to the SUPERTANK Laboratory Data Collection Project[1]

Introduction

The design of beaches to protect against storm erosion, flooding, and wave attack requires quantitative prediction of cross-shore hydrodynamics, sediment transport, and beach profile change. The U.S. Army Corps of Engineers (USACE) has pursued laboratory studies on beach erosion since the founding of the Beach Erosion Board (BEB) in 1930, the predecessor of the present coastal engineering research arm of the USACE, the Coastal Engineering Research Center (CERC), located at the U.S. Army Engineer Waterways Experiment Station.

In the early 1930s, the BEB designed a wave basin and conducted a series of laboratory experiments to examine the action of waves incident normal to an initial, approximately one to seven sloping sand beach, with and without tides (BEB 1936). The experiments were conducted in a basin approximately 6 m long and 4 m wide. (The terminology "basin" implies that both longshore and cross-shore processes can be modeled.) In the experiments, water elevation, waves, surface and bottom currents, and beach profile change were recorded. The evolution of numerous three-dimensional morphologic beach features found in the field were qualitatively reproduced and discussed, including berms, scarps, break-point bars and troughs, and channels that would now be termed rip-current channels. A summary of one aspect of the first four experiments in the series states "The results indicated that normal weather conditions tend to move the offshore sand toward the beach while storm conditions caused erosion of the beach and the formation of an offshore bar" (BEB 1936). The USACE thereafter conducted numerous small-scale laboratory experiments on beach profile change produced by wave action, and a review of these and other laboratory and field studies performed worldwide may be found in Larson and Kraus (1989).

Large wave tanks

From 1955, the BEB and later, its successor organization CERC, operated a tank 193.5 m long, 4.6 m wide, and 6.1 m deep that was equipped with a monochromatic wave generator. The terminology "tank" implies that cross-shore processes dominate over longshore processes. This facility began a new era of laboratory experimentation with length scales of the waves and beach sufficient to reproduce beach change of engineering significance on field beaches. The pioneering study of Saville (1956) using this facility demonstrated that scale effects in small laboratory facilities could lead to morphologic states different than those occurring at full scale. Although such effects were known to engineers (Johnson 1949), they could not be quantified until large facilities were available. The USACE large wave tank was mothballed in 1983, and the historic beach profile change experiments involving breaking waves up to 1.6 m in height and with periods up to 16 sec are documented in Kraus and Larson (1988). This data set continues to be a source of quantitative information for understanding beach profile change and for improving predictive tools such as numerical models of beach profile change.

A large wave tank (LWT) capable of producing waves and beach profile change without introducing scaling problems provides an inexpensive means, as compared with field data collection, of obtaining data for developing numerical simulation models of beach profile change and for investigating fundamental hydrodynamic and sediment-transport processes under controlled conditions. A number of LWT experiments on beach change have been performed (e.g., Kajima et al. 1982, Vellinga 1986, Dette and Uliczka 1987) since the pioneering study of Saville (1956), but none has taken advantage of the full range of modern instrumentation to capture the breadth of processes acting across the profile.

Genesis of SUPERTANK

In 1987, in support of numerical model development for predicting storm-induced beach erosion, staff at CERC concerned with numerical simulation of beach change and the associated hydrodynamics began planning an LWT research effort that was called the SUPERTANK Laboratory Data Collection Project, or, simply "SUPERTANK." The project was conducted by contracting for the LWT facility and supporting technical staff members located at the O.H. Hinsdale Wave Research Laboratory (WRL), Oregon State University (OSU). The WRL refers to this facility as a "channel" to connote that the processes developed in it are primarily two-dimensional or cross-shore, and that its major axis is aligned horizontally and not vertically. This usage will be maintained in discussions referring specifically to the facility. The WRL facility is the largest wave channel in the United States in which a sandy beach can be emplaced.

As planning progressed, it was realized that the offshore region could provide an ideal environment for hydrodynamic (waves and currents) and

2

sediment transport measurements for studying the movement of dredged sediment placed seaward of the surf zone. Thus, one unique characteristic of SUPERTANK was utilization of the entire length of the beach, extending from near the wave generator through the surf zone to the limit of runup, and both shore protection research work units and dredging-related research work units became involved.

Scope of chapter

This chapter presents an overview of the SUPERTANK Laboratory Data Collection Project. Project planning and the major test series are described to give a background on the motivation for the project and strategy for the tests performed. Some information is given on logistical details, because the great expense associated with numerous researchers at the site and contract time in the facilities required careful attention to logistics and coordination. The chapter also serves as an introduction to and background for the succeeding, more technical chapters on individual data collection activities.

Project Planning

SUPERTANK was conducted as a multi-institutional effort similar to cooperative field data collection projects first performed in the 1970s, for example, the Nearshore Sediment Transport Study in the United States (Seymour and Duane 1978), the Nearshore Environment Research Center Project in Japan (Horikawa and Hattori 1987), and USACE-sponsored projects such as DUCK85 (Mason, Birkemeier, and Howd 1987) and SUPERDUCK (Birkemeier et al. 1989). Cooperative efforts that pool expertise, instrumentation, and a wide range of research interests have led to advances unattainable by a single or small group of investigators. The advantages of cooperative research were readily carried over to the LWT environment of SUPERTANK.

The broad purpose of SUPERTANK was to collect data unbiased by scaling distortions to verify and refine existing predictive technology and provide data and insights on detailed physical processes for development of the next generation of coastal processes numerical and physical models. Thus, SUPERTANK provided data for present engineering research needs as well as for anticipated future research directions. The specific objectives of SUPERTANK were to:

   a. Collect data to verify and improve existing macro-scale beach profile change numerical simulation models (models that describe wave-averaged phenomena and beach change without reference to features such as bars and berms).

   b. Collect data to develop advanced hydrodynamic, cross-shore sand transport, and meso-scale beach profile change numerical simulation

models (models that describe primarily time-averaged phenomena and may include bars, berms, and similar morphologic features).

c. Collect data to quantify performance of sandbars ("nearshore berms") constructed offshore as a beneficial use of dredged material.

d. Test and compare sediment-sensing acoustic instruments in a controlled, field-scale environment in support of dredging research.

e. Collect data to improve understanding of micro-scale fluid and sand motion (time-dependent motion and spatial scales of ripples and the wave boundary layer).

The strength of the SUPERTANK project was integration of a wide range of instrumentation and expertise to achieve these objectives, resulting in extraordinarily comprehensive coverage of fluid and sediment motion along the channel.

Project design and coordination were the responsibility of a seven-person steering committee, whose members were also among the principal investigators. The steering committee developed initial project goals to meet research needs of CERC and served as facilitators for the large investigative group in arranging for resources for all investigators and promoting communication. The steering committee was comprised of the authors of this chapter, with the first author as chairperson; Dr. William Dally (Florida Institute of Technology); Dr. David Kriebel (U.S. Naval Academy); Dr. William McDougal (OSU); and Dr. Charles Sollitt (OSU), who also represented the WRL as its director. Other principal investigators were: Dr. Yogesh Agrawal (Northwest Research Associates, Inc.), Dr. Reginald Beach (OSU), Dr. Keith Bedford (The Ohio State University), Drs. John Fisher and Margery Overton (North Carolina State University), Dr. Daniel Hanes (University of Florida), Dr. Robert Holman (OSU), Dr. Paul Komar (OSU), Dr. Susumu Kubota (Nihon University, Japan), Mr. Atle Lohrmann (RD Flow, Inc.), Ms. Cheryl Pollock (CERC), and Dr. Edward Thornton (Naval Postgraduate School).

The steering committee, formed of CERC and non-CERC members, initially divided its efforts in three subject areas: (a) hydrodynamics, (b) sediment transport, and (c) beach profile change. Four investigator meetings were held to plan test series and coordinate instrumentation sharing, availability of support personnel, synchronization of data collection, and other practical matters.

During the course of periodic planning meetings the principal investigators found it convenient to form three operational groups, as follows:

a. Total-channel hydrodynamics and sediment transport.

b. Foreshore and beach profile change, including swash zone hydrodynamics.

4

c. Offshore measurements that centered around acoustic instruments, a laser-Doppler velocimeter (LDV), and instrument tests.

As described above, participants joining CERC at SUPERTANK came from universities, private research institutes, and industry. Many of these participants have contributed to this data report. In addition to the principal investigators and the teams from their institutions, students and other interested parties from Seatech, Inc., the University of California at Santa Cruz, the University of Delaware, and the University of Washington also participated. Observers were sent from the Danish Hydraulics Institute (Denmark) and the Delft Hydraulics Laboratory (The Netherlands). USACE personnel from several field offices also assisted SUPERTANK investigators in the data collection.

Project Procedure

SUPERTANK ran for the 8-week period from 29 July to 20 September 1991. The first and last weeks were dedicated to mobilization and demobilization, and waves were generated and data collected over the 6 weeks from 5 August through 13 September. Two 1-week trials of instruments were conducted 6 months and 1 month before the start of SUPERTANK. The steering committee encouraged participation in these instrument trials by all investigators to assure proper deployment and operation of the instruments, as well as to eliminate instrument cross talk and interference prior to the full deployment. These valuable shakedown trials allowed correction of instrument problems, improvements in mountings, and more detailed planning of the logistics of full instrument deployment. The instrument shakedown trials were the primary reason that data collection proceeded without major problems and little instrument downtime.

The channel was filled with sand the week prior to mobilization. Sand was trucked from the Oregon coast and placed in the channel with front loaders. The channel was first partially filled with water so that the sand would fall through the water and become wetted and somewhat washed. The sand was very well-graded with a median diameter (determined by sieving) of 0.22 mm and a fall speed of 3.3 cm/sec. Some tree bark and other dark-colored organic matter were contained in the sand. After extended periods of wave action or when new sand was added to the beach profile, such as in the construction of dunes, the water became cloudy and remained so until the tank was drained and new water added. When the channel was drained, some organic matter remained on the sand surface and was removed.

Waves were run in intervals of, typically, 10, 20, 40, or 70 min. The choice of these interval lengths was motivated by four considerations. First, profile change produced by waves of the same characteristics normally proceeds rapidly at first and gradually slows as the profile assumes an equilibrium shape. Therefore, the wave intervals were short at first and gradually increased to record the change with profile surveys. Second, there was con-

cern that long-period seiching would be amplified if long wave time series were used. Some seiching was recorded, and the degree of seiching depended on the type of waves (monochromatic or random), and on the shoreward beach configuration (a sloping beach or a seawall). Third, by stopping wave action after relatively short time intervals, the elevation from the sand surface to the sediment sensors could be measured for use in calculations, and these and other sensors could be repositioned as necessary. Fourth, because the wave gauges and current meters were sampled at 16 Hz and other instruments were sampled at 10 Hz, shorter runs gave data files that were manageable in size.

The SUPERTANK wave conditions were designed to balance the need for repetition of wave conditions to move the beach profile toward equilibrium and development of a variety of conditions for hydrodynamic studies. The TMA spectral shape, applicable to finite water depths (Bouws et al. 1985), was used to design all random-wave tests, with spectral width parameter γ between 1 (broad-banded) and 100 (narrow-banded). Other parameters that controlled the hydrodynamics, such as water level, bottom profile shape, and shoreward boundary (seawall, dune, and terrace), also varied between tests, changing the nearshore hydrodynamics for the same imposed offshore wave conditions.

The daily work schedule was 12 hr of wave action and associated data collection activities from Monday through Thursday and 8 hr on Friday, starting with a daily meeting of principal investigators at 7 a.m. Plans for the day were reviewed and optimized at the morning meetings, and in the evenings, data taken that day, particularly the beach profile change data, were inspected. Evenings and weekends were spent in major mechanical operations of beach profile reconstruction, emplacement and removal of dunes and seawalls, and inspection and moving of instruments, for which the tank was drained. For example, changes in wave conditions from higher to lower waves required shoreward translation of instruments to optimize measurement coverage in the vicinity of the breaker zone and in the surf zone.

Previous LWT projects (and most small-scale laboratory experiments) on beach profile change typically initiated tests from the same uniform slope, which required substantial sand transfer and profile regrading with heavy equipment. In the case of SUPERTANK, various researchers could be onsite for only a limited time and a large number of instruments were mounted inside the tank that required substantial effort to remove and re-emplace. Therefore, extensive regrading of the profile, with the associated delays, was not economically feasible. As a result, most tests were initiated using the final profile configuration of the previous run or a modified form of it. This substantial time savings was one way to obtain more data on physical processes of interest. Also, it was felt that numerical simulation modeling of profile change was sufficiently advanced to start from an arbitrary profile shape, and comparisons of all types of runs to a fixed initial profile were not considered necessary.

6

Most tests conducted in previous LWT projects ran waves over relatively long time periods, for example, 30 to 100 hr of wave action, to approach an equilibrium shape. Another departure of SUPERTANK strategy from previous LWT projects was use of short-duration tests to realize a wide variety of wave, initial beach profile, and foreshore or landward boundary combinations, instead of performing a small number of tests (perhaps four), as had been done in the past, to achieve effective equilibrium. Although a greater number of tests were run, many difficult decisions had to be made in prioritizing objectives. It was reasoned that previous LWT tests had provided much information on the approach to equilibrium profile shape and on the equilibrium shape itself, and that improvement of quantitative simulation models and mathematical models of the basic processes would better benefit from a wide variety of conditions. Some tests were run for sufficient time to clearly discern the approach to an equilibrium shape.

Although guided by a 6-week plan of tests, modifications and refinements for improving both the quality and scientific merit of the data collection were made on a weekly and even daily basis as experience was gained and tradeoffs were evaluated. These decisions were ultimately made by the two authors of this chapter as senior representatives of CERC. The pre-planned test series was modified and redirected as necessary through observation of the data and discussion among investigators. All data sets could be inspected during collection or shortly thereafter.

Channel, equipment, and operating procedures

The channel of the LWT at the WRL is 104 m long, 3.7 m wide, and 4.6 m deep, into which a 76-m-long beach was constructed for the SUPERTANK project. Figure 1-1 shows the interior of the WRL enclosure and computer control room, and Figure 1-2 is a view of the LWT during an instrument change. The beach was composed of approximately 600 cu m of sand. The direct, digital controlled servo-hydraulic wave generator was equipped to absorb energy at the peak spectral frequency that was reflected from the beach and structures, such as dunes and seawalls. Broad- and narrow-band random waves and monochromatic waves were run with zero-moment wave heights in the range of 0.2 to 1.0 m and with peak spectral periods in the range of 3 to 10 sec. As mentioned previously, waves were typically run in segments of 10-, 20-, 40-, and 70-min duration.

A coordinate system was set up at the LWT to reference all instrument positions. The zero point (x, y, and z = 0) was established at the beach end of the tank on the west wall (right side of the tank when standing on the beach and looking toward the wave generator). The positive x axis was directed offshore along the top of the wall, and the positive z axis was directed upward from the top of the tank wall in a right-handed coordinate system. A system of reference stations was also established along the west tank wall. Stations corresponded to the location of 1-in. threaded wall inserts used for instrument mounting. At each station inserts were paired horizontally (0.3-m spacing)
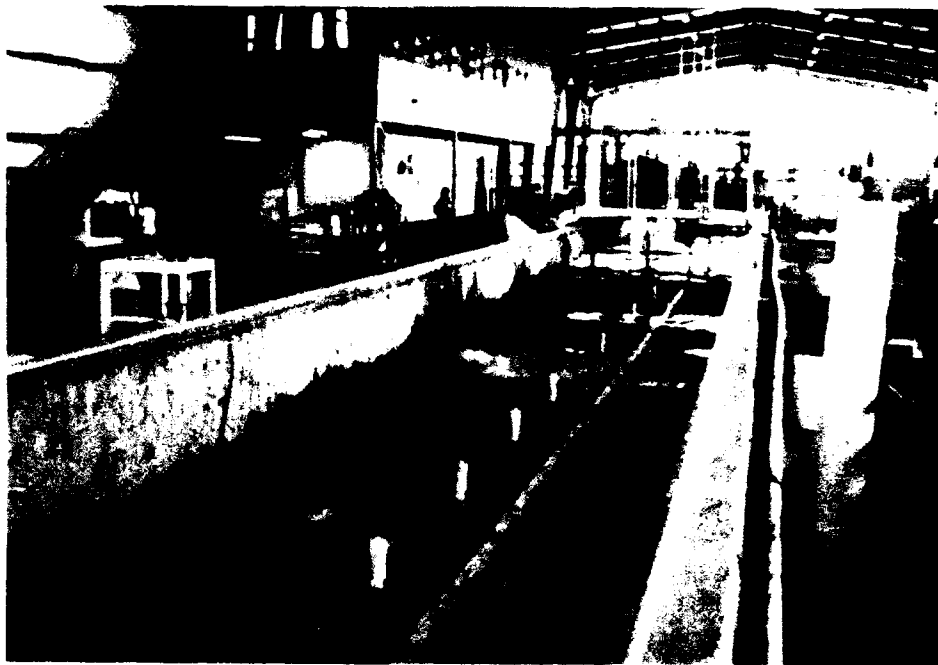
Figure 1-1. Wide-area view of LWT channel and control room during SUPERTANK (capacitance wave gauges in foreground)

Figure 1-2. Channel emptied for instrument change

and spaced vertically on 0.3-m centers over the entire depth. The stations were numbered with Station 1 at $x = 0.3$ m (location of the more seaward of the inserts in each pair where the wave gauges and current meters were mounted) and station numbers increasing at 3.7-m intervals offshore. Figure 1-3 shows the channel layout including stations.

SUPERTANK is believed to be the most densely and comprehensively instrumented nearshore processes data collection project conducted in the laboratory or field. At the peak of data collection activities, the LWT channel was instrumented with 16 resistance wave gauges, 10 capacitance wave gauges, 18 two-component electromagnetic current meters, 34 optical backscatter sensors (OBS), 10 pore-pressure gauges, 3 acoustic sediment concentration profilers, 1 acoustic Doppler current profiler, 1 four-ring acoustic benthic stress gauge, 1 LDV, 5 video cameras, and 2 underwater video cameras. The resistance wave gauges, capacitance wave gauges, and electromagnetic current meters formed the core of SUPERTANK data collection and were maintained throughout the project. Synchronous sampling by separate data acquisition systems was accomplished by digital input of a WWV time code (broadcast by National Institute of Standards and Technology, Fort Collins, CO, call letters WWV) to all computer clocks.

Core Measurements

Core measurements constitute data collection fundamental to all investigators. The core measurements consist of wave and current data collection and beach profile surveys. CERC investigators were responsible for these measurements.

Waves and currents

Water surface elevation was measured with 16 resistance wave gauges mounted on the west channel wall (left side of LWT in Figure 1-2), spaced 3.7 m (12 ft) apart. The array of resistance gauges extended from near the wave generator to a water depth of approximately 0.5 m. An array of 10 capacitance wave gauges extended from the most shoreward resistance gauge to the maximum runup limit. These gauges were also mounted from the west channel wall, but they were mobile with spacing that varied from 0.6 to 1.8 m. In addition to measuring wave transformation, the capacitance gauges also measured runup and the elevation of the sand surface at gauges that were intermittently submerged (Figure 1-4).

Fourteen Marsh-McBirney electromagnetic current meters were mounted on the east channel wall together with arrays of OBS (Figure 1-5). The current meters were deployed in vertical arrays of one to four sensors with vertical spacing of approximately 0.3 m, designed to quantify the undertow profile. Each array was configured to share a timing pulse (close-proximity
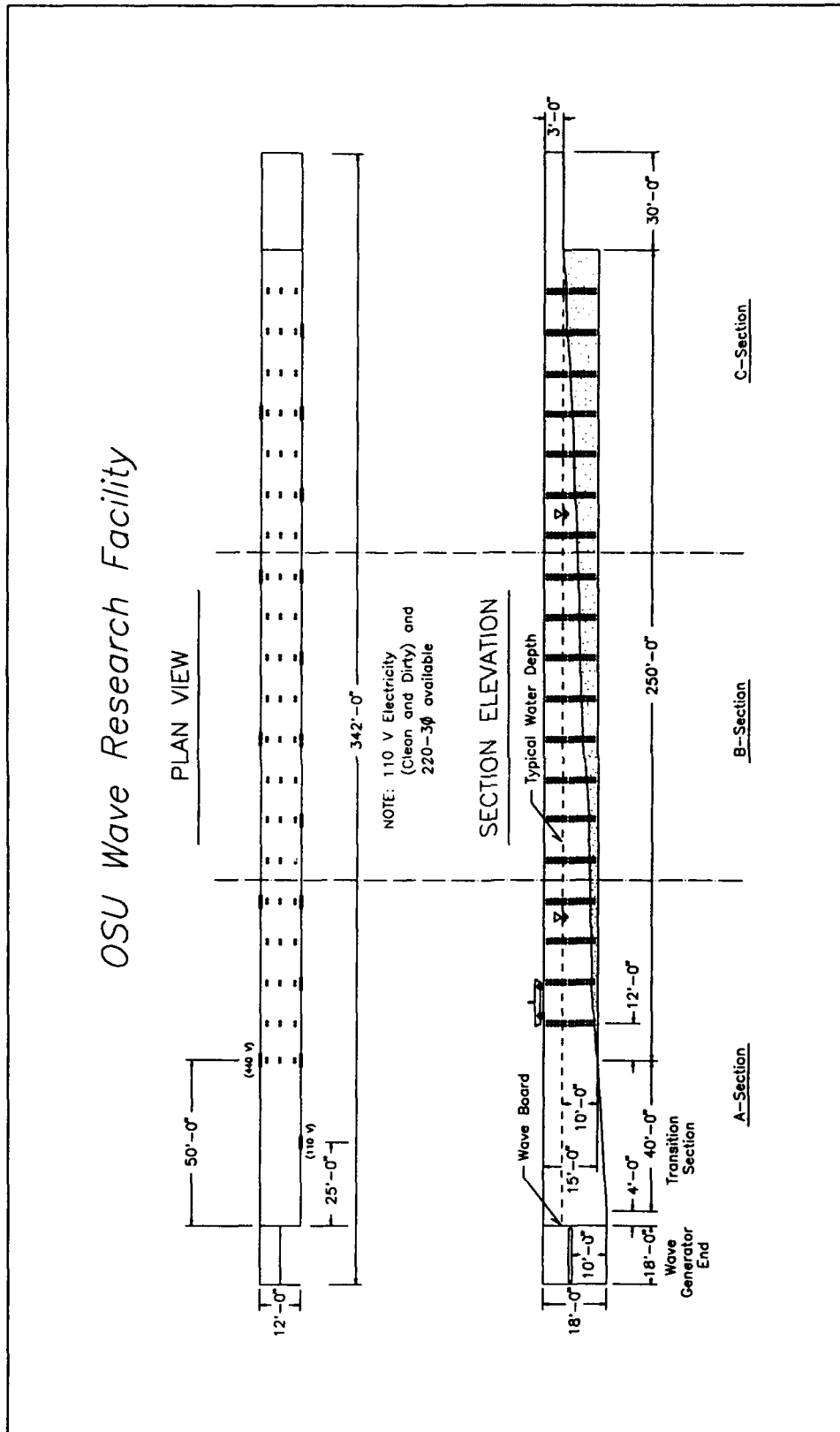
Figure 1-3. Arrangement of WRL channel for SUPERTANK

Figure 1-4. Capacitance bed surface and water surface gauges

Figure 1-5. Vertical arrays of current meters and OBS (roving carriage mast in foreground)

option) to reduce electronic interference. The meters were deployed in depths of 0.3 to 1.8 m, with selection of sensor position based on the wave conditions, water level, and bottom profile.

An additional four electromagnetic current meters, five OBS's, and one capaa..ance wave gauge were deployed on a roving carriage (Figure 1-6). The current meters were arranged in a vertical array (0.3-m spacing) off an adjustable wing extending beneath the carriage. The carriage was positioned prior to each test to locate the wave gauge, current meters, and OBS sensors in the incipient breaking zone, adjacent to a wall-mounted current meter array (for finer vertical resolution), or some other point of interest. Three video cameras, mounted on a scaffold overlooking the surf zone, recorded a continuous image of surf-zone wave transformation, swash, and runup. Ten pressure gauges were buried in the sand beach to measure pore pressure.

Portions of the hydrodynamic data were analyzed (spectra and time series) during or immediately after the tests for quality control and planning of subsequent tests. The instrumentation performed extremely well during the project. Instrument noise and crosstalk problems were identified and eliminated prior to the main project in shakedown tests. The wave gauges were calibrated once a week during the project by raising and lowering the water level. Wave gauge offsets were recorded at the beginning of each test. Current meters were calibrated before and after the project. See Chapters 3 and 4 for detailed descriptions of wave and current measu;.ements.

Beach profile surveys

Approximately 350 full-length surveys were performed to record the response of the beach profile to wave action and to changes in shoreward boundary conditions, such as emplacement of a seawall. Surveys were made with an auto-tracking, infrared Geodimeter, which targeted a prism attached to a survey rod mounted on a carriage that was pushed along the channel by two people. The survey rod, which could move freely in a sleeve with guide rollers, made contact with the bed via a pair of wide-tread wheels (Figure 1-7). Typically, 15 min were required to set up equipment and survey the profile with a horizontal nominal spacing of 0.3 m, but with much finer resolution over features such as dunes, steps, and bars, which had large across-shore gradients in elevation. At the start and end of a test, the profile was surveyed along the center line of the channel and on lines located 0.9 m from each of the channel walls to assess uniformity of the profile across the channel. Three-line surveys also were occasionally made when cross-tank flow was observed or suspected. Between wave runs of a given test, surveys were made only along the center line. See Chapter 2 for detailed discussion of the beach profiles.

Although not strictly part of the core measurements, OBS and fluorescent sand tracer measurements were supported by CERC and conducted by Drs. Reginald Beach and Paul Komar of OSU. The fluorescent sand tracer

12

Figure 1-6. Roving instrument carriage during data collection
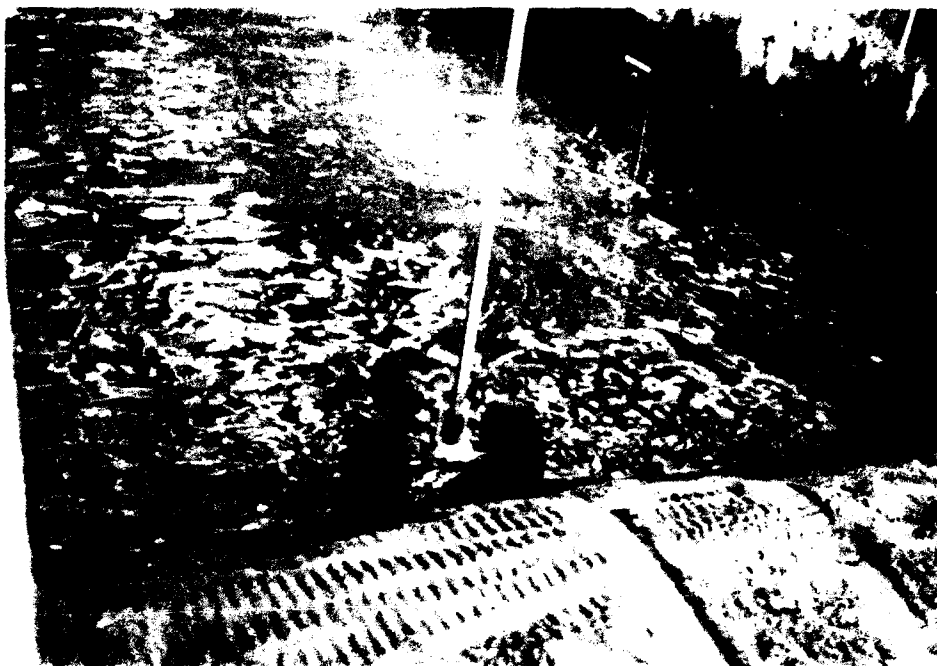
Figure 1-7. Survey wheels along the center survey line

experiments required sampling by SCUBA-equipped divers, and divers also measured and adjusted, as necessary, the bed-referenced elevations of OBS and other sensors at the end of each wave run. The tracer experiments measured dispersion of sand in the offshore, as a comparison to transport rates obtained with the OBS, and recorded macro-scale movement and layering of sand in regions of rapid morphologic change, such as in areas of bar formation and dune erosion. See Chapters 5 and 6 for detailed descriptions of the tracer and OBS measurements, respectively.

Test Series

The 20 major data collection tests performed during SUPERTANK are listed in Table 1-1. Wave conditions designed to produce erosion or accretion were selected using predictive criteria described by Kraus, Larson, and Kriebel (1991), both for monochromatic and random waves. Several tests had objectives separate from monitoring evolution of the beach profile, such as dedicated hydrodynamic, suspended sediment, and instrument tests that examined local fluid and sediment transport conditions.

Representative wave conditions are listed in Table 1-1. For tests involving random waves, the wave height is the significant (zero-moment) height, and the period is the peak spectral period. Sixty-six different wave conditions were run for a total of 129 hr of wave excitation; 70 percent of the wave conditions involved random waves. A detailed listing of the individual wave runs comprising each test, the associated water level, and comments on the test regarding unusual conditions or problems are given in Table 1-2. The table is long and is included at the end of this chapter and in Appendix A, which is contained in Volume II of this report.

Table 1-2 is essential for identifying data collection runs. Six-digit run numbers are given in the first column of Table 1-2. The first digit is the month (A for August and S for September), the second and third digits are the day of the month, the fourth and fifth digits give the hour (24-hr clock, Pacific Daylight Time), and the sixth digit is the run within the given hour (A denotes the first run, B denotes the second run, etc.). The standard water level in the channel was 3.0 m, meaning that the water level was located 1.5 m below the top of the 4.6-m channel walls. Those runs performed with different water depths are so designated explicitly in Table 1-2. If there is no depth information in the right-hand (comments) column, the water level was at 3 m.

In the following sections, a short description is given of each test, together with one or more pictures of conditions or actions representing the test.

Table 1-1
Summary of SUPERTANK Tests

Test Number	Description	Date	Representative Significant Wave Height, m	Period, sec
ST_10	Erosion toward equilibrium, random waves	8/05 – 8/09	0.8	3.0
ST_20	Acoustic profiler tests (random, monochromatic)	8/11 – 8/13	0.2-0.8	8.0-3.0
ST_30	Accretion toward equilibrium, random waves	8/14 – 8/16	0.4	8.0
ST_40	Dedicated hydrodynamics	8/19 – 8/21	0.2-0.8	8.0-3.0
ST_50	Dune erosion, Test 1 of 2	8/22	0.5-0.8	6.0-3.0
ST_60	Dune erosion, Test 2 of 2	8/23	0.5-0.7	6.0-3.0
ST_70	Seawall, Test 1 of 3	8/26	0.7-1.0	4.5
ST_80	Seawall, Test 2 of 3	8/27	0.7	4.5
ST_90	Berm flooding, Test 1 of 2	8/28 a.m.	0.7	3.0
ST_AO	Foredune erosion	8/28 p.m.	0.7	3.0
ST_BO	Dedicated suspended sediment	8/29 – 8/30	0.3-1.0	10.-3.0
ST_CO	Seawall, Test 3 of 3	9/02	0.4-0.8	8.0-3.0
ST_DO	Berm flooding, Test 2 of 2	9/03 a.m.	0.7	3.0
ST_EO	Laser Doppler velocimeter, Test 1 of 2	9/03 p.m.	0.2-0.8	3.0
ST_FO	Laser Doppler velocimeter, Test 2 of 2	9/04 a.m.	0.2-0.7	8.0
ST_GO	Erosion toward equilibrium, mono. waves	9/04 p.m.	0.8	3.0
ST_HO	Erosion, transition toward accretion, mono. waves	9/05 a.m.	0.5-0.8	4.5-3.0
ST_IO	Accretion toward equilibrium, mono. waves	9/05 – 9/06	0.5	8.0
ST_JO	Narrow-crested offshore mound	9/09 – 9/11	0.5-0.7	8.0-3.0
ST_KO	Broad-crested offshore mound	9/12 – 9/13	0.5-0.7	8.0-3.0

ST_10: Erosion toward equilibrium, random waves

Test ST_10 was the first and the longest test (21 hr of wave action) of SUPERTANK. This test was conducted to observe beach response to erosive random waves together with the associated hydrodynamics and sediment transport (Figure 1-8). Some changes were made in the spectral width of the random waves to observe the change in bar morphology and hydrodynamics. Several monochromatic wave runs were made for the acoustic instrumentation group. The combinations of random wave runs and monochromatic wave runs in the same test are expected to provide valuable data for improving beach profile change numerical simulation models.

Figure 1-8. Scarp formed in random wave erosion test

ST_20: Acoustic profiler tests, random and monochromatic waves

Three days of tests were performed with both random and monochromatic waves to provide varied conditions for the acoustic profiling instruments located in the offshore. The waves were generally lower in amplitude than ST_10. The tests were also of interest to the hydrodynamics group. Figure 1-9 shows two acoustic-Doppler current profile sensors raised out of the water for adjustment.

ST_30: Accretion toward equilibrium, random waves

This test was designed to produce accretion of the beach under low steepness random waves with long periods (6-10 sec) and heights of 0.4 to 0.5 m.

ST_40: Dedicated hydrodynamics

This 3-day test included time-varying wave conditions, varying spectral width, and bimodal spectra. The wave runs were 30 to 60 min in duration, covering a multiplicity of wave conditions.

16

Figure 1-9. Servicing of acoustic-Doppler current profilers between wave runs

ST_50: Dune erosion, Test 1 of 2

A dune was constructed and subjected to short-period high waves to cause erosion. The dune was not compacted. The water level was lower at the beginning of the test and higher at the end to provide data on erosion by runup and by direct wave impact. Figure 1-10 shows the dune configuration at the start of the test, and Figure 1-11 shows failure of the dune after approximately 90 min of wave action. The cross-section views of the dune face and failure line are indicators of good two-dimensionality of the hydrodynamic and sediment transport processes.

ST_60: Dune erosion, Test 2 of 2

A dune of approximately the same configuration as in the previous test was constructed and compacted with a vibrator for approximately 2 hr. Figure 1-12 shows the dune and dune toe just after major slumping.

ST_70: Seawall, Test 1 of 3

The profile was considered "sand rich" at this time, because most of the previous tests had removed sand from the upper portion of the profile and deposited it offshore. The break-point bar that had formed at Station 9 in

Figure 1-10. Dune Erosion Test 1, shortly after start of wave action
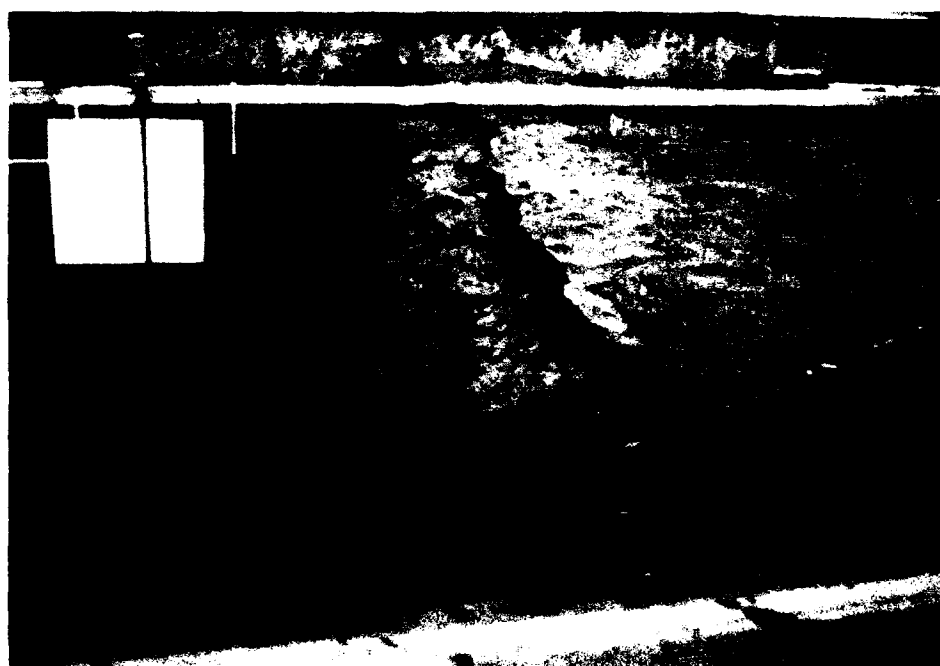
Figure 1-11. Cross-section view of dune during Dune Erosion Test 1 and initial failure line

Figure 1-12. Slumping of material at toe of dune during Dune Erosion
Test 2

previous tests was therefore leveled and the material removed from the channel to take sand off the profile that had been moved there from the beach and dune in previous tests. A portion of the beach and berm shoreward of the capacitance wave gauges was removed, and a seawall was emplaced at Station 1. This work took 8 hr and required several people and a small front loader. Wave conditions were designed to be erosive, but not top over the tank under the anticipated changed water levels. Figure 1-13 shows the shoreward side of the seawall during emplacement, and Figure 1-14 shows waves impacting the wall early in the test.

ST_80: Seawall, Test 2 of 3

Some sand was removed in front of the seawall to create a terraced profile so that waves could attack the wall more directly than in the previous test. The two seawall tests did not result in the erosion expected.

ST_90: Berm Flooding, Test 1 of 2

The evening before this test, a dune and berm were constructed in front of the seawall (Figure 1-15). The purpose of this test was to examine the process of sand transport under erosive wave conditions when a flat area is flooded.

Figure 1-13. Emplacement of wall in Seawall Test 1
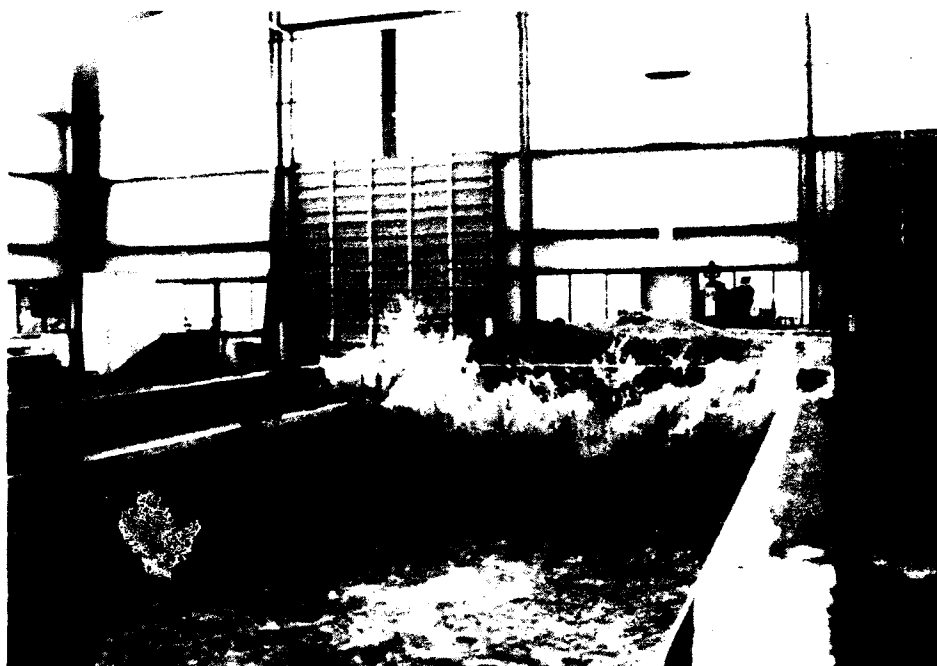
Figure 1-14. Waves impacting the wall in Seawall Test 1

Figure 1-15. Initial beach configuration for the Berm Flooding Test 1

ST_A0: Foredune Erosion

A small dune was emplaced on the terrace (Figure 1-16) to examine the process of dune breakthrough and overtopping. Figure 1-17 shows the foredune being overwashed just prior to its complete erosion.

ST_B0: Dedicated Suspended Sediment

Numerous very short wave runs (typically 1 to 2 min long) were performed with monochromatic waves of different heights and periods for studies of suspended sediment transport in and just seaward of the surf zone. The roving carriage was configured with dense arrays of current meters and OBS's (Figure 1-18), and it was positioned at the break point for each run.

ST_C0: Seawall, Test 3 of 3

An unscheduled (additional) seawall test was performed to assure that the previous tests were not unusual in showing no significant erosion. One day was spent with a front loader and shovels to remove sand from the channel. The seawall was placed at Station 4. All capacitance gauges and the shoreward current meters were removed prior to the profile lowering operations, and the gauges were reinstalled after the profile was formed, with current meter installations moved seaward. After the channel was filled with

Figure 1-16. Near completion of foredune in Foredune Erosion Test

Figure 1-17. Overwash occurring during the Foredune Erosion Test

22

Figure 1-18. Roving carriage being configured for the Dedicated Suspended
            Sediment Test

water, small waves were run to condition the profile to a natural state after the
sand-moving operations. Figure 1-19 shows three water spouts at the wall
upon wave impact.

ST_D0: Berm flooding, Test 2 of 2

Another berm was constructed to examine runup and swash transport.
The same waves were run as in ST_90, but with the water level 0.6 m lower.
Final runs were done with a narrow-banded spectrum and with monochromatic
waves to promote break-point bar growth.

ST_E0: Laser Doppler velocimeter (LDV), Test 1 of 2

Monochromatic waves with short periods were run for data collection by
the LDV in the offshore.

ST_F0: Laser Doppler velocimeter, Test 2 of 2

Longer period monochromatic waves were run for LDV measurements.

Figure 1-19. Wave impact on wall in Seawall Test 3

ST_G0: Erosion toward equilibrium, monochromatic waves

Erosive, monochromatic waves were run for an extended time to approach an equilibrium profile shape.

ST_H0: Erosion, transition toward accretion, monochromatic waves

Following the previous erosion test, wave height was decreased over several runs to produce accretionary conditions, as a gradual transition from storm waves to post-storm recovery waves.

ST_I0: Accretion toward equilibrium, monochromatic waves

Accretionary monochromatic waves were run for an extended time to approach an equilibrium profile shape.

ST_J0: Narrow-crested offshore mound

A weekend was spent filling the channel between Stations 12 and 13 with sand that was graded to form a massive narrow-crested mound to break waves. Three pipes were placed under the mound for water carried forward with the waves to circulate back to the offshore end of the tank. The current

24

meter and OBS arrays were relocated along the perimeter of the mound. Figure 1-20 shows waves breaking on the mound and the roving carriage positioned to collect data.

ST_K0: Broad-crested offshore mound

This test was similar to the previous test, except that more sand was added to create a wider mound in the offshore to examine the effect of mound width on wave dissipation. In both offshore mound tests, substantial dissipation of the incident waves occurred by breaking on the mounds.

Summary and Future Activities

Instrumentation at SUPERTANK performed very well, and data were collected for approximately 129 hr of wave action. The data sets contain a wealth of information ranging from foreshore beach processes to inception of sediment motion in the offshore, and they will be a valuable resource for coastal engineering research for many years.

Reduction and analysis of the enormous (multi-gigabyte) data sets were accomplished as part of this report. Significant effort has been dedicated to organizing and cleaning the data sets so that they may be accessed by all

Figure 1-20. Waves breaking on the narrow-crested offshore mound

researchers, including those who did not participate in SUPERTANK. The first year after SUPERTANK was devoted to reduction of all major data sets, converting quantities to engineering units, and cleaning and organizing the data, and the second year to preparation of this report. The third year will include data exchange among SUPERTANK investigators and more refined data analysis. In September 1994, 3 years after SUPERTANK was performed, the data will be made available to the public.

SUPERTANK succeeded as a cooperative multi-institutional data collection project in which investigators shared resources and expertise toward achieving common goals. Advancements in engineering tools, such as improvement of numerical models of beach change and wave transformation through the surf zone, as well as improved understanding of basic sediment transport and bottom boundary layer processes, are already emerging from the project.

Acknowledgements

SUPERTANK succeeded through the efforts of numerous individuals who assisted over several years in planning, instrument testing, mobilization, execution of the project, and subsequent demobilization.

The persistence and professionalism of the investigators and the technical support staff of the WRL will be forever engraved in the huge, high-quality data sets they created for coastal engineering. We thank Mr. Jesse Pfeiffer, formerly of Headquarters, USACE, for assisting in the difficult contracting process, and Messrs. Terry Dibble, William Hollings, and David Standley of the WRL and Mr. William Grogg of CERC for electronic, mechanical, and computer support. The logistics support (donuts, coffee, and barbecues) at the WRL provided by Ms. Cheryi Zedwick and Dr. Chuck Sollitt (who also came by at all hours of the night to check on channel water levels during filling) will also be remembered. The dedication of the entire SUPERTANK team -- investigators and students -- made SUPERTANK a success to provide researchers with data for probably decades of future studies of cross-shore hydrodynamic and sediment transport processes.

References

BEB (Beach Erosion Board). (1936). "Wave tank experiments on sand movement," Vol. 2, Office, Chief of Engineers, U.S. Army, Washington, D.C.

Birkemeier, W. A., Baron, C. F., Leffler, M. W., Hathaway, K. K., Miller, H. C., and Strider, J. B., Jr. (1989). "SUPERDUCK nearshore processes experiment data summary, CERC Field Research Facility," Miscellaneous Paper CERC-89-16, U.S. Army Engineer Waterways Experiment Station, Vicksburg, MS.

Bouws, E., Günther, H., Rosenthal, W., and Vincent, C. L. (1985). "Similarity of the wind wave spectrum in finite depth water; 1. Spectral form," *J. Geophys. Res.* 90 (C1), 975-86.

Dette, H. H., and Uliczka, K. (1987). "Prototype investigation on time-dependent dune recession and beach erosion." *Proc. Coastal Sediments '87.* ASCE, New York, 1430-44.

Horikawa, K., and Hattori, M. (1987). "The Nearshore Environment Research Center Project." *Proc. Coastal Sediments '87.* ASCE, New York, 756-71.

Johnson, J. W. (1949). "Scale effects in hydraulic models involving wave motion." *Trans. American Geophysical Union* 30(4), 517-25.

Kajima, R., Shimizu, T., Maruyama, K., and Saito, S. (1982). "Experiments on beach profile change with a large wave flume." *Proc. 18th Coastal Engrg. Conf.* ASCE, New York, 1385-1404.

Kraus, N. C., and Larson, M. (1988). "Beach profile change measured in the tank for large waves, 1956-1957 and 1962," Technical Report CERC-88-6, U.S. Army Engineer Waterways Experiment Station, Vicksburg, MS.

Kraus, N. C., Larson, M., and Kriebel, D. L. (1991). "Evaluation of beach erosion and accretion predictors." *Proc. Coastal Sediments '91.* ASCE, New York, 572-87.

Larson, M., and Kraus, N. C. (1989). "SBEACH: Numerical model for simulating storm-induced beach change; Report 1, Empirical foundation and model development," Technical Report CERC-89-9, U.S. Army Engineer Waterways Experiment Station, Vicksburg, MS.

Mason, C., Birkemeier, W. A., and Howd, P. A. (1987). "Overview of DUCK85 Nearshore Processes Experiment." *Proc. Coastal Sediments '87.* ASCE, New York, 818-33.

Saville, T. (1956). "Scale effects in two dimensional beach studies." *Trans. 7th General Meeting.* IAHR, 1, A3.1-10.

Seymour, R. J., and Duane, D. B. (1978). "The Nearshore Sediment Transport Study." *Proc. 16th Coastal Engrg. Conf.* ASCE, New York, 1555-62.

Vellinga, P. (1986). "Beach and dune erosion during storm surges," Delft Hydraulics Comm. No. 372, Delft Hydraul. Lab., Delft, The Netherlands.

Run	Time	Dur min	T_p sec	H_{mo} m	y	Elev ft	Pos in.	Ref Sta	Comments
Table 1-2									
SUPERTANK Test Series									
ST_10: EQUILIBRIUM EROSION (RANDOM)									
AUG 05	900	INITIAL SURVEY							
A0509A	945	20	3	0.8	20	13.58	87.	9	
A0510A	1045	40	3	0.8	20	13.58	87.75	9	
A0512A	1230	70	3	0.8	20	13.58	87.375	9	
A0515A	1520	70	3	0.8	20	13.58	87.25	9	CM17 RAISED 6" BEFORE RUN
A0517A	1730	70	3	0.8	20	13.58	88.75	9	
AUG 06	720	INITIAL SURVEY							
A0608A	805	20	3	0.8	3.3	13.58	88.5	9	CM1 RAISED 6" BEFORE RUN
A0609A	945	40	3	0.8	3.3	13.58	88.	9	
A0611A	1100	70	3	0.8	3.3	13.58	88.25	9	
A0613A	1335	70	3	0.8	MON	13.13	122.5	8	SAMP RATE = 0.06 SEC
A0615A	1558	20	3	0.8	3.3	13.58	86.	9	FORESHORE RESHAPED BEFORE RUN; CM1 BURIED AFTER RUN
A0617A	1725	20	3	0.8	3.3	13.58	89.5	9	W.L. @ 9.5 FT CM1 & 18 LOWERED 6"
A0618A	1822	40	3	0.8	3.3	13.58	88.75	9	W.L. @ 9.5 FT CM17 LOOSE AFTER RUN
AUG 07	745	INITIAL SURVEY							
A0709A	955	4	4.5	0.8	20	13.58	123.	8	CM18 AND 4 UP 6" CM17 TIGHTENED CM1, 2, 6, & 5 UP 6"
A0710A	1015	20	4.5	0.8	20	13.58	123.	8	
A0711A	1120	40	4.5	0.8	20	13.58	65.25	9	
A0713A	1305	70	4.5	0.8	20	13.58	74.5	9	
A0715A	1500	70	4.5	0.8	20	13.58	106.5	9	
A0717A	1700	70	4.5	0.8	20	13.58	148.75	9	
A0719A	1910	5	4.5	0.15	MON	13.58	149.25	9	NOT SURVEYED
A0719B	1930	5	4.5	0.8	20	13.58	149.25	9	NOT SURVEYED
AUG 08	700	INITIAL SURVEY							
A0808A	830	40	4.5	0.8	3.3	13.58	47.5	9	MOVED CM5 UP 6"
A0809A	950	70	4.5	0.8	3.3	13.58	48.	9	
A0812A	1240	20	4.5	0.8	3.3	13.95	4.	13	
A0814A	1425	20	4.5	0.8	3.3	12.14	81.	8	
A0815A	1530	20	4.5	0.8	3.3	13.85	89.	9	
A0816A	1625	20	4.5	0.8	MON	13.85	88.25	9	
A0817A	1730	20	4.5	0.8	MON	11.98	15.	9	

(Sheet 1 of 11)

Table 1-2
SUPERTANK Test Series

Run	Time	Dur min	T_p sec	H_{mo} m	y	Elev ft	Pos in.	Ref Sta	Comments
AUG 09	730	INITIAL SURVEY							
A0907A	756	5			APPRX	21			
A0908A	835	40	6	0.8	3.3	13.73	88.25	9	
A0910A	1010	40	5	0.5	3.3	13.73	88.25	9	
A0911A	1130	40	3	0.7	3.3	13.73	87.75	9	
A0912A	1255	40	3	0.9	3.3	13.73	84.75	9	
A0914A	1415	40	4.5	0.9	3.3	13.73	104.5	9	
A0915A	1535	40	5	0.7	3.3	13.73	81.25	9	DATA LOST
A0916A	1655	5	3	1.2/1.5	MON	13.73	217.5	9	
A0917A	CALIBRATION FOR WAVE GAUGES								
AUG 10	NEW METER DEPLOYMENT FOR ACCRETIONARY SERIES								
AUG 11	1500 REGRADE BEACH, USE AS INITIAL PROFILE								
ST_20: ACOUSTIC PROFILERS (RANDOM; MONOCHROMATIC)									
A1208A	848	5	ZEROS FOR CAL (10 FT)						
A1209A	910	40	8	0.2	3.3	12.55	66.5	9	
A1211A	1115	40	8	0.2	MON	12.55	68.25	9	
A1212A	1225	40	8	0.4	3.3	12.55	62.5	9	
A1213A	1355	40	8	0.4	MON	12.55	58.	9	
A1215A	1515	40	8	0.6	3.3	12.55	46.75	9	
A1216A	1630	40	8	0.6	MON	12.55	40.	9	CM9 ALMOST BURIED
A1217A									SPAN SET TO 91% EARLY IN RUN
A1307A	727	9	ZEROS FOR CAL (10 FT)						
A1307B	758	40	3	0.2	3.3	12.55	109.	9	
A1309A	900	40	3	0.2	MON	12.55	76.5	9	
A1310A	1005	40	3	0.4	3.3	12.55	86.	9	
A1311A	1122	40	3	0.4	MON	12.55	35.25	9	
A1312A	1236	9	ZEROS FOR CAL (10 FT)						
A1313A	1315	40	3	0.6	3.3	12.55	48.	9	
A1314A	1430	40	3	0.6	MON	11.19	72.	9	1430-1435
							0.	9	1437-1443
							72.	8	1444-1450
							0.	8	1453-1500
							72.	7	1503-1510
A1315A	1550	40	3	0.8	3.3	12.53	77.5	9	
A1317A	1700	40	3	0.8	MON	11.15	72.	9	1700-1705
							0.	9.	1708-1714

(Sheet 2 of 11)

Table 1-2
SUPERTANK Test Series

Run	Time	Dur min	T_p sec	H_{mo} m	y	Elev ft	Pos in.	Ref Sta	Comments
							111.75	8	1717-1723
							117.	7	1726-1731
							57.	9	1734-END
ST_30: EQUILIBRIUM ACCRETION (RANDOM)									
A1407A	706	9	ZEROS FOR CAL (10 FT)						
AUG 14	730	INITIAL PROFILE							
A1408A	810	20	8	0.4	3.3	12.59	84.75	9	
A1409A	918	20	8	0.4	3.3	11.17	52.5	9	
A1410A	1020	20	8	0.4	3.3	11.17	105.25	8	
A1411A	1120	70	8	0.4	3.3	11.17	102.5	8	
A1413A	1328	9	ZEROS FOR CAL (10 FT)						
A1413B	1358	70	8	0.4	3.3	11.17	83.5	8	
A1415A	1540	20	8	0.5	3.3	12.62	85.25	9	CM6 & CM8 DISCONNECTED
A1416A	1625	40	8	0.5	3.3	12.62	64.75	9	CM5 DISCONNECTED
A1417A	1725	70	8	0.5	3.3	12.62	68.25	9	OBS UNPLUGGED AT 1818
MOVED CM4 UP 6", MOVED CM8 UP 6", DISCONNECTED CM6 AND CM 10									
A1507A	714	9	ZEROS FOR CAL (10 FT)						
AUG 15	730	INITIAL SURVEY							
A1507B	750	20	9	0.4	20	12.62	82.5	9	
A1508A	845	40	9	0.4	20	12.62	78.75	9	
A1510A	1000	70	≤	0.4	20	12.62	52.	9	
A1511A	1135	70	9	0.4	20	12.62	74.5	9	
A1513A		9	ZEROS FOR CAL (10 FT)						
A1513B	1330	70	9	0.4	20	11.48	60.	8	
A1515A	1510	40	9	0.5	20	12.19	52.	9	W.L. @ 9.5 FT
A1516A	1615	70	9	0.5	20	12.19	54.25	9	W.L. @ 9.5 FT
A1518A	1805	9	ZEROS FOR CAL (9.5 FT)						
A1607A	703	9	ZEROS FOR CAL (10 FT)						
A1607B	740	40	6	0.4	3.3	12.19	51.75	9	
A1608A	855	40	7	0.5	3.3	11.65	4.5	8	
A1610A	1000	40	7	0.4	3.3	11.65	7.5	8	
A1611A	1120	40	10	0.4	3.3	11.65	5.25	8	
A1612A	1226	9	ZEROS FOR CAL (10 FT)						
A1613A	1300	40	6	0.4	MON	11.65	5.5	8	
A1614A	1420	40	7	0.5	MON	11.65	76.5	7	
A1615A	1530	40	7	0.4	MON	11.65	73.	7	
A1616A	1635	40	10	0.4	MON	11.65	77.75	7	

(Sheet 3 of 11)

Table 1-2
SUPERTANK Test Series

Run	Time	Dur min	T_p sec	H_{mo} m	y	Elev ft	Pos in.	Ref Sta	Comments
A1617A	1744	CALIBRATION FOR WAVE GAUGES							
ST_40: DEDICATED HYDRODYNAMICS									
AUG 19	730	INITIAL SURVEY							
A1909A	911	9	ZEROS FOR CAL (10 FT)						
A1909B	940	20	3	0.4	3.3	11.65	75.	8	
		20		0.8					
		20		0.4					
A1911A	1100	10	3	0.4	MON	11.65	52.75	8	DATA LOST
		10		0.8					
		10		0.4					
A1911B	1155	20	5	0.4	3.3	11.65	108.	8	
		20		0.8					
		20		0.4					
A1914A	1400	10	5	0.4	MON	11.65	129.	8	
		10		0.8					
		10		0.4					
A1916A	1628	10	5	0.2	MON	11.65	3.75	9	
		10		0.4					
		10		0.5					
		10		0.6					
		10		0.7					
		10		0.8					
		10		0.2					
A2007A	711	9	ZEROS FOR CAL (10 FT)						
A2007B	735	40	5	0.7	100	12.14	122.	7	
A2008A	857	40	5	0.7	20	12.2	126.25	7	
A2010A	1010	40	5	0.7	3.3	11.42	65.	8	CRASH - HY DATA LOST
A2013A	1332	40	5/8	0.7	20	11.42	88.125	8	WRONG INPUT
	5.0 s	1.64 ft			20	$\sigma = .09$			
	8.0 s	1.64 ft			20	$\sigma = .07$			
A2014A	1440	40	5	0.7	1.0	11.42	79.	8	
A2015A	1545	40	5/8	0.5	20	11.42	74.5	7	REPEATED A2013A
	5.0 s	1.64 ft			20	$\sigma = .09$			
	8.0 s	1.64 ft			20	$\sigma = .07$			
A2017A	1735	40	8	0.5	20	11.42	75.5	7	$\sigma_b = 0.07$
A2018A	1835	40	5	0.5	20	11.42	32.75	8	REPEAT A2015A W/ COR-RECT INPUT

(Sheet 4 of 11)

Table 1-2
SUPERTANK Test Series

Run	Time	Dur min	T_p sec	H_{mo} m	γ	Elev ft	Pos in.	Ref Sta	Comments
A2107A	724	9	ZEROS FOR CAL (10 FT)						
A2107B	745	40	5/8	0.7	100	11.42	101.	8	
	5.0 s	1.64 ft			100	$\sigma = .09$			
	8.0 s	1.64 ft			100	$\sigma = .07$			
A2108A	850	40	5/8	0.7	20	11.42	98.	8	
	5.0 s	1.97 ft			20	$\sigma = .09$			
	8.0 s	1.15 ft			20	$\sigma = .07$			
A2109A	955	40	3/7	0.7	20	11.42	47.5	9	
	3.0 s	1.97 ft			20	$\sigma = .09$			
	7.0 s	1.15 ft			20	$\sigma = .07$			
A2111A	1100	40	3/7	0.4	20	11.42	122.	8	
	3.0 s	1.10 ft			20	$\sigma = .09$			
	7.0 s	0.75 ft			20	$\sigma = .07$			
A2112A	1210	40	3/7	0.7	3.3/ 20	11.42	97.	9	
	3.0 s	1.97 ft			3.3	$\sigma = .09$			
	7.0 s	1.15 ft			20	$\sigma = .07$			
A2114A	1417	9	ZEROS FOR CAL (10 FT)						
ST_50: DUNE EROSION 1/2									
AUG 22	700	INITIAL SURVEY							
A2207A	755	9	ZEROS FOR CAL (10 FT)			W.L. @ 9.5 FT			
A2208A	845	10	3	0.8	3.3	11.5	6.5	9	W.L. @ 9.5 FT
A2209A	915	20	3	0.8	3.3	11.5	0.	10	W.L. @ 9.5 FT
A2209B	957	30	4.5	0.8	3.3	12.5	0.	10	W.L. @ 9.5 FT
A2210A	1055	30	6	0.8	3.3	12.5	0.	10	W.L. @ 9.5 FT
A2213A	1301	9	ZEROS FOR CAL (10.5 FT)			W.L. @ 10.5 FT			
A2213B	1332	30	3	0.8	3.3	12.5	0.	10	W.L. @ 10.5 FT SPAN SET TO 90% @ 13:37
A2214A	1440	30	4.5	0.7	3.3	12.5	0.	10	W.L. @ 10.5 FT
A2215A	1545	30	6	0.7	3.3	12.5	0.	10	W.L. @ 10.5 FT SPAN SET TO 90% @15:52
A2216A	1640	30	3/7	0.5	3.3/ 20	12.5	0.	10	W.L. @ 10.5 FT
ST_60: DUNE EROSION 2/2									
AUG23	700	INITIAL SURVEY							
A2307A	740	9				ZEROS FOR CAL (10.5 FT)			
A2308A	805	20	3	0.7	3.3	12.5	0.	10	W.L.@ 10.5 FT
A2308B	855	20	3	0.7	3.3	12.5	0.	10	W.L. @ 10.5 FT
A2309A	935	20	3	0.7	3.3	12.5	0.	10	W.L. @ 10.5 FT

(Sheet 5 of 11)

Table 1-2
SUPERTANK Test Series

Run	Time	Dur min	T_p sec	$H_{\_\_}$ m	y	Elev ft	Pos in.	Ref Sta	Comments
A2310A	1020	20	4.5	0.7	3.3	12.5	0.	10	W.L. @ 10.5 FT
A2311A	1100	20	4.5	0.7	3.3	12.5	0.	10	W.L. @ 10.5 FT
A2311B	1145	20	4.5	0.7	3.3	12.5	0.	10	W.L. @ 10.5 FT
A2313A	1303	9	ZEROS FOR CAL (11 FT)						
A2313B	1345	20	6	0.5	3.3	12.5	0.	10	W.L. @ 11.0 FT
A2315A	1525	20	6	0.5	3.3	12.5	0.	10	W.L. @ 11.0 FT
A2316A	1605	20	6	0.5	3.3	12.5	0.	11	W.L. @ 11.0 FT
A2316B	CALIBRATION FOR WAVE GAUGES								
24-25AUG91	∗ SAWALL MOVED SAND FROM SUBAQ PROFILE TO BERM AND OUT OF TANK; CHECKED MCM POSITIONS; BROKE AND REPLACED OSU WAVE GAUGES 6 AND 9								
ST_70: SEAWALL 1/3									
AUG 26	700	INITIAL SURVEY							
A2608A	800	6	ZEROS FOR CAL @ 10.5 FT (THEN DROPPED W.L. TO 9.5 FT AND DID 9-MIN CAL)						
A2609A	925	10	4.5	0.7	3.3	12.5	84.	12	W.L. @ 9.5 FT
A2610A	1000	20	4.5	0.7	3.3	12.5	84.	12	W.L. @ 9.5 FT
A2610B	1040	40	4.5	0.7	3.3	12.5	84.	14	W.L. @ 9.5 FT
A2612A	1215	9	ZEROS FOR CAL (10 FT)						
A2612B	1245	10	4.5	0.7	3.3	13	84.	14	W.L. @ 10.0 FT DATA LOST
A2613A	1321	20	4.5	0.7	3.3	13	84.	14	W.L. @ 10.0 FT
A2614A	1420	20	4.5	1	3.3	13	84.	14	FOUND CM1-4 DISCON-NECTED W.L. @ 10.0 FT
A2615A	1505	40	4.5	1	3.3	13	84.	14	CM1-4 OK, W.L. @ 10.0 FT
A2617A	1722	9	ZEROS FOR CAL (11 FT)						
A2617B	1745	10	4.5	0.8	3.3	14	84.	14	W.L. @ 11.0 FT
A2618A	1820	20	4.5	0.7	3.3	14	84.	14	W.L. @ 11.0 FT
A2618B	1855	20	4.5	0.7	3.3	14	84.	14	W.L. @ 11.0 FT
ST_80: SEAWALL 2/3									
AUG 27	700	INITIAL SURVEY							
A2707A	756	9	ZEROS FOR CAL (11 FT)						
A2708A	820	10	4.5	0.7	3.3	14	84.	14	W.L. @ 11.0 FT
A2708B	845	20	4.5	0.7	3.3	14	84.	14	W.L. @ 11.0 FT
A2709A	925	70	4.5	0.7	3.3	14	84.	14	W.L. @ 11.0 FT
A2710A	1055	20	4.5	0.7	MON	14	84.	14	W.L. @ 11.0 FT
A2711A	1145	40	4.5	0.7	MON	14	84.	14	W.L. @ 11.0 FT
AUG 27	LOWERED W.L. & SHOVELED SURF ZONE SAND LANDWRD FROM BAR TO FORESHORE; FILLED TANK								
ST_90: BERM FLOODING 1/2									
AUG 28	700	INITIAL SURVEY							

(Sheet 6 of 11)

Table 1-2
SUPERTANK Test Series

Run	Time	Dur min	T_p sec	H_{mo} m	γ	Elev ft	Pos in.	Ref Sta	Comments
A2809B	930	10	3	0.7	3.3	14	84.	9	W.L. @ 11.0 FT
A2810A	1025	20	3	0.7	3.3	14	84.	10	CART NOT PLUGGED IN W.L. @ 11.0 FT
A2811A	1120	20	3	0.7	3.3	14	84.	10	W.L. @ 11.0 FT
ST_A0: FOREDUNE EROSION									
AUG 28	1500	INITIAL SURVEY							
A2816A	1611	9	ZEROS FOR CAL (11 FT)						
A2816B	1637	10	3	0.7	3.3	14	84.	10	W.L. @ 11.0 FT
ST_B0: DEDICATED SUSPENDED SEDIMENT									
A2908A	833	9	ZEROS FOR CAL (10 FT)						
A2908B	855	100 S	10	0.6	MON	13			TEST TO FIND BP
A2909A	950	150 S	10	0.6	MON	13	120.	6	270 SEC RECORD
A2910A	1025	150 S	10	0.6	MON	13	48.	6	270 SEC RECORD
A2910B	1050	150 S	10	0.6	MON	13	72.	5	270 SEC RECORD
A2911A	1110	120 S	8.0	0.6	MON	13	72.	5	240 SEC RECORD
A2911B	1135	120 S	8.0	0.6	MON	13	0.	7	240 SEC RECORD
A2912A	1200	90 S	6.0	0.6	MON	13	17.5	7	210 SEC RECORD
A2912B	1231	90 S	6.0	0.6	MON	13	96.	6	210 SEC RECORD
A2912C	1255	90 S	6.0	0.6	MON	13	0.	6	210 SEC RECORD
A2915A	1505	67.5 S	4.5	0.6	MON	13	57.	7	187.5 SEC RECORD
A2915B	1530	67.5 S	4.5	0.6	MON	13	96.	6	187.5 SEC RECORD
A2915C	1549	60 S	3.0	0.6	MON	13	96.	6	180 SEC RECORD
A2916A	1618	120 S	8.0	0.8	MON	13	96.	6	240 SEC REC (90% SPAN)
A2916B	1638	120 S	8.0	0.7	MON	13	7.	8	240 SEC RECORD
A2917A	1720	90 S	6.0	0.8	MON	13	7.	8	210 SEC RECORD
A2917B	1746	90 S	6.0	0.8	MON	13	52.5	7	210 SEC RECORD
A2918A	1818	67.5 S	4.5	1.0	MON	13	26.25	8	187.5 SEC RECORD
A3007A	737	9	ZEROS FOR CAL (10 FT)						
A3009A	900	20	8.0	0.4	3.3	13	122.5	7	TO SMOOTH PROFILE
A3010A	1025	120 S	8.0	0.4	MON	13	26.	6	240 SEC RECORD
A3010B	1055	120 S	8.0	0.4	MON	13	72.	5	240 SEC RECORD
A3011A	1110	90 S	6.0	0.4	MON	13	72.	5	210 SEC RECORD
A3011B	1127	67.5 S	4.5	0.4	MON	13	72.	5	187.5 SEC REC.
A3011C	1156	67.5 S	4.5	0.8	MON	13	33.	7	187.5 SEC REC.
A3012A	1220	67.5 S	4.5	0.8	MON	13	132.5	7	187.5 SEC REC.
A3012B	1400	45 S	3.0	1	MON	13	84.5	8	165 SEC REC.
A3017A	1717	---	8.0	0.4	MON	13	20.	17	ABORTED

Table 1-2
SUPERTANK Test Series

Run	Time	Dur min	T_p sec	H_{mo} m	y	Elev ft	Pos in.	Ref Sta	Comments
A3017B	1727	40	8.0	0.4	MON	13	20.	17	RIPPLE MEAS. RUN
S0109A	925	9	ZEROS FOR CAL (10 FT)						
S0109B	945	20	8.0	0.4	3.3	13.5	84.	14	TO SMOOTH PROFILE
ST_C0: SEAWALL 3/3									
SEP 02	700	INITIAL SURVEY							
S0209A	932	9	ZEROS FOR CAL (9 FT)						
S0209B	955	10	3.0	0.8	3.3	13.5	84.	14	NO HYD. PRESS.; LOW WAVES 1ST 1/2 OF RUN
S0210A	1052	20	3.0	0.8	3.3	13.5	84.	14	WAVE GAUGE STA 17 MAL-FUNCTIONING, W.L. @ 9 FT
S0211A	1147	40	3.0	0.8	3.3	13.5	84.	14	W.L. @ 9.0 FT
S0213A	1350	9	ZEROS FOR CAL (10 FT)						
S0214A	1410	20	3.0	0.8	3.3	13.5	84.	14	LANDWARD 8 EMCM FOUND UNPLUGGED; RESUMED OPERATION, W.L. @ 9 FT
S0214B	1455	40	3.0	0.8	3.3	13.5	87.5	14	
S0216A	1605	40	3.0	0.4	3.3	13.5	86.5	14	
S0217A	1735	40	8.0	0.4	3.3	13.5	86.75	14	
S0218A	1842	40	8.0	0.7	3.3	13.5	86.75	14	RUN ABORTED AT 1918; WAVE BOARD LOCKED; RE-MOVED SEAWALL
S0220A	2000	9	ZEROS FOR CAL (10 FT)						
ST_D0: BERM FLOODING 2/2									
SEP 03	700	INITIAL SURVEY							
S0308A	831	9	ZEROS FOR CAL (10 FT)						
S0309A	900	20	3.0	0.7	3.3	13.5	86.75	14	WAVE GAUGE ON
S0310A	1005	20	3.0	0.7	3.3	13.5	86.5	14	
S0311A	1105	20	3.0	0.7	20	13.5	86.25	14	
S0311B	1150	20	3.0	0.7	MON	13.5	86.5	14	
ST_E0: LDV 1/2									
SEP 03	1300	INITIAL SURVEY							
S0314A	1412	9	ZEROS FOR CAL (9 FT)						
S0314B	1430	40	3.0	0.2	MON	13.5	100.75	18	
S0315A	1530	40	3.0	0.6	MON	13.5	100.75	18	
S0316A	1630	40	3.0	0.8	MON	13.5	100.75	18	
ST_F0: LDV 2/2									
SEP 04	700	INITIAL SURVEY							
S0409A	930	9	ZEROS FOR CAL (9 FT)						
S0409B	955	40	8.0	0.7	MON	15.8	101.5	18	SPAN = .98, W.L. @ 9 FT

(Sheet 8 of 11)

Table 1-2
SUPERTANK Test Series

Run	Time	Dur min	T_p sec	H_{mo} m	y	Elev ft	Pos in.	Ref Sta	Comments
S0410A	1055	40	8.0	0.4	MON	15.8	101.5	18	W.L. @ 9.0 FT
S0411A	1155	40	8.0	0.2	MON	15.8	101.5	18	W.L. @ 9.0 FT
ST_G0: EQUILIBRIUM EROSION (MONOCHROMATIC)									
S0413A	1348	9	ZEROS FOR CAL (10 FT)						
S0414A	1410	20	3.0	0.8	MON	12.3	37.	9	
S0415A	1500	40	3.0	0.8	MON	12.3	26.5	9	
S0416A	1615	70	3.0	0.8	MON	12.3	137.	8	
S0417A	1744	10	3.0	0.8	MON	12.3	125.	8	70 MIN ABORTED
S0418A	1820	70	3.0	0.8	MON	12.3	130.	8	
ST_H0: EQUILIBRIUM EROSION/TRANSITION (MONOCHROMATIC)									
S0507A	752	9	ZEROS FOR CAL (10 FT)						
S0508A	825	70	3.0	0.8	MON	12.3	140.	8	
S0510A	1006	40	4.5	0.7	MON	12.3	136.5	8	
S0511A	1110	40	4.5	0.6	MON	12.3	136.	8	
S0512A	1210	40	4.5	0.5	MON	12.3	13.5	9	
ST_I0: EQUILIBRIUM ACCRETION (MONOCHROMATIC)									
S0513A	1335	20	8.0	0.5	MON	12.3	11.5	9	
S0514A	1425	20	8.0	0.6	MON	12.3	105.25	8	
S0515A	1515	40	8.0	0.5	MON	12.3	138.5	8	
S0516A	1625	70	8.0	0.5	MON	12.3	136.	8	
S0517A	1755	70	8.0	0.5	MON	12.3	132.	8	
S0607A	712	9	ZEROS FOR CAL (10 FT)						
S0607B	755	70	8.0	0.5	MON	12.3	13.5	9	
S0609A	930	70	8.0	0.5	MON	12.3	86.5	9	
S0610A	1055	70	8.0	0.5	MON	12.3	90.	9	
S0612A	1225	70	8.0	0.5	MON	12.3	84.	9	
S0614A	1405	70	8.0	0.5	MON	12.3	67.	9	
SEP 06	1600	PRESURVEY FOR 1635 RUN							
S0616A	1635	40	8.0	0.5	MON	12.3	85.5	9	PLANED OFF FORESHORE SCARP & LANDWD; RISING TIDE END 10.6 FT
S0617A	1725	9	ZEROS FOR CAL (10.6 FT)						
ST_J0: NARROW-CRESTED MOUND									
S0908A	852	60	ZEROS FOR CAL (10 FT)						
SEP 09	1100	INITIAL SURVEY							
S0912A	1213	9	ZEROS FOR CAL (10 FT)						
S0913A	1330	20	3.0	0.7	3.3	12.3			
S0914A	1420	20	3.0	0.7	3.3	12.3			

(Sheet 9 of 11)

Table 1-2
SUPERTANK Test Series

Run	Time	Dur min	T_p sec	H_{mo} m	γ	Elev ft	Pos in.	Ref Sta	Comments
S0915	1510	40	3.0	0.7	3.3	12.3			
S0915A	1610	70	3.0	0.7	3.3	12.3			
SEP 09	1700	RESHAPE MOUND							
S0915A	1810	70	3.0	0.7	3.3	12.3	122.5	13	
S1007A	737	9	ZEROS FOR CAL (10 FT)						
S1008A	800	20	8.0	0.5	3.3	12.3	124 5	13	
S1008B	840	40	8.0	0.5	3.3	12.3	121.	13	
S1009A	940	70	8.0	0.5	3.3	12.3	116.5	13	
S1011A	1105	70	8.0	0.5	3.3	12.3	126.	13	
S1013A	1315	70	8.0	0.5	3.3	12.3	116.5	13	
S1014A	1445	20	3.0	0.7	MON	12.3	146.75	13	
S1015A	1520	20	3.0	0.7	MON	12.3	126.	13	
S1015B	1555	40	3.0	0.7	MON	12.3	116.	13	
S1016A	1659	70	3.0	0.7	MON	12.3	111.25	13	DATA LOST
S1018A	1832	40	3.0	0.7	MON	12.3	101.	13	
SEP 11	700	SCARP REMOVED							
S1107A	720	9	ZEROS FOR CAL (10 FT)						
S1107B	740	20	8.0	0.5	MON	12.3	126.5	13	
S1108A	815	40	8.0	0.5	MON	12.3	124.25	13	
S1109A	925	70	8.0	0.5	MON	12.3	117.25	13	
S1111A	1100	70	8.0	0.5	MON	12.3	126.5	13	ACTUAL RUN - 60 MIN
ST_K0: BROAD-CRESTED MOUND									
SEP 12	700	INITIAL SURVEY							
S1208A	805	9	ZEROS FOR CAL (10 FT)						
S1208B	825	20	3.0	0.7	3.3	12.3	3.75	15	
S1209A	910	20	3.0	0.7	3.3	12.3	5.5	15	
S1209B	950	40	3.0	0.7	3.3	12.3	4.5	15	
S1210A	1050	70	3.0	0.7	3.3	12.3	141.	14	
S1212A	1220	70	3.0	0.7	3.3	12.3	125.75	14	
S1214A	1420	20	8.0	0.5	3.3	12.3	130.75	14	
S1215A	1505	40	8.0	0.5	3.3	12.3	138.	14	CHAN 35-42 UNPLUGGED PART OF RUN
S1216A	1605	70	8.0	0.5	3.3	12.3	138.5	14	
S1217A	1730	70	8.0	0.5	3.3	12.3	5.	15	
S1307A	714	9	ZEROS FOR CAL (10 FT)						
S1307B	735	20	3.0	0.7	MON	12.3	6.25	15	STA 13 W.G. BAD
S1308A	815	20	3.0	0.7	MON	12.3	6.5	15	

(Sheet 10 of 11)

Table 1-2
SUPERTANK Test Series

Run	Time	Dur min	T_p sec	H_{mo} m	γ	Elev ft	Pos in.	Ref Sta	Comments
S1309A	905	40	3.0	0.7	MON	12.3	6.25	15	STA 13 W.G. OKAY
S1310A	1003	70	3.0	0.7	MON	12.3	7.5	15	
S1311A	1138	40	3.0	0.7	MON	12.3	8.	15	
S1313A	1313	20	8.0	0.5	MON	12.3	8.75	15	
S1314A	1405	40	8.0	0.5	MON	12.3	6.75	15	
S1315A	1505	70	8.0	0.5	MON	12.3	7.	15	
S1316A	1644	70	8.0	0.5	MON	12.3	4.5	15	
A1318A	1810	9	ZERO FOR CAL (10 FT)						
A1318B	1830	CALIBRATION FOR WAVE GAUGES							

(Sheet 11 of 11)

2 Beach Profile Surveys and Sediment Sampling at SUPERTANK[1]

Introduction

The SUPERTANK Data Collection Project was originally conceived to supply data for improving existing numerical simulation models of cross-shore processes and beach profile change and for developing the next generation of such models. The technical objectives of SUPERTANK were expanded in subsequent planning by the Principal Investigators, as discussed in Chapter 1 of this report, to encompass a wide range of interests in hydrodynamic and sediment-transport processes, and instrument testing. Information on the shape and evolution of the beach profile remained central to all SUPERTANK investigations, however. Interest in profile change measurement continued in the tradition of the pioneering data collection project conducted in the world's first large wave channel constructed and operated by the U.S. Army Corps of Engineers (Saville 1956, Kraus and Larson 1988). Accurate survey data are required for studying beach profile response, developing profile change simulation models, calculating wave transformation and cross-shore currents (which are major research objectives in themselves, besides being necessary for beach profile change modeling), and determining the vertical positions of instruments.

During SUPERTANK, approximately 350 profile surveys were made of the 70- to 80-m-long sandy bottom to record the response of the beach profile to wave action and to changes in shoreward boundary conditions, such as the presence of a seawall or dune. To put this number of surveys in perspective, in an ongoing 11-year program of beach profile surveys made every 2 weeks or more frequently at the Field Research Facility (FRF), located in Duck, NC, operated by the Coastal Engineering Research Center (CERC), U.S. Army Engineer Waterways Experiment Station (WES), the data set for the

most frequently traversed profile line is only now approaching 350 surveys (Howd and Birkemeier 1987).

In SUPERTANK project planning, it was considered essential to develop a survey system that would withstand intensive use and allow rapid surveying and immediate capture and examination of the data. Budgetary restrictions and the uniqueness of SUPERTANK precluded development of a fully automated system. Instead, a labor-intensive, semi-automated survey system was devised. This chapter describes the beach profile survey instrumentation, measurement procedure, and selected properties of the profile data set. Information on the beach sediment is also given. The beach profile survey data are listed in Appendix B of Volume II of this report, together with plots of the profiles taken along the center line of the channel. Chapter 12 discusses associated pore pressure and sediment density measurements.

Experiment Apparatus

At SUPERTANK, the beach profile was surveyed with an auto-tracking, infrared Geodimeter, a commercially available instrument, that was brought in for use in the project and positioned at the beach end of the channel. The Geodimeter targeted a prism attached to the top of a survey rod mounted on a manually operated carriage. The survey rod, which moved freely in a supporting roller guide, made contact with the bed through a pair of wide-tread pneumatic rubber wheels. The main components of the survey system were the rod with guide that was affixed to the carriage, the Geodimeter located outside the northern end of the wave channel (landward side of the beach), and a portable personal computer (PC) connected to the Geodimeter. The carriage rode on top of the channel walls and was dedicated to profile surveying. The basic survey system was developed by the third author of this chapter, and the survey rod and guide were designed and fabricated in the machine shops at WES. The system was modified and refined onsite during the mobilization week of SUPERTANK.

Survey rod

Figure 2-1 is a cross-section schematic of the survey rod and a portion of the carriage, as viewed from the Geodimeter position. There were two concerns in designing and operating the survey rod: disturbance of the sand bed and flexure of the rod. Minimization of bed disturbance was addressed by terminating a hollow, airtight aluminum rod with pneumatic tires, providing sufficient buoyancy such that the tires did not notably disturb the bottom under the weight of the rod. Minimal penetration of the wheels into the wetted sand bottom was confirmed visually along the shallow ends of the profile and on the subaerial beach, and by divers observing the action of the wheels in the deeper end of the channel.

40
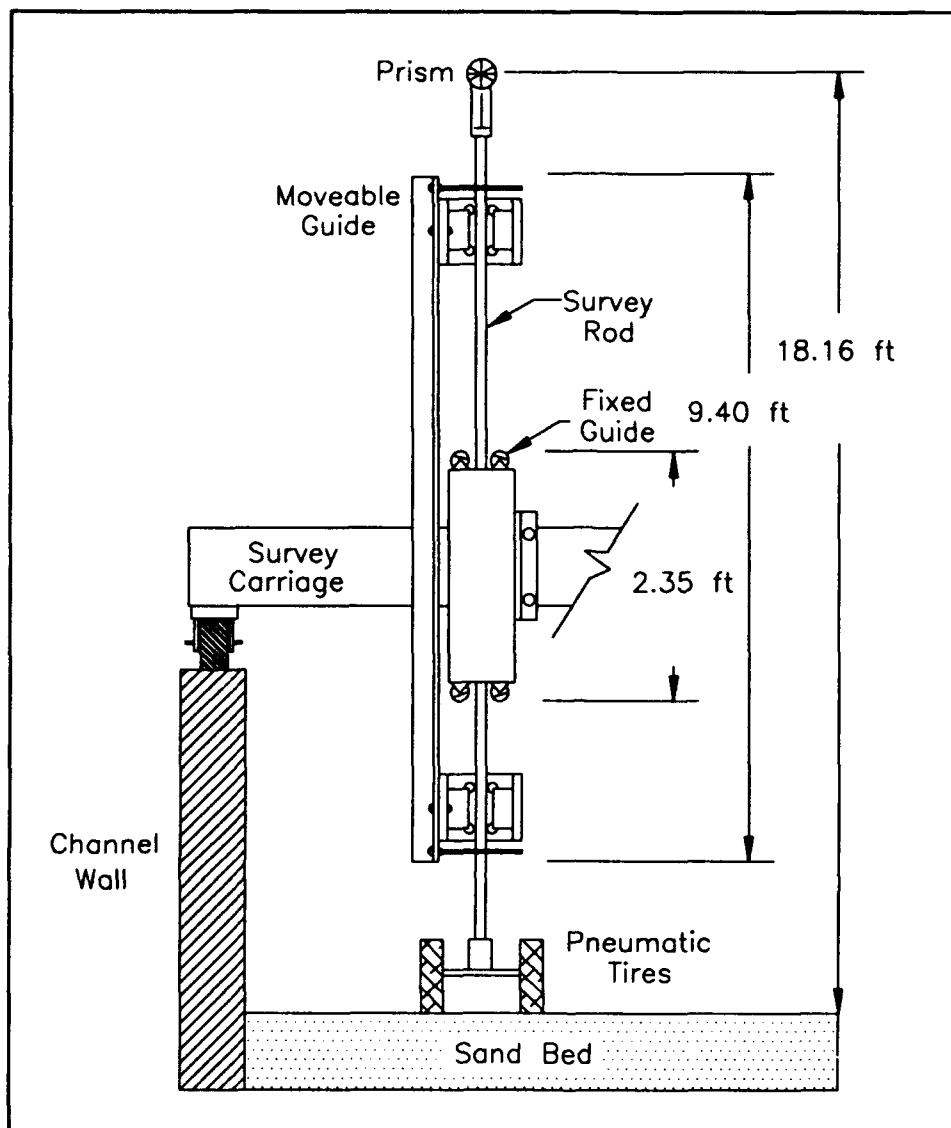
Figure 2-1. Cross-section sketch of the survey rod and carriage

The second concern, rod flexure, was addressed by mounting the rod in a fixed guide, as shown in Figure 2-1. The guide provided primary support of the rod and allowed ready relocation of the rod to one of three cross-channel positions on the carriage. Stainless steel roller bearings were placed on both ends of the guide to allow smooth vertical motion. A second, moveable guide was set to minimize the unsupported length of the rod, and, when raised in shallow water, to minimize horizontal sway of the prism. The movable guide provided additional rigidity to the rod as the tires moved over ripples and steep offshore bars. Because the rod was nearly neutrally buoyant and the rollers allowed easy vertical movement, an error called "floating of the wheels," signifying lifting of the wheels off the bottom, could occur if some downward force was not exerted by the operator.

Total survey station

A Geodimeter T140 total survey station was positioned outside of the tank (Figure 2-2) to track by an infrared beam the position of the prism mounted on the top of the rod. The Geodimeter obtained power from a 12-V battery. The coordinate system reference angle was set to zero on a back sight located on the wall of the channel. The maximum horizontal distance from the station to the channel was limited by the presence of the north wall of the environmental enclosure of the O. H. Hinsdale Wave Research Laboratory (WRL), Oregon State University (OSU), where SUPERTANK was conducted. Accuracy of the coordinates of the station is discussed below. Additionally, the Geodimeter was used to measure instrument locations, including current meters and sediment sensing instruments mounted in the channel, and video cameras located far from the channel.

Survey data acquisition program

The output signal from the Geodimeter was directed to a portable PC located on a raised table next to it (Figure 2-2). The PC ran a program written by Mr. William Birkemeier, Chief of the FRF, specifically for use with a total survey station. With the Geodimeter position, backsight information for a known point in the coordinate system, and prism elevation given, the program computed the horizontal and vertical coordinates of the bottom profile or other survey targets, such as repositioned gauges when the channel was drained.

The interactive data collection program displayed measured coordinates as they were read by the Geodimeter. The readings and input conditions used in the calculations were also written to a file by the program. The menu-driven program provided several features, including the capability to pause recording of data when the survey was interrupted (e.g., for routine lowering of the movable guide on the survey carriage). Other features included the capability to mark certain data points in the file corresponding to features of interest along the profile, such as location of the still-water line, the maximum point of runup, or a location where severe scarping had occurred.

Experiment Procedures

Profile survey

Procedure. Typically, 15 min were required to ready all equipment and survey the profile with a nominal horizontal spacing of 1 ft (0.3 m), but with much finer resolution over features such as dunes, steps, and bars, which had large across-shore gradients in elevation. Figure 2-3 shows a plan view schematic of the arrangement of the survey equipment. At the start and end of a

42

Figure 2-2. Geodimeter and portable data acquisition computer

major test, the profile was surveyed along the center line of the channel and on lines located 3 ft from each of the channel walls to assess uniformity of the profile across the channel. The three survey lines were designated as Line 3, Line 6, and Line 9 to denote locations as 3, 6 and 9 ft (0.9, 1.8, and 2.7 m) from the channel west wall; because the channel is 12 ft (3.66 m) wide, survey Line 6 is the center line. Three-line surveys were also occasionally made if cross-tank flow was observed or suspected. Between wave runs of a given test, surveys were made only along the center line to allow wave action to resume as soon as possible (Figure 2-4).

The beach profile survey procedure was designed to optimize speed, accuracy at a given survey point, and resolution of profile features. The coordinate system origin was chosen to coincide with the first of a series of instrument mounts (channel stations described in Chapter 1) located along the wall of the channel, and the top of the channel west wall was chosen as zero in the vertical. The horizontal coordinates were defined such that the x-axis was positive directed offshore, the cross-channel coordinate y was positive directed across the channel, and the vertical (z) axis was positive directed upward, to form a right-handed coordinate system.

It was difficult to zero the station on the origin due to glare from the windows of the enclosure and closeness of the origin to the Geodimeter. Therefore, a backsight was chosen at a known distance further along the channel. The coordinates from the origin to the Geodimeter and from the origin to the backsight were specified to the data-acquisition program for computing a
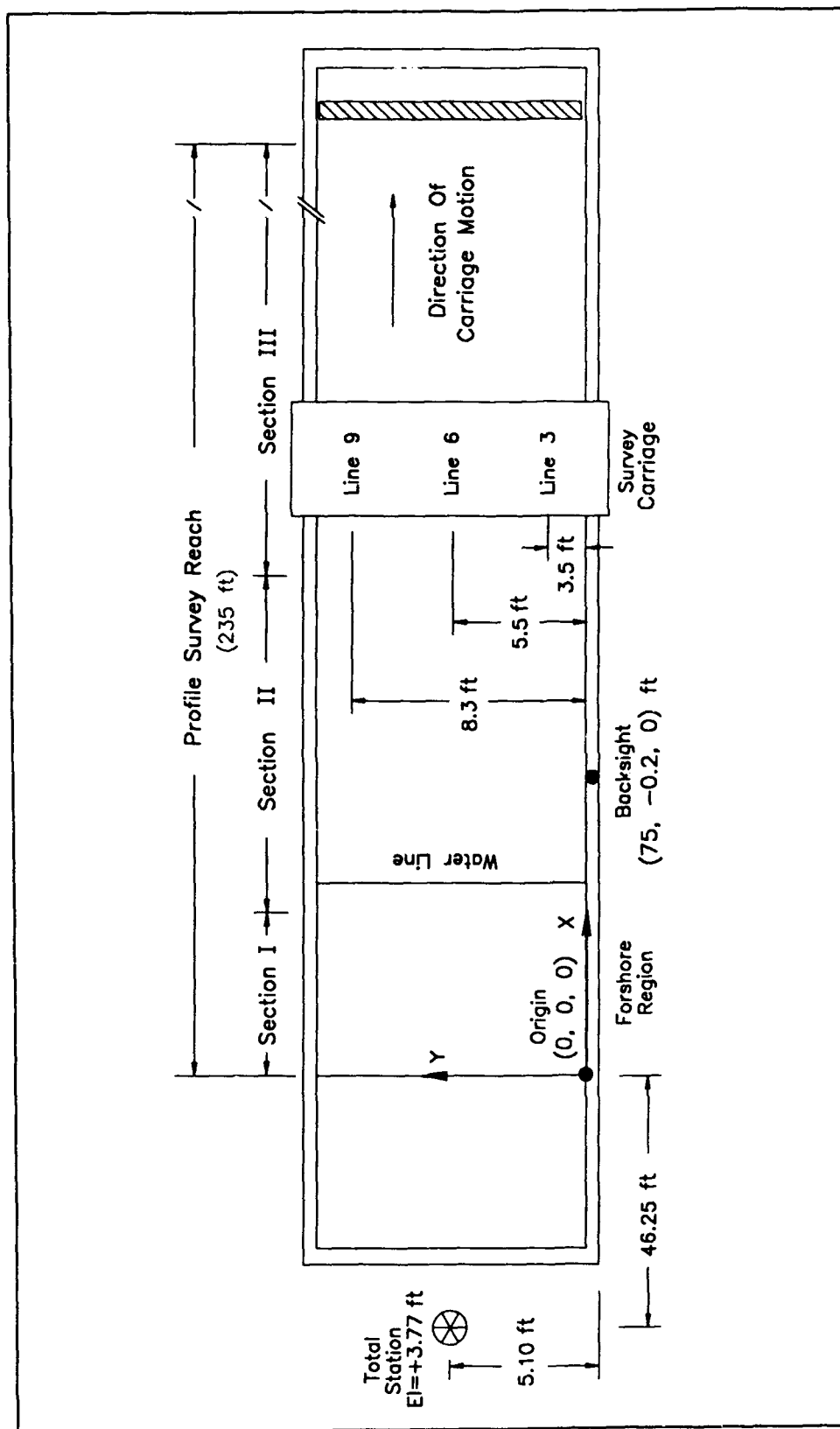
Figure 2-3. Plan view of the survey coordinate system and channel

Figure 2-4. Survey rod in operation on Line 6

survey position relative to the origin from the distance and angle measured by the Geodimeter. The correctness of these coordinate values was checked by comparing Geodimeter measurements to known locations on the tank and by comparing cross-tank (y) values along each profile line, because the y-value should not have changed for a given profile survey line as the carriage moved along the channel.

Beginning at the origin and moving offshore, the portion of interest of the channel (normally, the entire channel length up to the location of the other two carriages that were moved offshore to allow the profile survey carriage access to the channel) was surveyed in the three sections shown in Figure 2-3. During a few tests, lack of clearance under the survey carriage rod necessitated that Section I of the profile be surveyed by a hand-held rod with a top-mounted prism. Tracking of the prism was sometimes difficult in this section due to window glare and the proximity of the prism to the Geodimeter. The error introduced is discussed below, but it is noted that the water did not

reach this section for most tests so that measurement of this region was not crucial. When the hand-held rod reached the beginning of Section II, which was always on dry beach and well before the location of maximum runup, the data acquisition program was paused, a new prism elevation was entered, and the Geodimeter sighted on the carriage rod for continuation of the survey.

The Geodimeter-PC system in auto-tracking mode recorded at 0.4-sec intervals. With this sampling rate, the carriage speed was manually controlled as judged by its operators (rod handler and two carriage pushers), to resolve major geomorphic features and breaks in beach slope. Care was taken to resolve such features as a dune face, scarps, bars, and the large ripples that formed seaward of the breakpoint bar in some monochromatic wave tests. The system was thus adaptive in providing data at the appropriate resolution in minimum time and according to the existing morphology. Depending on the morphology and location on the profile, horizontal spacing between survey points ranged from about 0.1 ft (0.03 m) at distinct features to 2 to 5 ft (0.6 to 1.5 m) in the offshore, far seaward of the breakpoint bar.

Three profile lines could be surveyed within 45 min, acquiring approximately 100 to 300 data points on each line. The profile data were stored on diskette and immediately transferred to a PC located in the SUPERTANK Principle Investigator room, where the survey data were read, displayed, and analyzed, as necessary, with the Beach Morphology Analysis Package (Sommerfeld et al., in preparation). Once the profile data were examined and found to be in good order, wave action was resumed. Examination of the profile data took only a few minutes and assured that these fundamental measurements were correct. Occasionally, this inspection revealed errors, and portions of a survey were redone.

Example result. Figure 2-5 shows selected profile surveys along Line 6 and all net cross-shore transport rates calculated for two cases, the random wave erosion Test ST_10A and the random wave accretion Test ST_30A. The test series are described in Chapter 1. The symbol "A" appended to the test number indicates the first wave condition in the test series. Test ST_10, the first test of SUPERTANK, started from a profile configured as a planar foreshore joining to the subaqueous portion formed in a concave shape as $h = Ax^{2/3}$, where h is still-water depth, x is horizontal distance from the shoreline, and A is a shape parameter corresponding to a mean grain size of 0.30 mm according to data compiled by Moore (1982). This shape parameter produced an average profile slope somewhat steeper than that for the 0.22-mm sand employed at SUPERTANK (see section on sediment below) and provided adequate depth for the offshore group of measurements. Inspection of the natural variation of field profiled data at the FRF, which has fine-grained sand in the surf zone, indicated that the profile shape varies around the average to encompass a state described by an A parameter for 0.30-mm sand.
Test ST_10A thus started from a profile with no prominent morphologic features, and Test ST_30A started from an initial profile with a prominent bar that had been produced in previous tests.
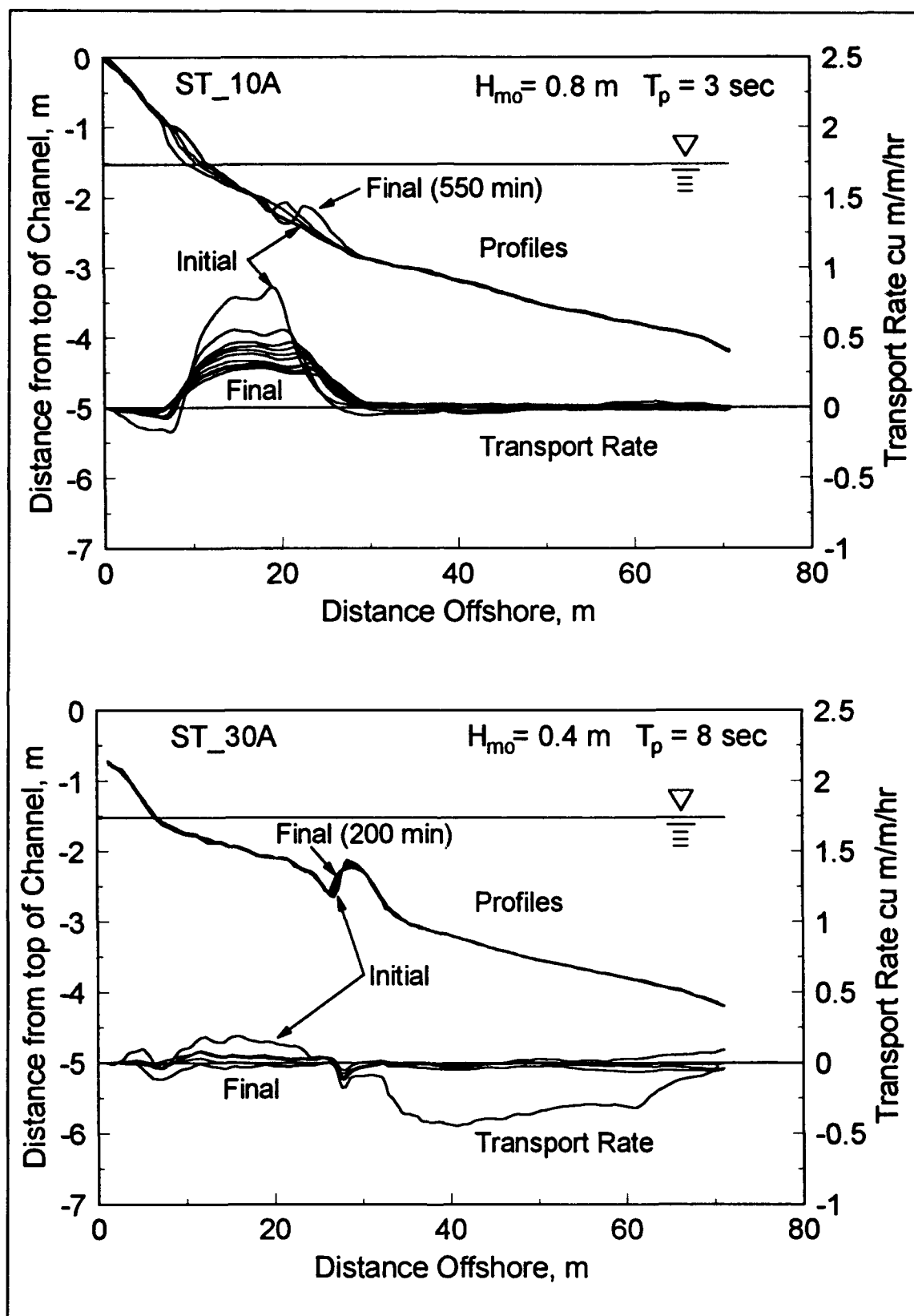
Figure 2-5. Examples of profile change during random-wave tests

Chapter 2 Beach Profile Surveys and Sediment Sampling

The input wave condition for Test ST_10A was narrow-banded random waves with H_{mo} = 0.8 m and T_p = 3.0 sec, where H_{mo} is the (significant) wave height calculated from the zeroth spectral moment, and T_p is the peak period of the input spectrum. The wave condition for Test ST_30A was H_{mo} = 0.4 m and T_p = 8.0 sec. Positive and negative rates respectively denote offshore and onshore transport.

The profile in Test ST_10A experienced significant erosion around the still-water shoreline, together with formation and migration seaward of a prominent breakpoint bar. For the random wave accretionary Test ST_30A, the transport rate and profile change were less extreme in rate and magnitude, respectively, than the erosional Test ST_10A. There was slight erosion of the foreshore as it adjusted under the higher runup of the long-period waves of Test ST_30A, and the bar slowly migrated onshore, decreasing in crest elevation and filling in the shoreward trough.

The net cross-shore transport rate is calculated by integration of the mass conservation equation, a process that involves the difference in consecutive profile-survey depths. Small errors in survey measurement, either in the horizontal or vertical, or changes in depth due to loss or gain of sand by local compaction or expansion of the bed under wave action, enter cumulatively in such a calculation and are manifested by nonclosure of the transport rate in deeper water. In calculation of the cross-shore transport rate by integration of profile elevation differences, therefore, one of the two profiles may have to be translated vertically by a small amount (Larson and Kraus 1989) to achieve closure of the rate offshore, where no transport occurred, as evidenced by absence of change in the profile between surveys. In examination of the SUPERTANK profile data, it has been found that some transport rates do not close without vertical adjustment, typically on the order of 0.5 cm. The next section discusses the reliability of the profile survey measurements.

Reliability of sur ·y procedure. Although the accuracy of Geodimeter T140 was satisfactory for the SUPERTANK project, it was necessary to estimate the reliability of the total survey system and operating procedure. Reliability was assessed in part by repetitive surveys of the same profile line (Kraus, Smith, and Sollitt 1992) after a particular day of testing with monochromatic waves, which left the profile with a well-defined breakpoint bar with steep vertical gradients. The 10 repetitive surveys were made with different personnel operating the Geodimeter, survey carriage, and rod to obtain an upper bound on potential survey error.

Repetitive surveying of a well-defined bar is expected to provide error bounds associated with the overall profiling system. Figure 2-6 shows the superposition of the 10 profile surveys that were made along the center line of the channel. The profile surveys began at Section I (Figure 2-3). The measurements in Section I, made with a hand-held rod, are not of direct interest here because the objective is to assess measurement of profile change produced by wave action as determined with the survey carriage and rod. The error associated with the hand-held rod is less than 0.1 ft (0.03 m), which was
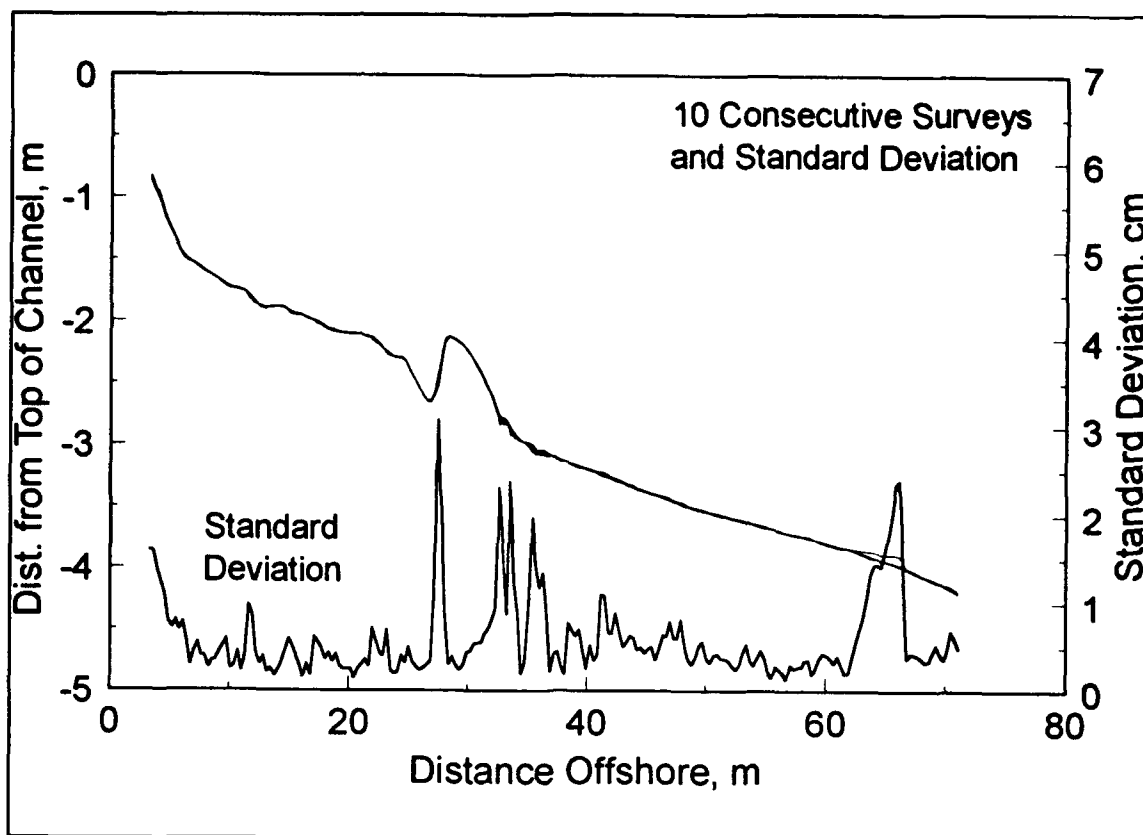
Figure 2-6. Repetitive profile surveys and standard deviation of profile elevation

on the order of the depth of footprints on the dry sand. All lines on
Figure 2-6 are coincident, with the exception of one line in the range of 62 to
66 m. This one obvious error was caused by wheel floating, which would
tend to occur in deeper water where the hollow survey rod was mostly
submerged and buoyant. Routine data inspection of the profile data at the end
of the survey, as described above, revealed most of these errors, and the data
were edited or the profile re-surveyed. In the present case, the obvious wheel
float was allowed to remain as an example.

Because measurements in the repetitive survey were not made at exactly
the same location along the channel, the data were interpolated to obtain uni-
form spacing, and the standard deviation in elevation in Figure 2-6 was com-
puted at each point. The standard deviation was less than 0.3 cm over most
of the profile. The deviation was greater, however, in the nearshore region
where the proximity of the Geodimeter to the prism tended to introduce error.
It was difficult to overcome this near-field error because the location of the
Geodimeter was limited by the wall of the enclosure. The standard deviation
was also relatively high on the shoreward side of the bar, where repeated
impact of the tires may have disturbed the bed, and on the offshore side of the
bar. On the offshore side of the bar, large ripples that were observed to form

under monochromatic waves may have contributed to increasing the variability as they were gradually obliterated by repetitive motion of the survey wheels. The standard deviation shown in Figure 2-6 is associated with an extreme profile shape, and a large part of the variability was probably caused by cumulative damage to the profile introduced by the repetitive survey. The error in a single profile survey is expected to be less than that obtained in the repetitive survey.

Sediment sampling

The origin of the sand from the Oregon coast and its emplacement in the channel are described in Chapter 12. In addition, Chapter 12 also describes bed density measurements that were made during the course of SUPERTANK to determine if compaction occurred.

Bed and suspended sediment samples were obtained by individual investigators and as part of background data collection associated with the profile change component of SUPERTANK. These samples were subsequently analyzed independently at CERC, OSU, and the Florida Institute of Technology (FIT) for the geometric grain size diameter through mechanical sieving. In addition, the hydraulic grain size diameter can be inferred through particle fall-speed measurements conducted at FIT.

Data Analysis

Profile surveys

After completion of data collection, the profile survey data were plotted and visually examined by three people, including the first two authors, who were involved with the majority of surveying operations at SUPERTANK. Inspection of the individual profile plots and comparison of three-line surveys revealed occasional small discrepancies as noise or obvious wheel floating. These points were eliminated and replaced through nearest-neighbor interpolation. Selected portions of the final profile survey data set have subsequently been subjected to intensive analyses in independent studies, such as for bar properties and net cross-shore sand transport rates, and the data have yielded consistent and reasonable results. The profile data listed and plotted in Appendix B of Volume II are the final cleaned values.

Sediment

At CERC, the mineralogy of a sediment sample taken from the surf zone during SUPERTANK was determined through visual inspection by microscope, as summarized in Table 2-1. The sediment consisted primarily of quartz and feldspar.

50

Table 2-1
SUPERTANK Sediment Mineralogic Composition

Composition by Weight	
Light minerals (SG* < 2.87)	94.9 percent
Heavy minerals (SG > 2.87)	5.1 percent
Composition of Light Fraction	
Quartz	64.2 percent
Feldspar	35.8 percent
Composition of Heavy Fraction	
Leucoxene	68.1 percent
Hornblende	18.2 percent
Tourmaline	4.4 percent
Other	9.3 percent

Note: SG denotes specific gravity; analysis performed by Mr. Edward P. Meisburger, formerly Research Physical Scientist (Geology), CERC.

Table 2-2 summarizes grain-size statistics of the same sample as determined by sonic sifter analysis. The sediment consisted primarily of very uniform fine sand with median grain-size diameter of 0.22 mm.

Table 2-2
SUPERTANK Sediment Content and Grain-Size Statistics

Sample Content by Weight, percent						
Classifi- cation	Gravel	Coarse Sand	Medium Sand	Fine Sand	Silt	Clay
Went- worth	0.034	0.197	14.487	85.255	0.027	0.000
Unified	0.000	0.034	0.244	99.668	0.054	0.000

Grain-Size Statistics					
Analysis Method	Median	Mean	Std. Dev.	Skew.	Kurt.
Moment, phi	--	2.23	0.28	-1.68	32.49
Folk Graphic, phi	2.21	2.22	0.24	0.12	1.08
Diameter, mm	0.22	0.21	--	--	--

The fall speed of surf zone sediment samples was measured in a settling tube. Figure 2-7 gives a representative result, in which the particle fall-speed distribution is plotted for five samples. The predominant peak occurs at 3.3 cm/sec.

Summary

A survey system consisting of an auto-tracking Geodimeter, manually moved carriage, and previously developed software was implemented at SUPERTANK to provide rapid surveys while preserving accuracy and resolution of major features of the beach profile. The system and associated operation procedure were shown to be accurate with error less than 0.3 cm in most areas of the profile exposed to wave action. Additionally, the survey system provided an integrated means of measuring instrument location inside and outside the channel. The large number of beach profile surveys made in conjunction with hydrodynamic and other measurements provides a reliable database for a wide range of profile change configurations with which to study cross-shore hydrodynamic and sediment transport processes.

The beach sediment, consisting primarily of very uniform fine-grained quartz and feldspar sand, was analyzed to have a median diameter of 0.22 mm and a fall speed of 3.3 cm/sec.
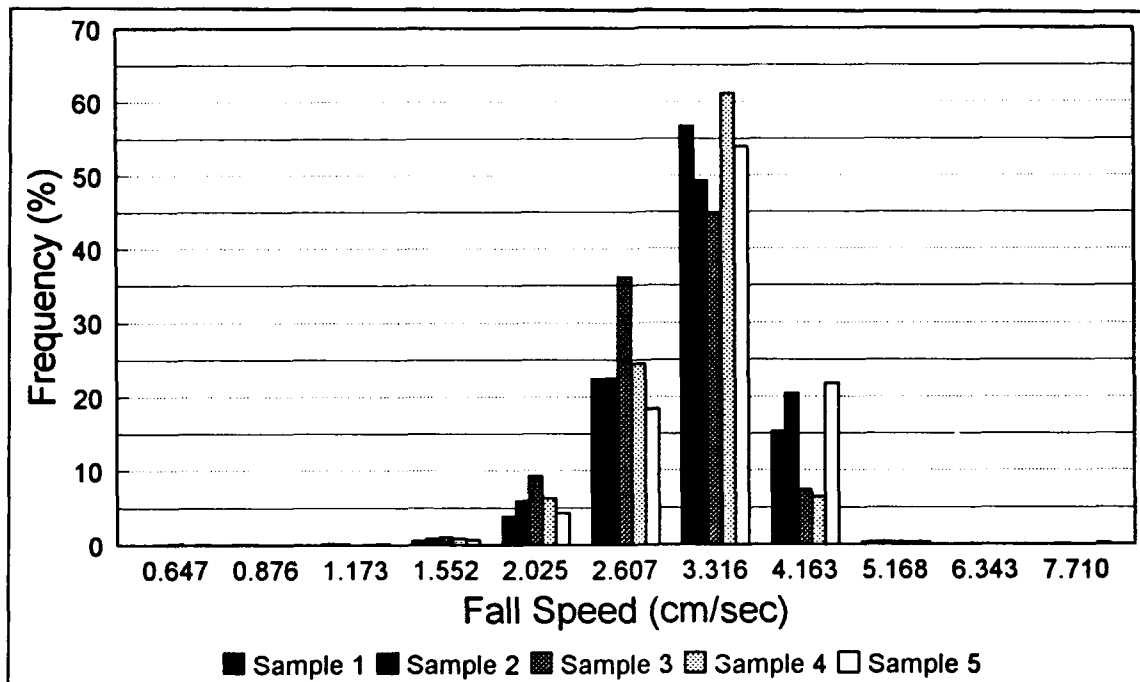
Figure 2-7. Fall-speed distribution of SUPERTANK surf zone sediment

Acknowledgements

References

Howd, P. A., and Birkemeier, W. A. (1987). "Beach and nearshore survey data: 1981-1984 CERC Field Research Facility," Technical Report CERC-87-9, U.S. Army Engineer Waterways Experiment Station, Vicksburg, MS.

Kraus, N. C., and Larson, M. (1988). "Beach profile change measured in the tank for large waves, 1956-19' ·d 1962," Technical Report CERC-88-6, U.S. Army Engineer Waterways Experiment Station, Vicksburg, MS.

Kraus, N. C., Smith, J. M., and Sollitt, C. K. (1992). "SUPERTANK Laboratory Data Collection Project." *Proc. of 23rd Coastal Engrg. Conf.* ASCE, New York, 2191-2204.

Larson, M., and Kraus, N. C. (1989). "SBEACH: Numerical model for simulating storm-induced beach change; Report 1, empirical foundation and model development," Technical Report CERC-89-9, U.S. Army Engineer Waterways Experiment Station, Vicksburg, MS.

Moore, B. (1982). "Beach profile evolution in response to changes in water level and wave height," M.S. thesis, University of Delaware, Newark, DE.

Saville, T. (1956). "Scale effects in two-dimensional beach studies." *Trans. 7th General Meeting*. IAHR, 1, A3.1-A3.10.

Sommerfeld, B. G., Mason, J. M., Larson, M., and Kraus, N. C. (1993). "Beach Morphology Analysis Package (BMAP)." *Proc. Coastal Zone '93*. ASCE, New York.

Sommerfeld, B. G., Mason, J. M., Kraus, N. C., and Larson, M. "BFM: Beach Fill Module, Report 1: Beach Morphology Analysis Package (BMAP) -- user's guide," in preparation, U.S. Army Engineer Waterways Experiment Station, Vicksburg, MS.

3 SUPERTANK Hydrodynamics[1]

Introduction

Background

At the SUPERTANK Laboratory Data Collection Project, waves and currents were measured along the wave channel with 16 resistance wave gauges and 18 electromagnetic current meters. Wave gauges were deployed at 12-ft (3.66-m) intervals from the mid surf zone to the wave paddle. The wave gauges measured the water surface elevation as a function of time to give wave height, wave period, and mean water level throughout the channel. Current meters were deployed in vertical arrays inside and just outside the surf zone. The current meters measured the cross-shore and vertical water velocities as a function of time to give mean wave-induced current velocities. Hydrodynamic data were processed with both spectral and time series analyses.

Objectives of hydrodynamic measurements

The first objective of the hydrodynamic measurements at SUPERTANK was to support the beach profile change studies, as waves and currents are the driving forces for beach evolution. Within this objective, the measurements also supported studies of sediment suspension and transport. The second objective of the hydrodynamic measurements was to collect data for the development and verification of advanced hydrodynamic models that describe such processes as vertical current structure, wave breaking, transformation of bimodal spectra, wave setup, and nonlinear wave transformation.

---

[1] Written by Jane McKee Smith, Coastal Engineering Research Center, U.S. Army Engineer Waterways Experiment Station.

Scope

The purpose of this chapter is to describe the collection and analysis of data from the resistance wave gauges and electromagnetic current meters and to document the analyzed data. The following sections describe the data collection and analysis procedures. Wave and current parameters resulting from the analyses are given in Appendix C, which is contained in Volume II of this report.

Experiment Apparatus

Instrument description

Resistance wave gauges. Sixteen resistance wave gauges measured the elevation of the water surface to determine mean water levels and wave parameters. The resistance wave gauges were fabricated by the staff of the O. H. Hinsdale Wave Research Laboratory, Oregon State University (OSU) (Dibble and Sollitt 1989), where the SUPERTANK project was conducted. Each gauge was 7 ft (2.1 m) tall and consisted of two 0.027-in. (0.69-mm), seven-strand stainless steel cables, spaced 2.5 in. (6.4 cm) apart. The resistance gauges use the conductivity of the water to determine the water elevation. The resistance between the two wires is inversely proportional to the depth of water. By monitoring the change in resistance, the water surface elevation can be determined. Each gauge is driven by a constant amplitude AC voltage source and the current drawn by the gauge is measured. By Ohm's law, with the voltage held constant, the current is inversely proportional to the resistance or directly proportional to the water elevation. Current sensing is accomplished by measuring the voltage drop across a 1-ohm resistor placed in series with the gauge. The conversion from volts to engineering units is determined by calibration of the gauges, as described under "Experimental Procedures."

Electromagnetic current meters. Cross-shore and vertical water velocities were measured with 18 Marsh-McBirney Model 512 electromagnetic current meters. Each current meter sensor consists of a 1.5-in.- (3.8-cm-) diam sphere, which contains an electromagnet. Four electrodes are equally spaced around the sphere. The electromagnet generates a magnetic field, and, as the water (a conductor) flows through the magnetic field, it produces a voltage that is proportional to its velocity (Faraday principle). The voltage is detected with the electrodes. A rod containing the instrument cable is attached to the sphere, which in turn is attached to a flat metal mounting bar.

56

Location

Resistance wave gauges. Wave gauges were deployed at 12-ft (3.66-m) intervals on the west wall of the channel. The most shoreward gauge was at Station 6, $x = 61$ ft (18.6 m), and the most seaward at Station 21, $x = 241$ ft (73.5 m), in SUPERTANK coordinates (Chapter 1). The gauges were numbered 1 to 16 with Gauge 1 being the most shoreward and Gauge 16 the most seaward. Gauge numbers correspond to the channels on which the data were collected. Wave gauges were attached to the tank wall using existing 1-in. (2.54-cm) wall inserts. Gauge mounts consisted of 1-in. (2.54-cm) aluminum rods, threaded on one end to attach to the wall inserts. The other end of each rod was machined to accept a Delrin plate, to which the wave gauge wires were attached. The gauge mounts extended horizontally out from the wall approximately 18 in. (0.46 m), $y = 1.5$ ft (0.46 m) and the gauges extended vertically from $z = -1.0$ ft to -8.0 ft (-0.3 m to -2.4 m). The top mount incorporated an adjustable eyebolt to set wire tension.

Electromagnetic current meters. Fourteen current meters were deployed on the east wall of the channel in vertical arrays of one to four gauges. The arrangement of the current meters varied from week to week, with some changes from run to run, to meet measurement objectives. Tables A2-A7 (contained in Volume II of this report) give the x, y, and z positions of the 14 wall-mounted current meters for the 6 weeks of SUPERTANK tests. The current meters were numbered CM1 to CM18. Current meters CM13, CM14, CM15, and CM16 were deployed in a vertical array (approximate 1-ft (0.3-m) vertical spacing) off a mobile carriage. The position of the carriage for each run is given in Table 1-2. The column labelled *Elev* is the vertical reference for the current meters deployed off the carriage. The z position of CM13, the bottom sensor in the array, is given by 4.9 ft (1.49 m) minus *Elev* (Table 1-2); plus 0.98 ft (0.30 m) for z of CM14, plus an additional 0.90 ft (0.27 m) for CM15, plus an additional 1.05 ft (0.32 m) for CM16. Columns labelled *Pos* and *Ref Sta* (Table 1-2) are the horizontal references for the carriage. The x position of the current meters is located *Pos* inches seaward of the given reference station.

The current meter mounts consisted of aluminum plates and rods. The plates were bolted into the wall inserts with 1-in. (2.54-cm) bolts. Spacers welded to the back of the plates set the plates approximately 2 in. (5 cm) out from the wall. A vertical array of rectangular slots was machined into the plates at 6-in. (15.2-cm) spacings. Three-quarter-in. (1.9-cm) aluminum rods, threaded and keyed on one end, slid into the slots in the plate and were fastened with a nut on the backside of the plate (the space between the wall and plate allowed access behind the plate). The elevation of the rods could be easily adjusted between runs by removing the nut behind the plate and refastening the rod into another slot. The opposite end of the rod was machined flat on one side, and the mounting bar of the current meter was attached to the flat portion of the rod with two small hose clamps. Current meter cables were secured to the plate with cable ties attached through small holes punched into the plate for that purpose. The meters extended
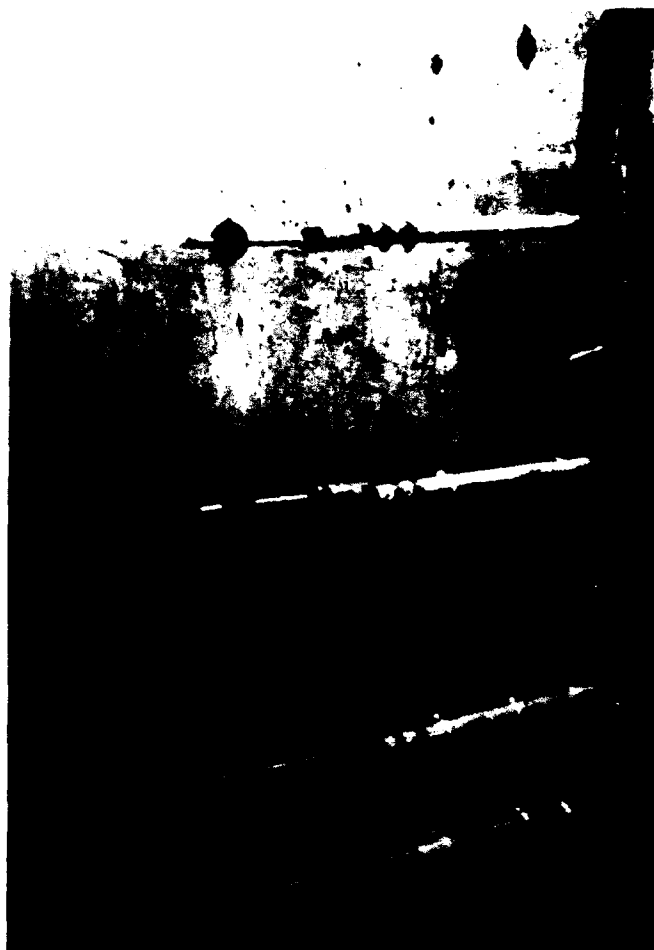
Figure 3-1. Current meter mounting configuration

approximately 2 ft (0.6 m) out from the channel wall. Figure 3-1 shows an example of the current meter mounting configuration. The current meters deployed off the carriage were hose clamped to angles bolted to an aluminum wing-shaped section hanging down from the carriage. The wing elevation was adjusted with a winch and clamped into place to provide a steady platform for the meters.

Instrument characteristics

Resistance wave gauges. The largest source of error in the gauge is expected to be the change in resistivity (change in conductivity of the water, contamination of the probes, or residual errors in the calibration procedure), typically about 2 percent. The range of the gauges was fixed by the vertical range of the wires, -1 to -8 ft (-0.3 to 2.4 m). Occasionally, waves exceeded the top of a gauge (produced by a combination of large wave height and high water level) and saturated the signal. Gauge calibrations were linear.

58

Electromagnetic current meters. The manufacturer's specifications state that the electromagnetic current meters have an accuracy of ± 2 percent. The range of the meter is ± 5 V, which translates to ± 5 m/sec (CM1 to CM16) or 3 m/sec (CM17 and CM18) (the difference between the meters is due to different factory calibrations). The meters were deployed in groups of two (CM17 and CM18) or four (CM1 to CM16) using the close proximity option. This reduced interference between closely spaced meters by driving all four meters with one timing pulse.

Experiment Procedures

Sequence of events

The sequence of a typical run was:

a. Specify wave conditions and data collection parameters. The wave conditions were either monochromatic (specified wave height and period) or random (specified target zero-moment wave height H_{mo}, peak period T_p, and peakedness parameter γ to generate a TMA spectrum). Data collection parameters included sampling frequency and run length. Wave conditions and run lengths are listed in Table 1-2.

b. Check gauges and water level. Checks were made of the gauges (checking gauge voltages) and the water level.

c. Position the carriage. The carriage with the current meters was positioned at a strategic location (e.g., in the expected incipient breaking zone, adjacent to wall-mounted meters, in the trough, etc.).

d. Begin wave action and data collection. One computer program controlled both the wave generation and the collection of the resistance wave gauge and electromagnetic current meter data. The data collection began as soon as the wave generation program began (although wave action did not begin immediately) and ended when the wave action ceased. Typically, wave action lasted 10 to 70 min.

e. Lab notes. Notes were kept documenting significant features of the run, e.g., breaker type and approximate position, instrument status, and visual observations of sand ripples.

f. Beach profile survey. At the beginning of the day and following each run, the beach profile was surveyed (the post-run survey typically served as the pre-run survey for the next run). Divers also measured the elevation of the lowest current meter in each vertical array and made any necessary meter adjustments. Current meter positions were surveyed once a week and after major changes in configuration.

g. Preliminary analysis of data for quality control. For at least one run a day (typically the first run of the day), plots were made of the time series and spectra for all gauges to ensure that the gauges were operating properly.

Calibration and zero reference

Resistance wave gauges. Wave gauges were calibrated once a week during the project. They were calibrated by slowly raising or lowering the water level (approximately 1 ft/hr (0.3 m/hr)) and recording the water level change with the gauges. Simultaneously, a video camera recorded the water level relative to a 0.1-ft- (0.3-m-) increment scale painted on the tank wall. Wave gauge data were linearly regressed with the video measurements to estimate gauge gains and offsets. Calibration gains for each day of the experiment were linearly interpolated between the weekly calibrations. Gains are given in Tables A8 through A13 (contained in Volume II of this report). Gauge offsets were calculated in the analysis software as the average water surface elevation during the quiescent period at the beginning of a run (average over the first 200 points in random wave runs, average over the first 20 points in monochromatic wave runs). The run-by-run offsets were calculated to adjust for small changes in water level between runs (leaking or filling of the tank) and changes in the sand level of the most shoreward gauges (due to beach profile change).

Electromagnetic current meters. Current meters were calibrated between 24 and 27 September 1991 at a U.S. Geological Survey Indoor Hydraulic Laboratory Facility in Bay St. Louis, MS. Although most of the meters had been calibrated within one year prior to the project, the post-project calibrations were used for all analyses. The calibration gains and offsets are given in Table A14. As with the wave gauges, the current meter offsets for submerged meters were calculated from the beginning of the data record. For gauges that were out of the water at the beginning of the run, the calibration offsets were applied.

Sampling and time reference

The OSU data acquisition system (Chapter 13) sampled the wave gauges and current meters at a rate of 16 Hz. The start time for a run was recorded in the data file header. Time was referenced to Pacific Daylight Time. The computer clock was updated to the WWV time standard (broadcast by National Institute of Standards and Technology, Fort Collins, CO, call letters WWV), which was used by all SUPERTANK participants. The approximate run start times are given in Table 1-2.

Pre-processing and filtering

A 10-Hz, fifth-order anti-aliasing Bessel filter was applied to both the resistance wave gauge and electromagnetic current meter analog data to eliminate noise and avoid aliasing.

Data Analysis

Analysis and interpretation methods

Frequency domain and time domain analyses were performed on the SUPERTANK hydrodynamic data. The analysis routines for the resistance wave gauge and electromagnetic current meter data were nearly the same, with only minor differences in the initial processing of the data and output parameters. The data were filtered to separate the incident-band wave motions from the low-frequency motions due to the channel seiche, and then spectral and zero up-crossing analyses were performed on the raw, low-pass, and high-pass signals.

Preprocessing. The electromagnetic current meter data required two types of processing prior to analysis. First, a low-pass filter with a 2-Hz cutoff was applied to remove high-frequency noise. High-frequency noise was present in some data records for deployments with the current meters spaced less than 30 cm apart. Second, the elevation of each current meter was compared with the water surface elevation (estimated from a resistance wave gauge at the same cross-shore location) to determine if the current meter was submerged. The criterion for submergence was that the water level was 5 cm or more above the surveyed current meter elevation. Current meter readings were set to zero (for that portion of the record) when the gauge was out of the water. The current meters deployed on the carriage and current meters shoreward of resistance wave Gauge 1 could not be checked for submergence. These gauges were analyzed assuming 100 percent submergence; thus, these results should be used with care.

Filtering. To separate incident-band wave motions from low-frequency motions due to channel seiche, a non-recursive, low-pass filter was applied. The period cutoff for the filter was set to twice the peak period of the incident waves (the peak period of the long-period motion was generally 20 sec or longer). The period response of the filter is shown in Figure 3-2 for a cutoff period of 6 sec. The filter was applied beginning with the 1,009th data point. The first 1,008 points were skipped to ensure that the waves had reached the most shoreward gauge. Two hundred points were sacrificed at the beginning (in addition to the 1,008 points that were skipped) and end of the data record in constructing the filter. The low-pass time series was output directly from the filter. The high-pass time series was obtained by subtracting the low-pass time series from the preprocessed data.

Spectral analysis. Spectral analysis was performed using a standard Fast Fourier Transform (Press et al. 1989). Data were divided into blocks of 4,096 points and the spectrum was calculated for each block. The total number of blocks per run was determined by the run length (20-min run = 4 blocks, 40-min run = 8 blocks, and 70-min run = 15 blocks). The average spectrum for each run was calculated by averaging the spectra over all blocks within the run. The confidence bands for each spectrum become tighter as the number of averages increases. The degrees of freedom (DOF) for the spectra are approximately twice the number of averages (20-min run = 8 DOF, 40-min run = 16 DOF, and 70-min run = 30 DOF).
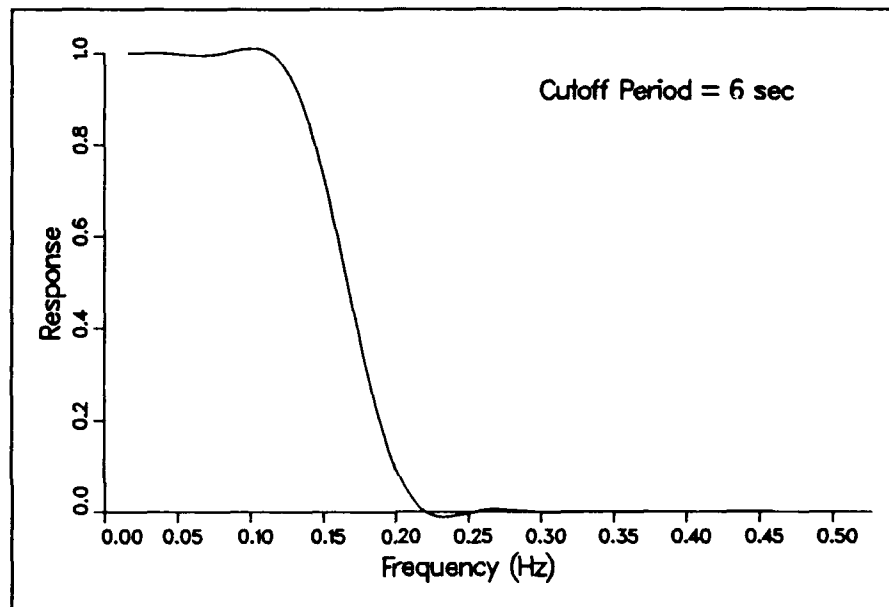
Figure 3-2. Period response of the low-pass filter for cutoff period 6 sec

Although most runs were 20, 40, or 70 min in length, shorter runs were also made. For 10-min runs, blocks of 4,096 points with two averages were used and for 5-min runs, blocks of 2,048 points with no averages were used. Runs of 1 to 3 min that were conducted to investigate sediment suspension (Runs A2908B through A3017B) were not analyzed for this report. The spectral parameters calculated for the resistance wave staffs are:

a. Setup and setdown or mean water elevation (relative to the still-water elevation)

$$\overline{\eta} = S(0) \tag{3-1}$$

where $S(0)$ is the energy density of the discrete water surface spectrum at the frequency f equal to zero.

b. Spectral estimate of the standard deviation of the water surface

62

$$\sigma = \sqrt{m_0} \qquad (3-2)$$

where m_0 is the zeroth moment of the water surface spectrum $S(f)$

$$m_0 = \int_0^{f_{ny}} S(f)\, df \qquad (3-3)$$

and f_{ny} is the Nyquist frequency. The spectral component $S(0)$ is excluded from the integration.

c. Root-mean-square wave height

$$H_{rms} = \sqrt{8\, m_0} \qquad (3-4)$$

d. Zero-moment wave height

$$H_{mo} = 4\sqrt{m_0} \qquad (3-5)$$

e. Peak spectral wave period T_p defined as the reciprocal of the frequency containing the greatest energy.

The spectral parameters calculated for the electromagnetic current meters are:

a. Mean cross-shore and vertical velocity components

$$\overline{u} = S_u(0)$$
$$\qquad (3-6)$$
$$\overline{w} = S_w(0)$$

where u is the cross-shore velocity component, w is the vertical component, and S_u and S_w are the spectra of u and w, respectively.

b. Spectral estimate of the standard deviation of the cross-shore and vertical velocities

$$\sigma_u = \sqrt{m_{0_u}}$$
$$\qquad (3-7)$$
$$\sigma_w = \sqrt{m_{0_w}}$$

where

$$m_{0_u} = \int_0^{f_{ny}} S_u(f)\, df$$
$$\qquad (3-8)$$
$$m_{0_w} = \int_0^{f_{ny}} S_w(f)\, df$$

The spectral components $S_u(0)$ and $S_w(0)$ are excluded from the integrations.

c. Peak spectral periods T_{pu} and T_{pw} of the velocity components defined as the reciprocal of the frequency containing the greatest energy.

Time series analysis. The time series analysis was performed with a zero-upcrossing definition of a wave. A wave is defined between two upward crossings of the water surface about the mean water elevation. The upcrossing definition was chosen because the saw-tooth shape of the nearshore wave profile gives distinct upward crossings, whereas downcrossings vary from wave to wave. The wave height H of an individual wave is defined as the difference between the highest and lowest water elevation between two zero upcrossings. The wave period T of an individual wave is defined as the time between zero upcrossings. Very small waves ($H < 0.6$ cm), associated with small surface variations near the mean water elevation, were not identified as individual waves. These very small waves were included as part of the preceding wave. The time series parameters calculated for the resistance wave staffs are:

a. Mean water elevation

$$\overline{\eta} = \frac{\sum \eta}{N} \tag{3-9}$$

where η is the measured water elevation and N is the number of data points.

b. Standard deviation of the water surface

$$\sigma = \sqrt{\frac{\sum(\eta - \overline{\eta})}{N - 1}} \tag{3-10}$$

c. Skewness of the water surface

$$\mu_3 = \frac{\sum(\eta - \overline{\eta})^3}{\sigma^3} \tag{3-11}$$

which is a measure of the horizontal asymmetry of the waves.

d. Kurtosis of the water surface

$$\mu_4 = \frac{\sum(\eta - \overline{\eta})^4}{\sigma^4} \tag{3-12}$$

which is a measure of the peakedness of the waves.

64

e.   Mean wave height

$$\overline{H} = \frac{\sum H}{M} \qquad (3\text{-}13)$$

where M is the number of individual waves identified by the zero-crossing analysis.

f.   Mean wave period

$$\overline{T} = \frac{\sum T}{M} \qquad (3\text{-}14)$$

g.   Root-mean-square wave height

$$H_{r,s} = \sqrt{\frac{\sum H^2}{M}} \qquad (3\text{-}15)$$

h.   Significant wave height H_s, defined as the average of the highest one-third of the wave heights.

i.   Significant wave period T_s, defined as the average period of the highest one-third waves.

j.   One-tenth wave height H_{10}, defined as the average of the highest one-tenth wave heights.

k.   One-tenth wave period T_{10}, defined as the average period of the highest one-tenth waves.

l.   Maximum wave height H_{max}.

m.   Maximum wave period T_{max}, defined as the period of the highest wave.

Time series parameters calculated for the electromagnetic current meters are:

a.   Mean velocity components

$$\overline{} = \frac{\sum}{N}$$

$$\overline{w} = \frac{\sum w}{N} \qquad (3\text{-}16)$$

b.   Standard deviation of the velocity components

$$\sigma_u = \sqrt{\frac{\sum(u - \bar{u})}{N - 1}}$$

$$\sigma_w = \sqrt{\frac{\sum(w - \bar{w})}{N - 1}}$$

(3-17)

c. Skewness of the velocity components

$$\mu_{3_u} = \frac{\sum(u - \bar{u})^3}{\sigma_u^{\,3}}$$

$$\mu_{3_w} = \frac{\sum(w - \bar{w})^3}{\sigma_w^{\,3}}$$

(3-18)

d. Kurtosis of the velocity components

$$\mu_{4_u} = \frac{\sum(u - \bar{u})^4}{\sigma_u^{\,4}}$$

$$\mu_{4_w} = \frac{\sum(w - \bar{w})^4}{\sigma_w^{\,4}}$$

(3-19)

e. Maximum velocity components u_{max} and w_{max}.

f. Minimum velocity components u_{min} and w_{min} defined as the largest negative velocities.

g. Percent of measurements with the gauge submerged.

Data file format

Resistance wave gauge and electromagnetic current meter data were saved in unformatted, direct access files with all channels for each run contained in one file. Data were archived on TK70 tape cartridges with the Digital Electronics Corporation VAX VMS backup utility.

Sample data

Resistance wave gauge. A sample of the raw resistance wave gauge data is shown in Figure 3-3 for Gauge 6, Run S0311A. Every fourth data point of the time series is plotted. The low-pass signal is also included in Figure 3-3, appearing as the smoother line. Figure 3-4 shows the time series of the high-pass signal for the same gauge and run. Wave groups are evident in the time

66
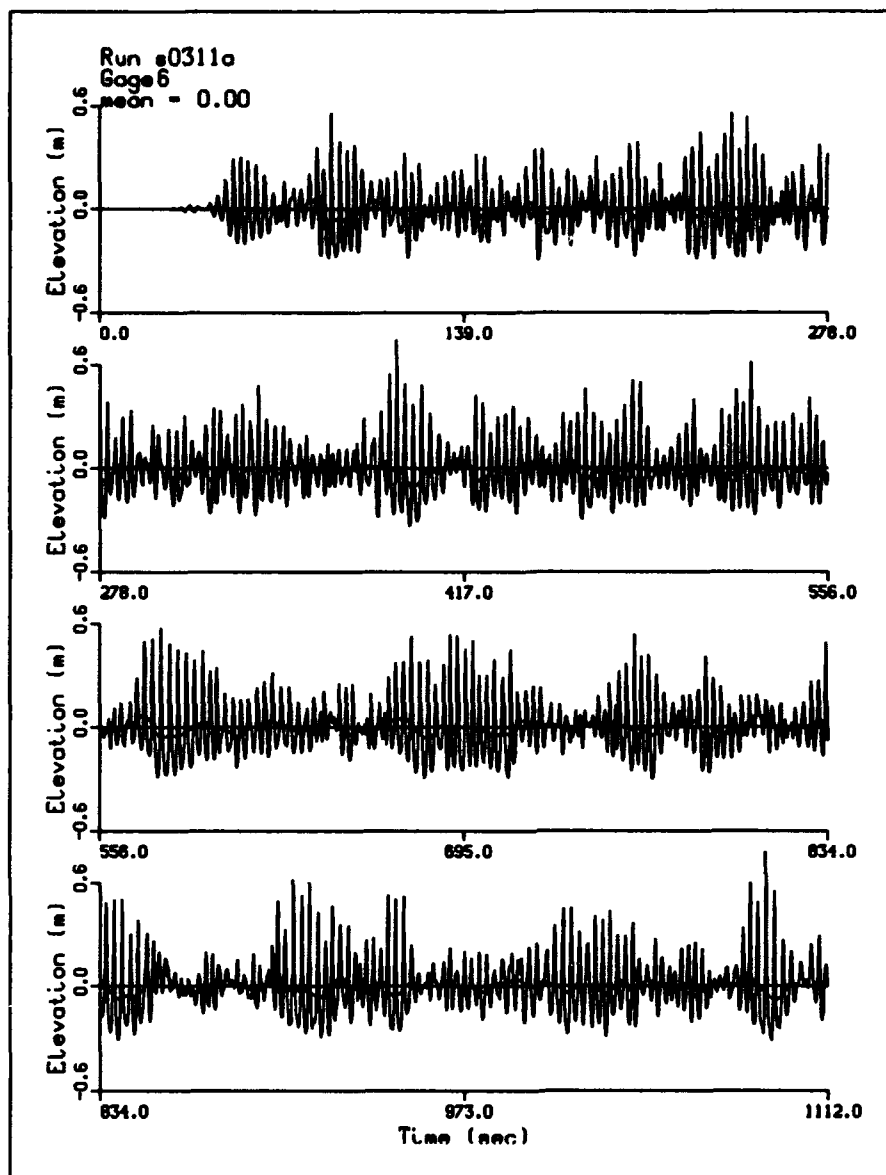
Figure 3-3. Time series of raw and low-pass water surface elevation
for Gauge 6, Run S0311A

series, as would be expected with the relatively narrow incident spectrum
($\gamma = 20$).

Smoothed spectra for the raw, low-pass, and high-pass signals for
Gauge 6, Run S0311A are given in Figure 3-5. For this example, the spectral
peak is located at 0.34 Hz (2.9 sec) and higher harmonics are apparent at
approximately 0.7 and 1.0 Hz. A low-frequency peak at 0.04 Hz (23 sec) is
also apparent. At Gauge 6, 96 percent of the wave energy is contained in the
high-pass signal and only 4 percent in the low-pass signal. The energy in the
low-pass signal tends to increase closer to shore.
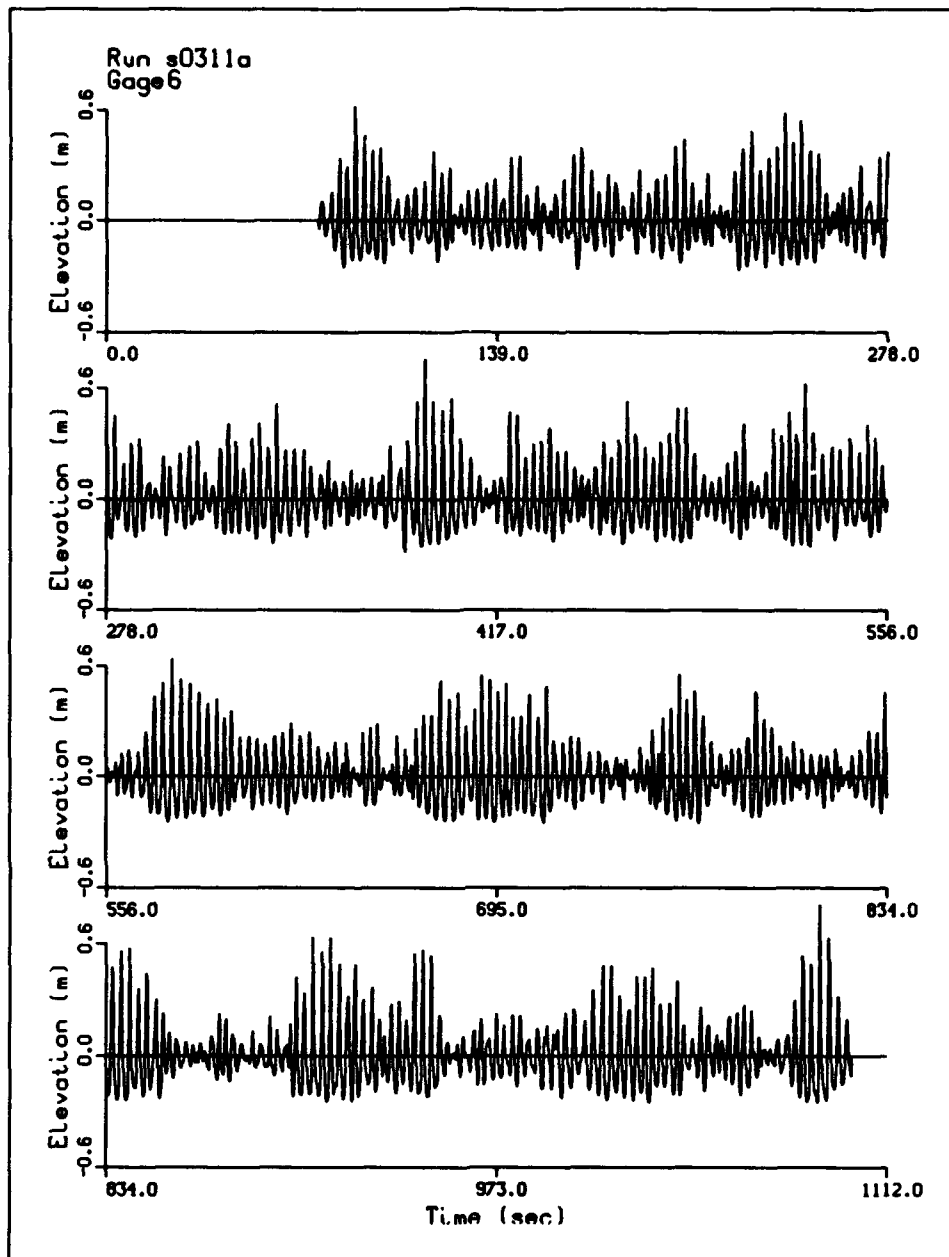
Figure 3-4. Time series of high-pass water surface elevation for Gauge 6, Run S0311A

Electromagnetic current meter. Figure 3-6 shows the spectrum for the raw signal and the raw and low-pass time series for Channel 36 (CM5, cross-shore component, located approximately 1.7 ft below the mean water elevation) for Run A3011A. Note that the general appearance of the raw time series is inverted from the wave time series in Figure 3-3. Because the SUPERTANK coordinate system defines the cross-shore coordinate as positive
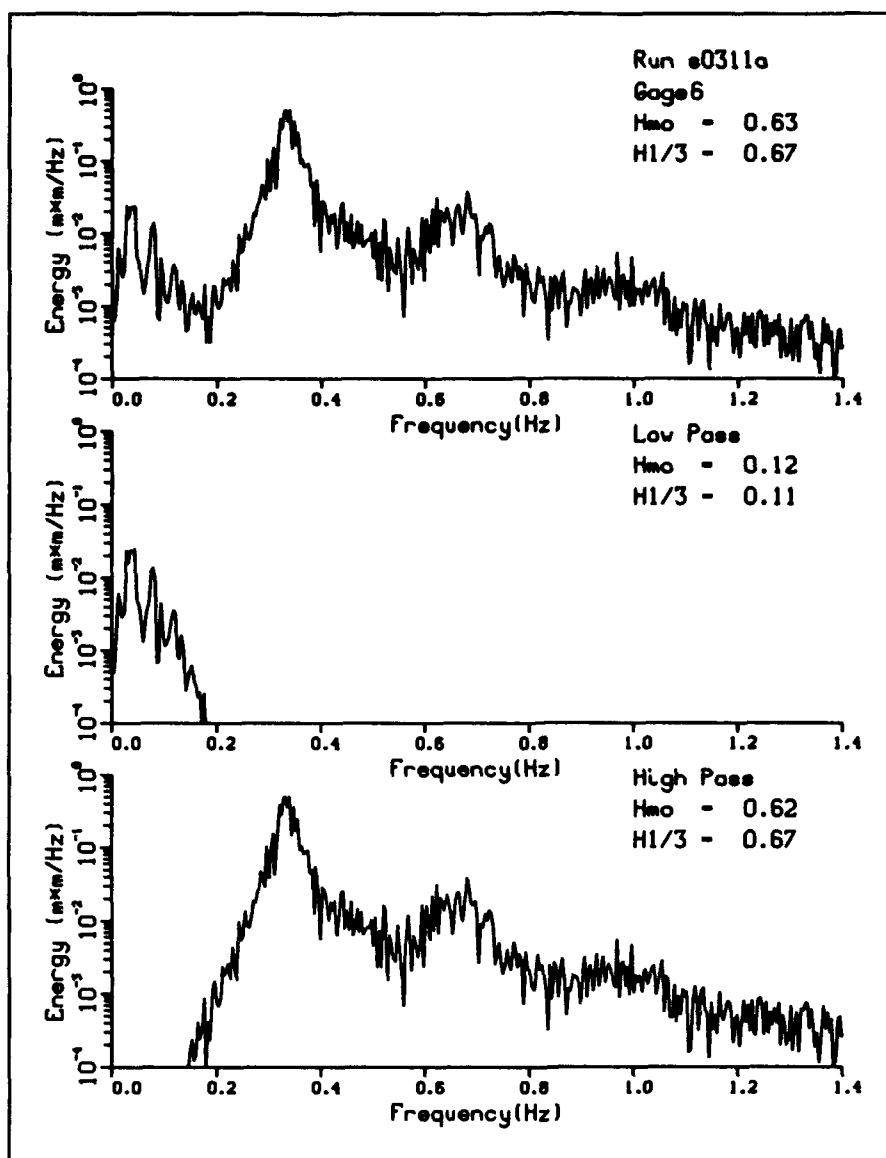
Figure 3-5. Wave spectra for the raw, low-pass, and high-pass water surface elevation for Gauge 16, Run S0311A

offshore, the positive (offshore) velocities correspond to the passage of a wave trough (negative elevations), and the negative (onshore) velocities correspond to the passage of a wave crest (positive elevations). The mean velocity at this gauge was 0.13 m/sec, directed offshore. The energy spectrum of the velocity is similar to the wave spectrum in Figure 3-5. The primary peak is at 0.33 Hz with harmonics at 0.7 Hz and 1.0 Hz. Approximately 14 percent of the energy is contained in the low-pass signal (the current meter is located 24 ft shoreward of wave measurement at Gauge 6) and the low-frequency peak is at 0.02 Hz (50 sec).
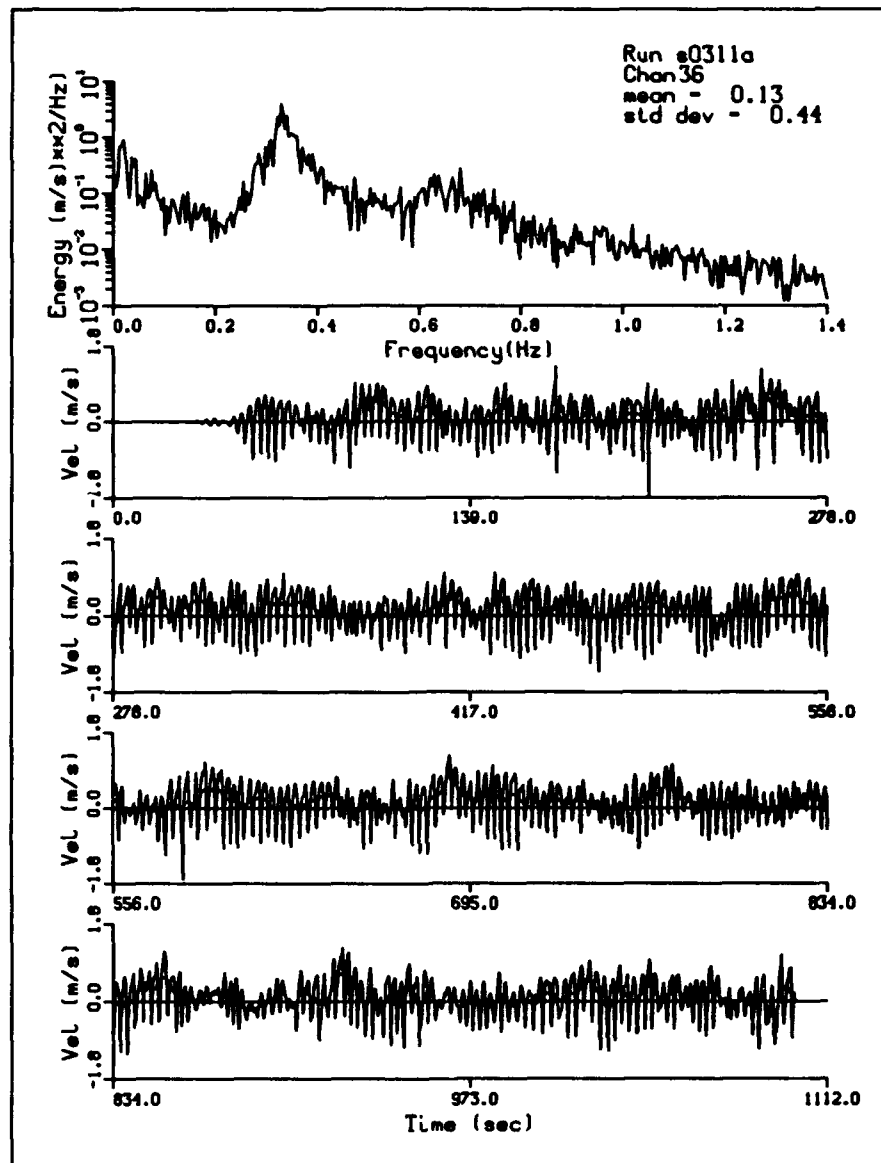
Figure 3-6. Current meter raw spectrum and time series of the raw
and low-pass signal for Channel 36, Run S3011A

Summary of data characteristics

Resistance wave gauge. Spectral analysis results for the wave gauges are
given in Table C1, and time series results are given in Table C2, both
contained in Volume II of this report. Figure 3-7 gives an example summary
of the wave transformation for a typical run (A0814A). Wave height
increases (through shoaling) up to breaking and then decays. Energy in the
low-frequency portion of the spectrum increases in shallower depths as shown
in the lower half of Figure 3-7. Energy also increases at harmonics of the
peak frequency in shallower depths which can be seen with the increase in
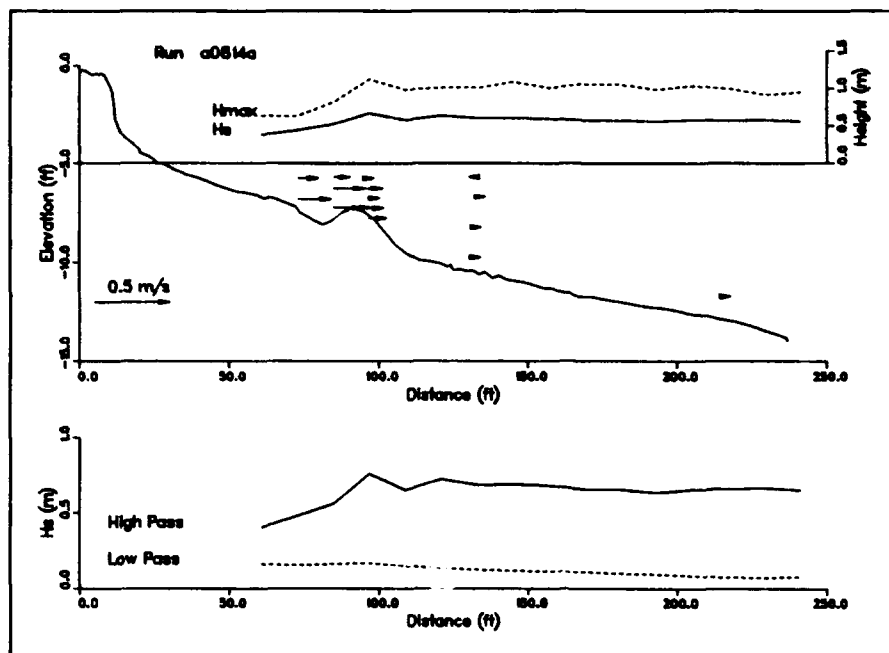
Figure 3-7. Summary of wave transformation and cross-shore current
for Run A0814A

kurtosis. Wave skewness increases as the waves become asymmetric in the
surf zone.

Electromagnetic current meter. Spectral analysis results for the current
meters are given in Table C3, and time series results are given in Table C4,
contained in Volume II of this report. Table A14 gives the channel numbers
associated with each current meter to relate the gauge positions and channel
numbers given in Tables C3 and C4. The odd-numbered channels are vertical
velocity, and the even-numbered channels are cross-shore velocity. The mean
cross-shore velocities for Run A0814A are shown in Figure 3-7 as vectors.
The current meters show a tendency for onshore flow above trough level and
offshore flow below trough level. Also, the velocity magnitude is much lower
outside the surf zone than inside. There is a marked decrease in the cross-
shore flow seaward of the bar.

Identification of marginal data sets

In general, the quality of the hydrodynamic data is considered to be good.
Care should be taken interpreting results from current meters that were located
near the mean water elevation and shoreward of the resistance gauges or on
the carriage, because these data were not filtered for being "in" or "out" of
the water. These data could be reanalyzed on a case-by-case basis using
capacitance wave gauges for filtering. Run A0916A should be viewed with
caution due to cross waves (standing waves in the y direction) during this run.

Comments on the status of particular gauges, such as on lost data, are given in the *Comments* column in Table 1-2.

Summary

Review of experiments and results

A large data set of hydrodynamic measurements was obtained during the SUPERTANK Laboratory Data Collection Project to support beach profile change, sediment transport, wave transformation, and cross-shore flow studies. This chapter describes the procedures used to collect and analyze these data. Results from spectral and time series analysis are presented in Appendix C, which is contained in Volume II of this report.

Recommendations

The analysis described in this chapter is only the first step in the SUPER-TANK data analysis process. The data are now in a usable form for application to beach profile change, wave transformation, and cross-shore current research and modeling. The data contained in Appendix C can also be used to identify trends in the data and lead to more detailed analysis including correlation of wave and current measurements to suspended sediment concentration, time varying wave and current parameters, and transformation of multiple wave trains.

Acknowledgements

References

Dibble, T. L., and Sollitt, C. K. (1989). "New designs for acoustic and resistive wave profiles," *Proc. Workshop on Instrumentation for Hydraulic Laboratories*, IAHR.

Press, W. H., Flannery, B. P., Teukolsky, S. A., and Vetterling, W. T. (1989). *Numerical Recipes*. Cambridge University Press, Cambridge, England, 390-5.

4 SUPERTANK Swash Measurements[1]

Introduction

Background

Ten capacitance-based wave gauges were placed at 2- to 6-ft (0.61- to 1.83-m) intervals in the vicinity of the shoreline and on the beach face to measure water surface and sand bed elevations in the swash zone. These gauges complement the 16 resistance wave gauges that were positioned at 12-ft (3.66-m) intervals from the wavemaker to the mid surf zone (Chapter 3). As a result, mean and time-varying water surface elevations were measured at 26 locations along the full length of the wave channel. In the swash zone, the capacitance-based wave gauges measured wave propagation (uprush and down-rush) on the beach face. In addition, these gauges were partially buried in the sand beach and recorded the elevation of the saturated sand surface during those times when the sand was exposed between successive wave events.

Objectives of the swash measurements

The major objective of the swash measurements at the SUPERTANK Laboratory Data Collection Project was to provide data on both mean water level and wave transmission in the nearshore and swash regions. This infor-mation includes both spectral and statistical, or time-series, wave parameters at each gauge location. Data were analyzed in three ways: (a) the total water level as originally measured, (b) the low-frequency water level based on low-pass filtering of the total record, and (c) the high-frequency water level based on high-pass filtering of the total record. This data set supplements that ob-tained from the resistance wave gauges installed offshore and provides wave transformation information to near the runup limit.

---

[1]W itten by David L. Kriebel, U.S. Naval Academy.

Experiment Apparatus

Instrument description

A general configuration of the capacitance wave gauges is depicted in Figure 4-1. These gauges consisted of a single loop of Teflon-insulated, 20-gauge copper wire which was lightly twisted so that both ends of the wire were attached to one terminal at the base of a PVC electronics housing. The electronics housing was attached to a stainless steel support frame. A ground wire from the electronic circuitry was then attached directly to this frame to make ground contact with the water in the wave tank. The bottom of the sensing wire loop was attached to the support frame by a non-conductive rubber band. The purpose of this rubber band was to maintain a constant tension in the sensing wire while keeping the sensing wire parallel to the support frame at a fixed distance.

The capacitance wave gauges were installed vertically with each gauge partially buried in the sand as depicted in Figures 4-1 and 4-2. With this configuration, the initial zero elevation of each gauge was taken to be either: (a) the still-water level if the gauge was located seaward of the still-water shoreline where the sand bed was not exposed at the beginning of the run, or (b) the wet sand surface if the gauge was located landward of the still-water shoreline where the sand bed was exposed at the start of the run. Water surface elevations and wave heights were then measured relative to this initial reference datum.

Location

The locations of the capacitance wave gauges varied for each run and are listed in Table D1 in Appendix D. Gauges were usually placed on 3- or 6-ft (0.91- or 1.83-m) spacings in the inner surf zone and swash zone. The 10 gauges were numbered from A to J at the start of the experiment. In almost all tests, Gauge A was located approximately 1 ft (0.30 m) seaward of Station 5 at horizontal position x = 49.8 ft (15.18 m) in SUPERTANK coordinates (Chapter 1) and, thus, 11 ft (3.35 m) landward of the first resistance wave gauge. Starting from Gauge A and proceeding landward, Gauges B, C, D, E, and F were normally located at 6-ft (1.83-m) intervals, though this spacing changed frequently. Gauges G, H, I, and J were then used as "gauges of opportunity," either as spare gauges or to fill in between the other gauges to achieve a 2- or 3-ft (0.61- or 0.91-m) gauge spacing throughout the anticipated swash zone. As a result, gauge positioning did not follow alphabetical order.

A typical configuration of the gauges as used for the first three weeks of SUPERTANK is shown in Figure 4-2. Note, however, that this configuration changed frequently later in SUPERTANK, especially for the dune erosion
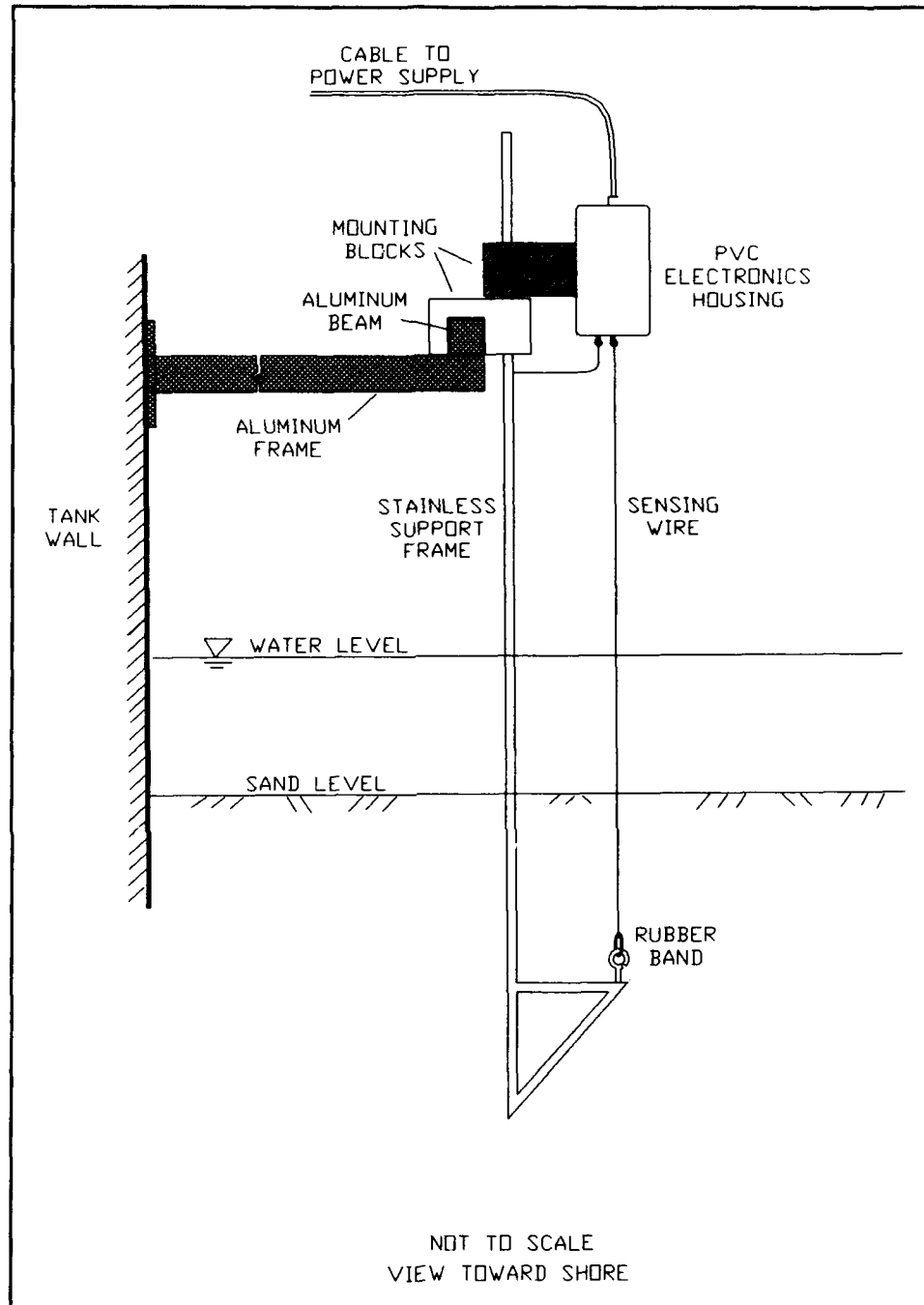
```
CABLE TO
POWER SUPPLY

MOUNTING
BLOCKS

                                    PVC
ALUMINUM                            ELECTRONICS
BEAM                                HOUSING

ALUMINUM
FRAME

TANK            STAINLESS           SENSING
WALL            SUPPORT             WIRE
                FRAME

    ▽ WATER LEVEL

    SAND LEVEL
    ///  \\  ///        //\      ///  \\  ///

                              RUBBER
                           ⊘  BAND

            NOT TO SCALE
        VIEW TOWARD SHORE
```

Figure 4-1. Schematic of capacitance wave gauge used in swash
measurements

tests. In most tests, Gauges A and B were located in water of sufficient depth
that the sand surface was never exposed. The other gauges were often located
near or landward of the still-water shoreline where the sand bed was exposed
intermittently. Some gauges were located near (or even above) the wave

76
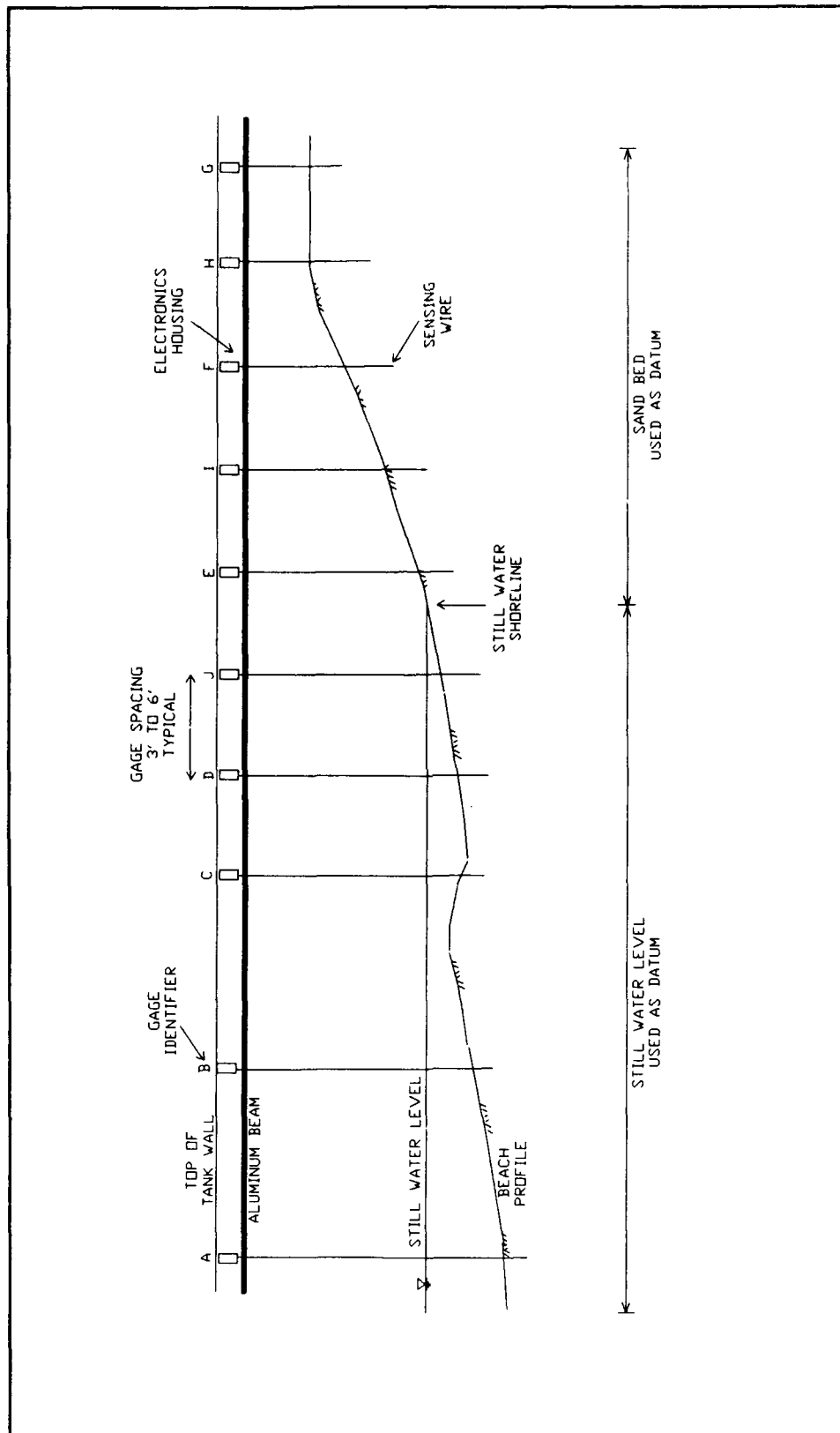
Figure 4-2. Wave gauge locations in inner surf zone and swash zone

Chapter 4 SUPERTANK Swash Measurements

runup limit and were seldom (or never) activated by wave action during a particular test.

Capacitance wave gauges were supported by an aluminum frame which was attached to the west wall of the wave tank. This frame consisted of canti-levered supports which extended 2 ft (0.61 m) out from the tank wall every 12 ft (3.66 m) at Stations 1 through 5. A 2-in. (5.1-cm) square aluminum box beam was then placed on top of these cantilevered supports parallel to the tank wall. This beam formed a continuous horizontal support for the wave gauges that extended from just landward of Station 1 to just seaward of Station 5. The centerline of this beam was located 1.94 ft (0.59 m) out from the west tank wall. The top of this aluminum beam formed a convenient reference datum for swash measurements and was located at an elevation of -0.63 ft (-0.19 m) below the top of the wave tank wall.

Instrument characteristics

Capacitance wave gauges were designed and constructed at the Coastal and Oceanographic Engineering Laboratory of the University of Florida. The gauge design has been used for many years in the ocean engineering laborato-ries at both the University of Florida and the University of Delaware. The gauges are reliable, in that they have a linear response over almost the entire length of the sensing wire and they maintain their calibrations over many days without changes due to temperature or other factors.

Output voltage from the gauges is proportional to the total capacitance of the system. This is composed of the capacitance of the wetted sensing wire, which is linearly proportional to the immersed length of the sensing wire, plus the internal capacitance in the gauge electronics, which is based on installation of three capacitors in series and in parallel with the sensing wire. During preliminary tests, sensing wires with lengths of 3 to 6 ft (0.91 to 1.83 m) were tested and internal capacitors were then selected to provide a desired gauge sensitivity for all sensing wire lengths.

The electronics housing of the wave gauges contained internal gain and offset potentiometers that were preset based on bench-testing of the wave gauges. The gauges were then connected to a power supply and signal condi-tioning unit. This unit contained a 40-Hz filter for each channel to remove high-frequency electrical noise from the signals. Each channel had separate gain and offset potentiometers located in the power supply and signal condi-tioning unit that were used to routinely adjust the sensitivity of the gauges and the zero of the signals.

Prior to deployment at SUPERTANK, all gauges were tested in the Hydro-mechanics Laboratory at the U.S. Naval Academy. This regimen involved static tests in which the gauge calibrations were checked over a period of up to 2 weeks to ensure absence of long-term gauge drift. Tests were then con-ducted in the Naval Academy large wave tank to evaluate the dynamic re-

78

sponse of the gauges in regular waves. The capacitance gauges were placed side by side in the wave tank with commercial resistance wire wave gauges of known reliability. In all cases, the capacitance gauges performed identically to the commercial resistance wave gauges in nonbreaking waves. The gauges were not tested in breaking waves where the foaming water surface with entrained air bubbles might affect the gauge response. Static calibrations were also performed at the Naval Academy in wet and saturated sand. It was confirmed that the gauges could record the wet sand/water surface if the sand was fully saturated. Some degradation of the response was found if the sand was not fully saturated.

Data collection and storage were performed on a personal computer (PC) that was separate from the main Oregon State University, O. H. Hinsdale Wave Research Laboratory (WRL) data collection system, the system used for the other hydrodynamic measurements. Lack of data channels on the main SUPERTANK data collection system prevented use of this common system for the swash data. The PC-based system used a MetraByte 12-bit, 16-channel Analog-to-Digital interface board. Data sampling was controlled using the LabTech Notebook data acquisition software package.

Experiment Procedures

Calibration

Capacitance wave gauges were calibrated once each week, but additional gauge calibrations were performed more frequently if a gauge was repositioned or if the length of the sensing wires was changed. Gauge calibration differed from that used for the resistance wave gauges because it was too time-consuming to frequently raise the channel water level high enough to ᴛ ivate the capacitance gauges that were near the runup limit. Instead, a separate calibration tank was built and placed outside the wave tank. The swash gauges could be removed from the wave channel and placed in the calibration tank without disconnecting the power supply or signal cables. To facilitate calibration, the stainless steel support rods that held the gauge electronics housing and sensing wire were pre-drilled with 1/8-in.- (3.2-mm-) diameter holes spaced every 2 in. (5.08 cm). This support rod could then be moved up and down in the calibration tank in 2-in. (5.08-cm) intervals over the entire length of the sensing wire. The gauges were found to be linear over almost the entire length of the sensing wire.

Calibration of the capacitance gauges was accomplished by adjusting the gain or sensitivity potentiometer of the power supply/signal conditioning unit to give an output of 0.1 V/in. (0.04 V/cm) change in water level. This value was adopted as a standard calibration value for all gauges. Based on the rated resolution of the data acquisition board, water surface measurements could in theory have been resolved to the nearest 1/400 of an inch (0.006 cm), although data storage was limited to the nearest 1/100 of an inch (0.025 cm).

By adopting a standard calibration for all gauges, data conversion from volts to engineering units of inches of water surface was performed during measurement, and data were stored in units of inches in the archived data files.

Initial depth and zero reference

Zero reference levels for the gauges were established in two ways during the SUPERTANK project. Initially, gauge zeros were selected during the gauge calibration at the midpoint of the sensing wire. Once installed in the channel, however, this zero point was often several inches above the actual still-water surface. As a result, this method was modified. In subsequent tests, gauges were calibrated, installed in the wave channel, and then the offset potentiometers were adjusted to give approximately zero volts output based on the initial sand bed or water surface elevation. For gauges placed seaward of the still-water shoreline, gauge zero reflects the approximate initial still-water level. For gauges placed landward of the shoreline on the beach face, gauge zero reflects the approximate initial saturated sand bed elevation.

Reference elevations for the capacitance gauges are therefore dependent on the local water depth or sand bed elevation at each gauge. At the start of each run, sand bed elevations were measured by holding a survey rod next to each gauge and reading the distance between the sand bed and the top of the aluminum box beam that ran the length of the measurement region. Since the top of this beam was at a known elevation of -0.63 ft (-0.19 m) below the top of the wave tank, sand bed elevations could be determined in the SUPERTANK coordinate system. Measurements were also taken of the still-water surface elevation and referenced to the top of the tank wall. From these measurements, the initial bed elevation was determined relative to the still-water level. These values are listed in Table D1, where positive values indicate that the sand bed was above the still-water level and negative values indicate the initial water depth at the gauge was below the water level datum.

Sampling and time reference

The PC-based data acquisition system, using the LabTech Notebook software package, sampled all 10 capacitance wave gauges at a 16-Hz rate, the same as that used by the WRL data collection system. Because of data storage limitations on the PC, data sampling run lengths varied throughout SUPERTANK. Normally, sampling lengths of 10 to 20 min were used to create data files that were small enough to store and transfer by diskette on the PC. Because of this procedure, runs of 40 or 70 min required two to four data collection runs and produced two to four data files. The typical sequence of events was to collect data for 20 min, save the data file, and then re-run the software to collect another data file. This resulted in some "downtime" between the end of one file and the beginning of another (typically 1 or 2 min).

80

The PC clock was continually updated to the same WWV time standard used by all SUPERTANK investigators. A problem in the data collection software, however, prevented the correct starting time from being recorded in the header of each data file. This problem was not detected during SUPERTANK and was found later upon inspection of the data. The data collection software requires two key strokes to start sampling data. Unfortunately, the software program recorded the start time based on the first keystroke, whereas data collection did not begin until the second keystroke. There was an elapsed time of several minutes to more than 1 hr between these keystrokes. As a result, all start times recorded for the swash data files are in error. The 10 capacitance gauges are properly sequenced in time from one to another; however, the capacitance gauges are not linked in time to other SUPERTANK gauges.

Data Analysis

Analysis methods

Analysis of the swash zone wave records was nearly identical to that performed on the other hydrodynamic data, as summarized in Chapter 3. Both frequency- and time-domain analyses were performed. Data were also filtered so that these analyses were performed on three signals: (a) the total water surface record (denoted "T"), (b) the low-frequency water surface record based on low-pass filtering of the data (denoted "L"), and (c) the high-frequency water surface based on high-pass filtering of the data (denoted "H"). The only major difference between the analysis of the swash data and the other hydrodynamic data involved the treatment of the sand bed if the bed was exposed during the wave record.

Identification of offset. As noted, the reference (zero) datum for each gauge is the initial water surface elevation for gauges seaward of the shoreline or the initial wetted sand surface for gauges landward of the initial shoreline. At the beginning of a run, the signal for each wave gauge was adjusted to give approximately zero volts output for this initial reference elevation. These initial "zero-voltage" readings were only approximate, however, and in practice each gauge had a small initial voltage offset. In the data analysis software, the signal for each gauge was averaged over the initial 200 data points, before waves arrived at the gauges, to determine the offset. This average offset was then subtracted from the entire wave record to rectify the signal to a reference datum.

Preprocessing. In preliminary testing of the capacitance gauges, it was found that high-frequency noise was introduced as a result of gauge interference. At a gauge spacing of 6 ft (1.83 m) this noise was almost undetectable. At a spacing of 3 ft (0.91 m), the noise was noticeable but of minimal importance and about the equivalent of 0.05 to 0.1 in. (0.13 to

0.25 cm) of water surface change. To reduce these noise levels, a 3.33-Hz, low-pass filter was applied to the wave records.

Identification of sand bed. The sand bed was exposed at some gauges in between the wave down-rush and the subsequent wave uprush. In the wave records, this exposure appears as a flat or clipped wave trough. For gauges located seaward of the still-water shoreline, these bed exposures were infrequent, unless the wave period was long so that there was little interference between the wave run-down and the next wave uprush. Landward of the shoreline, however, the bed was frequently exposed. Near the runup limit, the bed was often exposed more than it was submerged, as only a few waves reached the wave gauge.

For gauges with frequent bed exposures (gauges landward of the initial shoreline), the bed generally eroded or accreted during a test so that the elevations of the bed decreased or increased, respectively, over time. This produced large trends in the measured wave record. To remove these trends, an algorithm was developed to identify the sand bed during the exposures, to interpolate sand beds in between exposures (during the wave uprush), and then to remove the sand bed record from the original signal.

The sand bed surface was defined numerically as a minimum in the wave record for which the signal remained essentially constant (flat) for longer than 1 sec (16 data points). This was based on trial calculations in which it was found that flat strings of less than 1 sec were often actual water surface rather than the sand bed. Because of small variations and remaining noise in the signals, the bed was considered flat if elevations were within ± 0.05 in. (0.13 cm). This criterion was also verified by trial calculation.

Once sand bed exposures were identified, an approximate time series for the sand bed elevation was generated. For the duration of the bed exposure, from the end of one back-rush to the beginning of the next uprush, the average bed elevation was determined. Between bed exposures, as the next wave passed, bed elevations were linearly interpolated to connect one exposed bed level to the next. As a result, a bed elevation time series was generated at the same 16-Hz sampling rate used in the gauge measurements. This bed elevation record was then subtracted from the original signal (with offset also subtracted) to produce a time series of the water surface elevations with any trend due to erosion or accretion removed. It is noted, however, that the resulting signal may not be stationary, as, for example, the average wave height may increase over time if the sand bed eroded significantly.

Filtering. Once the sand bed signal was removed, the remaining water surface signal was filtered again to separate the signal into low- and high-frequency components. This procedure was identical to that performed on the other hydrodynamic data in which the filter cut-off frequency was selected as one-half of the peak wave frequency based on the target wave spectrum input into the wavemaker. Following this filtering, three time series were available for analysis: (a) the original (de-trended but unfiltered) total wave record,

82

(b) the low-frequency wave record containing wave group and tank seiching frequencies, and (c) the high-frequency wave record containing the wavemaker frequencies and higher harmonic components.

Spectral analysis. Spectral analysis of the three wave records followed the same procedures used for the other hydrodynamic data as described in Chapter 3. The only difference is that wave records obtained on the PC-based data acquisition system for the swash measurements are typically shorter than those obtained on the WRL system for the other wave gauges and current meters. For this reason, up to four individual data files, each containing 20 min of data, were sometimes required during a 40- or 70-min run. For spectral analysis, each shorter record was analyzed in blocks of 4,096 data points (256 sec) so that, for example, four blocks of data would be analyzed in a 20-min data file. Over the two to four data files required for a 40- to 70-min run, this provided 8 to 16 blocks of 4,096 data points for which individual wave spectra were calculated and then averaged to give the final result.

Spectral parameters determined from the block-averaged spectra are given in Equations 3-1 through 3-5 in Chapter 3 and are listed in Table D2 in Appendix D (contained in Volume II of this report). Two changes were made in the spectral analysis routines to compute the first and second spectral moments of the spectrum, m_1 and m_2. These were used to compute the mean wave period as $Tm_1 = m_0/m_1$ and the mean zero-crossing period as $Tm_2 = (m_0/m_2)^{1/2}$. These wave period parameters are reported in addition to the peak spectral period because they better describe the changes in the wave spectrum as waves propagate through the inner surf zone and into the swash zone. In many cases, the peak period varies suddenly and inconsistently from one gauge to the next. The mean period and the mean zero-crossing period, on the other hand, tend to vary in a systematic way from gauge to gauge.

Time series analysis. The time series analysis was also nearly identical to that performed on the other hydrodynamic data and equations describing the calculated parameters are given in Equations 3-9 through 3-15. Results of the time series analysis are given in Table D3 in Appendix D. The wave setup or the mean-water level of the record was first determined. Statistical parameters such as the standard deviation, skewness, and kurtosis of the water surface were then calculated using all of the data points in the wave record (excluding some points at the beginning and end of the records). Individual waves were then identified from a zero up-crossing analysis, and statistical parameters for wave height and period were determined.

Sample Data

Gauges located seaward of still-water shoreline

Typical results from a location seaward of the still-water shoreline are shown in Figures 4-3 and 4-4. The sample time series in Figure 4-3 is from Gauge A during Run A0509A. The incident wave conditions for this run were based on a narrow spectrum (γ = 20) with a peak period of 3 sec (peak frequency of 0.33 Hz) and a zero-moment wave height of 0.8 m near the wavemaker. Gauge A was located inside the surf zone approximately 3.7 m seaward of the still-water shoreline where the water depth was initially 0.37 m.

In Figure 4-3, the initial zero offset has been removed from the time series and every fourth data point has been plotted to show a smoothed version of the original wave record. In addition, the low-pass signal showing time-varying wave setup and setdown is plotted as a dashed curve. As shown in Figure 4-3, waves arrived at Gauge A about 40 sec after the start of data recording. Data recording was initiated at the same time that wavemaker commands were initiated by the host computer. The 40-sec delay in waves reaching the wave gauge is then due to two factors: (a) a time delay between the initiation of these wavemaker commands and the start of the wavemaker motion, and (b) the propagation time of waves travelling from the wavemaker to the wave gauge.

The wave record in Figure 4-3 is fairly typical of gauges that were located inside the surf zone but seaward of the shoreline where the sand bed was never exposed during the wave run. Almost all waves are breaking or broken as they pass this gauge and individual waves exhibit the characteristic "saw-tooth" shape of shallow-water waves in the inner surf zone. The incident waves were highly grouped in this example and some evidence of the wave group structure is shown in Figure 4-3, both from the individual (high-frequency) waves and from the low-pass signal. The low-frequency signal may be interpreted as a record of the dynamic wave setup and setdown that, relative to the high-frequency waves, represents a slowly varying mean water level. By averaging the low-frequency signal, the mean wave set-up averaged over the entire data run was determined to be 4.5 cm at Gauge A.

In Figure 4-4, the smoothed (block-averaged) wave spectra are shown for the total water surface signal, the low-pass signal, and the high-pass signal, respectively. Dominant wave energy is concentrated around the intended peak frequency of the incident spectrum near 0.33 Hz, but significant low-frequency energy is also found. Higher harmonics are evident at about two and three times the peak frequency. In this case, the zero-moment height from the high-frequency signal dominates and is about 0.39 m, whereas the low-frequency zero-moment height is about 0.22 m.
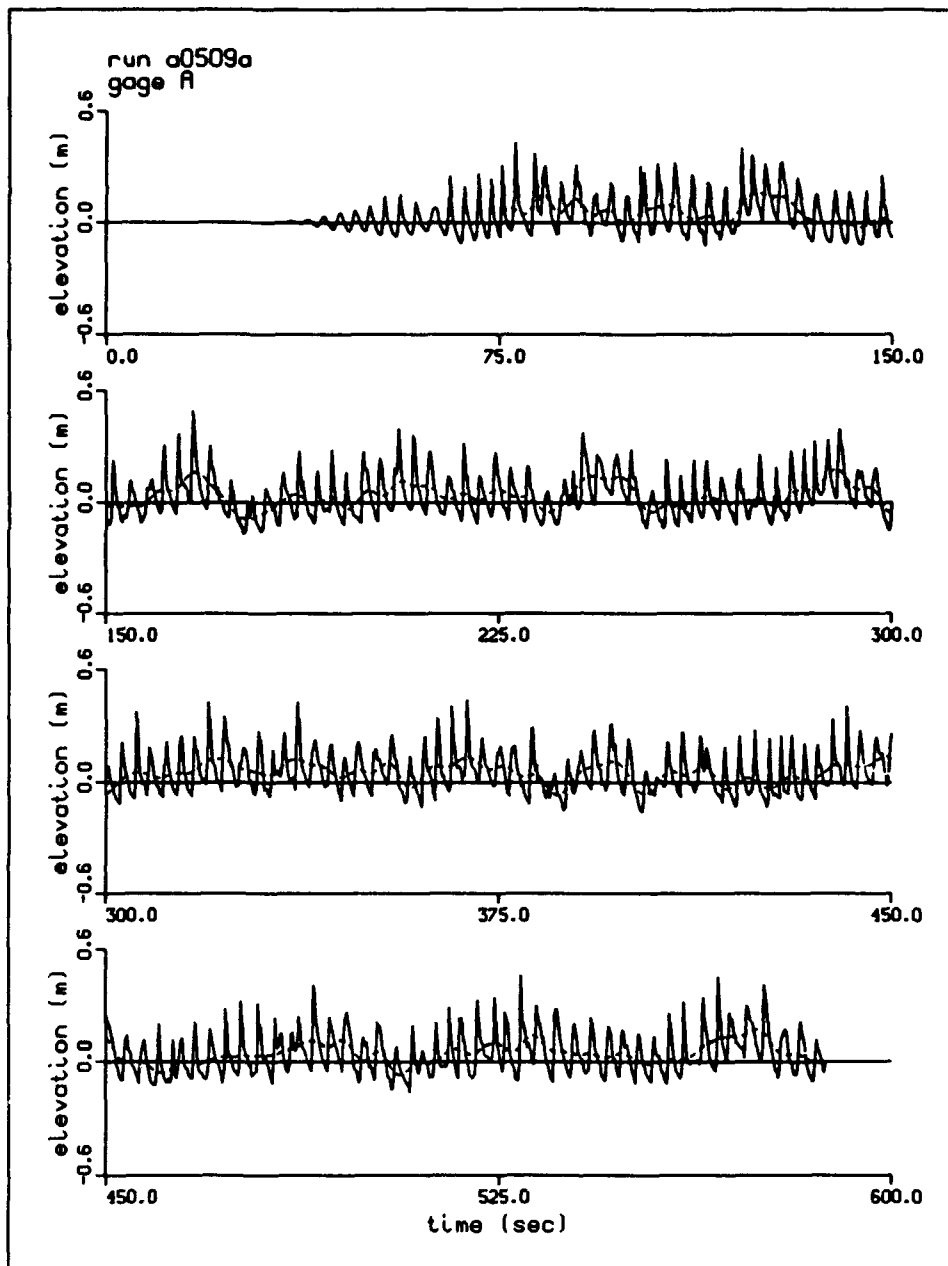
84

Figure 4-3. Sample of raw and low-pass signals from Gauge A,
Run A0509A

Gauges located landward of still-water shoreline

Typical results from a gauge located landward of the still-water shoreline are shown in Figures 4-5 and 4-6. In Figure 4-5, a sample time series is shown from Gauge I during Run A0509A. The incident wave conditions again consisted of a narrow spectrum ($\gamma = 20$) with a peak period of 3 sec and a zero-moment wave height of 0.8 m at the wavemaker. Gauge I was
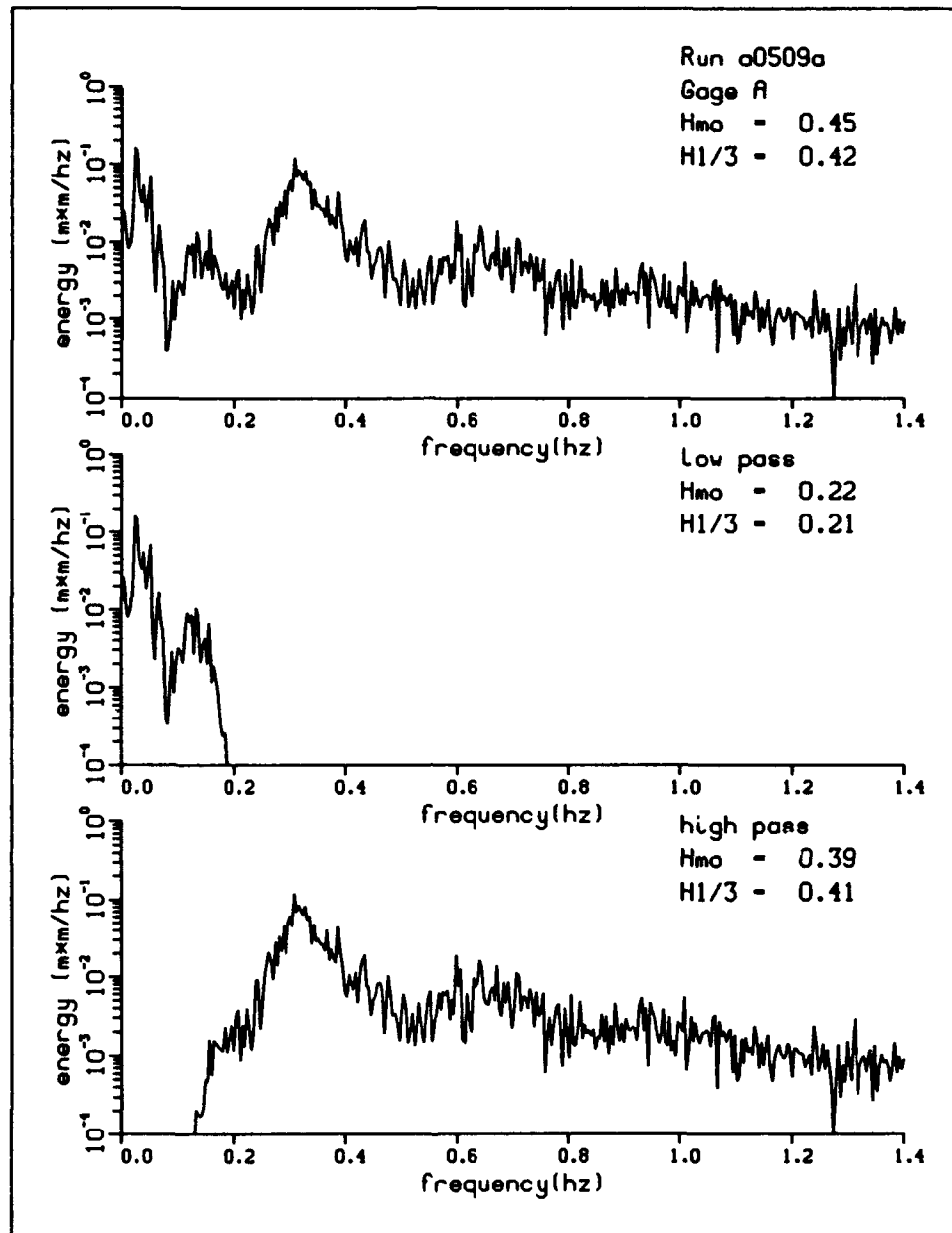
Figure 4-4. Smoothed wave spectra from Gauge A, Run A0509A

located approximately 2.7 m landward of the still-water shoreline, about mid-way up the beach face between the still-water shoreline and the runup limit. The maximum runup, the runup limit, reached an elevation of about 0.3 m above the still-water level in this case.

Figure 4-5 shows the wave record after the initial voltage offset has been removed. Once again, the original wave record has been smoothed by plotting only every fourth data point. The low-frequency signal, based on
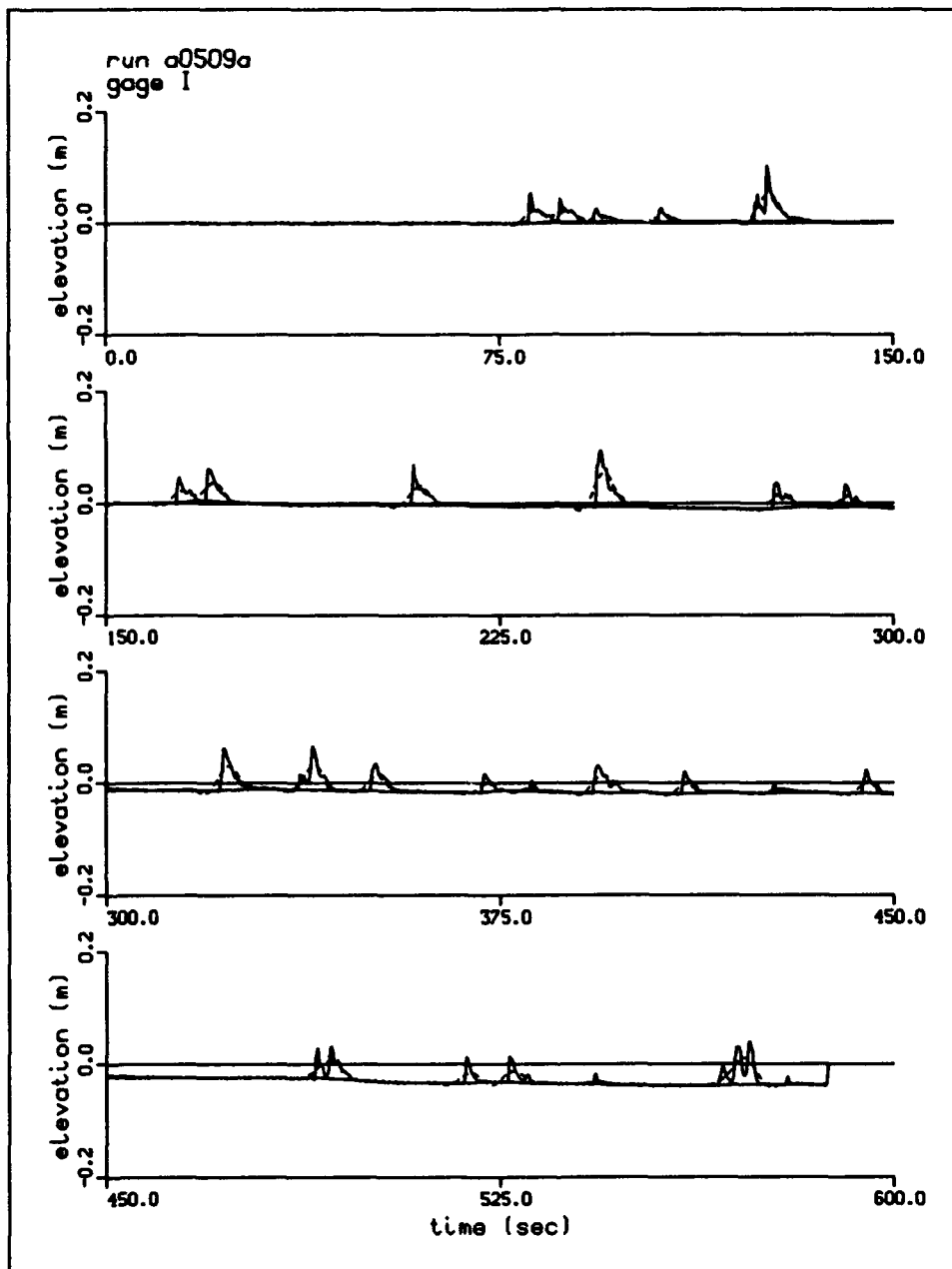
Figure 4-5. Sample of raw and low-pass signals from Gauge I, Run A0509A

application of the low-pass filter with a cutoff frequency of one-half the peak frequency of the incident spectrum, is again shown as the dashed curve. In addition, Figure 4-5 also shows the sand bed signal as identified by the algorithm described in the previous sections. In this case, the downward trend in the signal indicates that the sand bed is eroding over time. After 9 min of wave action, the sand surface eroded 3.4 cm in this case. After a second 9-min data sample (not shown), with some intervening downtime while data
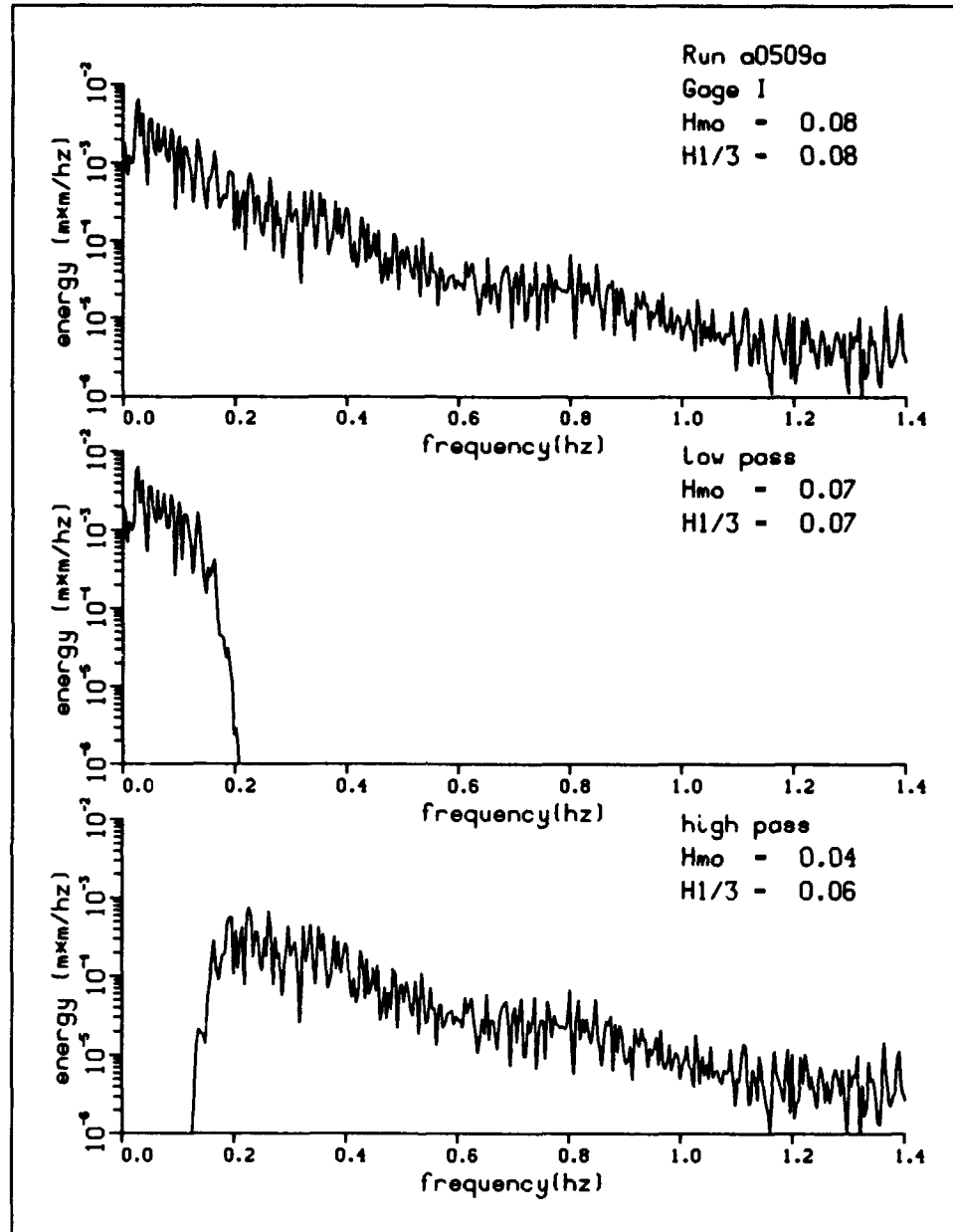
Figure 4-6. Smoothed wave spectra from Gauge I, Run A0509A

files were transferred, the bed eroded 10.0 cm, and, at the end of the wave run, the sand bed eroded 13.5 cm at this location.

The wave record in Figure 4-5 is fairly typical of gauges that were located landward of the still-water shoreline. As shown in Figure 4-5, the first swash event to reach Gauge I occurred after about 77 sec of data recording. Swash events occur intermittently and depend on the group structure of the incident high- and low-frequency waves. Comparison of Figure 4-5 with Figure 4-3 indicates that the first swash event corresponds to the first large wave group

(the first large waves with an elevated wave setup) recorded at Gauge A, with a phase lag related to the 6.4-m spacing between Gauges A and I. Other large swash events may also be traced to the occurrence of elevated mean water levels (maximum dynamic wave setup) and large incident waves at Gauge A. These wave records also show the apparent downshifting in wave frequency as 187 waves pass Gauge A whereas only 25 waves pass Gauge I in the same length of time.

In Figure 4-6, the smoothed wave spectra are shown for Gauge I for the total signal, the low-pass signal, and the high-pass signal, respectively. The energy content in this case is concentrated at low frequencies due to the long period of time between successive swash events. It is, in fact, difficult to discern the intended peak wave frequency in the wave spectra. Further evidence of the domination of low-frequency components is found in the energy-based significant wave height. The zero-moment wave height for the total wave record is 0.08 m in this case. If separated into components, however, the low-frequency wave height dominates and is 0.07 m, whereas the remaining high-frequency signal has a zero-moment height of 0.04 m.

Summary of data characteristics

Figure 4-7 shows a summary of mean water level and selected wave parameters for Run A0509A for all 10 swash gauges. The initial beach profile is also shown for reference with elevations defined relative to the still-water-level datum. As shown in Figure 4-7a, mean water levels (mean wave setup averaged over the length of the data run) increase in the shoreward direction from Gauge A to Gauge C (located at the still-water shoreline) where the setup is maximum and equal to 9.9 cm. Shoreward of Gauge C at Gauge I, the mean setup is 0.7 cm, while at Gauge E (next gauge landward from Gauge I) the setup is 0.3 cm.

Wave transformation across the profile is indicated by both the zero-moment wave height and the maximum wave height. The zero-moment wave height diminishes from 0.45 m at Gauge A to 0.30 m at Gauge C (still-water shoreline). Landward of Gauge C, the zero-moment wave height decays by one order of magnitude to 3.0 cm at Gauge E (next gauge landward from Gauge I) and then decays less dramatically to less than 1 cm at Gauge G (landwardmost gauge). The maximum wave height follows a similar decay across the inner surf zone and swash zone. It may be observed, however, that the maximum wave height does not decrease systematically but actually increases slightly just landward of Gauge C. The reason for this variation is the presence of reflected waves moving seaward from the upper limit of the swash and colliding with incoming waves in this region.

In Figure 4-7b, the zero-moment wave height is further decomposed into low- and high-frequency components based on the low- and high-pass filtering described earlier. It may be seen that the high-frequency wave component dominates in the surf zone, but, landward of the still-water shoreline, the low-
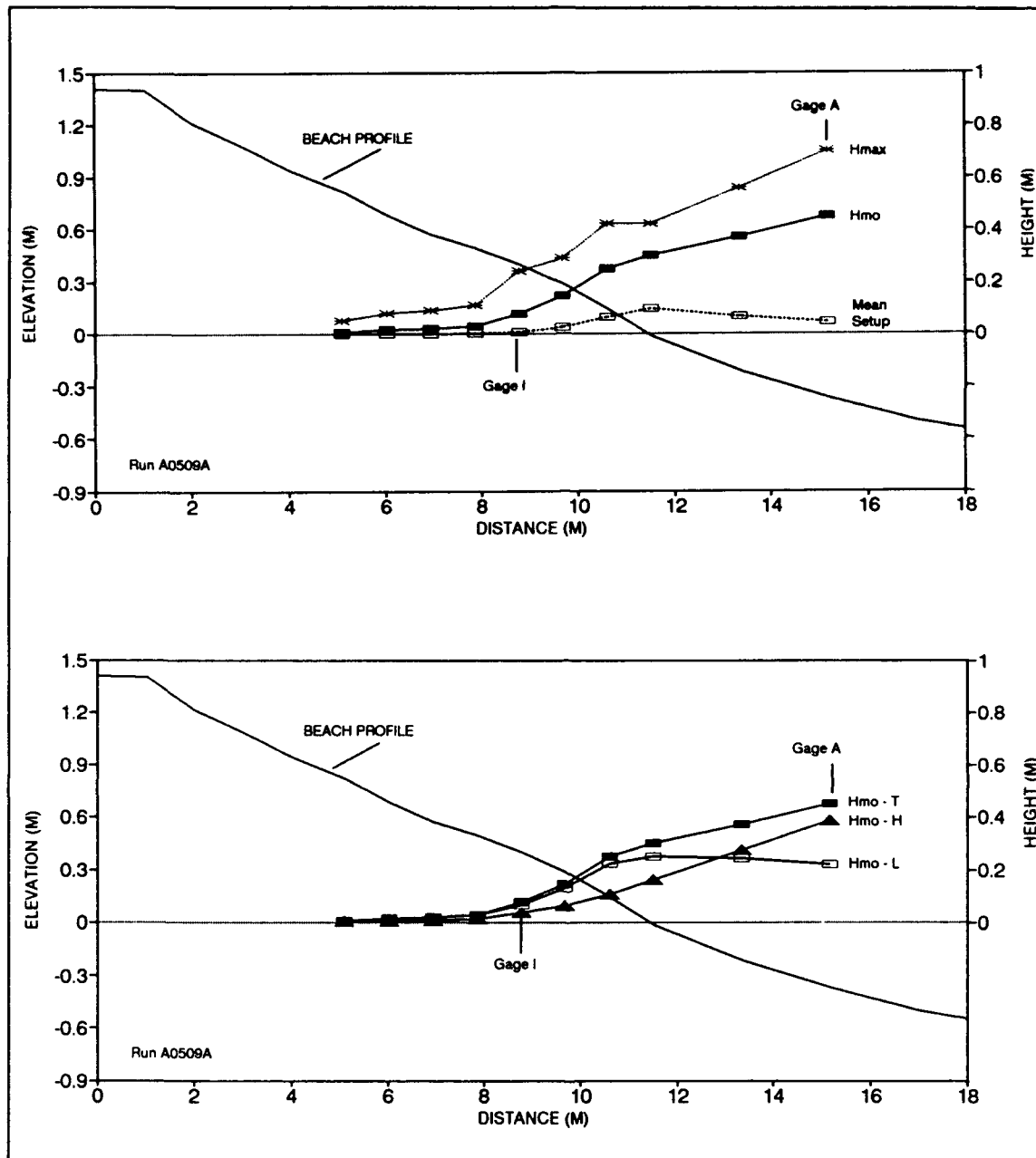
Figure 4-7. Summary of mean water level and selected wave parameters across inner surf zone and swash zone for Run A0509A

frequency component dominates. The low-frequency component increases in magnitude to a maximum value at the initial shoreline and exhibits a spatial variation similar to that of the mean wave setup in Figure 4-7a. The high-frequency wave component, in contrast, decays continually from the surf zone to the runup limit.

90

Summary

Swash measurements made at the SUPERTANK project are summarized in Appendix D, contained in Volume II of this report. These include tabulations of water level and wave parameters calculated by both spectral and statistical analysis methods. These data complement other water level and wave data reported in Chapter 3 and Appendix C, which is also contained in Volume II of this report. Swash measurements included sand bed elevation measurements when the sand bed was exposed between successive swash events. Because of the extensive beach profile measurements described in Chapter 2 and tabulated in Appendix B, however, these sand bed measurements are not included in this report.

Acknowledgements

5 Tracer Measurements of Sand Dispersion During SUPERTANK[1]

Introduction

Background

There have been considerable advances in recent years in our understanding of sediment transpor* processes in the nearshore and in our ability to predict transport rates under a given set of wave conditions. However, many unknowns remain, in part resulting from the diversity of measurement techniques and uncertainties as to how they are related. On the one hand, most data for comparing longshore sand transport rates on beaches to the causative waves and nearshore currents have come from sand-tracer measurements, which permit one to follow immense numbers of grains in an integrated fashion. Examples of the use of fluorescent sand tracers to measure longshore sediment transport rates on beaches are provided by the studies of Komar and Inman (1970), Knoth and Nummedal (1977), and Kraus et al. (1982). A recent review of the technique and the collected field data is given by Komar (1990). The tracer technique measures the total sediment transport rate, bed load, and suspended load, because all grain sizes represented in the sand are tagged in their natural proportions.

Sand tracers have also been employed to follow cross-shore sand movements and grain sorting across the beach profile (e.g., Ingle 1966), as well as to reveal sediment transport patterns in a qualitative manner in complex engineering situations (e.g., Sasaki and Sakuramoto 1984). At the same time, measurements have been made by a number of investigators using arrays of optical backscatter sensors (OBS) to determine suspended-sediment concentrations, which, when combined with measurements of currents obtained by electromagnetic current meters, yield assessments of the net suspended sedi-

---

[1] Written by Paul D. Komar, Oregon State University.

ment flux. Published results of such analyses include Sternberg, Shi, and Downing (1984) and Beach and Sternberg (1987). Chapters 6 and 7 of this report document the OBS approach and measurements undertaken during the SUPERTANK Laboratory Data Collection Project.

There is a similar dichotomy of sediment transport measurements in the offshore, that is seaward of the surf zone but at depths shallow enough for active sediment movement by waves. Examples of the use of sand tracers in this offshore zone include the field studies of Inman and Chamberlain (1959) and Murray (1967), and the combined field and laboratory wave-channel investigation of Miller and Komar (1979). In this offshore zone the sediment movements are produced by the oscillatory wave-orbital motions over a bed covered by ripples, and the sediment is placed in suspension by the vortices that develop adjacent to the ripples and is periodically ejected above the bed. A net advection of this suspended sediment can be produced by unidirectional currents superimposed on the oscillatory wave motions or by asymmetries in the onshore versus offshore components of the wave orbits.

Sand tracers and OBS measurements provide somewhat different views of the sediment transport processes as well as measurements of quantities of sediment movement. Although direct comparisons need to be made between the measured quantities of sediment transport from these two techniques, such simple comparisons are not entirely valid and not particularly informative. A more enlightened approach is to recognize that the two techniques compliment one another in providing fuller documentation of sediment-transport processes, and that simultaneous measurements using both sand tracers and arrays of OBS will yield more complete understanding of sediment movements. It was with this view that fluorescent sand tracers were used during SUPERTANK to investigate the movement of sand in both the offshore and within the surf zone. The results of the experiments document the dispersion of large numbers of sand grains, results that could be important to the development of models for the movement of nearshore sediments.

Objectives of sand tracer measurements

The objective of this component of SUPERTANK was to obtain measurements of sand-tracer dispersal patterns in both the offshore and within the surf zone, patterns that can be analyzed to determine cross-shore (along-channel) rates of sand advection and diffusion. Some experiments were designed specifically to document the movement of sand between the bars and the beach berm as part of measured profile response to changing wave conditions. These latter experiments were primarily intended to provide qualitative information, to be evaluated both by visually observing the tracer movement, for example, as seen during overwash, and by tracer counting.

The offshore sand-tracer experiments undertaken during SUPERTANK compliment and extend those made by Miller and Komar (1979) in the same wave channel located at the O. H. Hinsdale Wave Research Laboratory at Oregon State University (OSU). That earlier study was limited to monochromatic waves with periods of 3, 4, and 5 sec, and offshore wave heights in the range of 15.9 to 37.6 cm. In addition to providing new data with monochromatic waves, some SUPERTANK tracer experiments were undertaken with random waves. Furthermore, the wave energy levels were considerably higher than in the study of Miller and Komar (1979). That earlier study yielded only measurements of sand diffusion under different wave conditions, as there were no significant displacements of tracer that could be interpreted to represent net advection. The rates of diffusion, the "mass spreading coefficients" (Miller and Komar 1979), were quantitatively related to an assessment of the rate of entrainment based on the wave orbital motions following the approach of Madsen and Grant (1976) and to a random-walk model of grain movement that yielded a relationship to d_o^2/T, where d_o is near-bottom wave orbital diameter, and T is wave period. There was some uncertainty as to the correspondence between the wave-channel data with monochromatic waves versus two measurements obtained under higher-energy field conditions. The scope of the offshore SUPERTANK sand-tracer measurements is such that analyses of the data may resolve questions as to how to relate data on sand movements obtained with monochromatic waves to that obtained under random waves, as well as providing quality data at higher wave-energy levels.

The surf zone tracer experiments were conducted to provide information for supplementing the beach profile survey measurements (see Chapter 2). These qualitative tracer experiments were designed to address such questions as where material originates that forms the break-point bar and how the over-wash process takes place.

Experiment Technique

The development of a sand tracer involves tagging the natural sediment with a coating of fluorescent dye that does not alter the hydrodynamic properties of the grains or the overall distribution of sizes as found in the environment to be studied. Teleki (1966), Yasso (1966), and Ingle (1966) provide summaries of the techniques involved in tagging the sand, but the approaches are complex and messy, especially for large samples. The tracers employed at SUPERTANK were dyed professionally by the Great American Color Company in Los Angeles. Large splits of the natural quartz-feldspar sand used at SUPERTANK were trucked to Los Angeles for coating with fluorescent dye. Separate quantities of sand were dyed with five colors: red, green, blue, yellow, and maroon. Availability of several colors was important so they could be used successively and distinguished from tracer introduced in previ-

ous runs. In tracer experiments performed within the surf zone, multiple injections were used with different colors injected into the beach face versus, for example, the offshore bar.

Experiment procedure

In the offshore experiments, the tracer sand was injected in a narrow line across the width of the wave channel. This was accomplished by a diver using SCUBA gear so that the tracer emplacement would be in the prescribed position and would have an even distribution across the channel width. Just prior to injection, a large sample of the bottom sediment was collected to determine the quantity of "background" tracer that might remain from earlier experiments. In the experiments within the surf zone, the injection was made on a line across the channel or sometimes at a point on the midline of the channel, generally on the beach face or over the offshore bar. This was accomplished by wading. In all cases the injection operation was completed during still-water conditions prior to wave generation. The tracer was placed in plastic bags so that it could be pre-wetted prior to injection, and a small quantity of liquid dish soap was added to reduce grain surface tension which can cause the particles to float to the water surface or to adhere to one another in clumps.

After an interval of wave generation and sand movement, the wave generator was turned off and samples were obtained on a grid along the length of the midline of the wave channel. This procedure ensured that all samples would be synoptic with respect to the sand dispersion processes. In the offshore experiments, a SCUBA-equipped diver systematically sampled the bed (Figure 5-1). The diver was guided by a weighted line, to which sample vials were attached, that was lowered to the beach profile (Figures 5-2 and 5-3). The vials were labeled to identify the sample-grid locations. The grid varied somewhat between experiments and within the series of sample runs in each experiment, governed by the energy of the waves and the expected tracer dispersal distances. In general, the grid samples were obtained at 0.5-m increments close to the injection line ($\pm$ 3 m from the injection line) and spaced at 1-m increments at greater distances. All samples were taken by the same person, who attempted to sample consistently to a depth of 1 cm into the bed. The inshore samples were obtained on a grid marked along the wall of the wave channel. In the inshore, sampling was accomplished by wading.

Five offshore sand-tracer experiments were completed. Table 5-1 summarizes the dates of the offshore experiments, including the colors and quantities of tracer used and the sampling times. The Δt-values given in Table 5-1 are time intervals after injection for the first sample run and the time intervals between subsequent sample runs. Ideally, each experiment would consist of at least three to four sample runs so that dispersion of the tracer with time could be documented. This was accomplished in four of the five experiments, but the fifth (28 August) offshore tracer experiment was terminated after two sam-

Figure 5-1. SCUBA-equipped diver with bag holding tracer samples

ple runs when there was an abrupt change in the wave parameters required by other SUPERTANK participants.

The surf zone tracer experiments are summarized in Table 5-2. Tracer injected on the subaqueous portion of the profile, such as on the berm, was observed visually. Qualitative descriptions of tracer movement from the visual observation are not discussed further here.

All sand samples from the tracer experiments were air-dried and inspected for tracer content using an ultraviolet light in a dark room. Samples containing a large amount of tracer were reduced with a sample splitter to render counting of tagged grains a manageable task. Weighed samples or splits were spread to one-grain thickness on a flat-black surface for counting. This procedure yields the number of tracer grains in the measured weight of the sample, which can then be used to calculate the concentration in terms of tracer grains per gram of sample, to place all samples on the same basis for comparisons.

Data Analysis

Tracer concentrations for the offshore sample runs are listed in Table 5-3. Station numbers refer to local grid position with respect to the injection line (0.0), with positive and negative numbers respectively signifying offshore and onshore directions. Magnitudes of the station numbers denote distance in me-

Figure 5-2. Weighted tracer sampling line with vials attached at fixed
intervals

ters from the injection position. As presented in Table 5-3, the data immedi-
ately provide an impression of the dispersion of the sand tracer during the
experiments. It is apparent that generally during an experiment there is a
progressive decrease in tracer concentration at the injection line, with a corre-
sponding increase at grid-sample locations away from the injection site. This
decrease in concentration is produced by the progressive diffusion of the
tracer, presumably as it is lifted above the bed within suspension vortices shed
from ripples and subsequently drifts along the length of the wave channel.
The measured concentrations in Table 5-3 also reveal that, in most experi-
ments, there is an asymmetry in the concentrations about the injection line.
Generally more tracer was carried onshore than offshore, probably represent-
ing a net tracer advection, although an along-channel variation in the rate of
diffusion cannot be ruled out.

Figure 5-4 shows examples of histograms for representative sample runs of
the data listed in Table 5-3. The histogram for 7 August, Run 13A, plots the
tracer distribution after 100 min of wave action following tracer injection.

Figure 5-3. Tracer sampling line being lowered into the channel

Table 5-1
Offshore Sand Tracer Experiments during SUPERTANK

Date	Color	Weight lb (kg)	Run	Sampling Interval Δt, min
7 Aug	green	21 (9.5)	10A 11A 13A	20 40 40
8 Aug	red	35 (15.9)	13A 14A 15A 16A	20 20 20 20
14 Aug	green	33 (15.0)	08A 09A 10A 11A	20 20 20 70
28 Aug	red	27.5 (12.5)	10A 11A	20 20
5 Sep	green	32 (14.5)	13A 14A 15A	20 20 20

Table 5-2
Foreshore and Surf Zone Sand Tracer Experiments During SUPERTANK

Date	Color	Weight lb (kg)	Run	Location of Injection by Color
5 Aug	Green Red Blue	1.0 (0.45) 1.0 1.0	09A	Station 3.5 Station 3.9 Station 4.4
5 Aug	Green Red Blue	1.0 (0.45) 1.0 1.0	10A	Station 8 (bar trough) Station 10 (on bar) Station 12 (offshore)
8 Aug	Blue Orange	10.0 (4.5) 10.0	12A	Seaward end of berm Shoreward end of berm
26 Aug	Blue Orange	4.7 (2.1) 4.7	12B 17B	In front of seawall In front of seawall
28 Aug	Blue	8.5 (3.9)	09B	Station 0 + 9 (on berm)
28 Aug	Red Blue	2.0 (0.9) 2.0	16B	Top of foredune Shoreward toe of foredune

This distribution is typical in showing an onshore movement of tracer, with the maximum concentration displaced toward the beach 0.5 to 1 m from the injection position. The distribution is strongly asymmetrical, with higher concentrations onshore of the maximum concentration, as compared with offshore positions. The asymmetry suggests a non-uniformity in the rate of diffusion along the length of the wave channel, as well as the injected tracer acting as a quasi-continuous source rather than being an "instantaneous" injection (quasi-continuous source behavior was also found by Miller and Komar (1979)).

The patterns of measured concentrations seen in the histograms of Figure 5-4 show that the variations are not smooth and systematic, but instead "jump," with adjacent grid samples yielding significantly different concentrations. In future analyses of the measurements, it will likely be necessary to smooth the results or to match analytical grain-dispersion equations to yield minimum-error fits to the data. The cause of the concentration variability is uncertain. One possibility is that it represents sampling effects, with perhaps some vials having reached into the bed and sampled sediments having lower concentrations. Another possibility is that the concentration variability reflects the irregular bottom topography with areas of scour and fill. While undertaking sampling operations, the diver noted that during most experiments there was large-scale waviness in the bed and localized scour holes, as well as small-scale vortex ripples. In view of this three-dimensionality of the observed bottom topography, such as shown in Figure 5-5, the author's mea-

surements and analyses of the two-dimensional dispersion of tracer along the length of the wave channel may be overly simplistic.

Table 5-3
Tracer Counts in Grains/Gram for the Offshore Experiments

Sta-tion	A0710A	A0711A	A0713A	A0813A	A0814A	A0815A	A0816A	A1408A
7.0	0.802	0.020	0.159	0	0	0	0	1.41
6.0	0.889 0.258	0.318	0.116	0	0	0.107	0	0.735
5.0	0.079	0.877	0.962	0	0	0.246	1.01	0.412
4.0	0.449	10.6	8.43	0	0	0.259	0.246	1.07
3.0	13.8	24.1	6.72	0	0.517	27.3	3.43	5.11
2.0	9.51	12.3	16.4	0.106	0.519	264.0	6.81	18.3
1.5	39.0	179.0	35.3	16.7	534.0	1.28×10^3	145.0	26.7
1.0	16.6	146.0	91.4	228.0	1.33×10^3	2.48×10^3	575.0	524.0
0.5	378.0	13.4	175.0	534.0	2.72×10^3	1.92×10^3	148.0	4.00×10^3
0.0	1.40×10^4	951.0	230.0	2.25×10^4	2.54×10^3	3.70×10^3	497.0	2.96×10^4
-0.5	1.05×10^3	562.0	2.06×10^3	2.03×10^3	144.0	1.02×10^3	149.0	1.75×10^3
-1.0	728.0	735.0	2.04×10^3	329.0	933.0	1.92×10^3	0.420	241.0
-1.5	360.0	506.0	652.0	1.41×10^2	2.12×10^3	650.0	253.0	98.6
-2.0	1.91×10^3	976.0	1.62×10^3	54.1	141.0	446.0	336.0	50.0
-3.0	181.0	536.0	656.0	11.0	305.0	137.0	1.96	80.6
-4.0	133.0	490.0	317.0	1.33	61.1	34.4	8.84	60.4
-5.0	14.7	192.0	650.0	0.418	2.82	2.87	0.518	67.5
-6.0	13.3	87.1	709.0	0	0.500	2.75	14.9	55.0
-7.0	1.40	122.0	322.0	0.088	1.04	1.02	12.0	65.7
-8.0					2.66	0.923	1.83	61.0
-9.0					0	4.30	2.46	26.0

(Continued)

Table 5-3 (Concluded)								
Stat-ion	A1409A	A1410A	A1411A	A2810A	A2811A	S0513A	S0514A	S0515A
7.0	0.733	1.09	1.52	0.219	0.702	0.186		0.333
6.0	1.31	1.28	2.29	0.739	1.60		0.325	0.165
5.0	1.77	2.10	9.28	2.12	0.765	0.518	0.348	0.195
4.0	1.33	8.56	5.13	1.74	0.666	0.417	0.344	0.913
3.0	10.7	24.4	15.2	3.62	0.823	3.25	1.92	0.832
2.0	31.9	203.0	56.3	10.9	24.0	1.25	1.60	3.35
1.5	238.0	641.0	157.0	39.7	43.0	2.79	1.44	
1.0	1.04×10^3	3.46×10^3	591.0	97.9	364.0	13.2	4.52	11.9
0.5	7.40×10^3	2.84×10^4	4.09×10^3	6.19×10^3	2.46×10^3	82.4	42.4	
0.0	2.35×10^4	3.99×10^3	2.49×10^3	1.84×10^3	1.96×10^3	2.25×10^3	247.0	
-0.5	6.80×10^3	3.10×10^3	1.18×10^3	844.0	6.78×10^3	6.07×10^3	2.90×10^3	
-1.0	2.44×10^3	1.43×10^3	5.03×10^3	610.0	774.0	3.77×10^3	3.61×10^3	1.28×10^3
-1.5	298.0	349.0	2.39×10^3	322.0	342.0	1.35×10^3	2.40×10^3	
-2.0	71.4	174.0	654.0	117.0	154.0	688.0	1.78×10^3	2.60×10^3
-3.0	62.3	60.1	520.0	102.0	79.4	149.0	563.0	1.62×10^3
-4.0	46.9	57.0	117.0	99.5	90.7	33.4	142.0	899.0
-5.0	59.1	44.5	66.3	63.6	75.0	22.1	26.7	496.0
-6.0	67.6	57.4	56.9	63.1	62.5	19.0	26.1	146.0
-7.0	68.2	63.9	65.2	73.7	57.2	22.9	31.9	91.5
-8.0	57.8	48.5	53.4	41.9	54.5	28.9	44.3	53.9
-9.0	3.64	26.7	25.7	42.4	35.2	33.9	39.3	40.0
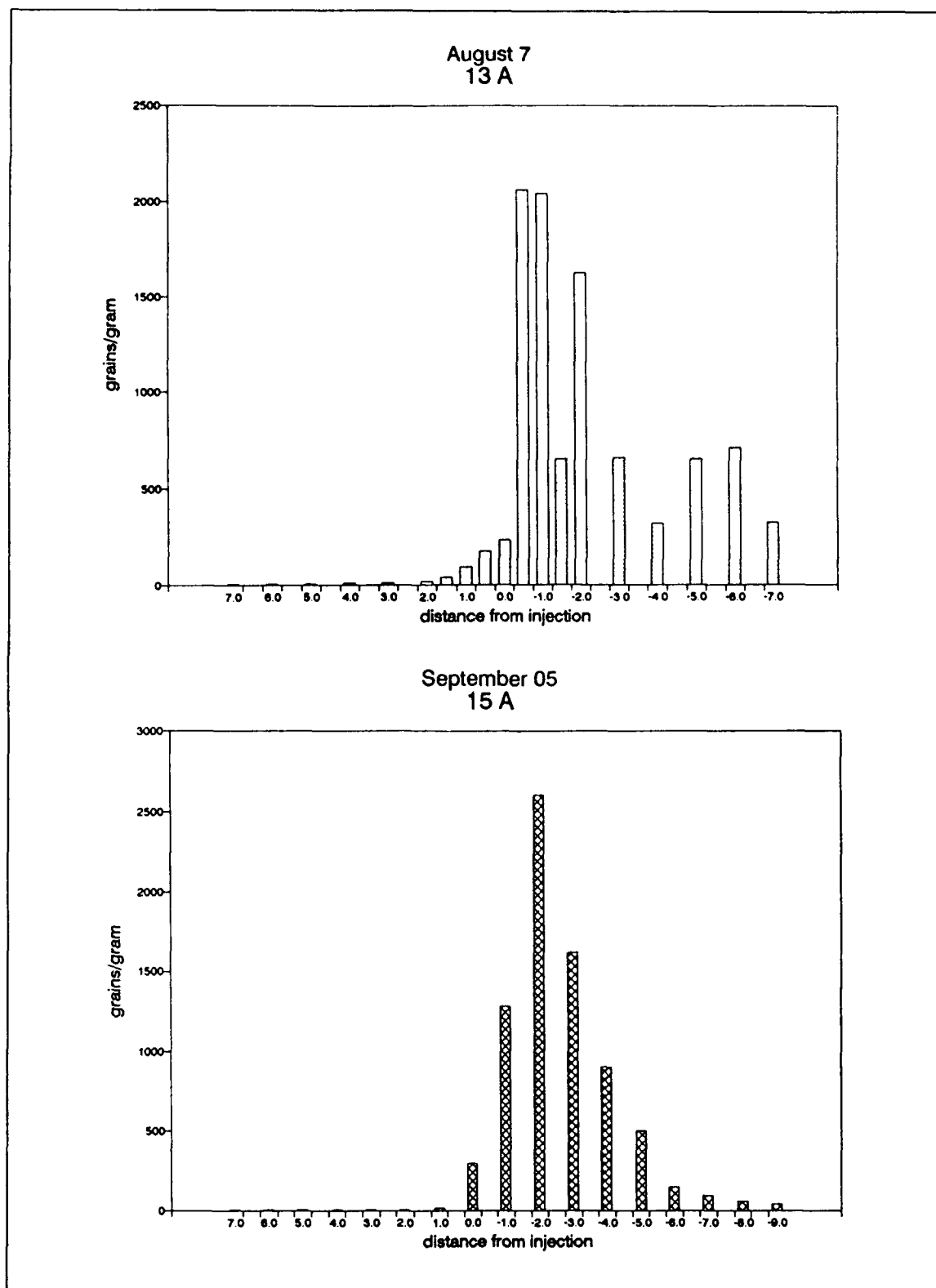
Figure 5-4. Example tracer concentration histograms
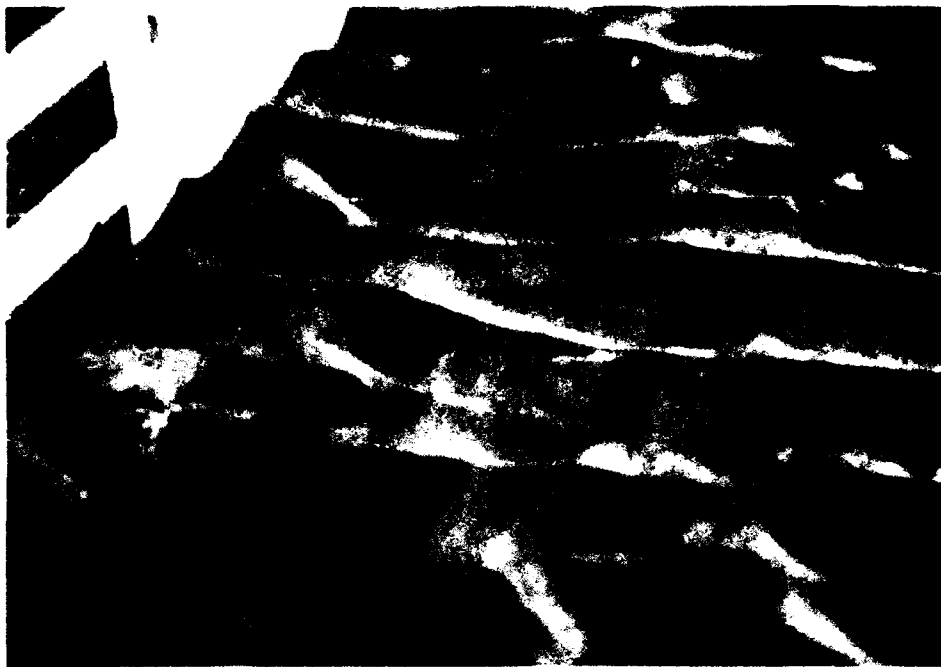
Figure 5-5. Example of offshore bottom with irregular ripples

Summary

Fluorescent sand tracers were used during SUPERTANK to measure sand
dispersion (advection and diffusion) seaward of the breaker zone. Additional
experiments were conducted within the surf zone to document the exchange of
sand between the beach face and sandbars.

Five offshore experiments were completed, including sixteen sampling runs
encompassing a wide range of wave conditions. For the most part, the results
show the expected diffusion of tracer with time, and often an apparent net
onshore advection. Future analyses will be undertaken to calculate average
diffusion and advection rates for the experiments, with a comparison of the
results to the wave parameters and direct measurements of suspended sediment
concentrations. The analyses will expand the range of results reported in the
comparable study by Miller and Komar (1979), in that the SUPERTANK data
extend to significantly greater wave-energy levels and include measurements
under random as well as monochromatic waves. More sophisticated analyses
of the offshore sand-tracer dispersion measurements obtained during
SUPERTANK could involve the development of a sand dispersion model
which utilizes the OBS measurements of the temporal and spatial variation in
sediment concentrations, models that would yield a greatly improved under-
standing of the processes and patterns of sediment transport under waves.

Acknowledgements

References

Beach, R. A., and Sternberg, R. W. (1987). "The influence of infragravity motions on suspended sediment transport in the inner surf zone." *Proc. Coastal Sediments '87*. ASCE, New York, 913-28.

Ingle, J. C. (1966). *The movement of beach sand*. Elsevier, New York.

Inman, D. L., and Chamberlain, T. K. (1959). "Tracing beach sand movement with irradiated quartz," *J. of Geophys. Res.* 64, 41-7.

Knoth, J. S., and Nummedal, D. (1977). "Longshore sediment transport using fluorescent tracer." *Proc. Coastal Sediments '77*. ASCE, New York, 383-98.

Komar, P. D. (1990). "Littoral sediment transport." *Handbook on Coastal and Ocean Engineering*. J.B. Herbich, ed., Gulf Pub. Co., Houston, TX, 2, 681-714.

Komar, P. D., and Inman, D. L. (1970). "Longshore sand transport on beaches," *J. of Geophys. Res.* 75, 5514-27.

Kraus, N. C., Isobe, M., Igarashi, H., Sasaki, T. O., and Horikawa, K. (1982). "Field experiments on longshore transport in the surf zone." *Proc. 18th Coastal Engrg. Conf.* ASCE, New York, 969-88.

Madsen, O. S., and Grant, W. P. (1976). "Sediment transport in the coastal environment," Ralph M. Parsons Lab. for Water Resources and Hydrodynamics Report No. 209, Mass. Institute of Technology, Cambridge, MA.

Miller, M. C., and Komar, P. D. (1979). "Measurements of sand spreading rates under near-bottom wave orbital motions," *J. of Geology* 87, 593-608.

Murray, S. P. (1967). "Control of grain dispersion by particle size and wave state," *J. of Geology* 75, 612-34.

Sasaki, T. O., and Sakuramoto, H. (1984). "Effect of rip current barrier on harbor shoaling." *Proc. 19th Coastal Engrg. Conf.* ASCE, New York, 2091-106.

Sternberg, R. W., Shi, N. C., and Downing, J. P. (1984). "Field investigation of suspended sediment transport in the nearshore zone." *Proc. 19th Coastal Engrg. Conf.* ASCE, New York, 1782-1798.

Teleki, P. G. (1966). "Fluorescent sand tracers," *J. of Sedimentary Petrology* 36, 469-85.

Yasso, W. E. (1966). "Formulation and use of fluorescent tracer coatings in sediment transport studies," *Sedimentology* 6, 287-301.

6 Suspended Sediment Concentration Measurements at SUPERTANK[1]

Introduction

Background

Early work on suspended sediment transport measurement in the surf zone attempted to characterize the mean suspended sediment profile as a function of cross-shore position, beach slope, and incident wave characteristics (Watts 1953, Fairchild 1972, Thornton and Morris 1977, Inman 1978, Kana 1979). The resultant mean profile was either generated from a pump sample (Watts 1953, Fairchild 1972, Thornton and Morris 1977) or from averaging a large number of instantaneous samples (Kana 1979, Zampol and Inman 1989). These investigations firmly established that suspended sediment concentrations decrease rapidly with height above the bed and that mean concentration varies between 0 and 20 g/ℓ near the bed to less than 1 g/ℓ at 60 cm. Physical processes that apparently govern the variation of the mean suspended sediment profile are: (a) breaker type, with plunging waves suspending more than spilling waves (Kana 1979); (b) position relative to the breakpoint, where concentration reaches a maximum shoreward of the breakpoint (Kana 1979); and (c) cross-shore position, where maximum concentrations are found near the breakpoint and in the inner surf zone close to the swash (Kana 1979). Although these observations provide a general understanding of the spatial distribution of suspended sediment, the first attempts at characterizing the temporal variation of suspended sediment on time periods short relative to the wave period were made by Brenninkmeyer (1975, 1976a,b) and Thornton and Morris (1977). These investigators utilized forward-scattering optical devices to monitor changes in turbidity; Brenninkmeyer used an "almometer," capable of simultaneously monitoring conditions at many elevations above the bed,

---

[1]Written by Reginald A. Beach, Oregon State University.

whereas Thornton and Morris monitored a single elevation with a nephelometer. Although the almometer seemed to have potential for a breakthrough in the field of sediment transport measurement, it was difficult to calibrate was not responsive to the full range of sediment concentrations observed in the surf zone, and has not been used in the field by others. Thornton and Morris reported that peaks in the suspended sediment spectra occurred at approximately twice the frequency of peaks in the velocity spectra, indicating two or more maxima per wave period. They also concluded that suspended sand concentration decreased exponentially with height above the bed and that the rate of decrease and total concentration were related to the mean bed shear stress.

Several years later, Downing (1984); Sternberg, Shi, and Downing (1984); and Jaffe, Sternberg, and Sallenger (1984) used Optical Backscatter Sensors (OBS) (Downing, Sternberg, and Lister 1981) and Marsh-McBirney electromagnetic current meters to observe time-dependent fluctuations of suspended sediment and fluid forcing, respectively. The combinations of these two types of fast-response instrumentation allowed, for the first time, the calculation of suspended sediment flux. These pioneering studies indicated that suspended sediment re-suspension events were episodic and exhibited considerable low-frequency modulation at wave group and edge wave frequencies. Calculations by Jaffe, Sternberg, and Sallenger (1984) showed that net suspended sediment flux was dominated by transport associated with oscillatory velocities rather than mean currents. These results indicated that the onshore movement of a bar crest could be accounted for by the net movement of the suspended load. These exciting results were further substantiated by Huntley and Hanes (1987) who indicated that the direction and magnitude of suspended sediment transport were functions of frequency; that is, net transport of sediment was a result of several competing processes, mean flows, and incident-band and infragravity-band forcing.

The SUPERTANK Laboratory Data Collection Project was guided by these and subsequent field studies, and utilizes the approach of combining rapid, synchronous measurement of suspended sediment concentration and fluid flow to understand fluid-sediment interactions and to calculate net suspended sediment flux.

Objectives

The primary objective of this investigation was to increase understanding of cross-shore sediment transport processes in response to a wide variety of offshore wave conditions. Establishing the degree to which suspended load transport is responsible for observed beach profile change is of fundamental importance. Addressing this single objective requires accurate measurement of the time-varying concentration field, fluid forcing, and beach profile change. The large wave channel at Oregon State University's O. H. Hinsdale Wave Research Laboratory (WRL) provided an unparalleled opportunity to control sensor elevations, cross-shore locations, and offshore wave conditions to a degree unattainable in the field.

Scope

During SUPERTANK, as many as 25 OBS for monitoring suspended sediment concentration were deployed. Typically, these sensors were deployed in vertical stacks of five sensors each, at five positions on a cross-shore transect spanning the surf zone. Data for 166 experimental runs were collected, encompassing a wide range of wave and breaking conditions. This chapter contains background information on sediment concentration measurement equipment and procedures employed during the SUPERTANK project and provides coefficients for the conversion of the raw sensor output to scientific units, instrument positions (horizontal - x, elevation - z), and basic statistics of sensor output for all runs.

Experiment Apparatus

Instrument description

Suspended sediment concentration measurements were made using OBS which were first developed at the University of Washington and are presently fabricated by Downing and Associates Instrument Company, Port Townsend, Washington. The OBS used in this project had two configurations, but utilize the same principle of operation. A typical sensor consists of a stainless steel housing, 19 cm in diameter by 11 mm in length (Figure 6-1). It houses an infrared emitting diode (IRED) with peak radiant intensity at 950 Å, a silicon photo-voltaic cell with peak spectral response at 900 Å, and an appropriate filter to limit transmittance from incident light. The optical components are encapsulated in the sensor head with clear epoxy resin. When operating, a scattering volume of approximately 1.3 cc is irradiated through a 5.6-mm-diam aperture at the geometric center of the photo-detector by an IR-beam with a half cone angle of 14 deg (0.24 rad). Backscattered radiation (110-165 deg (1.92-2.88 rad)) from suspended solids is converted to photocurrent by the detector oriented in a plane normal to the emitter beam axis and located close to it (Downing, Sternberg, and Lister 1981). The quantity of backscattered light is linearly proportional to the mass concentration of sediment present (see following section for calibration results).

Two OBS configurations were used during the project; sensors which are pre-configured in vertical stacks and individual sensors.

OBS: AO1-AO4, BO1-BO4, CO1-CO4. These three arrays of four sensors each are the original OBS developed for the Nearshore Sediment Transport Study (NSTS) in 1979 (Downing, Sternberg, and Lister 1981). The four individual sensors are housed in a vertical stack with inter-sensor distances of 3, 3, and 5 cm for a total vertical coverage of 11 cm. Figure 6-2 shows one of these sensor arrays deployed during SUPERTANK.
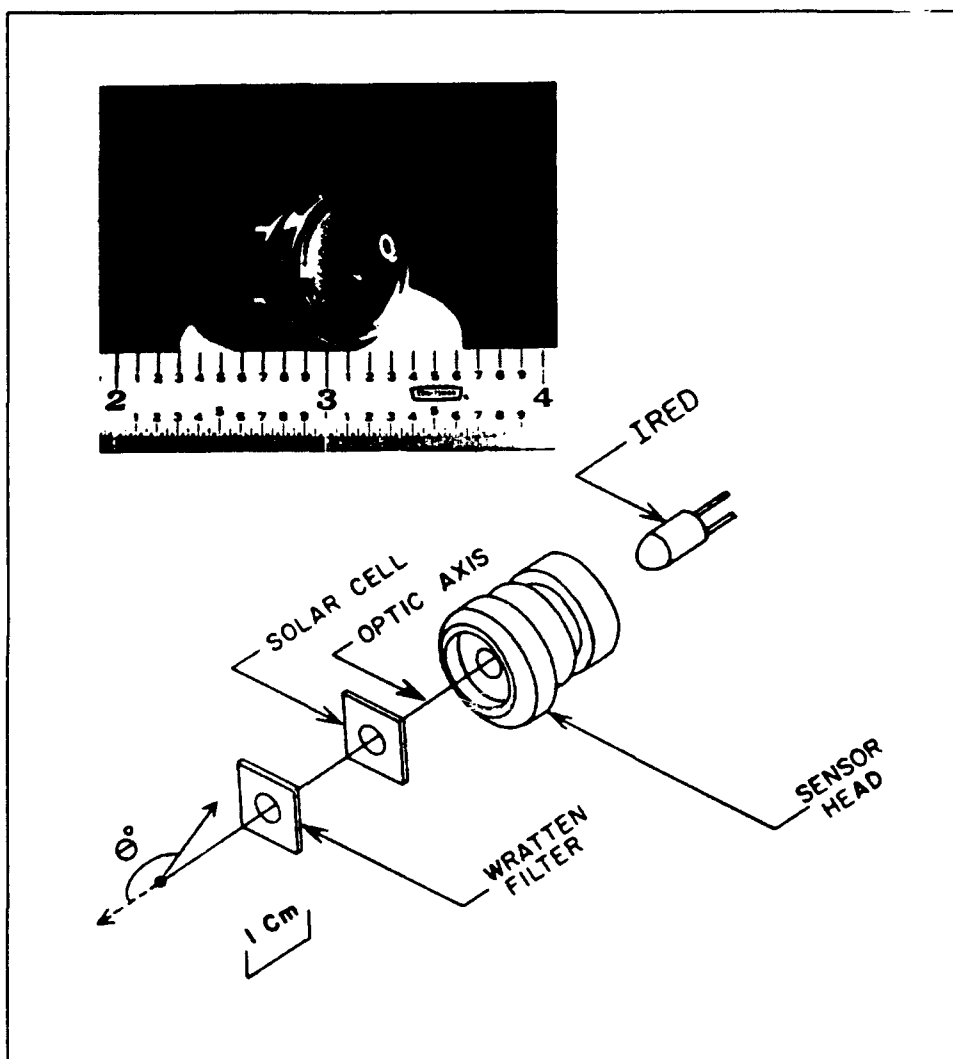
Figure 6-1. Optical Backscatter Sensor (OBS) and cut-away view (Downing, Sternberg, and Lister 1981)

OBS: AM1-AM5, BM1-BM5, PO1-PO3. These 13 sensors are Model OBS-1P from Downing and Associates. They are individual sensors but were primarily deployed in vertical stacks (Figure 6-3). The distances between sensors in the vertical arrays were not necessarily constant between stacks, project runs, or over the entire experiment. The three PO sensors were primarily used to augment the vertical stacks AO, BO, and CO. These 13 sensors were on loan to R. Beach and are the property of Dick Sternberg (eight sensors, University of Washington) and Dave Cacchione (five sensors, U.S. Geological Survey, Menlo Park, California).

Location

All OBS locations coincided with the fixed wall positions where current meters and wave staffs were deployed. Table F1 (contained in Volume II of
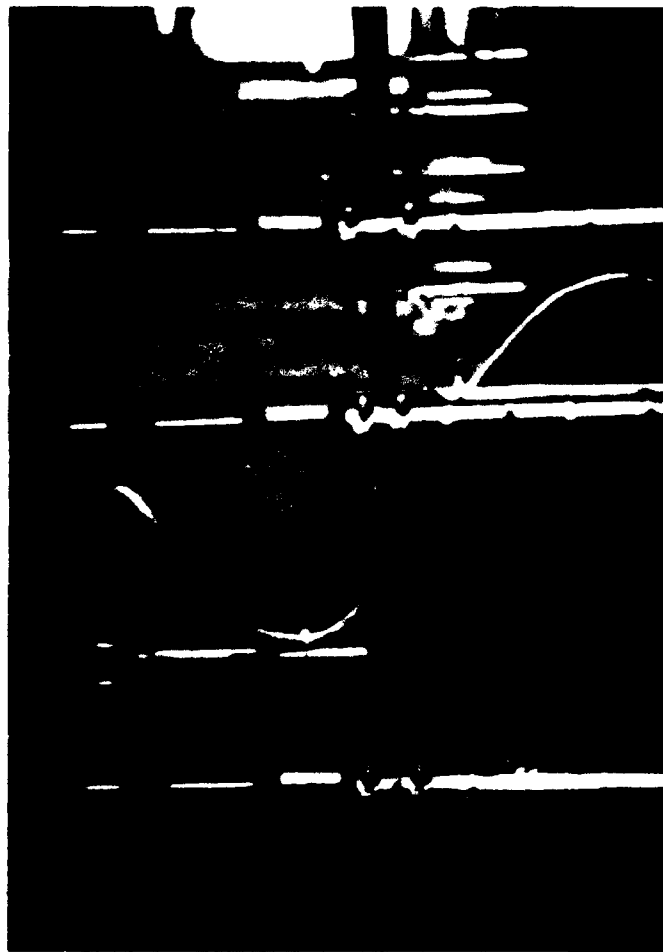
Figure 6-2. Example of OBS array; AO, BO, or CO. Sensor array is shown displaced 1 ft shoreward from the current meters, Runs A0509A - A0915A

this report) provides a listing of the along-channel coordinates, x (ft), and sensor elevation above the bed prior to, z_b (cm), and after, z_a (cm), an experimental run. Any differences between z_b and z_a indicate bed elevation changes associated with erosion or accretion. Negative z-values indicate that the sensor was buried. Generally, sensor stacks remained at a specific along-channel, x, position for the duration of a test series.

All vertical stacks of the OBS were cantilevered either from the east wall of the wave channel (Figure 6-2) or from pipes jetted into the bed (Figure 6-4). During the entire project all vertical stack locations coincided with one or more Marsh-McBirney electromagnetic current meters. During the first week of runs, A0509A - A0915A, the vertical stacks of OBS were located 1 ft shoreward, (-x), of the corresponding current meters (Figure 6-2). During the remainder of the project, OBS and current meters were located at the same x coordinate, but displaced in the cross-channel y direction (Figure 6-4). This "longshore" displacement was typically less than 2 ft.

110
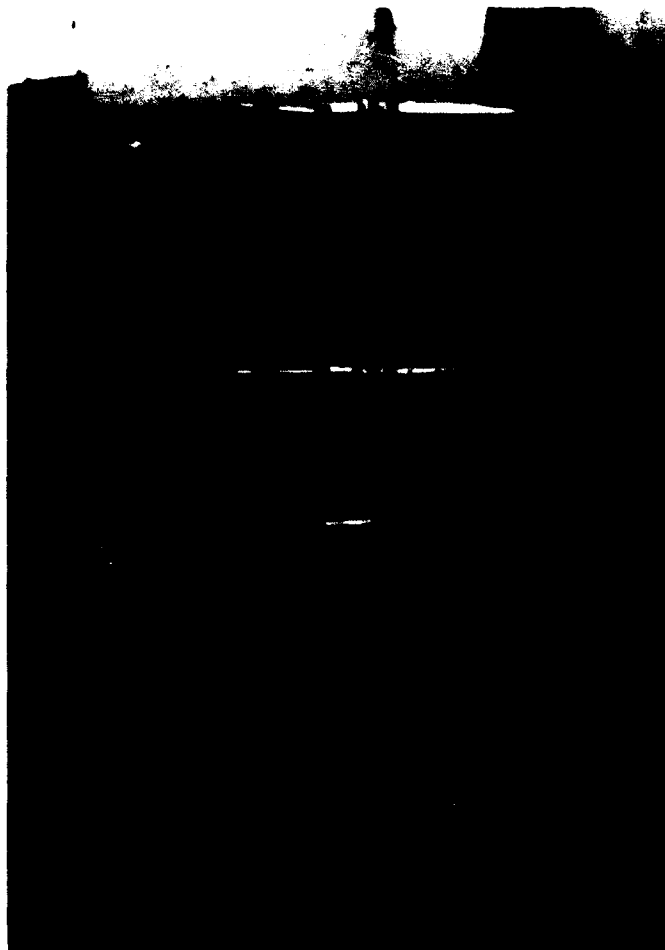
Figure 6-3. Example of OBS -1P array; AM, BM, or PO

Instrument characteristics

The OBS series of sensors are mature instrumentation. Their characteristics include a linear response to suspended particulates (see below), a wide dynamic range, and a 10-Hz bandwidth. The OBS-1P have built in temperature compensation to reduce sensor drift. The NSTS sensors have a voltage output range of + 5 V, and the OBS-1P output range is 0 to 3.5 V. Consequently, for the same sensor gain (and sensitivity), the NSTS sensors have a greater dynamic range than the OBS-1P.

The 12-bit analog to digital converter (A/D) used to record all OBS sensors was the PC-Mate Lab Master by Tecmar Inc. (now Scientific Solutions), and it sampled all sensors simultaneously (sample and hold) at a 10-Hz rate. Because all of the OBS have different (though comparable) responses to suspended particulates, their absolute sensitivity is limited by the 12-bit resolution of the A/D. For one-bit accuracy and a typical sensor response of 10 g/ℓ/V, the resolution of the A/D is 0.04 g/ℓ.
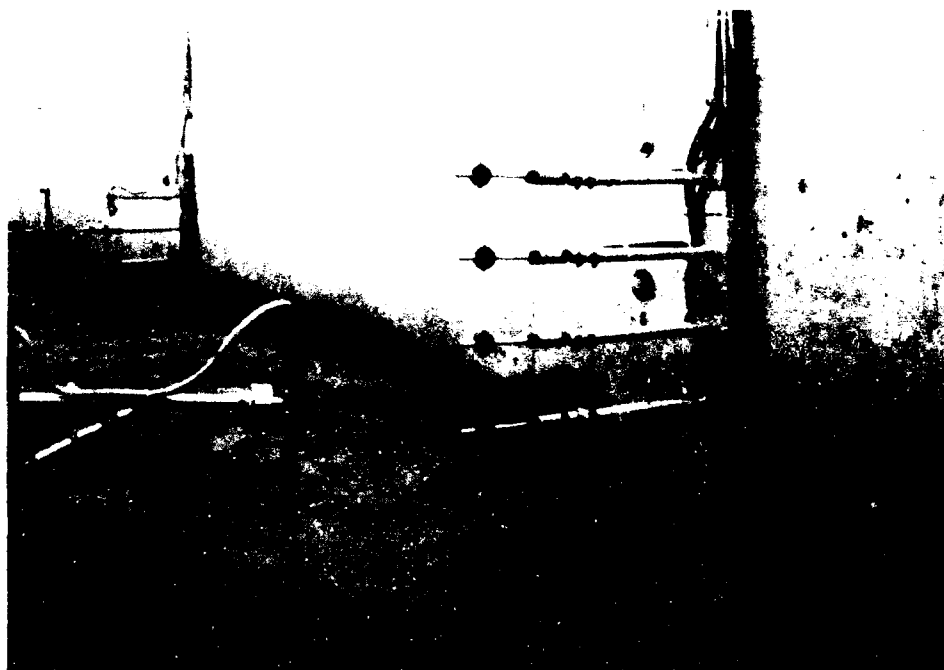
Figure 6-4. Example of OBS array; AO, BO, or CO. Longshore displacement from current meters is less than 20 cm

Experiment Procedures

Sequence of events

A typical data run was conducted after all OBS heights above the bottom had been measured and recorded. The OBS data logging system was started approximately 15-30 sec prior to the official start time of a run to record the "clear-water" offset of each OBS. Data collection continued for approximately 15-30 sec after the official stop time of the run to record whether the clear-water offset had changed during the run. Comments on wave conditions, difficulties encountered, or noteworthy events observed during the run were logged into notebooks. Divers were then deployed to measure OBS heights above the bed, describe bed configuration (ripples, plane, etc.), and readjust the OBS stacks such that the lowermost sensor was set to $z = 3.5$ cm, in preparation for the next run. These pre- and post-run instrument elevations were recorded in the logbooks.

Sampling and time reference

All data were recorded on a personal computer (PC) located in the SUPERTANK Principle Investigator room at the WRL. All data channels were simultaneously sampled at a 10-Hz rate. The time of each data sample

(to 0.01 sec) was also recorded to allow synchronization with other independently recorded data sets. During A0509A - A0915A, the sampling time was taken from the A/D clock, which was set "by hand" (to 0.1 sec) to Coordinated Universal Time. For the remainder of the project runs, the sampling time was taken from a precision clock installed in the PC and linked via radio (call letters WWV) to Coordinated Universal Time.

Pre-processing and filtering

Prior to sampling, the analog signals are low-pass filtered to 20 Hz by a one-pole passive filter. This filter reduces signals at 20 Hz by 3 db (50 percent). There is no appreciable alteration of the 10-Hz signal of interest.

Calibration and zero reference

The sizes and refractive indices of sediment particles strongly influence light scattering characteristics, and, consequently, OBS must be calibrated with the sediment from the area where they were deployed. OBS calibrations were performed in the laboratory using a recirculating tank from which pump samples of the ambient concentration can be drawn (Downing and Beach 1989). The procedure consists of adding sediment, recording sensor output, and drawing a pump sample. This procedure is repeated for increasing sediment concentrations until the range of sensor output in the field is covered. After a calibration run, the water is decanted from each pump sample, and the volume of water is recorded. The sediment is dried, and its weight and volume are determined. The sediment parameters are then used in conjunction with the known volume of water to calculate a mass concentration. Response, typically, is linear over a wide concentration range. Table 6-1 lists the gains and linear regression coefficients calculated for the sensors used during SUPERTANK.

Offsets, or zero reference values, were determined for each sensor for each run and are included in Table F1, which is contained in Volume II of this report. These offsets represent "clear" water values measured prior to the start of wave action and are indicative of the background turbidity of the channel. These offsets changed from run to run depending on the previous wave action and on longer time scales as the channel was drained and refilled for logistical reasons. Changes in background turbidity are seen by the instruments as a constant shift. Because the gains of each sensor are different, removal of this constant shift prior to conversion to scientific units is essential. Consequently, the value in the offset column represents an electronic offset seen by the instrument and is in A/D units. The offset value was established for each sensor by taking the mean of the 30-sec (approximate) data segment recorded prior to the official start time of each run. Table F1 provides a listing of these offsets as a function of instrument and run.

Table 6-1
BS Gain and Linear Regression Coefficient (R^2)

OBS Instrument ID	Gain, g/l	Regression Coefficient
AO1	7.73	0.995
AO2	8.32	0.993
AO3	8.16	0.995
AO4	9.26	0.993
PO1	9.02	0.995
BO1	6.29	0.999
BO2	6.52	0.998
BO3	8.55	0.998
BO4	15.47	0.997
PO2	9.38	0.997
CO1	7.45	0.999
CO2	7.93	0.998
CO3	8.94	0.998
CO4	86.61	0.980
PO3	9.69	0.990
AM1	33.91	0.995
AM2	105.76	0.980
AM3	68.84	0.985
AM4	55.00	0.986
AM5	41.80	0.989
BM1	71.27	0.990
BM2	14.43	0.999
BM3	7.99	0.998
BM4	18.39	0.997
BM5	7.58	0.998

Data Analysis

Reduction and interpretation methods

All 166 raw data files, in DOS format, were transferred to a SUN workstation, converted to UNIX format, and archived on optical disk. All subsequent data reduction and processing were performed on a SUN workstation.

To convert the raw sensor output R (A/D units) to concentration C (g/ℓ), the following algorithm was used

$$C = G \frac{(R - O)}{204.8} + B \qquad (6\text{-}1)$$

where G is the sensor gain (g/ℓ/V), O is the clear-water offset (A/D units), 204.8 is the conversion factor from A/D units to volts, and B is the background turbidity present in the channel (g/ℓ). Absolute measurements of background turbidity were not made during the project, and, consequently, B is assumed to be zero.

Data file format

Data were recorded on a PC in binary format. A sample record consists of 8 bytes of time in one of two formats, a ground channel (2 bytes) and N channels of OBS output (2 bytes each), where N is the number of sensors deployed for that run. For Runs A0509A - A0915A, time was stored as four 2-byte integers (HH MM SS HH); for all subsequent runs, time was stored as an 8-byte real number in seconds since midnight. These two formats reflect differing clock outputs; the former being taken from the A/D clock (which was set to WWV), and the latter directly from the WWV clock.

A common number of channels recorded was 34; thus, the corresponding record would be 8 + 2 x 34 = 76 bytes. Subsequent records (at 10 Hz) are simply appended to the file. Typically, a 70-min run had 42,000 records and was 3.2 MB in size. All data files have been archived in two formats, on QIC-40 tapes in the original PC format and on optical disk in UNIX format.

Sample data

A 20-min segment of suspended sediment concentration data (g/ℓ) collected during Run A1417A (70-min duration) is shown in Figure 6-5. During this random wave forcing run, the peak wave period T_p was 8 sec, the zero-moment wave height H_{mo} was 0.5 m, and γ, the TMA spectral width parameter, was 3.3. Figure 6-5 shows the time-dependence of nearbed concentration ($z = 3.5$ cm) at five cross-shore positions progressing from offshore (panel A) to onshore (panel E). General observations of sediment dynamics evident in Figure 6-5 are:

a. Seaward of the surf zone, suspended sediment concentrations are considerably lower (panels A, B) than shoreward of the breakpoint (panels C - E).

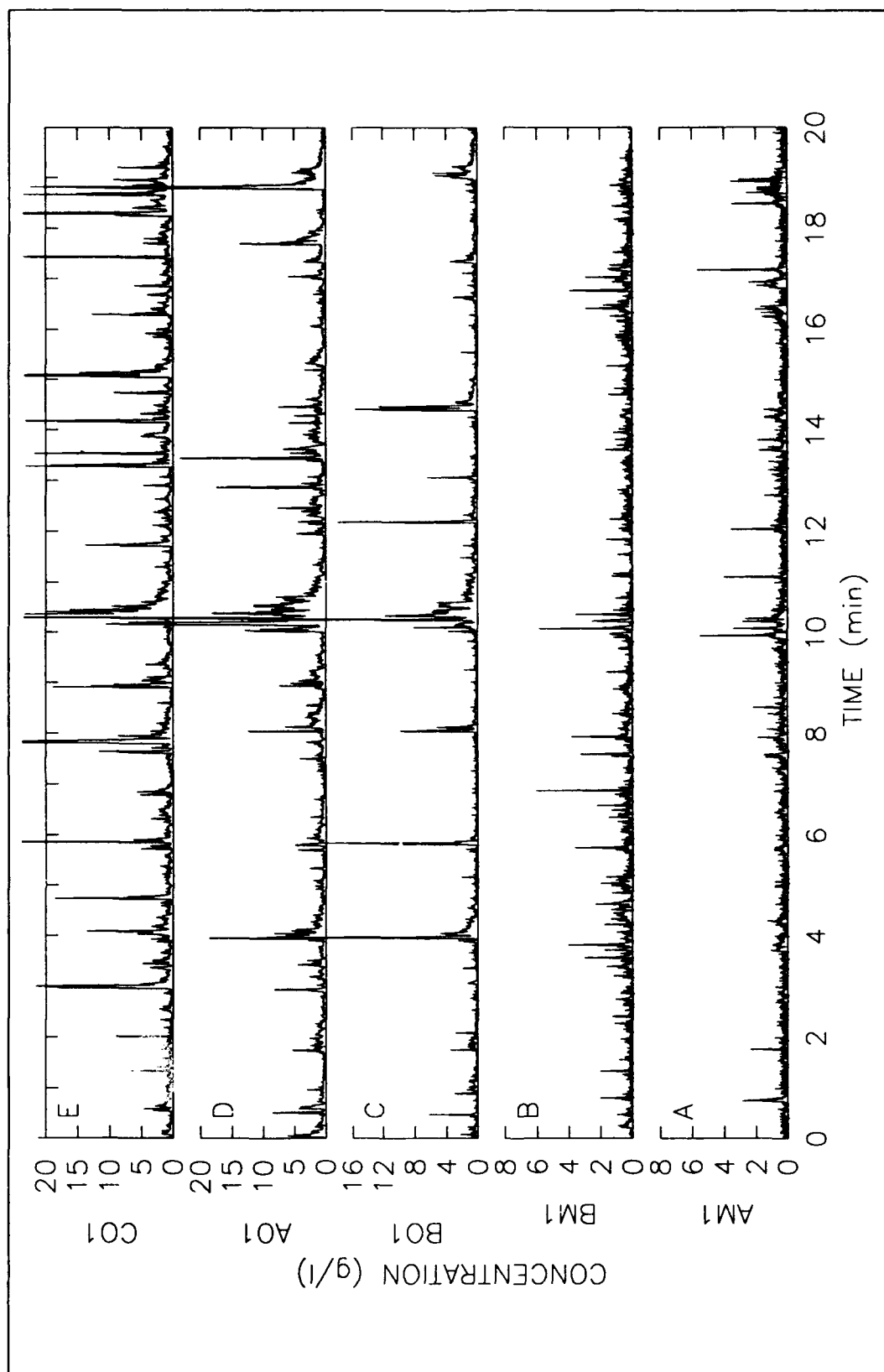b. The highest peak concentrations are found at the innermost positions, panels D and E (note scale change).

Figure 6-5. Time series of suspended sediment concentration (z = 3.5 cm) at five cross-shore locations, Run A1417A

c. While suspension events associated with individual waves are evident (sharp spikes), the largest concentrations are at low frequencies and are associated with wave groups.

d. Suspension events associated with wave groups persist in the water column for a considerably longer time than those associated with individual waves.

e. The low-frequency modulation of sediment re-suspension is present at all cross-shore locations, but is most evident in the inner surf zone.

Summary of data characteristics

Table F1 summarizes the output of the fixed OBS for all runs collected. The two columns on the right indicate the mean and standard deviation of sensor output (g/ℓ) for all runs. These mean and standard deviation values may be used to identify data sets that have larger dynamic signals and hence, may be of more interest for study.

Identification of marginal data sets

The overall OBS data set is considered to be of good quality, and, while there are often malfunctioning sensors in each run, all of the data runs have usable data. It is suggested that sensors near the sea surface be filtered using data from the resistance wave gauge to eliminate data when the sensors are out of the water. Data sets in which known difficulties were encountered are listed in Table 6-2.

The sheer volume of data collected during SUPERTANK has precluded a rigorous treatment to eliminate spurious signals which may be present. Spurious signals are most often caused by floating debris (in this case, wood chips) or rapid transition from water to air and back into water, rather than electronic noise. It is suggested that all data be plotted as time series prior to use in numerical calculations to avoid inclusion of contaminated signals. Elimination of outliers, such as discussed in Chapter 7, using robust techniques is recommended along with the following observations. Generally, concentration consistently decreases with elevation, along with the dynamic range seen at a particular level. Hence, concentration profiles that have inversions or sensors that fluctuate widely immediately above a rather quiescent sensor should be viewed as suspect, for there is no reasonable physical explanation for these observations. Sensors with these characteristics should be investigated prior to their inclusion in any analysis.

Table 6-2
Marginal Data Sets

Run	Explanation
A0613A	Sampling time not constant, check clock output
A0615A	Recorded A/D clock time off by 4.93 sec from WWV
A1217A	Hard disk failed causing A/D program to hang
A3010A-S0414A	Stack CO drawing excess power, use with caution

Summary

Review of experiments and results

The OBS measurements made during SUPERTANK were one of the largest efforts to date. The data set covers a broad range of offshore wave conditions and allows comparison of suspended sediment response to both random and monochromatic forcing. If used in conjunction with hydrodynamic and beach profile change data, the potential for advancing the state of knowledge of nearshore sediment transport is considerable. This report is the first step towards achieving this goal by providing necessary background information (Table F1, contained in Volume II of this report) required for advanced studies.

Recommendations

Concentration of suspended sediment decays rapidly with height above the bed. Bed-level fluctuations over the course of a run lead to changes in OBS elevation and consequently, changes in dynamic signal, even if offshore wave forcing remains constant. Consequently, knowledge of OBS elevation relative to the bed is essential for proper interpretation of their output. The ability to turn off the waves at SUPERTANK allowed measurement of these bed-level fluctuations and readjustment of sensor height between runs, but required considerable diver support. It is recommended that future investigations attempt to use some remote means (sonic altimeter, sonic concentration sensor, etc.) to keep track of bed-level fluctuations and hence, OBS elevation.

Acknowledgements

The author is most grateful to S. Barkaszi (Florida Institute of Technology (FIT)), A. Ogston (University of Washington), and J. Smith (Coastal Engineering Research Center (CERC)) whose tireless dedication (well, okay,

118

it WAS tiring) made the suite of OBS measurements possible. Thanks also go to B. Dally (FIT), K. Scott (University of California at Santa Cruz), and C. Church (Naval Postgraduate School) who helped out at crucial moments. The support of the WRL and the U.S. Army Engineer Waterways Experiment Station CERC staff during the long summer is most appreciated. Post-processing of the data was enhanced by the efforts of M. Muddarm (Oregon State University). Special thanks to Nick Kraus (CERC) for conceiving and sponsoring the SUPERTANK project and for his continuing enthusiasm and support of surf zone research.

References

Brenninkmeyer, B. M. (1975). "Mode and period of sand transport in the surf zone." *Proc. 14th Coastal Engrg. Conf.* ASCE, New York, 812-27.

_____. (1976a). "In situ measurements of rapidly fluctuating high sediment concentrations," *Marine Geology* 20(2), 117-28.

_____. (1976b). "Sand fountains in the surf zone," S.E.P.M. Special Publication 24, 69-91.

Downing, J. P. (1984). "Suspended sand transport on a dissipative beach." *Proc. 19th Coastal Engrg. Conf.* ASCE, New York, 1765-81.

Downing, J. P., and Beach, R. A. (1989). "Laboratory apparatus for calibrating optical suspended solids sensors," *Marine Geology* 86, 243-9.

Downing, J. P., Sternberg, R. W., and Lister, C. R. B. (1981). "New instrumentation for the investigation of sediment suspension processes in the shallow marine environment," *Marine Geology* 42, 19-34.

Fairchild, J. C. (1972). "Longshore transport of suspended sediment." *Proc. 13th Coastal Engrg. Conf.* ASCE, New York, 1069-88.

Huntley, D. A., and Hanes, D. M. (1987). "Direct measurement of suspended sediment transport." *Proc. Coastal Sediments '87.* ASCE, New York, 723-37.

Inman, D. L. (1978). "Status of surf zone sediment transport relations," *Workshop on coastal sediment transport, with emphasis on the National Sediment Transport Study*, Sea Grant Rep. DEL-SG-15-78, 9-20.

Jaffe, B. E., Sternberg, R. W., and Sallenger, A. H. (1984). "The role of suspended sediment in shore-normal beach profile changes." *Proc. 19th Coastal Engrg. Conf.* ASCE, New York, 1983-96.

Kana, T. W. (1979). "Suspended sediment in breaking waves," Tech. Rep. No. 18-CRD, Univ. of South Carolina, Columbia, SC.

Sternberg, R. W., Shi, N. C., and Downing, J. P. (1984). "Field investigations of suspended sediment transport in the nearshore zone." *Proc. 19th Coastal Engrg. Conf.* ASCE, New York, 1782-98.

Thornton, E. B., and Morris, W. D. (1977). "Suspended sediments measured within the surf zone." *Proc. Coastal Sediments '77.* ASCE, New York, 655-68.

Watts, G. M. (1953). "Field investigations of suspended sediment in the surf zone." *Proc. 4th Coastal Engrg. Conf.* ASCE, New York, 181-99.

Zampol, J. A., and Inman, D. L. (1989). "Discrete measurements of suspended sediment." *Nearshore Sediment Transport.* R. J. Seymour, ed., Plenum Press, New York, 259-72.

7 Sediment Suspension Measurements from a Mobile Platform at SUPERTANK[1]

Introduction

Background

A fundamental feature of the surf zone that is obvious to even the casual observer is the suspension of sand by breaking waves. In following a single wave as it crosses the nearshore, the pattern of suspended sand left behind often resembles bands of clouds that stretch along the shore. Usually, sand concentrations are at their greatest in the zone of initial wave breaking, especially if the breakers are plunging (Kana 1979; Kennedy, Erlich, and Kana 1981), and a well-defined boundary between regions of high and low turbidity is evident just seaward of breaking. In addition to the zone of initial breaking, if wave re-forming is prevalent, a second "suspension boundary" can be found near the toe of the swash. Strong cross-shore gradients in mean suspended load exist in these zones, so the potential for strong gradients in mean transport also exists. Gradients in mean transport lead to the creation of depositional and erosional features, such as the swash step and the longshore bar and trough. Because the sediment is also carried by the longshore current, the location and intensity of these peaks in suspension are also of paramount importance in longshore transport processes. In short, it is clear that basic measurement and modeling of sand suspension across the entire surf zone, with particular emphasis on the regions where suspension is greatest, is a key element in the development of process-based formulas for coastal sediment transport, as well as improved beach evolution models.

The measurement technology available to study suspended sediment in the surf zone can be divided into two categories: (a) direct physical sampling and (b) inference based on radiation scattering. Suction sampling (e.g., Watts 1953; Fairchild 1974; Coakley et al. 1978; Nielsen, Green, and Coffey 1982),

---

[1] Written by Stephen F. Barkaszi and William R. Dally, Florida Institute of Technology.

in which a pump or siphon head is used to draw the fluid-sediment mixture into retaining bottles, can only establish mean concentrations. Streamer traps (Kraus 1987) have also been used to measure the mean suspended load carried in the longshore direction. Arrays of Niskan-type bottles (Kana 1979) provide "snapshot" water-sand samples, taken at a single instant in time. Although physical sampling is especially valuable in that the grain size distribution in each sample can be examined, analysis of the samples is labor-intensive and time-consuming.

Radiation-scattering detection technology utilizes a source of radiation (i.e., light or ultrasound) and an electronic detector that measures the energy that is scattered from any particulates present in the water. Output is at very high speeds, so temporal resolution is greatly enhanced. Acoustic backscattering devices can measure the entire vertical profile of sand concentration almost instantaneously (see, e.g., Hanes 1988); but unfortunately, they cannot be used in the aerated water of the surf zone. The infrared Optical Backscatterance Sensor (OBS) (Downing, Sternberg, and Lister 1981) can continuously monitor local concentration of suspended solids in aerated water, and has greatly expanded data collection capabilities in the surf zone.

Although characterizing suspension in the zones of initial wave breaking is arguably the most important facet of the complete description of sand suspension in the surf zone, little is known quantitatively, and only limited predictive capabilities exist. In the field, study of suspension in the zone of initial breaking is complicated by practical considerations. Establishing a priori where initial breaking will take place during the experiment is extremely difficult. In addition to the underlying randomness of the incoming waves, the outer boundary of the surf zone moves as (a) the tide rises and falls, (b) the wave climate and wind conditions change, and (c) the nearshore bar migrates and changes shape. During the field experiments reported in Sternberg, Shi, and Downing (1984), Beach and Sternberg (1988), and Beach (1989), five vertical arrays of five sensors each were installed in various planform configurations. Although there were times at which individual waves broke in the vicinity of an array, spacing of the arrays was too great (2-7 m) to directly resolve the structure of sand clouds and the suspension boundary.

In a small-scale laboratory wave channel, Shibayama and Horikawa (1982) focussed on the formation of the sand cloud created under plunging breakers. Using high-speed photography, it was confirmed that the large-scale vortex created during initial breaking generated the cloud, which the authors coarsely mapped from the photographs. Because of the control that can be exercised on breaking conditions, the laboratory is an excellent place for basic examination of discrete suspension events under breaking waves. However, in the tests conducted to date, sediment and wave scales have been mismatched, i.e., full-sized sand and small-scale waves were used.

Objectives

The major objective of this component of the SUPERTANK Laboratory
Data Collection Project was to measure instantaneous suspended sand
concentration and relevant fluid flow parameters at high cross-shore resolution
in the region of incipient and initial wave breaking. A secondary objective
was to measure, at high temporal and spatial resolution, the formation,
dispersal, and settling of the sand clouds created by plunging breakers.

Scope

To address the first objective stated above, a capacitance wave gauge, a
video camera, a vertical array of four electromagnetic current meters, and a
vertical array of five OBS were mounted to a carriage that spanned between
the walls of the wave channel (Figure 7-1). With this apparatus, time series
measurements of suspended sediment concentration, and other relevant param-
eters, were obtained in the region of transition from nonbreaking to fully
broken waves. The mobile array also enabled concentration measurements to
be obtained anywhere along the channel, to fill in between the fixed arrays.
In a few cases, high spatial resolution across shore was attained by moving the
carriage in a stepwise manner along the channel during a test. Initial analysis
of the concentration data shows significant change in sand suspension across
the zone of initial breaking, both in the behavior of the time series as well as
in the vertical distribution of mean concentration.

Figure 7-1. Movable carriage for measurements in breaking waves

To address the second objective, a two-day abbreviated experiment was conducted with an OBS matrix, fabricated using all 33 available sensors. The OBS were mounted in four vertical arrays, spaced at 0.75-m intervals. Four electromagnetic current meters (EMCMs), one for each array, the wave gauge, and the video camera were also employed. The matrix was suspended from the carriage, which was positioned at different locations in the zone of initial breaking. Data were collected across a range of incident wave heights and periods.

Experiment Apparatus

Instrument description

Mobile OBS array. A stacked array of five OBS was used to detect suspended sediments in the outer surf zone. The main components of an OBS are an infrared emitter that irradiates the water near the sensor and a co-located photoelectric cell that is filtered to detect only infrared radiation. The emitter produces a beam with an elliptical cone shape which has half-power points at 50 and 30 deg (0.87 and 0.52 rad) from the beam axis. Sediment particles within this conical region scatter the infrared radiation. That which is reflected 140 deg (2.44 rad) or more from the beam axis (i.e., backscattered) is received at the photoelectric cell (Downing, Sternberg, and Lister 1981).

The five OBS sensor heads were screwed into PVC cylinders, which were back-filled with epoxy resin to provide a watertight housing. Electrical connections were made from each sensor head to a neoprene jacketed multi-conductor cable, which transmitted the voltage produced by the photoelectric cell to a housing containing signal conditioning boards and a power supply. Each OBS head must be paired with its own signal conditioning board, which amplifies the signal for transmission, compensates for temperature, and provides synchronous switching of multiple sensors.

An aluminum sailboat mast of elliptical cross section (9.52 cm x 5.72 cm) was used to deploy the mobile OBS array (Figure 7-1). Forty holes at 3.8-cm spacing were drilled through the mast along the major sectional axis, so that sensors would mount horizontally with only the sensor head protruding. The sensor beam axis was oriented across the channel and set screws held each of the sensor heads in their respective positions. Unoccupied holes were covered with tape to provide a smooth surface. Cables from the sensors ran up the inside of the mast to the electronics housing.

The aluminum mast was mounted to the shoreward side of an existing motorized carriage that spanned the walls of the wave channel, thus allowing the cross-shore position of the sensors to be changed with relative ease. The mast was held vertically by clamping it between two steel I-beams that were

124

bolted to the carriage structure. A pulley and winch system was used to adjust the elevation of the base of the mast.

Capacitance wave gauge. A capacitance wave gauge, used to determine local free-surface displacement, utilizes the dielectric properties of water and air to detect the position of the air-water interface. The gauge consisted of a small PVC electronics housing, a jacketed wire sensing lead, and a d-c power supply. The sensing lead was approximately 2 m in length, and was oriented perpendicularly to the still-water surface.

The capacitance wave gauge was mounted to a second sailboat mast, attached vertically to the carriage in the same cross-channel plane as the OBS array. The sensing lead ran parallel to the mast from its bottom, up to the electronics housing, and was held in slight tension. The wave gauge could also be moved vertically to compensate for changes in still-water conditions.

Video camera. An 8-mm-format video camera was used to record the waves as they passed by the OBS array and wave gauge. From this, local wave form and turbulence intensity were visually documented. The camera's internal clock was manually synchronized with Coordinated Universal Time to facilitate comparison with sensor records. The video camera was mounted on a wooden frame which extended approximately 1 m shoreward of the carriage. From this position, an oblique view was obtained of all instruments deployed from the carriage.

Electromagnetic current meters. As described in Chapter 3, a stacked array of four EMCMs was also mounted to the instrument carriage. The gauges, which measured vertical and cross-shore velocities, were located in the same cross-channel plane as the OBS and wave gauge.

Location

The instrument carriage was used to measure and observe sediment suspension and associated fluid properties at any position between Stations 5 and 18, which spans a distance of approximately 50 m. However, the majority of measurements were taken in the outer surf zone, between Stations 7 and 10. The bottommost OBS was typically located within 8 cm of the bed and the topmost sensor nominally 35 cm from the bed.

The capacitance wave gauge, OBS array, and EMCM array were fixed in the same cross-channel plane. In this plane the wave gauge was positioned along the line $y = 105$ cm, the OBS array was at $y = 150$ cm, and the EMCM array was at $y = 260$ cm from the zero reference for the SUPER-TANK coordinate system (Chapter 1). Cross-channel positions for the wave gauge, the OBS array, and the EMCM array were constant for the SUPERTANK project with the exception of the relocation of the EMCMs for the dedicated suspended sediment test, ST_BO.

For the two days of tests dedicated to investigating the sand cloud created under plunging breakers, all 33 OBS and four EMCMs were attached to a frame that was suspended underneath the carriage. Four stacked arrays of 7 to 9 sensors were spaced at intervals of 0.75 m, and the wave gauge was installed adjacent to the shoreward-most array.

Instrument characteristics

The specifications for the OBS in the mobile array are the same as those in the stationary OBS arrays described in Chapter 6. Signals from the five sensors in the mobile OBS array were recorded on the same system used for the stationary arrays.

For the wave gauge, zero and span adjustments allow this instrument to be used under a wide range of conditions. The analog output signal can be adjusted to a maximum of $\pm$ 5 V, and the still-water level can be set to read 0 V. The capacitance wave gauge output was transmitted to a personal computer (PC) operated by the researchers from the U.S. Naval Academy (Chapter 4). The computer contained a DAS-16 analog-to-digital (A/D) conversion board. The voltage data output from the capacitance wave gauge, collected at a sampling rate of 16 Hz, was immediately converted to free surface elevation (referenced to still-water level) and saved as a time series in ASCII format.

Experiment Procedures

Sequence of events

Before each run began, a cross-shore position was selected for the sensors on the carriage. Some of the factors that determined the positioning of the carriage were:

a. Breaker height.

b. Breaker type.

c. Wave period.

d. Shape of the bottom profile.

e. Objectives of the upcoming test.

Once the carriage was in position, the OBS array was lowered until the bottommost sensor was a few centimeters from the bed. All necessary electrical connections were made and the parameters characterizing the run were recorded in a logbook.

Data collection began approximately 45 sec before the wave generator was started, so that still-water offsets for the wave gauge and OBS array could be determined. The video camera was manually started at the beginning of the run and did not require any further adjustment. While the run was under way, the sensors could be monitored in real-time using graphical displays of their output.

After the wave generator was shut down at the end of each run, data were collected for an additional 45 sec to measure the wash load. The distance from the bed to the bottom of the OBS array was measured again. Once the sensor elevation was recorded, electrical connections were undone. The OBS array was raised to avoid other instruments or sandbars, and the carriage was moved to the seaward end of the channel in preparation for beach profile surveying.

Calibration and zero reference

Calibration of the OBS was accomplished by immersing the individual sensors into a tank containing a sand-water mixture. The mixture was stirred continuously, to promote uniform turbidity in the region of the sensor. Sensor data were collected starting at a relatively low concentration, from which a mean sensor reading could later be determined. A pump sample was then drawn from the tank, before sand was added to increase the concentration. This process was then repeated, incrementally increasing the concentration in the calibration tank. Each sample was decanted and the volume of water recorded. The concentration at each incremental level was determined by drying the sand and measuring the weight with a laboratory balance. With this information, the calibration parameters for the individual OBS were established. The OBS has been shown to be highly linear, so a simple regression analysis provided the gain and offset for each sensor. Table 7-1 and Figure 7-2 present the calibration constants and curves, respectively.

Table 7-1 Mobile OBS Array Calibration Constants		
SENSOR*	GAIN (g/ℓ/V)	OFFSET (g/ℓ)
AAA	49.83	3.32
BBB	16.81	-0.19
CCC	16.00	0.08
DDD	22.57	0.10
EEE	16.38	-0.14
* Sensor AAA is closest and sensor EEE is furthest from the bed.		
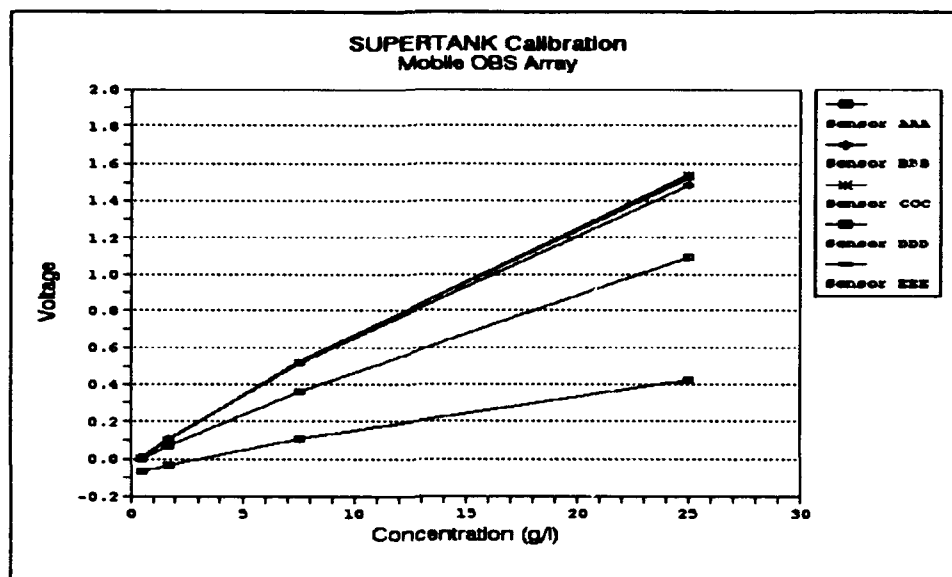
Figure 7-2. Calibration curves for mobile OBS array

Calibration of the capacitance wave gauge was a fairly simple process. Markings were made on the mast in 3-in. (7.6-cm) increments. The mast was then immersed in still water to the midpoint of the sensing lead, and a trim pot on the circuit board was adjusted so that the output was 0 V. A second trim pot allowed the gain to be adjusted to a chosen value of 0.1 V/in. (0.04 V/cm). The calibration was verified by immersing the sensing lead to different levels and measuring the output to ensure that the gain was constant over the length of the sensing lead.

Sampling and time reference

The sampling rate chosen for the mobile OBS array was 10 Hz (identical to that for the stationary OBS arrays). Ten samples per second was acceptable resolution for the changes in sand concentration and kept the size of the data records within the storage limitations of the PC used in data acquisition.

A computer time standard system was installed to link the PC to Coordinated Universal Time. The system consisted of a circuit board with a 10-Mhz radio receiver, a high-precision clock, and a powered antenna and cable. The clock was sampled with every data collection pass to ensure proper operation of the data collection system.

The capacitance wave gauge was sampled at a rate of 16 Hz. The A/D converter received a voltage in the ±5-V range, after which the voltage representation was converted to inches of displacement from the still-water level, prior to being saved to disk.

128

A computer time standard system similar to that in the OBS data collection system was installed in the computer used to collect all of the capacitance wave gauge signals. At the beginning of each run the clock was to be sampled to provide the exact time at which the data collection began. Using this initial time and assuming that the interval between samples was 1/16 sec, the time each data point was collected could be determined. Unfortunately, there was a problem with this procedure, and the time which appears in the header of the file is not the time of the first sample. An accurate method to determine the exact time at which data collection for the wave gauge began has not yet been identified.

Pre-processing and filtering. Hardware filtering of the OBS signal was performed to remove high-frequency electrical noise on the data lines. The A/D units, which represent the line voltage at the converter, were not processed in any way before being sampled and saved to disk.

Data Analysis

Reduction and interpretation methods

Original data files were written to the hard disk of a PC and then transferred to cartridge tapes. These files contained 35 columns of data. The first column was the time for each sample in seconds from midnight, and the second was a ground reference channel. The next 28 columns were data from stationary OBS arrays, and the final five channels were the data from the mobile OBS array.

The first step in the data reduction process was to convert the files from binary to ASCII format. Data for the mobile OBS array were then converted from A/D units to scientific units using the calibration constants presented in Table 7-1. The conversion was performed by: (a) dividing the raw data R (in A/D units) by 204.8 (volts per A/D unit), (b) multiplying by the gain G $(g/\ell/V)$, and (c) adding the offset O (g/ℓ). A mean background concentration C_B was determined from the data collected prior to the start of the run under still-water conditions using the above procedure. This mean background concentration was subtracted during the conversion procedure so that all sensors would have the same zero reference, so converted data are given by:

$$C(g/\ell) = G \frac{R}{204.8} + O - C_B \qquad (7\text{-}1)$$

Converted data files were created containing six columns of data, comprised of the time and the data from each of the five sensors in the mobile OBS array. These files had the same name as the raw data file with the extension changed to .CON, and the files were subsequently saved on a single tape.

Inspection of the time series plots revealed spikes in the OBS record created by single outlying points. It is believed these points were caused by noise on the data lines and not by rapid fluctuations in concentration. To remove outlying points, the data were filtered using a program which identifies the doubtful point and replaces it with a value interpolated from the adjacent data.

Basic statistics were calculated for the sensors in the mobile OBS array. The mean and standard deviation for each sensor are presented tabularly in a ledger file that accompanies each of the data files. Also included in the ledger file are instrument positions, start and stop times, and descriptive information.

Conversion of raw data from the capacitance wave gauge to scientific units was performed during the collection process. The software used to interface the gauges and the data collection system, LabTech Notebook, allowed for calibration constants and offsets to be updated prior to each run. Original wave gauge data files contain a header that provides information about the run and the column of wave gauge data. The original data files are in ASCII format and required no post-processing or reduction.

Data file format

Table 7-2 presents a 1-sec segment of the data file A1314AOB.CON. These data have been converted according to Equation 7-1, and no filtering has been performed. The first column is the time in seconds from midnight Pacific Daylight Time. For example, 53070.0 sec from midnight is 14:44:30.0 on the 24-hr clock. The second, third, fourth, fifth, and sixth columns are converted data for sensors AAA, BBB, CCC, DDD, and EEE, respectively. Figure 7-3 graphically presents a 15-sec segment of sensor AAA output from the file A1314AOB.CON. The 1-sec segment of data presented in Table 7-2 is contained within this larger segment.

Table 7-2 Sample of Converted, Raw Data					
	C, g/l				
Time, sec	AAA	BBB	CCC	DDD	EEE
53070.0	3.95623	2.87198	3.59375	2.87415	2.87850
53070.1	4.44285	4.43150	3.20313	2.87415	1.99871
53070.2	43.37254	4.67774	5.31250	1.55169	1.11893
53070.3	5.17278	3.03614	4.45313	1.66189	1.75877
53070.4	3.46961	2.70782	2.42188	2.21292	1.35887
53070.5	2.98299	2.78990	2.57813	1.99251	1.43885
53070.6	2.98299	2.87198	2.96875	2.98435	1.59881
53070.7	2.98299	2.46158	2.42188	2.76394	1.51883
53070.8	2.49637	2.87198	2.57813	2.43333	1.43885
53070.9	3.46961	4.02110	2.96875	3.86599	2.15867

Data Filtering

The third value in the second column of Table 7-2, is an order of magnitude greater than the neighboring values. It is not sensible that the concentration should increase by an order of magnitude and then decrease by the same in two-tenths of a second. This is even less realistic considering the behavior of the surrounding data, as well as the corresponding data from the other sensors. In Table 7-3, this point has been replaced with a value interpolated from the neighboring data. Figure 7-4 graphically presents the filtered version of the 15-sec segment of data presented in Figure 7-3. The 1-sec segment of data presented in Table 7-3 is contained within this larger segment.

Table 7-3					
Sample of Converted, Filtered Data					
Time, sec	C, g/l				
	AAA	BBB	CCC	DDD	EEE
53070.0	3.9550	2.8584	3.5655	2.8349	2.8472
53070.1	4.4216	4.2038	3.1923	2.8602	2.0022
53070.2	3.5847	4.5529	4.5344	1.6225	1.1904
53070.3	5.0068	3.0332	4.4030	1.6577	1.7500
53070.4	3.4773	2.6959	2.5800	2.1973	1.3543
53070.5	2.9845	2.7767	2.5691	1.9870	1.4331
53070.6	2.9830	2.8585	2.9539	2.8800	1.5926
53070.7	2.9830	2.4492	2.4126	2.7534	1.5130
53070.8	2.5000	2.8571	2.5672	2.4278	1.4331
53070.9	3.4579	3.9047	2.9483	3.5656	2.1172

Summary of data characteristics

Each of the data files for the mobile OBS array has an associated ledger file which contains run information, statistics, and sensor positions. Table 7-4 is a sample ledger file for Run A1314AOB and contains information about the converted, filtered file presented above.

The first line of the ledger file identifies the run and is followed by the SUPERTANK test number, wave generator file, and a short description of the test. Test conditions are presented in the second section of the ledger file. Design wave heights ranged from 0.2 to 1 m and the periods ranged between 3 and 10 sec for both random and regular wave conditions. Start and stop times found in the ledger file provide the interval of wave generation during which the OBS sensors were collecting data. This is the segment of data used to determine concentration statistics.

Instrument positions were measured in feet from the channel origin. English Units were chosen as the convention because the wave channel was originally designed using this system. The mean and standard deviation for

131
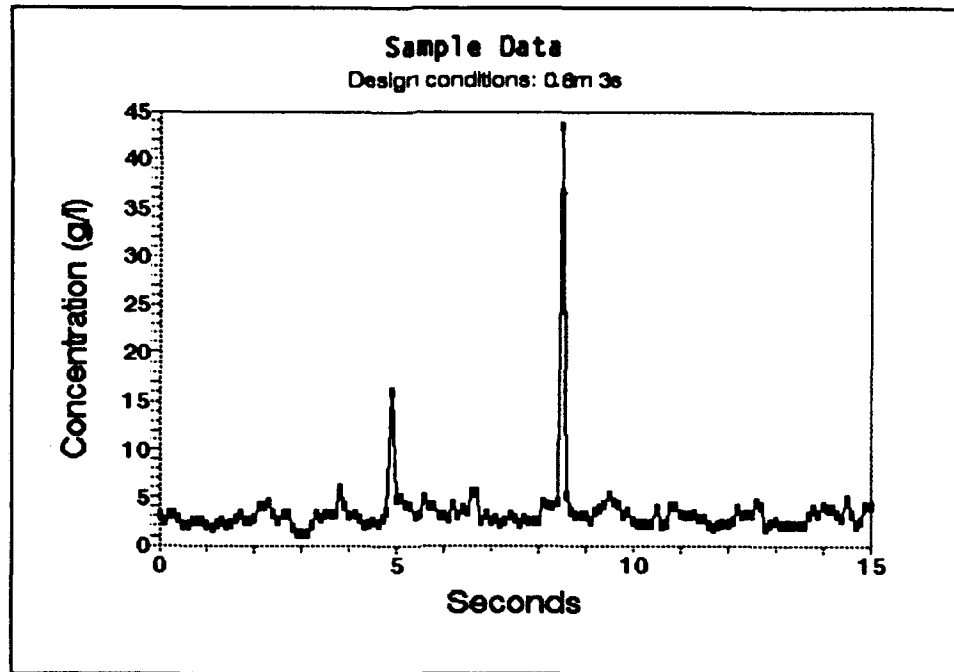
Figure 7-3. Sample converted, raw OBS data
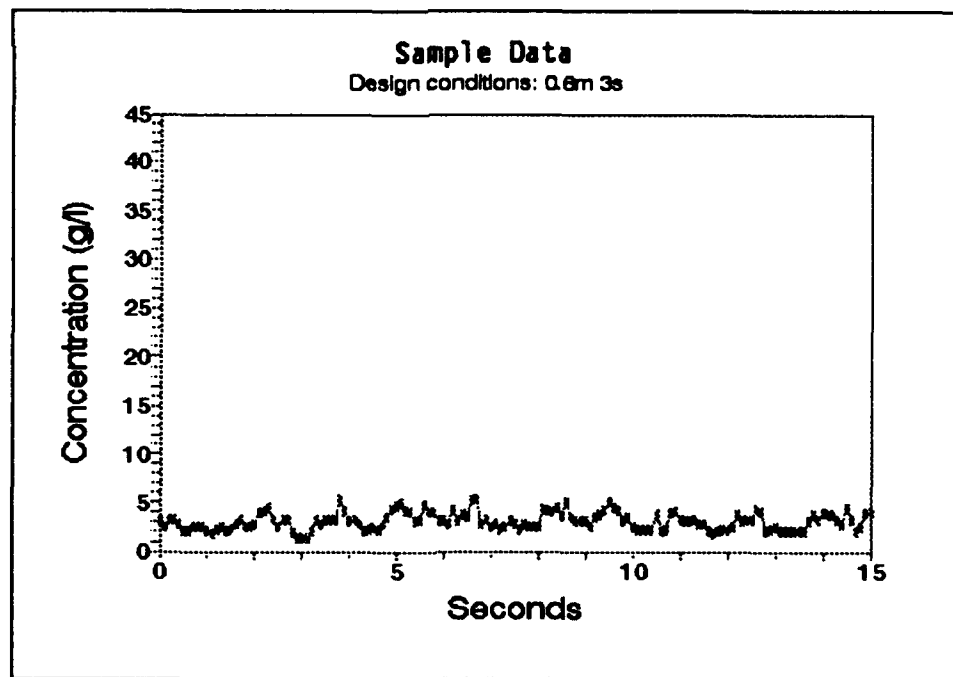
Figure 7-4. Sample converted, filtered OBS data

each of the five sensors in the mobile OBS array is tabulated along with the sensor distances from the bed, measured before and after the run.

Identification of marginal data sets

The carriage was used in a total of 212 runs; however, for 44 of the runs no OBS data were collected. For three of the 212 runs no wave gauge data were collected. In general, during the runs for which no OBS data were collected, the sensors were being calibrated, or the OBS were being prepared for special tests.

The usefulness/validity of the data from several of the runs may be questioned in instances where problems were encountered. However, sections of these marginal data files may be recoverable. Table 7-5 identifies these marginal data sets and the problems encountered.

Table 7-4
OBS Data Ledger File

RUN IDENTIFICATION : A1314AOB

Test Number : ST_20
Wave File   : A1209A
Description : Acoustic Profilers

TEST CONDITIONS
Wave Height : 0.6 m
Wave Period : 3.0 sec
Wave Type   : REGULAR

START TIME : 14:44:00.0
STOP TIME   : 14:50:00.0

INSTRUMENT POSITIONS
OBS Array : 101.50 ft
Wave Gauge : 101.67 ft

	AAA	BBB	CCC	DDD	EEE
Mean (g/ℓ)	3.38	2.77	2.41	1.89	1.61
STD DEV (g/ℓ)	1.54	1.14	0.97	0.89	0.77
SENSOR DISTANCES FROM THE BED					
Initial (cm)	6.9	10.7	14.5	22.1	29.7
Final (cm)	6.9	10.7	14.5	22.1	29.7

Table 7-5
Marginal Data Sets

RUN ID	Problem Encountered
A0509A	Capacitance wave gauge not operating properly
A0613A	Problem with OBS data collection software
A0814A	Sensor EEE in mobile OBS array exposed periodically
A0912A	Mobile OBS array not positioned correctly until 12:58:00
S0409B	Problem with the coordinated time in the OBS data file
S0508A	Initial distance from the bed of the mobile OBS array may be incorrect (corrected after 09:02:00)
S1309A	Mobile OBS array - beam axis parallel to flow
S1310A	Mobile OBS array - beam axis parallel to flow
S1311A	Mobile OBS array - beam axis parallel to flow

Summary

Review of experiments and results

During the SUPERTANK Laboratory Data Collection Project a mobile carriage was used to deploy a variety of instruments across the outer surf zone, with emphasis on documenting sediment suspension in the initial stages of wave breaking. For the majority of experiments conducted, data from a vertical array of five OBS, a vertical array of four EMCMs, and a capacitance wave gauge were collected, and test conditions were recorded on videotape. In addition, a two-day series of tests, dedicated to the collection of data in the sand cloud created by plunging breakers, was conducted using a matrix of 33 tightly spaced OBS.

Initial analysis of the carriage data shows that there is a strong cross-shore gradient in suspended sand load in passing along the channel from the region of incipient breaking into the surf zone. This gradient is accompanied by remarkable change in the behavior of the time series of sediment concentration from an oscillatory signal outside the breakpoint to one comprised of irregular events superimposed on a mean load in the zone landward of initial breaking. The structure of the vertical profile of mean concentration also shifts from its classical exponential shape seaward of breaking to a more linear distribution in the surf zone, and in some cases even inverts.

Recommendations

Sand concentration data from the carriage should be subjected to both statistical and spectral analyses. Up/downcrossing analysis would be meaningful for records that displayed an oscillatory behavior (i.e., outside the turbulent zone), whereas threshold-crossing/duration techniques should be used to characterize suspension events inside the surf zone. Attempts to correlate total suspended load with breaking wave parameters such as breaker height or Irribarren Number should also be attempted.

In future laboratory investigations, it is recommended that some means of measuring the local near-bed turbulence be incorporated. This was the one important parameter that was not measured during SUPERTANK. Use of a laser-Doppler or hot-film velocimeter should be explored. It is also recommended that the mobile array be used to traverse the entire surf zone, collecting data at high cross-shore resolution to better distinguish zones of high suspended load. Including a sonic concentration profiler on the carriage would also be extremely useful for side-by-side comparison and augmentation of the OBS data, especially in regions of low aeration.

Acknowledgements

References

Beach, R. A. (1989). "Suspended sediment transport in the surf zone," Ph.D. diss., Univ. of Washington, Seattle, WA.

Beach, R. A., and Sternberg, R. W. (1988). "Suspended sediment transport in the surf zone: Response to cross-shore infragravity motion," *Marine Geology* 80, 61-79.

Coakley, J. P., Savile, H. A., Pedrosa, M., and Larocque, M. (1978). "Sled system for profiling suspended littoral drift." *Proc. 16th Coastal Engrg. Conf.* ASCE, New York, NY, 1764-75.

Downing, J. P., Sternberg, R.W., and Lister, C.R.B. (1981). "New instrumentation for the investigation of sediment suspension processes in the shallow marine environment," *Marine Geology* 42, 19-34.

Fairchild, J. C. (1974). "Longshore transport of suspended sediment." *Proc. 13th Coastal Engrg. Conf.* ASCE, New York, NY, 1069-88.

Hanes, D. (1988). "Intermittent sediment suspension and its implications to sand tracer dispersal in wave dominated environments," *J. of Geology* 81, 175-83.

Kana, T. W. (1979). "Suspended sediment in breaking waves," Tech. Rep. No. 18-CRD, Univ. of South Carolina, Columbia, SC.

Kennedy, J. F., Erlich, R., and Kana, T. W. (1981). "The non-normal distribution of intermittent suspension of sediments below breaking waves," *J. of Sedimentary Petrology* 51, 1103-8.

Kraus, N. C. (1987). "Application of portable traps for obtaining point measurements of sediment transport rates in the surf zone," *J. Coastal Res.* 3(2), 139-52.

Nielsen, P., Green, M. O., and Coffey, F. C. (1982). "Suspended sediment under waves," Coastal Studies Unit Tech. Rep. No. 82/6, Univ. of Sydney, Sydney, Australia.

Shibayama, T., and Horikawa, K. (1982). "Sediment suspension due to breaking waves," *Coastal Engrg. in Japan* 25, 164-76.

Sternberg, R. W., Shi, N. C., and Downing J. P. (1984). "Field investigations of suspended sediment in the nearshore zone." *Proc. 19th Coastal Engrg. Conf.* ASCE, New York, NY, 1782-97.

Watts, G. M. (1953). "Field investigations of suspended sediment in the surf zone." *Proc. 4th Coastal Engrg. Conf.* New York, NY, 181-99.

8 Acoustic Doppler Current Profiler Measurements at SUPERTANK[1]

Introduction

Background

The participation of RD Flow in the SUPERTANK Laboratory Data Collection Project was part of a long-term program to study the relationship between acoustic backscatter and suspended sediment concentration. The focus of this program, the PLUmes MEasurement System (PLUMES) (Kraus, Thevenot, and Lohrmann 1992), concerns the objective of detecting and monitoring the long-term fate of dredged material after ocean discharge. The SUPERTANK project provided an excellent testing ground to determine the appropriate implementation of acoustics to serve this purpose.

The use of acoustics is motivated by its profiling capability and its remote sensing character. The profiling capability is important because suspension phenomena exhibit strong vertical gradients that are difficult to resolve with single-point measurement devices. Also, the vertical location of interest may change, either because the bottom elevation changes (as in SUPERTANK) or because the plume of suspended material is moving. The remote sensing character is important to avoid disturbances in the flow field. This is especially true in the highly dynamic regime simulated in the SUPERTANK project.

Objectives

The objectives of the Acoustic Doppler Current Profiler (ADCP) measurements at SUPERTANK were:

---

[1] Written by Atle Lohrmann and Craig A. Huhta, SonTek, Inc.

a. Provide background velocity data for the deep end of the wave channel, the "offshore" region.

b. Increase understanding of how acoustic systems must be designed and operated to extract information about the concentration of suspended sediment, resuspension events, and near-bottom transport. Several special equipment tests were made during the experiment as part of this objective.

c. Evaluate the performance characteristics of a newly developed 2.4-Mhz Broadband Acoustic Doppler Current Profiler (BB-ADCP). This included the capability of the instrument to measure turbulent quantities (e.g., $<u'^2>$, $<w'^2>$, and $<u'w'>$, where u' and w' are the horizontal and vertical turbulent velocities and triangular brackets denote time averages) as well as an assessment of its feasibility as a tool to resolve and quantify highly dynamic sediment transport processes such as resuspension.

Scope

It is emphasized that the instrumentation and data sampling strategies were of an experimental nature. As could be expected, some of these elements were not as successful as desired, and, in hindsight, the project served as a rude awakening to the highly dynamic flow regime found in the nearshore region. First, the variation in the acoustic signal strength (5 to 6 orders of magnitude) greatly exceeded expectations. Second, the BB-ADCP was found to have its own set of problems caused by the large wave orbital accelerations.

As a result, the wealth of information gathered during the project has primarily been used as an instructive lesson in instrument design for dynamic flow regimes. The analysis of data has had direct impact on instrument design and implementation, both for current meters and acoustic backscatter profilers.

The impact of the data on instrument design is not addressed in this report. Instead, emphasis is placed on objective (*a*), the average conditions in the offshore region of the wave channel. Data were collected for the first 2 weeks of the SUPERTANK project and cover both erosive and accretionary conditions. The *Experiment Apparatus* section describes the equipment being used, its physical configuration, and its location in the channel. The *Experiment Procedures* section discusses the range normalization of the backscatter data and findings that have implications for the interpretation of the velocity data. The *Data Analysis* section contains a description of the data analysis. The final section contains the summary. As an additional reference, Appendix H includes: a complete listing of all the data files, one sample set of 2.4-Mhz data from each run, and a personal-computer- (PC-) based conversion program for reading and separating the binary data files. All data files are stored on two magnetic tapes and can be retrieved on a PC-based Colora-

138

do Memory Systems QFA-700 tape drive. The data tapes and a tape drive are stored at the U.S. Army Engineer Waterways Experiment Station.

Experiment Apparatus

Instrument description

RD Flow operated two acoustic systems during the first 2 weeks of SUPERTANK. One system was a prototype of an off-the-shelf instrument designed primarily for water velocity measurements. The second was an experimental system built from modules procured individually. The two systems were not equivalent; the return echo, for example, was processed quite differently.

Instrument 1. A 2.4-MHz prototype BB-ADCP measured the acoustic backscatter and the radial velocity component along multiple acoustic beams. In SUPERTANK, the BB-ADCP had three operating beams: one vertical beam and two beams slanted 30 deg (0.52 rad) from the vertical. One of the slanted beams pointed onshore and one pointed offshore (Figure 8-1). The radial velocity components measured along each beam were used to form spatially averaged estimates of the along-channel velocity component u and the vertical velocity component w. The measurements were made at a series of vertical levels spaced 8 cm apart.
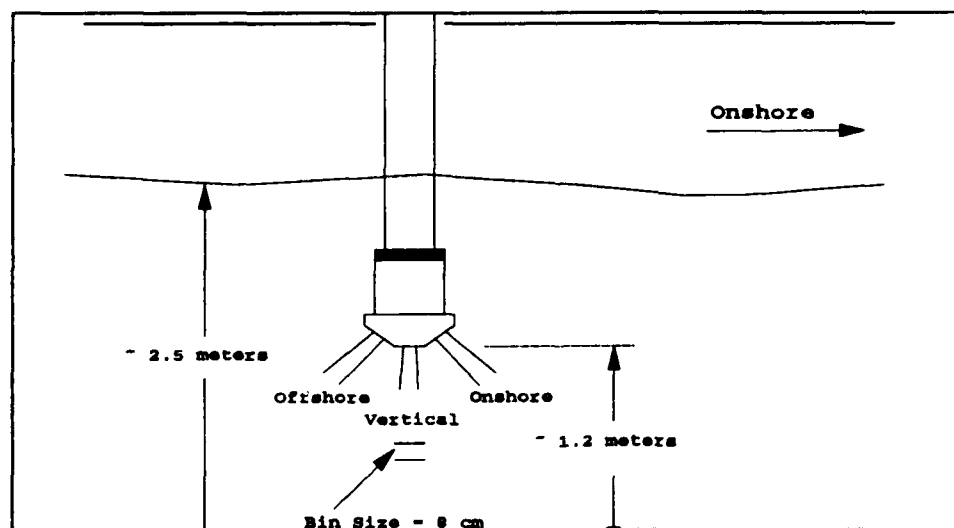
Figure 8-1. Orientation of the three-beam BB-ADCP

As the name indicates, the BB-ADCP is distinguished from other ADCPs by having a higher acoustic and processing bandwidth. Roughly speaking, this improvement translates into a better vertical resolution.

Instrument 2. The second system was a single-beam, 600-kHz transducer looking straight down. The system was built as a purely experimental tool and was employed to detect rapid changes in the concentration of suspended particles. The system consists of a large-bandwidth acoustic transducer, transmit and timing circuitry, a pre-amplifier, and an analog-to-digital (A/D) converter. This setup allows considerable flexibility in data collection strategy, and it was used to investigate both the scatter from the water column and to test velocity-measuring algorithms.

Location

RD Flow operated in the offshore region of the wave channel, near instruments operated by the University of Florida (UF), Ohio State University (OSU), and Quest Integrated, Inc. The 2.4-MHz and 600-kHz systems were attached in the middle of a mobile carriage mounted on top of the channel walls (Figure 8-2). OSU mounted their instrument array on the onshore side of the carriage. UF and Quest mounted their instruments to the channel walls. Between each run, and sometimes within a run, the carriage was moved to different locations within the offshore region and aligned with either of the two instrument groups fixed to the wall.
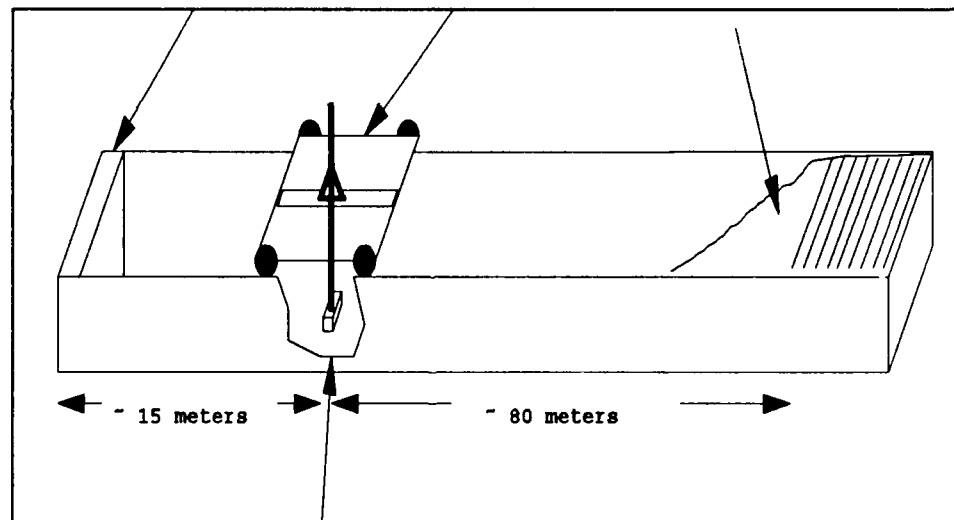
Figure 8-2. Position of the offshore instrument carriage

The two acoustic instruments were mounted in a frame attached to a vertical pole mounted through the center of the carriage. The two instruments were located approximately 1.0 m below the water level. Depending on the exact lateral position, the distance to the bottom was 1.0 to 1.2 m. The pole was secured with guide wires to prevent movement during wave action.

Figure 8-3 shows the relative position of the offshore instrument arrays. The Benthic Acoustic Stress Sensor and Profilometer systems operated by

140
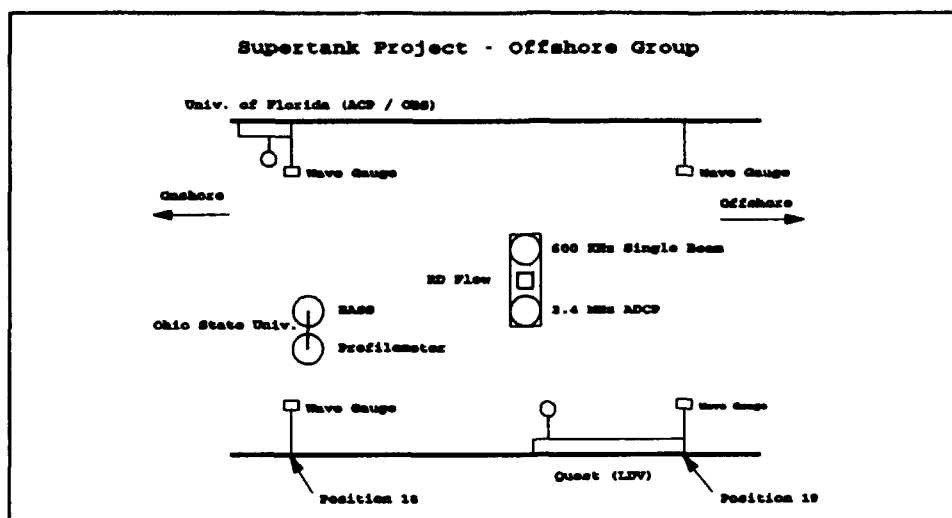
Figure 8-3. The relative position of offshore instruments

OSU were mounted on the mobile carriage, approximately 1 m shoreward of the center pole. Appendix H (contained in Volume II of this report) includes a figure showing the six locations where data were collected and the relative instrument alignments resulting from each location. The file listings in the appendix include the position of the instruments for each file.

Instrument Characteristics

Instrument 1. The 2.4-MHz system processes the data for both velocity and amplitude information. In the configuration used in SUPERTANK, the system had three operational transducers, each with a ceramic diameter of 3.18 cm. The total dynamic range is approximately 70 db.

The acoustic return signals from the 2.4-MHz transducers are fed into a pre-amplifier and then processed using a logarithmic amplifier (Signetics SA 604). The amplifier has two outputs: a hard-limited signal that preserves the phase information of the input and a Receive Signal Strength Indicator (RSSI). The first output is used to calculate the Doppler shift. The RSSI is a 0- to 5-V signal that is proportional to the logarithm (base 10) of the filtered input signal. The RSSI is low-pass filtered twice. The time constant of the filters is 50 μsec, equivalent to a 4-cm propagation distance. After filtering, the output signal is fed into an 8-bit A/D converter (0-255 "counts") and recorded. The sampling rate is set such that the vertical resolution in the RSSI data is roughly 2 cm.

The response of the logarithmic amplifier was calibrated by feeding a signal directly into the receiver and monitoring the output, as the input level changed. The calibration curve is shown in Figure 8-4. The input has units of decibels and is referred to a 1-V reference signal. A least-squares fit gives
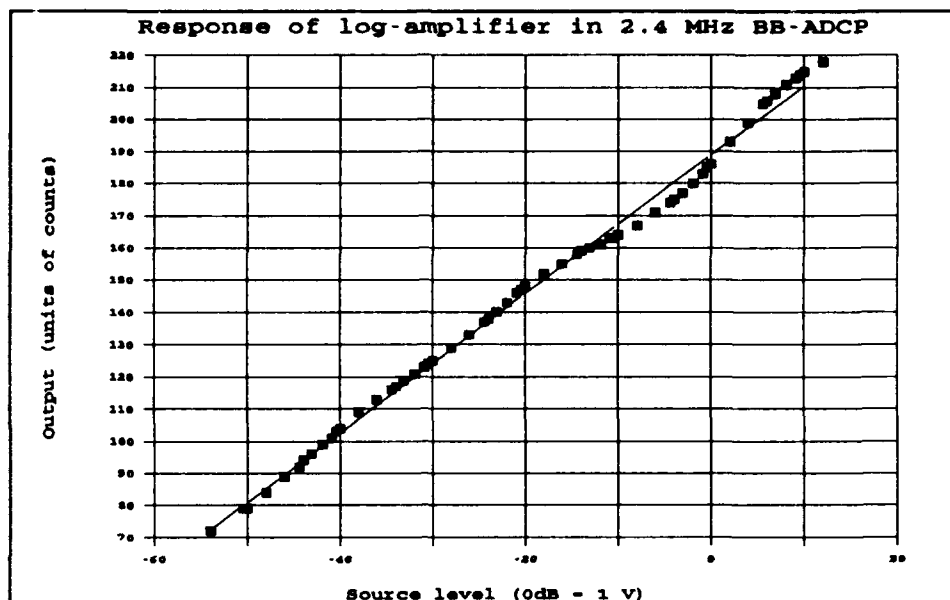
Figure 8-4. The RSSI output as a function of source level. The coefficients derived in Equation 8-1 are based on linear regression.

the following coefficients for a linear regression:

$$db = counts*0.46 + constant \tag{8-1}$$

The response of the log amplifier is close to linear over the full range. The maximum deviation observed in Figure 8-4 is 2 db in the range between 170 and 180 counts.

Instrument 2. The 600-kHz system uses a single transducer with a diameter of 10.16 cm. It processes all information linearly, with about 42 db of instantaneous dynamic range in any one configuration, and a total range of approximately 100 db. To use the full dynamic range, the system must be stopped and restarted.

Signal processing in the 600-kHz system provides considerable flexibility. The return signal from the transducer is fed into a linear pre-amplifier, providing between 0 and 50 db of gain. The pre-amplifier gain is software selectable before each data collection period. After amplification, the signal is fed into an 8-bit analog-to-digital (A/D) converter, sampling at 5 MHz. The output from the A/D is stored directly onto the computer hard drive. The high sampling rate allows for complete resolution of the return signal and considerable flexibility in post-processing. It is also computationally intensive, producing as much as 12 KB/sec. Backscatter from the water column and from the bottom cannot be resolved within a single ping since the difference in scattering strength exceeds the instantaneous dynamic range of 42 db.

142

To reference all the data collected with the 600-kHz system to a common level, an accurate calibration of the pre-amplifier must be obtained. This was done using a transmit hydrophone (Model E27) from the Naval Research Laboratory. The hydrophone transmits signals of known power, and the output from the 600-kHz system was recorded for different pre-amplifier gain settings. The gain was set to a value between 28 and 115, and the value determines the driving voltage for the amplifier. Limits on gain settings are determined by the power requirements and saturation limits of the circuit. Figure 8-5 shows the calibration curve for the pre-amplifier. Using this curve, all the 600-kHz data can be referenced to a common level even if the data were collected at different pre-amplifier settings. The curve shows strong changes in gain at lower settings and levels off as the setting approaches saturation.
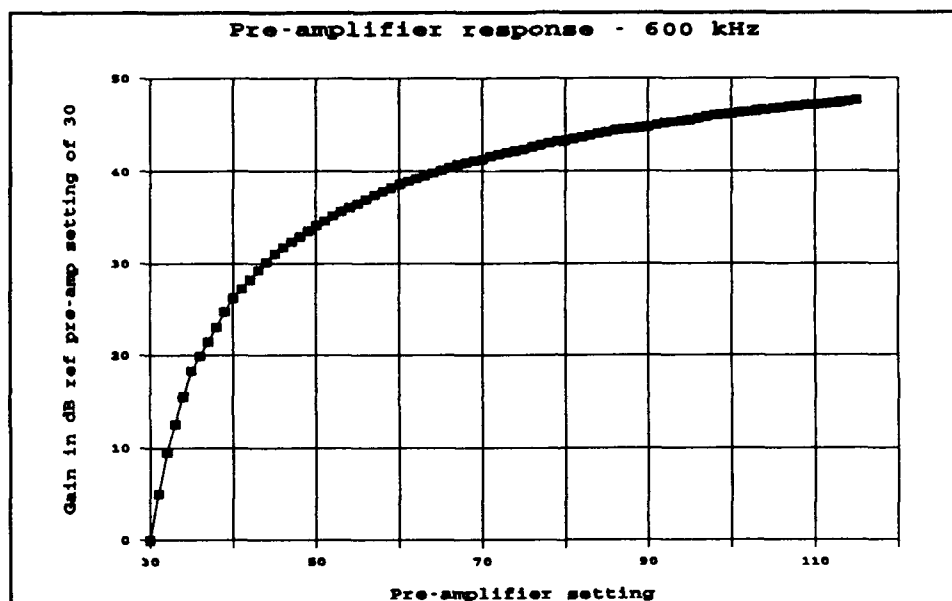
Figure 8-5. Calibration of 600 kHz pre-amplifier

In addition to the pre-amplifier, the sensitivity of the A/D board can be varied. For this project, three different settings were used, and sensitivity is shown in Table 8-1. All tests indicate that the A/D board has a linear response over the range of signals used.

Table 8-1 8-bit A/D Converter Sensitivity	
A/D Gain Setting	Input Voltage Sensitivity
0	1 mV/bit
1	2 mV/bit
2	5 mV/bit

Table 8-2 provides a summary of the properties of the two systems. This includes transducer dimensions and frequency, parameters of the two receivers, and typical pulsing schemes used. Additionally, the last two categories show the orientation of the two systems (horizontal or vertical profiling) and the goals of each mounting arrangement.

Table 8-2
Overview of the 600-kHz and the 2.4-MHz Systems Used During SUPERTANK

	600-kHz System	2.4-MHz BB-ADCP
Transmit Frequency	614,400 Hz	2,457,600 Hz
Transducer Diameter	10.16 cm	3.175 cm
Transducer/Receiver Bandwidth	70-80 percent	7-8 percent
Resolution (Sampling)	0.16 mm (5 MHz)	20 mm
Resolution (Filtering)	1.6 mm (500 kHz)	40 mm (20 kHz)
Resolution (Transmit pulse)	2.5 mm (2λ)	5 mm (16λ)
Minimum Operating Distance	0.50 m	0.25-0.3 m
Typical X-mit Pulses	a) 2.5 mm (minimum) b) 8.5 cm	a) 5 mm (minimum) b) 50 mm
Vertical Operation	a) Intercomparison	a) Velocity profiles b) Monitor sediment suspension
Horizontal Operation	Model transmission losses	not used

Experiment Procedures

Sequence of events

Data collection was normally initiated 30 to 60 sec before the first waves became apparent in the velocity data. In a standard run, data were collected with both instruments and in several different configurations. Only rarely was a continuous record collected for the full duration of the run. In most cases, data collection was stopped in the middle of a run and the carriage realigned with another offshore instrument group. Data recording was normally monitored continuously during the run.

Calibration and zero reference

The acoustic instruments are not calibrated in the common sense of the word, i.e., by finding precise estimates of one or two coefficients. Raw data are not immediately meaningful, but must be processed substantially before physical interpretations are possible.

Range normalization of backscatter data. As stated in the introduction, acoustic techniques have obvious advantages over single-point measurement methods because they are both profiling and non-intrusive. The profiling capability, however, makes the measurement more complex because the strength of the outward propagating pulse is reduced as it propagates through the water column. This variation in incident energy must be accounted for before the data can be analyzed. This is referred to as range normalization of the data.

Raw acoustic backscatter data, hereafter referred to as echo level (EL), were collected with both acoustic systems throughout the first 2 weeks of wave action at SUPERTANK. The uncorrected echo level varies as a function of depth even if the concentration is constant along the path of the acoustic pulse. Range normalization includes the following elements:

a. Water absorption.

b. Geometrical spreading.

c. Attenuation due to particles in the water column.

The first part, water absorption, can be accounted for by adding a linear term (in logarithmic units) to the echo level. The magnitude of the coefficient is determined mainly by the acoustic frequency but varies with water temperature and salinity.

The second part of the range normalization, geometrical spreading, is simple when the acoustic scattering volume is located in the acoustic far field, defined as the volume beyond the Rayleigh distance $r=\lambda^2/d$, where d is the diameter of the transducer and λ is the acoustic wave length. For the 600-kHz and the 2.4-MHz systems, this distance is about 4.0 and 1.5 m, respectively. In SUPERTANK, the distance from the transducers to the bottom was 1 to 1.2 m, and all the data were collected in the near field. A numerical model must be used to correct for spreading effects. The model is described in Ma, Vardan, and Vardan (1987), and the results for the 2.4-MHz system are shown in Figure 8-6.

It is difficult to correctly account for attenuation provided by particles in the water column. This is especially true when the suspended concentration is high and a combination of fine and coarse particles are present. To correctly estimate the attenuation, we ideally need to know the suspended load as a function of particle size. Since this is not possible, the attenuation can be estimated using the following information:

a. A good model for attenuation as a function of relative particle size must be used. Such a model is established (Flammer 1962).

b. The measured bottom echo will vary as a function of the integrated attenuation. In the case of the SUPERTANK project, it can be assumed that the attenuation is low before a run is started. This information can be used to constrain the system of coupled equations.

c. The system can be constrained by imposing physical constraints. The mean concentration, for example, can be required to increase toward the bottom.

d. A model of particle distribution as a function of depth can be included.
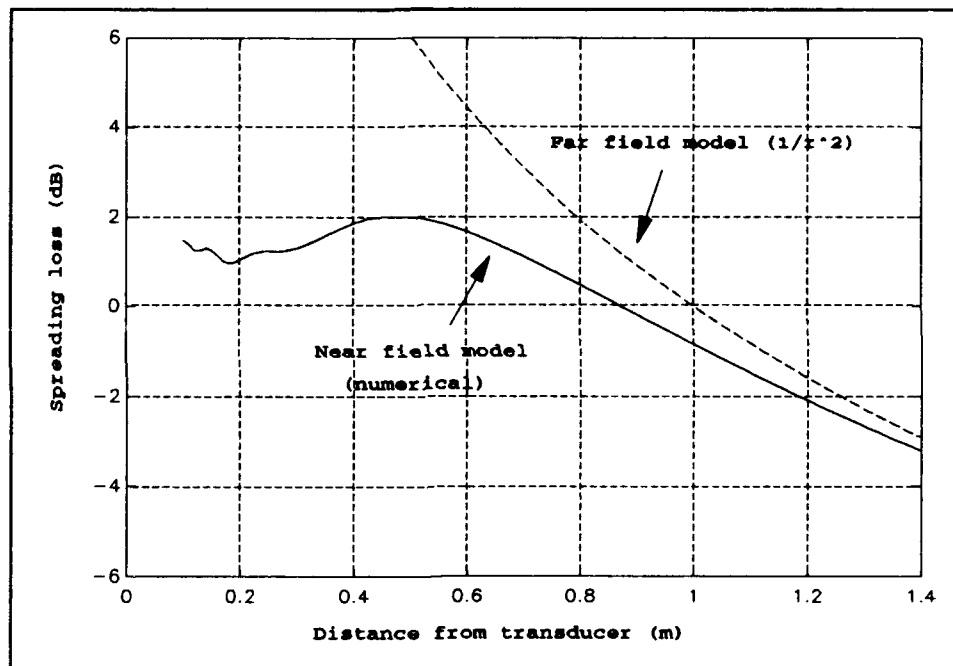
Figure 8-6. Spreading models for the 2.4-MHz system. The near-field model was applied to the data shown in Appendix H

In practice, steps (*a*)-(*d*) require substantial work as well as hardware that can measure all the pertinent parameters. The 2.4-MHz system fails in this regard because of the strongly filtered output. For the data in Appendix H, we have limited the correction to a fixed value of 2.8 db/m (one-way) for the combined effect of particle attenuation and water absorption.

Velocity measurements. The 2.4-MHz BB-ADCP was calibrated at the tow tank at Memorial University, Newfoundland, after the SUPERTANK project was completed. Tow carriage velocities were adjustable from 1 to 200 cm/sec. In the short-range mode (see pre-processing and filtering) used

146

during the project, the horizontal velocity matched within 2 percent of the carriage velocity. The time delay has little effect on the validity of the calibration because there are no individual parts or elements in acoustic Doppler systems that have significant "drift."

Sampling and time reference

Two types of data files were collected with the 2.4-MHz BB-ADCP. The first is based on single ping velocity estimates, recorded at approximately 1.8 Hz. The other file contains data that are averaged over 20 or 50 pings, recording one average profile every 3 to 8 sec.

The 600-kHz system collected three different types of data files. The first contains raw data from individual pings recorded at a rate of approximately 6 Hz. These pings alternate between short pulses (two carrier cycles) and longer coded pulses (34 carrier cycles). Due to the large amount of data collected in this mode (typically 12 KB/sec), these files were generally only collected over 2-min intervals. In the second configuration for the 600-kHz system, time-averaged root-mean-square values of the signal were recorded. The signal was averaged over a 40-sec interval, using a short pulse, and each rms file covers approximately 8 min. In the third mode, various pulse combinations were tried for later experimentation with Doppler calculations. Appendix H contains a complete list of file naming conventions, for both systems, as well as a list of files recorded with each wave set.

The computer operating the 600-kHz unit was hooked up to a UTC satellite receiver. This receiver continuously updates the computer clock from information contained in the satellite transmissions. The computer clock is subsequently used to tag the data files. The time was also transmitted over the serial line at regular intervals to update the clock in the computer operating the 2.4-MHz BB-ADCP. The clock in the computer operating the 2.4-MHz system was noted to drift 1 to 5 sec over a 1-hr run. The time was thus not synchronized as well as hoped for.

Pre-processing and filtering

The BB-ADCP measures the velocity by measuring the phase shift of the echo from two or more transmit bursts. In "short-range mode" (or pulse-to-pulse coherent mode), the second pulse is transmitted after the first pulse has died down, leading to a velocity estimate with low statistical uncertainty. Through a series of algebraic manipulations, along-beam velocities can then be used to measure the vertical profile of turbulent kinetic energy and of Reynolds stress (Lohrmann, Hackett, and Roed 1990).

Due to the inherent problem of measuring phase changes larger than $\pm \pi$ ("wrap-around" or "ambiguity problems"), the measurement scheme required to operate in short-range mode is complicated and requires pre-processing to

resolve the correct phase change. For the SUPERTANK project, this meant transmitting a series of pulses with increasing separation and decreasing unambiguous velocity range. Under the assumption of quasi-stationary conditions during this burst of "micro-pings," the correct velocity can be resolved even for the last pulse-pair -- which has the desired characteristics of low statistical uncertainty.

Data Analysis

Analysis and interpretation methods for data presented in Appendix H

The 2.4-MHz BB-ADCP collected profiles of along-beam velocities as well as profiles of relative acoustic scattering strength. The horizontal velocity u was calculated by combining the Doppler measurements along two opposing beams slanted 30 deg with respect to the vertical. The vertical velocity w and the relative scattering strength EL were obtained directly from the third beam pointing straight down between the two slanted beams.

Each profile of u, w, and EL was recorded at regularly spaced intervals. The depth intervals and the distance from the transducers to the first depth cell were kept constant through the project and are given in Table 8-3. There is a difference in cell position between the u and w components because the slanted beams are used to calculate u and the vertical beam is used to calculate w. Backscatter strength was sampled four times faster than velocity.

Table 8-3 Position of Depth Cells for Different Data Types			
	u	*w*	*EL*
Position of first depth cell	26.6 cm	30.8 cm	18.2 cm
Vertical extent of depth cell	6.9 cm	8.0 cm	1.9 cm

Velocity data. Velocity data were pre-processed to resolve ambiguity errors. Where this pre-processing failed, post-processing was used to retrieve the correct velocity. For single-ping data, the retrieval procedure was successful for most of the runs.

Four plots (see Appendix H, contained in Volume II of this report) have been generated for each run. Each plot shows an aspect of the velocity statistics during a 5-min interval. In all plots, u (positive toward the beach) is shown as a solid line and w is shown as a dashed line. Table H1 includes the start time and the length of the data segment used to generate the plots. The four velocity plots are:

148

a. Mean horizontal velocity profile over the averaging period.

b. Largest magnitude of *u* and *w* velocity over the measurement interval.

c. Profile of standard deviation of *u* and *w* components. This profile is a measure of the wave energy as a function of depth.

d. Power spectra of *u* and *w* shown at middepth. The spectra are averaged over three adjacent bins located midway between the transducers and the bottom.

Backscatter data. Range normalized backscatter data are presented in units of decibels relative to the background noise level. Before computing statistics, data were range normalized as described in *Experiment Procedures*. After applying the corrections for water absorption and for geometrical spreading, the resulting profiles still seemed to contain a loss term that was linear with range. The most likely explanation for this loss is scattering and/or viscous particle attenuation. A fixed value of particle attenuation of 1.3 db/m (one-way) removed most of this trend and subsequently was applied to all the data presented in Appendix H (contained in Volume II of this report). For each run, three backscatter plots were generated for the same time intervals as the velocity plots:

a. Profile of minimum (dashed), mean (solid), and maximum (dash-dot) range normalized scatter strength.

b. Standard deviation of the scattering strength over the 5-min measurement interval. These numbers represent the sum of natural variations in the amount of suspended material and a fixed contribution from purely statistical effects.

c. Power spectra of the scattering strength recorded 5 cm (solid), 10 cm (dashed), and 30 cm (dash-dot) above the bottom.

Data file format

Both 600-kHz data and 2.4-MHz data were recorded in a binary file format with a rather large and complex format. Source code and executable programs for decoding and conversion to ASCII are available along with the data tapes from the U.S. Army Engineer Waterways Experiment Station, from RD Instruments San Diego, CA, or from SonTek, Inc., San Diego, CA.

Identification of marginal data sets

Instrument 1. To make the short-range mode work for the 2.4-MHz BB-ADCP, all hardware and software modules must work well to achieve good quality data. Unfortunately, this was not the case. The 2.4-MHz BB-

ADCP had two specific problems: electrical cross-coupling between the conductors in the cable between the transducer head and the electronics, and a significant velocity bias error at short pulse separation. These errors led to the breakdown of the velocity resolution scheme (*Experiment Procedures -- Pre-processing and filtering*) in highly dynamic conditions or when the horizontal velocity was 50 cm/sec or above. For single-ping data files, the data are partly recoverable through ambiguity resolution methods that can be applied in post-processing. Multiple-ping data are unrecoverable.

Instrument 2. The main problem with the 600-kHz data was the lack of adequate instantaneous dynamic range. Many of the wave runs contain data that far exceed the 42-db range in the 5-cm layer close to the bottom. The output saturated the system and the data are not fully recoverable for the most dynamic events.

Summary

Review of experiments and results

The objectives of the ADCP measurements at the SUPERTANK project were fulfilled, but the scientific content of the data is not as good as was anticipated, and the data quality is mixed. First, the statistics of the velocity data from the offshore region were obtained for each run (Appendix H). Detailed time series, however, are garbled for the larger orbital velocities, due to ambiguity errors. Second, much was learned about the design of acoustic backscatter and velocity systems for use in the surf zone. The lessons, however, were not small perturbations on what was already known, but a radical departure from pre-conceived ideas about dynamic range. Third, the possibility of using BB-ADCPs to measure turbulent stress and kinetic energy was evaluated. The conclusion, however, was that a measurement scheme that has previously worked well for deep-ocean conditions was inadequate in the surf zone. Even if all hardware and software problems are fixed, the temporal resolution must be increased by one or two orders of magnitude before the system is robust enough to allow routine measurements of any flow other than the mean current. For backscatter measurements, the BB-ADCP beams should ideally be multiplexed, the dynamic range must be increased, and the filters opened up to properly resolve the bottom boundary layer.

Recommendations

The authors recommend that no further work be done with the present data set. Although acoustic methods have a future as a tool to uncover the mechanism for energy transfer and transport in the surf zone, the hardware used in SUPERTANK must be radically improved before these goals can be reached.

Acknowledgements

References

Flammer, G. H. (1962). "Ultrasonic measurements of suspended sediment," *Geological Survey Bulletin*, 1141-A.

Kraus, N. C., Thevenot, M. M., and Lohrmann, A. (1992). "PLUMES: An integrated acoustic and in situ sampling system for synoptic measurement of sediment concentration, current, and position." *Proc. First Thematic Conf.: Remote Sensing for Marine and Coastal Environments*. Environmental Research Institute of Michigan, Ann Arbor, MI, 377-90.

Lohrmann, A., Hackett, B., and Roed, L. P. (1990). "High resolution measurements of turbulence, velocity and stress using a pulse-to-pulse coherent sonar," *J. of Atmospheric Oceanic Tech.* 7, 19-37.

Ma, Y., Vardan, V. V., and Vardan, V. K. (1987). "Acoustic response of sedimentary particles in the near field of high frequency transducers," *IEEE* UFFC-34, 3-7.

9 The Ohio State University Measurements at SUPERTANK[1]

Introduction

Background

As part of its mission to maintain the nation's major waterways, ports, and harbors through dredging operations, the U.S. Army Corps of Engineers has initiated the Dredging Research Program (DRP). One of the technical areas of the program focuses on obtaining an improved understanding of the physical processes occurring at and around dredged-material disposal sites. The area includes development of improved site monitoring techniques, acquisition of field data sets to improve understanding of processes occurring within the bottom boundary layer (BBL) at the water/sediment interface, and development of computational techniques which may help predict the short- and long-term fate of materials associated with dredged material disposal areas.

Design and construction of the Acoustic Resuspension Measurement System (ARMS) at The Ohio State University (OSU) have been completed in partial fulfillment of these goals. ARMS is a bottom-sitting suite of acoustic instruments and their associated electronics. The instrument package collects and processes in situ data pertaining to the resuspension and transport of sediments by the combined effects of waves and currents in the BBL. Previous versions of ARMS have been deployed at open-water, dredged-material disposal sites; see, for example, Bedford et al. (1990) and Bedford, Wai, and van Evra (1987), but such instruments have never before collected data within the controlled conditions of the laboratory.

---

[1]Written by Keith W. Bedford, Sean O'Neil, Robert van Evra III, and Jongkook Lee, The Ohio State University.

Laboratory research on sediment movement due solely to wave motion has previously been concerned with the initiation of motion, transport of material in the form of bed load, and formation of ripple patterns on the bed. Most of these experiments attempted to use monochromatic waves created by a variety of methods including wave paddles, swinging trays in still water, and U-tube oscillatory flow tunnels. There are a number of concerns, however, which limit the usefulness of most of these data, including scale effects, wall and shore reflections, and improper boundary conditions such as the oscillatory flow tubes having no free surface. Other researchers have attempted to characterize the geometry of the concentration profiles observed under wave inducement, and these studies suffer from some of the same defects. It should also be mentioned that concentration measurements in the past have been made with instruments which are highly invasive of the BBL physics.

Objectives

The SUPERTANK Laboratory Data Collection Project was in part conceived to give DRP researchers an opportunity to study the processes and effects of sediment motion induced only by waves under controlled laboratory conditions with field-scale waves of known spectral composition. This was achieved by a precisely controlled wave paddle in a large wave channel that could be programmed to account for wave reflections from the beach and seiching. A modified version of ARMS was assembled for use in the wave-channel environment and was included as part of the offshore group, an ensemble of DRP researchers and their instrumentation, studying sediment motion offshore of the wave breaker zone. The primary focus of the OSU deployment and data collection system was to compare bed and boundary layer response to monochromatic and equivalent spectral waves. This includes obtaining profiles of the suspended sediment concentration as well as characterizing the complex three-dimensional hydrodynamics which effect sediment resuspension. It was also planned that corroborative information would be obtained through cooperation with other members of the offshore group.

Scope

There are three main sections to this chapter. The first section is a description of the experiment apparatus including how the devices operate, their locations both in the wave channel and with respect to other instruments in the offshore group, and a review of some unique characteristics of each device. The second section outlines how data were obtained by the OSU instrumentation through a description of the sequence of events of a wave run, the sampling regimen, calibration procedures, and electronic processing and filtering before the data were stored. The last section provides a description of the interpretation and analysis of the raw data. This section includes samples of the raw and interpreted data as well as a summary of the pertinent characteristics for several comparisons of similar wave runs. The chapter concludes with

a summary, and further data are presented in Appendix I (contained in Volume II of this report).

Experiment Apparatus

Each instrument used during SUPERTANK is physically described along with an explanation of its principle of measurement. The instrument system was a laboratory version of the ARMS field data collection package designed and developed at OSU. ARMS, its components, and its operating principles have been described previously by Bedford (1989) and van Evra and Bedford (1992).

Instrument description

Acoustic Concentration Profiler. The Acoustic Concentration Profiler (ACP) is a device used by the OSU Coastal Engineering Laboratory to obtain high-resolution vertical profiles of suspended sediment in the water column up to 1.5 m above the bottom. Originally designed as a high-resolution depth sounder by the Edo Corporation (1981), the instrument has been modified to enhance performance near the transducer and allow for range-gating of the near-field reflected acoustic signal. These modifications include a diamond-shaped ceramic transducer which produces an extremely narrow beam width and reduction of side lobes which are present in all instruments of this type.

The ACP transducer and electronics are contained in a 29-cm-long by 14-cm-diam cylindrical pressure housing made of stainless steel, shown in Figure 9-1. One endcap has the acoustic transducer mounted into its external face within a protective rubber potting compound which allows the transducer to vibrate without excessive flexure. The other endcap is attached to an internal circuit chassis which holds three circuit boards containing the transmitting and receiving electronics. On the outside of this endcap is a 10-pin underwater electrical bulkhead connector which links the instrument via an underwater cable to control and signal-conditioning hardware. The external hardware supplies power, triggering, and gain control to the ACP, receives the analog signal output from the ACP, and processes the data for presentation to a storage device.

The ACP operates by transmitting a 3-MHz acoustic pulse, which insonifies a narrow conical cross section of the water column from the face of the transducer to the bottom sediments. Immediately after the pulse has been transmitted, the transducer is internally switched over to a receiving circuit, which allows the transducer to act as a hydrophone. Detected return signals are amplified and filtered internally, and the resulting analog voltage trace is sent out of the ACP to the conditioning hardware. Output signals are then digitized according to the distance travelled, or range gated, 110 times, thus partitioning them into volumetric bins approximately 1 cm in depth.
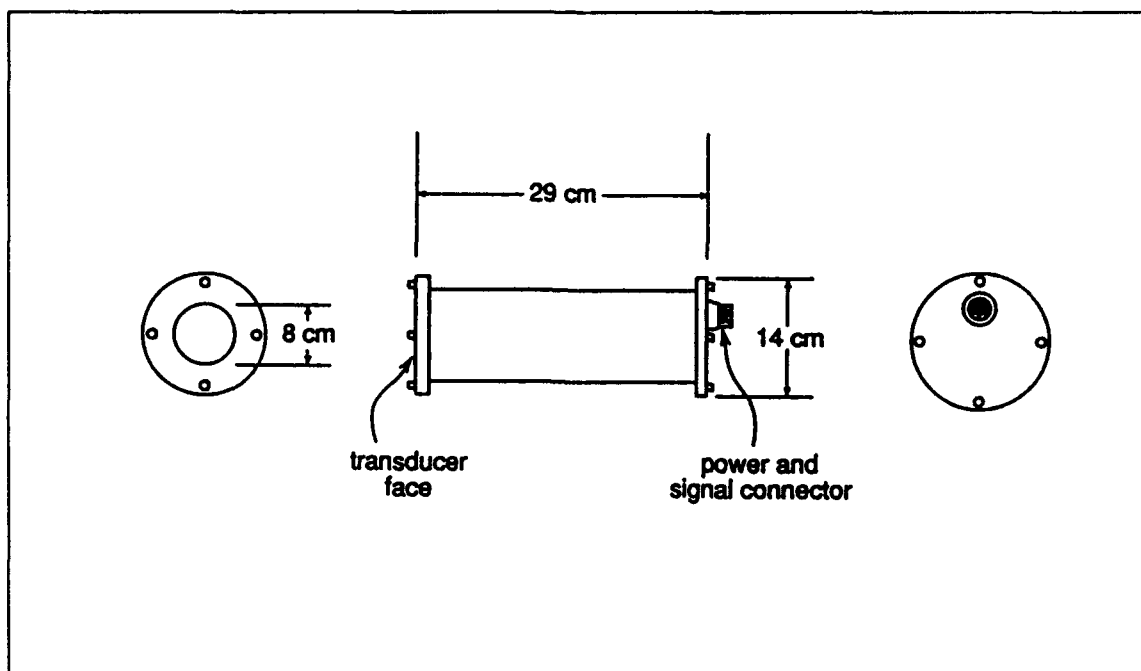
154

Figure 9-1. OSU Acoustic Concentration Profiler

Benthic Acoustic Stress Sensor. Flow field hydrodynamics are measured non-invasively, also in profile and within 1.5 m of the bottom, by the Benthic Acoustic Stress Sensor (BASS), developed at the Woods Hole Oceanographic Institution (Williams 1990). BASS is an acoustic time-of-travel velocimeter with transducers arranged on four vertically aligned rigid frames and can fully resolve velocities in three dimensions. BASS can measure at high enough speeds to provide the velocity data needed to resolve turbulent-scale fluctuations within the flow. Also, the vertical profile of measurements allows for better estimates of the shear stresses near the bottom, which can ultimately be correlated with the amount of sediment within the water column.

Four pairs of acoustic transducers for each BASS sensor array are mounted facing each other at 45-deg (0.79-rad) angles on the support rings of a 34-cm-long by 12-cm-diam cylindrical stainless steel frame as shown in Figure 9-2. The four transducer pairs are arranged so that their acoustic beam axes are coincident at the center of the cylindrical volume. Four BASS frames are attached end to end, and the transducer coaxial cables are individually secured to different struts of the BASS frame. The cables from each BASS sensor array frame are wrapped together with PVC spiral wrap to keep the cables protected and immobilized in one bundle. The cables transmit and receive signals from the BASS electronic circuitry, which is housed in a specially designed pressure canister. The electronic system controls sampling rate and processing of data for serial transmission to an external data storage device.
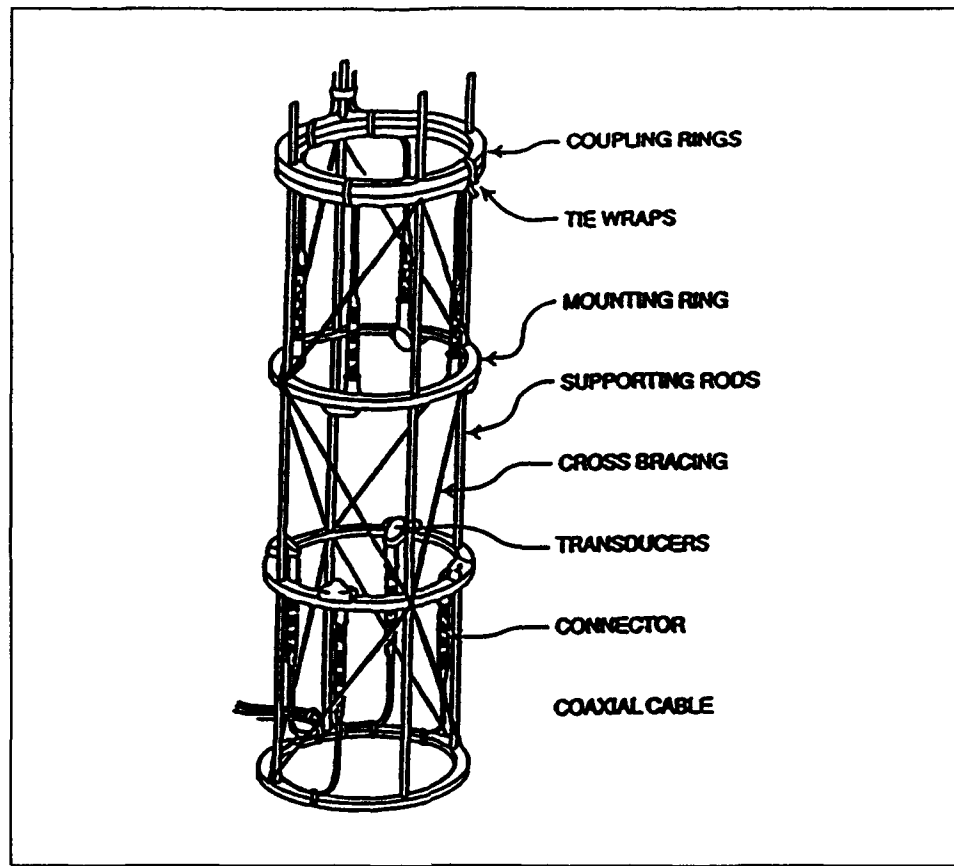
Figure 9-2. OSU BASS sensor array and frame

The BASS transducers transmit and receive 1.75-MHz acoustic pulses with each opposing pair transmitting and receiving twice during one sampling interval. Within the BASS electronics package the two time-of-travel measurements from each pair of sensors are subtracted and digitized, and the four resulting velocity measurements from each BASS array are output for storage. The four velocities correspond to four flow direction vectors which intersect at one point within the sampling volume and can thus be trigonometrically converted to three orthogonal velocity vectors during the data analysis process.

Pressure sensor. The hydrodynamic pressure history for each wave run was recorded using a Model ST-420 pressure sensor manufactured by Wika Instrument Corporation (Wika 1989). The instrument has a range of 0-5 psi and is principally used to record the dynamic pressure near the sampling volume of the ACP and BASS array. Another use of the pressure sensor is for the reconstruction of the surface wave climate history. The instrument simply measures the instantaneous ambient pressure at the transducer compared to a previously established datum.

The pressure transducer contains a piezo-resistive sensing element, which is protected from the media by a stainless steel diaphragm, and an isolating

silicone potting gel separates the sensor from the electronics. The bulk of the pressure sensor is contained within a capped 18.5-cm-long by 6-cm-diam galvanized steel pipe, with the threaded stainless steel transducer housing fitting through one endcap. A bulkhead connector on the other endcap accepts a transmission cable, which is connected to conditioning and controlling circuitry, where the sampling rate is controlled and the signal is digitized and combined with the concentration profile data.

PC array. Two personal computers (PC's) were used throughout the data collection process. PC1, in Figure 9-3, was solely used for receiving and storing the data streams as they came from the ACP and BASS microprocessors. PC2 was used primarily for performing an elementary analysis of 10-min samples of wave runs which were written to a floppy disk during each run on PC1. PC1 contained software pertinent to receiving the serially transmitted data to a named file, as well as the software for reading the WWV (broadcast by National Institute of Standards and Technology, Fort Collins, CO, call letters WWV) time signal and storing data to magnetic tape. PC2 contained software applicable to data analysis including a FORTRAN compiler and Matlab™, a numerical computation package.

PC1 was a 33-MHz, 386-based microprocessor with serial ports connected to the instrument data streams. Extra hardware was installed for the magnetic tape drive and the WWV time signal. PC2 was also a 33-MHz, 386-based microprocessor, but was not connected to any of the instruments. Both machines contained one 5¼-in. and one 3½-in. floppy disk drive and were connected to VGA color monitors.

Other instruments. Other important instruments to the data collection process include a 24-V power supply used to power the ACP and BASS microprocessors and transducers. An oscilloscope was used to examine the instantaneous signals from the ACP to monitor the reflections from the profile range bins. A self-contained, high-density magnetic tape drive was employed for permanently storing data from PC1's hard disk.

Location

The ACP, BASS, and pressure sensor were located close together on a specially designed mounting apparatus. Generally, the sensors were located between SUPERTANK Stations 18 and 19 for all wave runs, in close proximity to instruments belonging to other members of the offshore group. The specific location of the instruments with respect to the stations and other offshore group devices for each wave run are given in Table 9-1 and Figure 9-4. The locations of the instruments with respect to the edge walls, again for each run, are given in Table 9-1 and Figure 9-5.

The mounting assembly holding the ACP, BASS, and pressure sensor is shown in Figure 9-6. The assembly consists of aluminum seats for the ACP and the BASS frame assembly, with the instruments attached to their seats
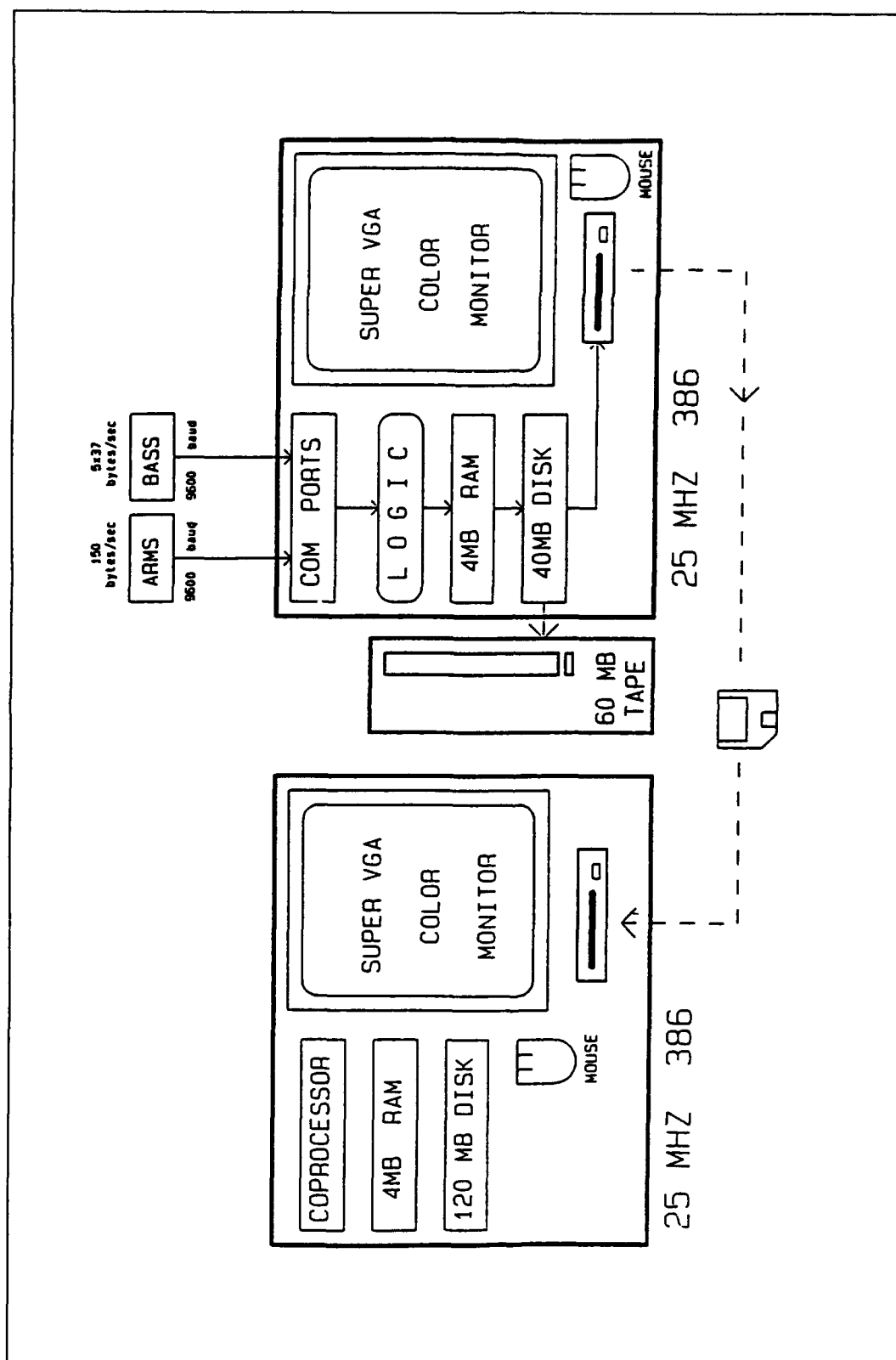
Figure 9-3. OSU PC array: PC2 left, PC1 right

Table 9-1							
OSU Instrument Position Key (Refer to Figures 9-4 and 9-5)							
Wave Run	**Position**	**Wave Run**	**Position**	**Wave Run**	**Position**	**Wave Run**	**Position**
A0509A	E,P1	A0912A	A1,P1	A1213A	D,P2	A1315A	B,P2
A0510A	E,P1		20 min		10 min		20 min
A0512A	E,P1		D,P1		C,P2		C,P2
A0515A	E,P1		20 min		10 min		20 min
A0517A	E,P1	A0914A	A1,P1		A1,P2	A1317A	B,P2
A0608A	E,P1		20 min		10 min		20 min
A0609A	E,P1		D,P1		B,P2		C,P2
A0611A	E,P1		20 min		10 min		20 min
A0613A	E,P1	A0915A	A1,P1	A1217A	C,P2	A1408A	B,P2
A0615A	E,P1		20 min		20 min	A1409A	C,P2
A0617A	E,P1		D,P1		B,P2	A1410A	D,P2
A0619A	E,P1		20 min		10 min	A1411A	B,P2
A0709A	A,P1	A1209A	D,P2	A1307A	C,P2	A1413A	C,P2
A0710A	A,P1		10 min		20 min	A1415A	B,P2
A0711A	A,P1		A1,P2		B,P2	A1416A	C,P2
A0713A	D,P1		20 min		20 min	A1417A	A2,P2
A0715A	D,P1		C,P2	A1309A	B,P2	A1507B	B,P2
A0717A	D,P1		10 min		20 min	A1508A	C,P2
A0719A	D,P1	A1211A	B,P2		C,P2	A1510A	B,P2
A0719B	D,P1		10 min		20 min	A1511A	A2,B2
A0808A	D,P1		A1,P2	A1310A	C,P2	A1513A	D,P2
A0809A	D,P1		10 min		20 min	A1515A	D,P2
A0812A	D,P1		C,P2		B,P2	A1516A	A2,P2
A0814A	D,P1		10 min		20 min	A1607A	B,P2
A0815A	D,P1		D,P2	A1311A	B,P2	A1608A	B,P2
A0816A	D,P1		10 min		20 min	A1610A	B,P2
A0817A	A1,P1	A1212A	D,P2		C,P2	A1611A	B,P2
A0908A	A1,P1		10 min		20 min	A1613A	A2,P2
A0910A	A1,P1		C,P2	A1313A	B,P2	A1614A	A2,P2
	20 min		10 min		20 min	A1615A	A2,P2
	D,P1		A1,P2		C,P2	A1616A	A2,P2
	20 min		10 min		20 min		
A0911A	A1,P1		B,P2	A1314A	B,P2		
	20 min		10 min		20 min		
	D,P1				C,P2		
	20 min				20 min		
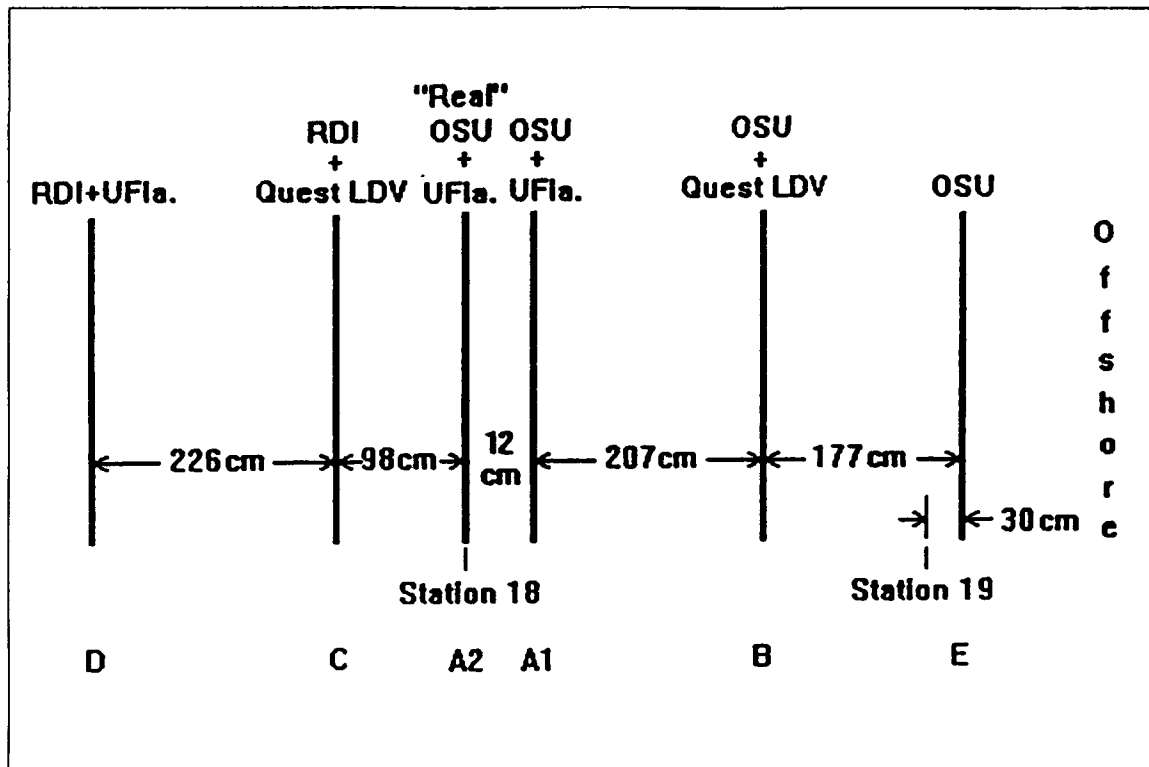
Figure 9-4. OSU instrument position along tank length
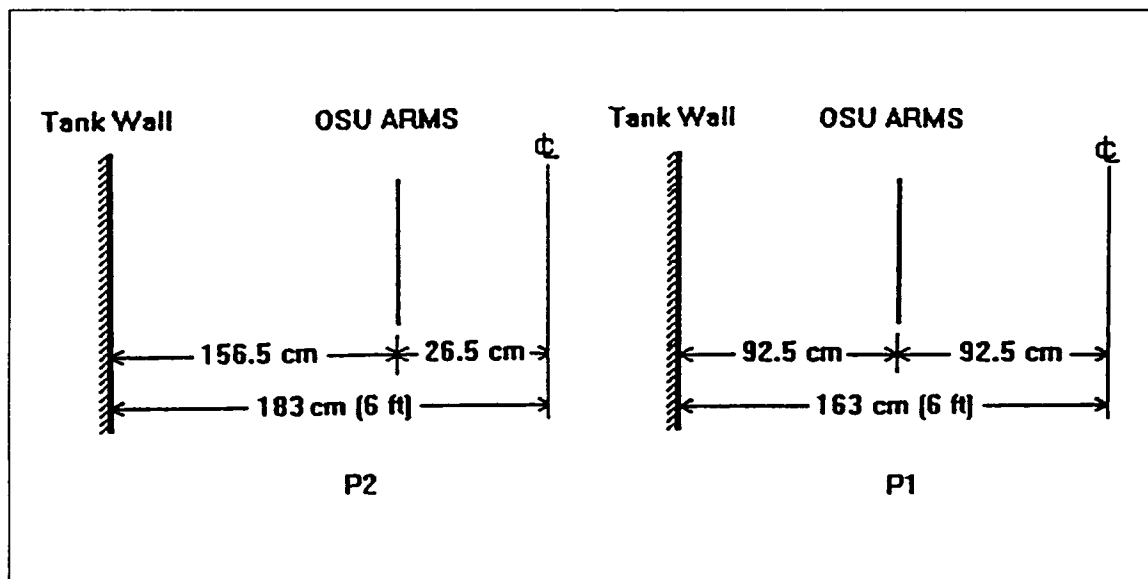
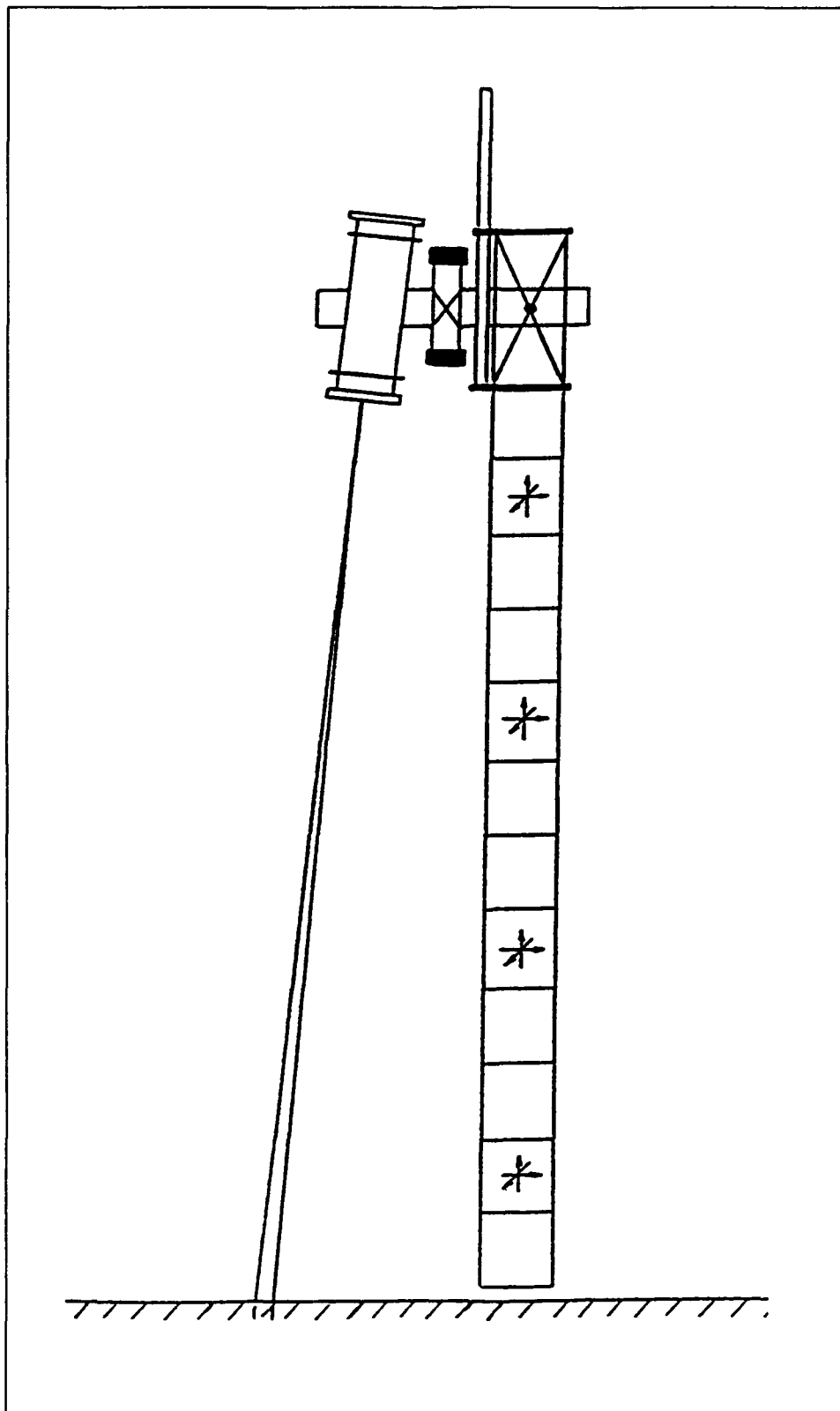Figure 9-5. OSU instrument position with tank width

Figure 9-6. Laboratory deployment of ARMS

with standard 5¼-in. (13.3-cm) U-brackets. The seats were attached to an aluminum cross brace with ⅝-in. (1.59-cm) bolts that allowed for the precise alignment of the instruments with respect to each other. The pressure sensor was situated between the ACP and BASS seats and was affixed to the cross brace using two plastic cable ties, with the transducer located just above the midpoint of the ACP cylinder.

The aluminum cross brace was in turn attached to a section of 1-in. (2.54-cm) galvanized steel pipe which ran up to the offshore moveable cart. The pipe was held in place with two 5¼-in. (13.3-cm) U-brackets at a particular vertical level depending on the cart location along the length of the channel. Guy wires, to prevent cross-channel instrument movement, were attached to the aluminum cross brace and ran diagonally toward the side walls to the bottom offshore corners of the offshore moveable cart. To prevent on-offshore movement caused by the waves passing through the instrument mounting assembly, another section of 1-in. (2.54-cm) galvanized steel pipe was attached to the vertical steel pipe near the cross brace and connected to the lower offshore edge of the cart.

All of the extra apparatus such as PC's, power supply, oscilloscope, magnetic tape drive, and other tools were located close to but outside the channel wall, between Stations 18 and 19.

Instrument characteristics

ACP. Because the ACP is designed as a depth sounder, it is specified to have a range of 6 to 10 m; however, use of the instrument in the presence of suspended sediment causes a high attenuation of its acoustic signal with distance from the transducer face, and thus limits the range of the instrument. Close to the transducer, however, the so-called near-field response to reflectors is quite sensitive. The reflected response of scatterers in each range bin to the transducer face can be modeled to convert acoustic signals to sediment concentrations, and the conversion process is discussed in the data analysis section of this chapter.

An external gain control of the receiver pre-amplifier allows for fine-tuning of instrument response to optimize for different sampling environments. The gain is adjusted to ensure that reflection from the sediment-water interface registers a full-scale output while maintaining statistically significant output from suspended particles within the water column sampling volume. The resulting output is a 0- to 5-V analog signal time trace, which is eventually digitized into 8-bit, 256-increment (hexadecimal 00 to FF) reflected intensity values and fed directly onto the data bus of the system microprocessor.

BASS. The BASS velocimeter package contains its own microprocessor to control the sampling process for all 16 transducer pairs of the four vertically aligned BASS sensor array frames. Each measurement along a transducer pair axis takes 100 msec to cross the sampling volume. Because one measurement

is taken with the sensors connected normally and one taken with the sensor connections reversed, it takes slightly more than 200 msec to obtain one velocity from each transducer pair. The travel time of the acoustic pulse is 1.33 nsec per cm/sec of velocity component. The two measurements are subtracted and then digitized by an analog-to-digital (A/D) converter to give a signed 12-bit word with a scale factor of 0.03 cm/sec per bit. The full-scale range of a sensor pair is 120 cm/sec (hexadecimal 0FFF).

The difference of the two measurements is obtained to remove electronic drift in the amplifiers, comparators, integrators, and A/D converter. The output on the signal line is a 9,600-baud RS232 UART in which the digitized range of each velocity is from -4,096 bits to +4,095 bits (hexadecimal F000 to 0FFF where 0000 is zero and FFFF is -1). The first hexadecimal digit, 0 or F, represents the sign of the velocity component. If the signal from one transducer is not received within a window of time, corresponding to 5 percent of 1,500 m/sec, a flag with hexadecimal value 8000 is written to the output. The cause of such a null response is the attenuation of sound by an acoustic inhomogeneity such as a bubble or other object within the sampling volume.

Each measurement from a transducer pair must be adjusted to account for a zero offset which is caused by capacitance in the cables from the transducers and the BASS electronics canister. The offset is different for each configuration of the cables and is obtained by stilling the medium within the sampling volume and taking measurements for several minutes. Changes in temperature and pressure affect the offset values by a maximum of 0.3 cm/sec.

Pressure sensor. The pressure transducer has a 0- to 5-V analog output that is sampled for 5.12 msec and digitized to an 8-bit number by an A/D converter separate from that used for the ACP signals. The 0- to 5-psi (0- to 34.5-kPa) range of the device has an overall accuracy of 0.0125 psi (0.086 kPa), but is digitized to 0.0195 psi (0.134 kPa) per bit increments. The sampling sequence is the same as that for the ACP since it is controlled by the same microprocessor.

Experiment Procedures

Sequence of events

A typical wave run, including the preparations needed to collect the data, is described:

a. The offshore moveable carriage is moved into place. The position along the length of the channel is chosen in consultation with other members of the offshore group so that sensors will be aligned in shore-parallel positions taking corroborative data.

b. Instrument mounting is moved into place so that the bottom of the BASS frame is roughly 2.5 cm above the bottom to prevent scouring around the frame. The vertical plumb of the mounting is checked, guy wires are tightened, and cables from the instruments to the signal conditioning and microprocessor hardware on the cart are immobilized.

c. Power cables and data transmission lines are connected from the electronic and microprocessor hardware on the cart to the PC's outside the channel, and equipment is powered up.

d. A test run of the instruments is made checking data on the PC's and the oscilloscope. BASS output is examined for capacitive drift due to partial immersion of the sensor cables running up from the instrument mounting through the water surface to the electronics. The profile of signals from the ACP is checked for proper background gain level and also to ensure that the instruments are positioned properly relative to the bottom.

e. Instruments are started before the wave run begins to observe the "spin-up" period of the suspended sediment. At this time a 10-min sample of the wave run data is written to a floppy disk which is then copied into PC2 where the data can be examined.

f. Data from the ACP, BASS, and pressure sensor are continuously collected and written to the hard disk of PC1 during the whole wave run. During this time a grab sample of the sediment-water mixture is collected using a Niskin bottle sampler from over the side of the channel just shoreward of the ACP.

g. Following completion of wave generation, a few more minutes of data are taken to obtain an idea of the settling characteristics of the suspended material. Data collection is ended and the instruments are turned off. Power and data transmission lines to and from the power supply and PC's are disconnected, and the instrument mounting is raised to prevent dragging on the bottom as the offshore cart is moved towards the wave paddle to facilitate the beach profile survey.

h. Data files are then copied to a properly named file designating the wave run. At the end of each day the saved files are copied onto two different magnetic tapes, one a backup and the other a working copy.

Calibration and zero reference

ACP. The procedure with which the ACP is calibrated is complicated and is fully discussed in Libicki, Bedford, Lynch (1989) and Libicki (1986). The method uses a model of the various parameters that influence reflected acoustic intensity, and data collected by the transducer, based on the active

sonar equation. Three components of the acoustic signal pathway must be modeled: the incident beam from the transducer face to the scattering field, the backscattered signal from the scatterers to the transducer, and the attenuation of the signal during each transit. The first two components can be approached from known solutions obtained by acoustic wave theory and are geometry-dependent. The attenuation component is the result of both the medium (parameterized by the temperature, pressure, viscosity, and frequency) and the effect of signal dispersal due to the density of scatterers. Effects of noise from the reflected signal and the processing hardware of the instrument must also be taken into account. The model has been verified with test data supplied by the instrument manufacturer as well as laboratory and field data.

BASS. Any calibration of the acoustic sensors of the BASS system is done by adjusting the integrator current sources on the microprocessor board within the BASS electronics package and was performed by the manufacturer prior to shipping. The BASS velocity interpretation is self-calibrating due to the redundant acoustic interpretive method it employs. Final interpretation of BASS data depends on shifting recorded values by capacitive zero offsets. Zero offsets are determined by taking several minutes of data in still water, or because still water is elusive in field conditions, taking a "bagged" zero offset by wrapping the BASS frame and transducers in an isolating sheathing, such as plastic, which can still the water within the sensor sampling volume. These should be obtained prior to or after any BASS deployment. Zero offsets obtained before and after SUPERTANK are used in the data conversion and analysis section of this report.

Pressure sensor. Internal calibration of the pressure sensor is performed by the manufacturer at the factory, and there is no need to obtain any offset values. Measurements of pressure values from calm periods before and after each wave run were stored and examined. This provides an exact reference of the instrument position below the still-water level, and thus the water depth, since the position of the instrument array was varied along the length of the channel.

Sampling and time reference

ACP. The controlling circuitry of the ACP is specified to sample profiles at rates up to 200 Hz, but at SUPERTANK, 32 complete profiles (110 range bins each) were obtained each second. The 16-msec sampling of each vertical increment of the profile dictates the 1-cm height of the range bins, and the 32 values for each bin are averaged providing one complete profile per second. The purpose of averaging is to minimize configurational noise, due to the changing orientation of individual scatterers within the insonified volume. Based on commonly encountered flow rates it has been judged that the 1-Hz stored data are adequate to reveal appreciable changes in concentration. The value of 32 Hz as the actual sampling rate was chosen as a compromise

between a denser sampling rate and the rate at which the internal binary computations for the averaging are done most efficiently.

At the time of execution of the data collection program within PC1, the first task is to read the output of the installed WWV time circuit. This precise time is stored as the first four bytes of the data file. Immediately following this the data stream from the ACP microprocessor is accessed, since the ACP is already actively taking data. Timing for sampling is provided by the system microprocessor. Each 110-byte data segment for the profile represents a second of elapsed time counting from the time taken from the WWV output.

BASS. Controlling circuitry within the BASS electronics canister can be programmed to sample up to 5 Hz, but for SUPERTANK deployment, 4 Hz was judged to be adequate. For each of the four BASS frames, the four transducer pairs were sampled sequentially, from A to D looking down from the upper ring of a BASS frame (see Figure 9-7) at four 0.25-sec intervals. The two measurements for each transducer pair are subtracted, and the difference in travel time between transducers is a flow velocity along that acoustic beam path. For each 0.25 sec, the 16 two-byte hexadecimal data words for each sample are sent to the data stream along with header and checksum bytes.

Similar to the case for the ACP, at the initiation of data collection, the WWV time is read and stored to the data file as the first four bytes. After that, each sample record represents an elapsed time of 0.25 sec. Timing for each of the four BASS sensor arrays is controlled by its own circuit board, and overall timing is controlled by the BASS microprocessor.

Pressure sensor. The processing circuitry of the ACP is also programmed to control the sampling rate of the pressure sensor. The sampling rate at SUPERTANK was set to 2 Hz, although samples can be collected at up to 20 Hz. The passive nature of the pressure sensor means that a sample can be obtained at any moment, and thus the instantaneous pressure is timed with the ACP. Twice a second, at 0.5-sec intervals, the output of the pressure transducer was sampled and stored in a buffer until the whole ACP data record was ready to be sent to the output data stream.

Pre-processing and filtering

Signals from the ARMS instruments were sampled, digitized, and transferred to storage under the control of two separate microprocessors. BASS was controlled by a Tattletale IV manufactured by Onset Corporation, and the ACP and pressure sensor were controlled by a CDP18S601 manufactured by RCA Corporation. The dual microprocessor setup proved to be flexible in being able to independently access the instrumentation via separate communication ports on PC1 during SUPERTANK.
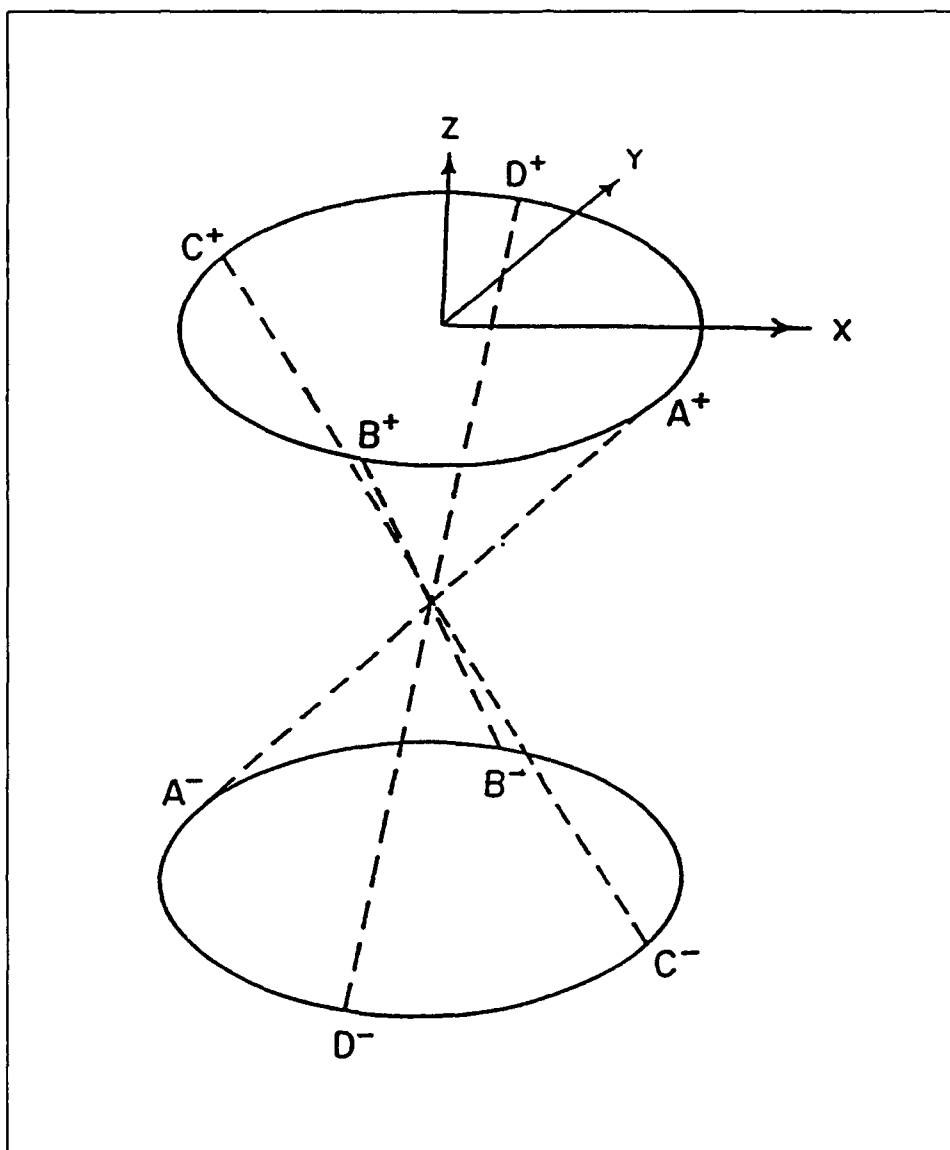
Figure 9-7. BASS sensor geometry

BASS. The Tattletale IV is a 6303-based microprocessor that is pro-grammed in BASIC. The operational sampling algorithms of the BASS are programmed into random access memory (RAM), and it executes the routines upon command. It is mounted onto one of the circuit boards of the BASS electronics and directly controls the functions of the instrument. The serial port of the Tattletale IV is the data output of the BASS as well as the interface for programming and checking the RAM contents.

In addition to providing timing for the system, which was later checked directly against the WWV signature at PC1, the BASS program controls the conversion and processing of the acoustic signals. The A/D converter of the Tattletale IV is used to convert the final values prior to output, and a detailed

167

description can be found in Williams (1990). The microprocessor transmits raw velocity vector information along with a time signature and pre-transmission checksum byte for each record.

ACP/Pressure sensor. To extend independent control of and data output streams from the ACP and pressure sensor, they were controlled separately by an 1802-based CDP18S601 single board computer. The electronic hardware used was similar to that described by van Evra (1983), with direct computer control of the timing, sampling, and conversion of the ACP and pressure sensor signals. The coded hexadecimal machine language operational program of the 601 board is contained on EPROM. Similar to the Tattletale IV, the program controls serial output through an RS232 port that also serves as an interface to perform system checks via PC1 and an oscilloscope.

The 601 controlled two separate A/D converter boards, one for the ACP and one for the pressure sensor. The ACP signal is converted sequentially by dual sample-and-hold circuits fed into the two matched A/D converters, the outputs of which are connected directly to the computer board data bus. The pressure electronics utilize a gated voltage-to-frequency circuit that is digitized at intervals matched to the ACP timing.

The ACP is triggered 32 times a second, and each 110 range-bin profile is added to a RAM buffer on the 601. The summed profiles at the end of each second are divided by 32 to provide the 1-sec ensemble-averaged profile. The averaged profile along with a timing counter and checksum are sent out serially through the output port to PC1. The 2-Hz pressure values are also included in the data stream with the ACP profile values.

Data Analysis

Analysis and interpretation methods

The complete description of the data obtained using the laboratory version of the ARMS data collection system used at SUPERTANK includes a number of analysis methods as well as different levels of analysis. It includes checking raw data integrity, as well as converting raw data to a physically descriptive format. With the data in this format it is also necessary to describe the context in which the data were taken, and thus a description of the wave environment and background sediment environment is needed. Finally, these different components are put together and the data from the different instruments are combined to obtain a picture of the water motion and its effect on the motion of the sediment.

Once data are obtained and stored, the first requirement is to check the whole data file for gaps and to check each data record for missing bytes. Examining each record for missing bytes is accomplished by counting the

number of bytes in the record, checking for the correct header byte, and adding data bytes to confirm that the checksum byte is correct. Because some bytes in each record do not correspond to actual data, it is possible to replace these bytes with place holders if it is determined that the missing bytes occurred in those places.

Along with examining each byte of a data record, it is possible to track the bytes allotted to keep track of time. Each data record has a few bytes allotted to count the actual clock time or to keep track of the record number which would be referenced to the time from the microprocessor which is sending the data. Again, because these bytes can be tracked, they can be replaced if found to be missing by referring to previous records. If any ACP acoustic intensity bytes, BASS velocity bytes, or pressure sensor bytes are lost, these cannot be replaced and the time of the occurrence of such a data record must be noted and a tally kept of such records for each data file.

The next order of analysis includes examining some basic statistics of the raw data. Because BASS data and pressure sensor data are directly converted algebraically, the best way to examine these data is to convert them to their final form. Data obtained from the ACP, however, can be examined for statistical regularity before conversion, and this process is described in a later section. Other analysis and interpretation focuses on the final converted data and includes determining a proper averaging time and using that averaging time to construct average profiles of ACP concentration data and BASS velocity data.

Data file format

ACP/Pressure sensor. To implement a completed ARMS data collection system including the BASS array, two separate data streams were used for the laboratory version of the system at SUPERTANK. The format for the ACP data stream is the same as that used for previous ARMS deployments and includes data from the pressure sensor. The data file format from the BASS, including some bytes allocated to keep track of the clock time, was designed to be used specifically for SUPERTANK.

The ACP data file for each 1-sec record of data contains a total of 128 bytes of 2 hexadecimal digits each, of which there are 110 bytes used for the reflected acoustic intensity. At the beginning of each data record there are 16 bytes allocated for data from other instruments, and the first and last bytes contain a constant valued header byte and a checksum byte. The format has the form

$$\text{H XRRBXXXXPXXXXXPX CCC...CCC S} \qquad (9\text{-}1)$$

where H represents the header byte, R's represent the record number, B is the block number, P's are the two pressure measurements, C's correspond to the 110 reflected acoustic intensities, S is the checksum byte, which is the sum of

the reflected acoustic intensities, and X's represent 11 extra bytes inserted as spacers and contain no useful information.

BASS. The BASS data file format contained 38 bytes for each 0.25-sec record. For each of the four vertically aligned BASS sensor arrays there are four values of two bytes each, containing four hexadecimal digits, corresponding to the velocity components along the four transducer axes. The four bytes previous to the 16 double-byte velocity words are used to record a time counter which contains the day, hour, minute, and second of that data record. Each data record also contains a constant-valued header byte and a checksum byte which is the sum of the 16 velocity component values and can be represented as

$$
\begin{array}{llll}
\text{H TTTT} & \text{VV} & \text{VV} & \text{VV} & \text{VV} \\
& \text{VV} & \text{VV} & \text{VV} & \text{VV} \\
& \text{VV} & \text{VV} & \text{VV} & \text{VV} \\
& \text{VV} & \text{VV} & \text{VV} & \text{VV} \text{ S}
\end{array} \tag{9-2}
$$

where each character represents one byte and each byte is made up of two hexadecimal digits. H is used for the header byte, T represents the time bytes, S is the checksum byte, and VV corresponds to the two-byte velocity components.

Sample raw data

An example of a single 1-sec ACP data record, in the format discussed above, is given in Table 9-2. Because each record is fairly lengthy, ACP data can be separated from the pressure data and stored as a separate data file for later interpretation. The pressure data can be stored as a 2-Hz time trace from any desired starting time and duration.

Each of the ACP data bytes represents an integer value from 0 to 255, where the actual stored data are from hexadecimal 00 to FF. A preliminary examination of the raw data begins by reading a 10-min block of data and averaging the values in each range bin which gives the average reflected acoustic signal for that particular range bin. Figure 9-8 shows the distribution of the average raw signal for a 10-min period from wave run A0608A; other figures showing distributions of average raw signals for seven other wave runs can be found in Appendix I (Figures I1-I7), contained in Volume II of this report.

The distribution in the figure shows that at range bin 108 the average signal value is the maximum of 255 for the 10-min averaging period. The maximum value, which indicates a strongly reflected signal, is always seen to occur in range bin 108 and can be interpreted as the reflected response from the bottom. For a particular data record a maximum reflected signal may occasionally occur at range bin 107 or 109, but it always occurs at range bin 108. The dip towards the bottom of the profile shows attenuation of the

170

Table 9-2 A Raw Data Record from the ACP/Pressure sensor											
H	X	RR	B	XXXX	P	XXXXX	P	X	C		S
98	FB	00 CF	FF	FF 00 00 00	93	00 00 00 00 00	A1	00	F2 F0 EF EB F2 EC E7 EF F0 F0		6 2
									EF E9 EE E3 EC E3 EB EA EC DC		
									E2 DF C9 E2 DF DD D5 D2 D6 E3		
									E3 CC D3 D7 C8 D0 CF D5 D9 D8		
									C9 C3 C8 CA C5 C8 B7 BA B4 B4		
									BE AF BB BA AB B8 B9 AA B6 AB		
									A3 96 99 A8 8F 88 8A 81 90 A8		
									9A 86 91 80 79 6A 75 7C 7B 6D		
									6E 67 71 77 69 78 5B 6F 6F 6A		
									66 6F 69 62 4B 4B 58 55 4A 55		
									50 47 5F 67 93 AB F6 FF FE DB		

reflected acoustic signal with distance from the face of the transducer. The extent of the dip is adjusted by changing the external gain of the transducer preamplifier. The sawtooth nature of the curve is due to the independent offsets of the two A/D converters processing the ACP data stream.

Another way to look at the raw ACP data is to examine a histogram of the signals in each bin over the averaging period. Figure 9-9 shows this at four points in the profile, where each range bin is represented by the average of three range bins, including one above and one below each point. The four points correspond to the vertical positions of the sampling points of the BASS velocity values. The figure shows that reflected intensities obtained at each range bin are distributed normally at all four points within the profile. If this were not the case, using average values to represent the concentration profiles might be questionable, or the sampling rate could need adjustment. Similar figures are shown in Figures I8-I14 of Appendix I (contained in Volume II of this report).
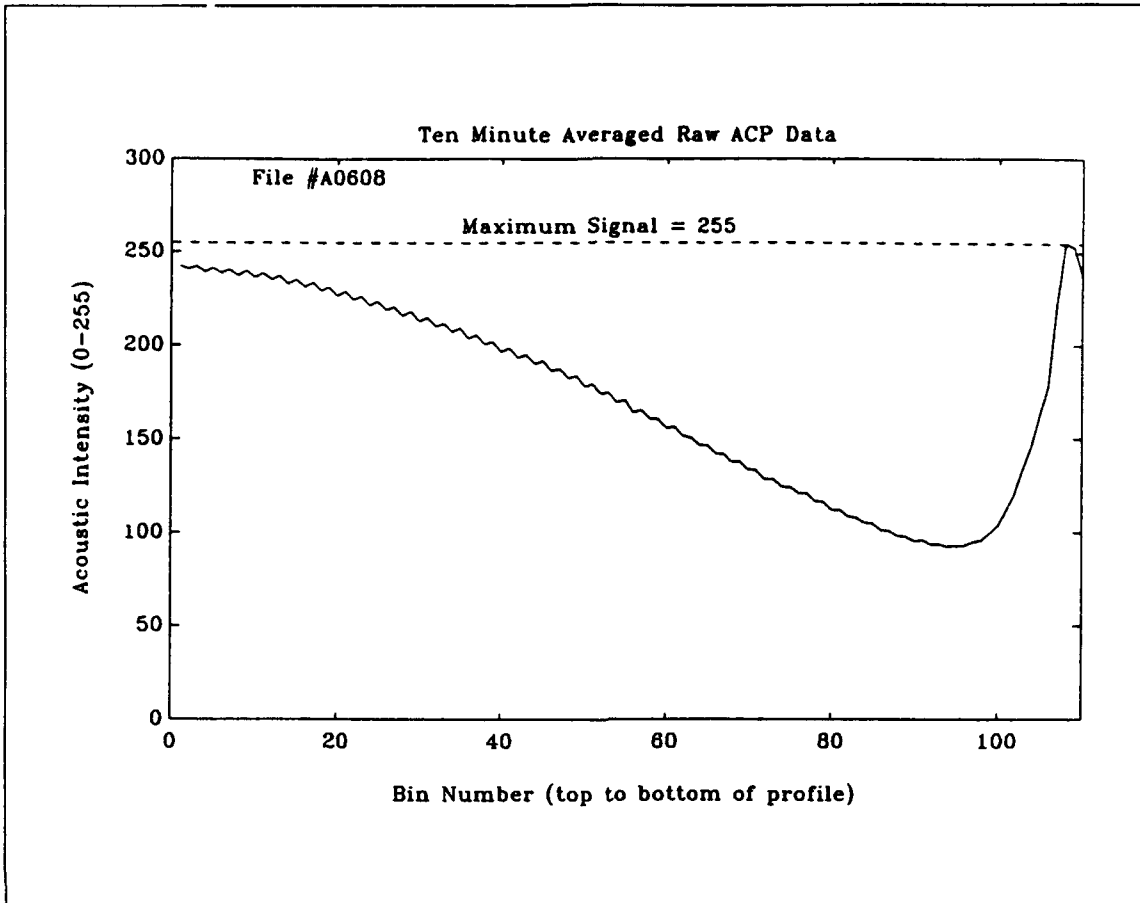
Figure 9-8. Averaged profile of the raw ACP signal

Table 9-3 Raw Data Record from the BASS Sensor Set										
						Sensor Pair				
						A	B	C	D	
H	**T**	**T**	**T**	**T**		**VV**				**S**
55	01	00	0B	01	**BAS S I**	FED8	FBE8 FCD4	FE86 FFB6	0164 01E0	9C
					BAS S II	FE7E	FCEE FDFA	FF74 004E	01AE 0166	
					BAS S III	FF48				
					BAS S IV	FF1A				

Raw data obtained from the BASS sensors are shown in Table 9-3, where
the data correspond to each BASS frame, and the sensor axes A, B, C, and D
areshown. The table shows one record of BASS velocity data, which is taken
every 0.25 sec, and there are four rows for the velocity data since there are

172
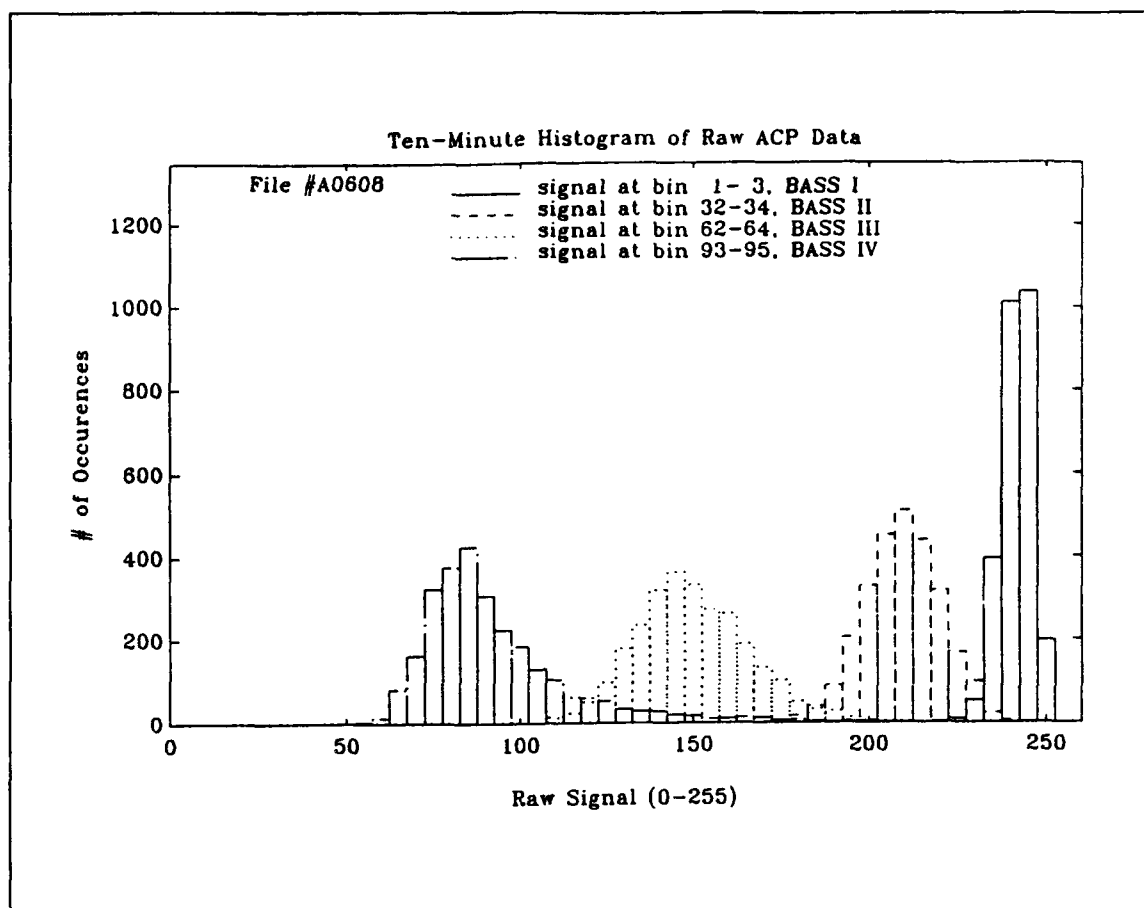
Figure 9-9. Histogram of the raw ACP signals at four BASS locations

four BASS frames stacked in the profile. The time bytes represent day (which is always one when the program is first run), hour, minute, and second; thus, for each second there will be four records, like the one in the table, with the same time numbers.

Sample interpreted data

ACP. The process of converting reflected acoustic intensity values obtained from the ACP involves many steps before the values can be described as suspended sediment concentration. Grab samples of the sediment-water mixture obtained during a wave run are examined for particle size distribution as well as for total solids in the sample. The total solids per volume is a background representation of the concentration which is used to fine-tune the model used for the conversion of the raw acoustic signals (Libicki, Bedford, and Lynch 1989).

Samples of the sediment-water mixture, approximately 1 ℓ in volume, were obtained once per day during the 2-week period that the OSU team was at SUPERTANK; however, two of the samples were lost in transport from the wave channel. Particle size distribution was measured using three 5-mℓ aliquots from each of the samples using the HIAC Model PC-320 Automatic Particle Size Analyzer. As samples are channeled through a narrow tube past a light emitter-detector pair, particles within the sample occlude a portion of the light detected by a photo sensor and decrease the light intensity detected, which results in a lower output voltage and is expressed as a function of particle diameter. The particle size analyzer is calibrated with polystyrene beads of known size distributions. The device contains a counter with 12 voltage threshold values; thus, as a particular sensor voltage is detected, the event increments one of the 12 values. The particle counts in each of these voltage ranges can then be plotted, yielding a grain size distribution for the grab sample. One limitation of using this particle size analyzer is that it can only reliably interpret particle diameters within the range of 1 to 100 μm, losing resolution of larger sizes.

A total solids analysis was performed with the remaining portion of the grab samples. The samples were divided into three 200- to 250-mℓ aliquots and analyzed using the method for determining total solids prescribed in *Standard Methods for the Examination of Water and Wastewater* (American Public Health Association 1989). Table 9-4 shows the results of the analysis.

The converted sediment concentration profiles obtained from the model are averaged over the time that was required to take each grab sample, as well as over the number of range bins of the profile that the sampler covered in space. For example, the grab sample took about 1 min to complete and was taken with a 32-cm by 14-cm-diam cylindrical Niskin bottle that was suspended with its axis arranged vertically at 33 to 65 cm above the bottom, the corresponding range bins are 54 to 82, where the higher-numbered range bins are closer to the bottom. Thus, sixty 1-sec partial profiles, from bins 54 to 82, were averaged together, and the resulting concentration in mg/ℓ was compared to that of the averaged grab sample concentration. The ratio represents a scale factor, which every model-calculated range bin concentration value in a profile is multiplied by.

A sample profile for a 15-min averaging time is shown in Figure 9-10. The concentration profile depicted in the figure is from the wave run numbered A0608A, and the 15-min average is taken at nearly the same time as the 10-min average raw intensity shown in Figure 9-8. The figure shows the mean of the concentration, the mean plus and minus one standard deviation for each range bin, and the maximum and minimum concentration values in each bin. The sample profile was taken at a time during the wave run when a time trace from any one bin would not show large changes over time in the concentration; i.e., an equilibrium period some time after any "spin up" effects have ceased.

174

Table 9-4
Total Solids Analysis of the Water/Sediment Grab Samples

Sample No.	Mass of Filter g	Mass of Filter with Solids g	Sample Volume ml	Sample Total Solids mg/l	Mean Total Solids mg/l	Standard Deviation
1-1	0.2001	0.2017	198.0	8.08		
1-2	0.2029	0.2043	197.5	7.09	7.70	0.54
1-3	0.2031	0.2048	214.0	7.94		
2-1	0.2011	0.2046	248.0	14.11		
2-2	0.2019	0.2055	248.0	14.52	14.58	0.50
2-3	0.2034	0.2071	245.0	15.10		
3-1	0.2026	0.2041	243.5	6.16		
3-2	0.2026	0.2043	241.0	7.05	6.71	0.48
3-3	0.2045	0.2062	246.0	6.91		
4-1	0.2029	0.2050	197.0	10.66		
4-2	0.2055	0.2078	198.5	11.59	11.07	0.48
4-3	0.2023	0.2045	201.0	10.95		
5-1	0.2074	0.2099	247.0	10.12		
5-2	0.2040	0.2065	246.5	10.14	10.38	0.44
5-3	0.2091	0.2118	248.0	10.89		
7-1	0.2113	0.2120	242.5	(2.89)		
7-2	0.2065	0.2083	244.0	7.38	6.78 (5.48)*	0.86 (2.32)
7-3	0.2006	0.2021	243.0	6.17		
8-1	0.2014	0.2030	243.0	6.58		
8-2	0.1964	0.1983	251.5	7.55	7.07 (12.37)	0.69 (9.20)
8-3	0.2073	0.2130	248.0	(22.98)		
10-1	0.2009	0.2013	197.0	2.03		
10-2	0.2020	0.2025	200.0	2.50	2.02	0.49
10-3	0.2047	0.2050	198.0	1.52		

* Numbers in parentheses represent outliers, and statistics including outliers.

BASS. Using the averaged zero offset values from Table 9-5, the sampled 2-byte velocity values can be converted to three-dimensional velocities. The conversion procedure is provided by the manufacturer and is made up of a set of equations that convert the four axial velocities to three orthogonal velocity component values. The conversions are

$$v = 0.0207 \ (A - A_0 - C + C_0) \qquad (9\text{-}3)$$
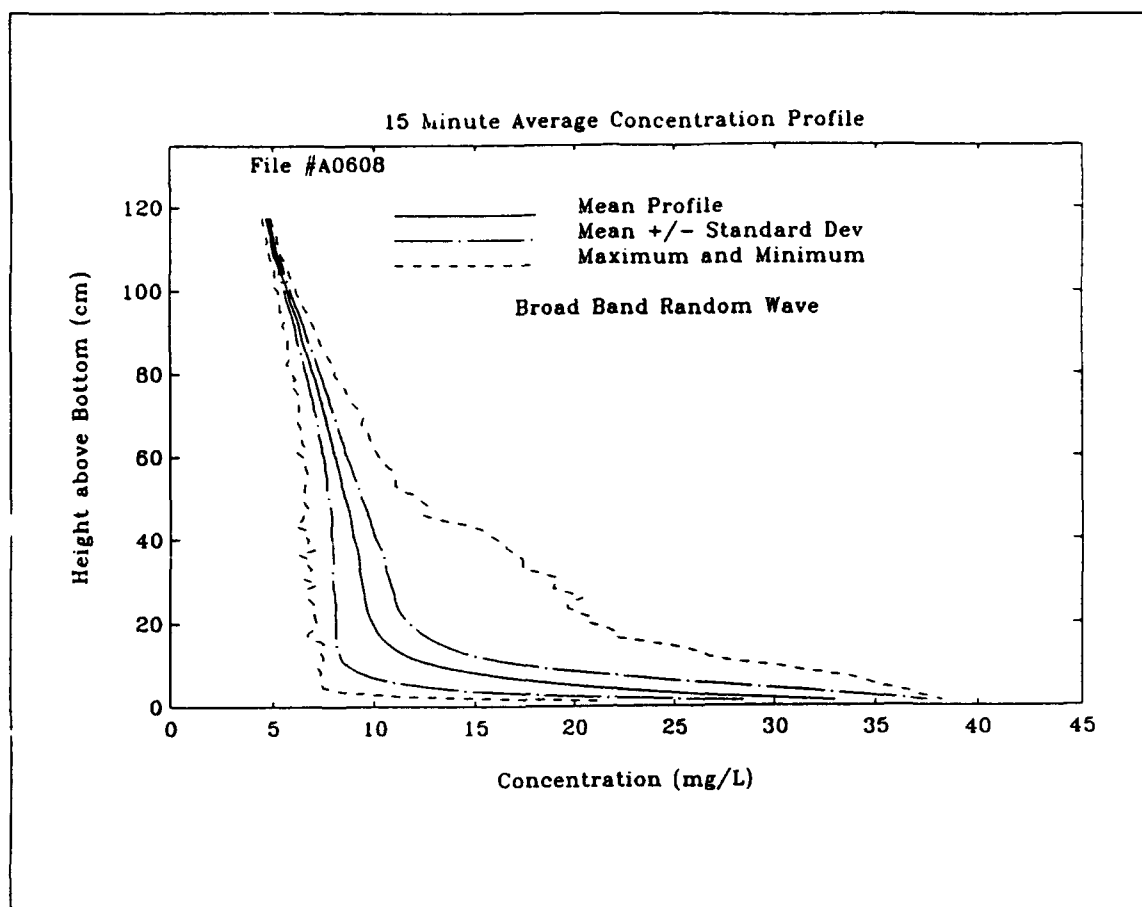
Figure 9-10. Interpreted concentration profile

$$u = 0.0207 \ (B - B_0 - D + D_0) \qquad (9\text{-}4)$$

$$w = 0.0207 \ (A - A_0 + C - C_0) \qquad (9\text{-}5)$$

or

$$w = 0.0207 \ (B - B_0 + D - D_0) \qquad (9\text{-}6)$$

or

$$w = 0.0207 \ (A - A_0 + B - B_0 + C - C_0 + D - D_0) \qquad (9\text{-}7)$$

where

u	$=$	horizontal (along the channel length), positive offshore velocity component (cm/sec)
v	$=$	horizontal, cross-channel velocity component (cm/sec)
w	$=$	vertical, positive-upwards velocity component (cm/sec)

Table 9-5				
Averaged Zero Offsets for Supertank Deployment				
	Sensor Pair			
	A	**B**	**C**	**D**
BASS I	0003 (3)	0000 (0)	FFFF (-1)	0000 (0)
BASS II	0001 (1)	0000 (0)	FFFE (-2)	0001 (1)
BASS III	0000 (0)	0003 (3)	FFFF (-1)	0000 (0)
BASS IV	FFFE (-2)	FFFD (-3)	FFFC (-4)	0002 (2)

A,B,C,D = integer velocity data values from the four sensor pairs of each BASS array

A_0, B_0, C_0, D_0 = zero offset values corresponding to A,B,C,D

In the above, the constant multiplier is due to trigonometric conversion as well as the value of velocity in cm/sec per bit of integer data.

As with the ACP data, it is possible to arrange the velocity data into averaged profiles or time series over the 15-min time period. Both of these yield a different kind of information; a time series trace of velocity components reflects the instantaneous wave characteristics and an average profile shows net fluid motion during the period. Because not all velocity data for each 15-min period are intact (there may only be two out of four points in a particular profile), the velocity data which are intact will be presented as a time trace. An example of the interpreted velocity data for the u-velocity component, which is along the channel and positive offshore, at a depth parallel to the sampling point of the third BASS sensor down from the top of the instrument mounting, is shown in Figure 9-11.

Pressure sensor. Each 1-sec ACP data record contains 2-Hz pressure data which is stored in 2-byte places within the first 17 bytes of the record (Equation 9-1). The conversion of the data to units of pressure is easy, due to the linearity of the instrument. Thus the integer-valued data, represented as hexadecimal digits from 00 to FF, are converted by multiplying by a constant. The value is 0.0125 psi (0.086 kPa) per bit or 0.88 cm of water per bit. The data can be stored in a separate data file as a time trace, and a sample of data is shown in Figure 9-12 for wave run A0608A and the same 15-min period used for average ACP concentration and BASS velocity values.

Summary of data characteristics

Eight wave run data files have been selected as representative sample files collected by OSU at SUPERTANK. These files comprise at least one of each type of wave run spectra, i.e., one each of broad-banded random waves, narrow-banded random waves, and monochromatic waves. There are two
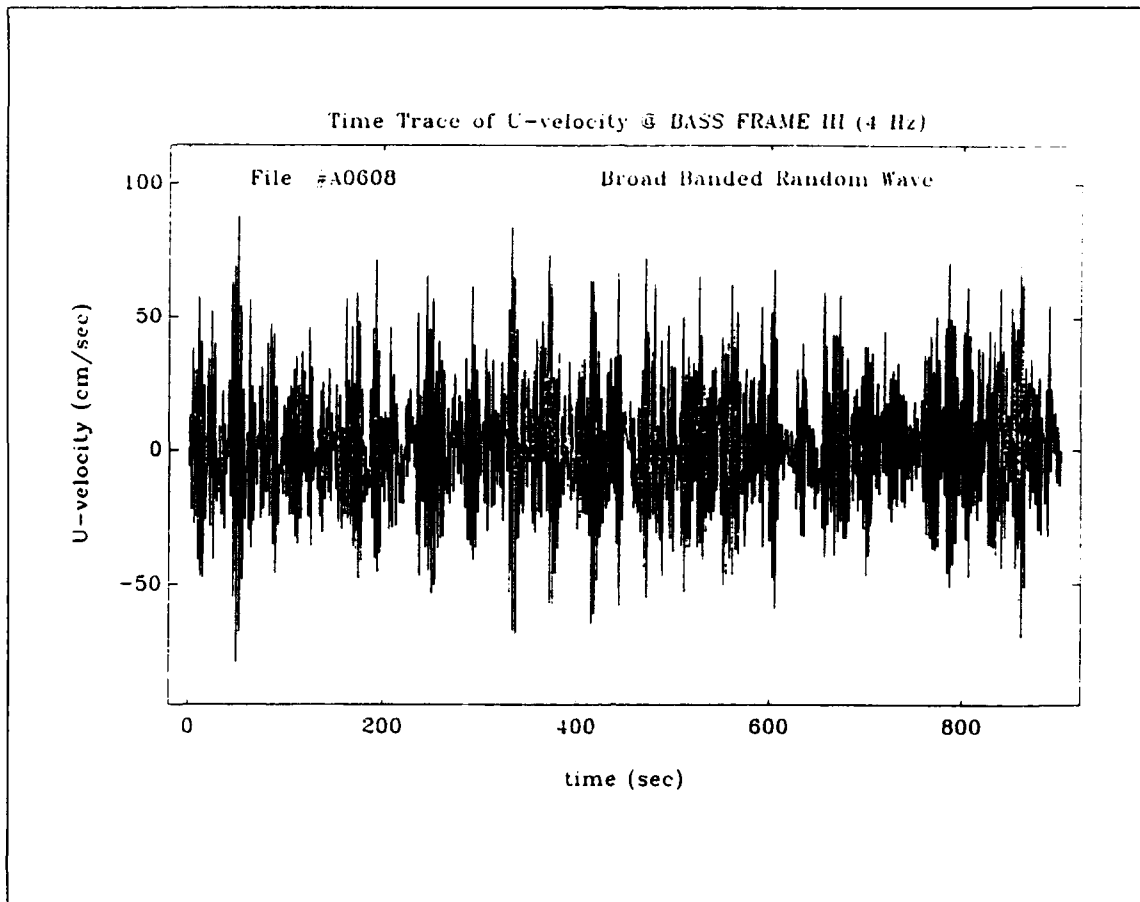
Figure 9-11. Time trace of interpreted velocity data

wave periods represented, four data files have wave periods of 3 sec and four data files have wave periods of 4.5 sec. The wave heights of all eight data files are statistically equal to 0.8 m. These files were selected because it is necessary to compare spectrally similar waves for a better understanding of how the different kinds of waves affect sediment resuspension. The velocity files comprise one figure for each velocity component, for each of the four BASS sensor arrays. Thus for each wave run there is a maximum of twelve possible separate figures; only two of the eight wave run data files contained this much uncompromised data.

It can be seen from the concentration profiles exhibited in Figure 9-10 and Figures I15-I21 that profiles induced by waves of similar spectral width have a similar shape. The broad-banded waves have the least total suspended sediment mass within the profile, followed by the narrow-banded waves having more total suspended sediment as evidenced by the kink in the L-shaped profiles moving upwards and to the right. This effect is even more pronounced on the monochromatic wave profiles.

178
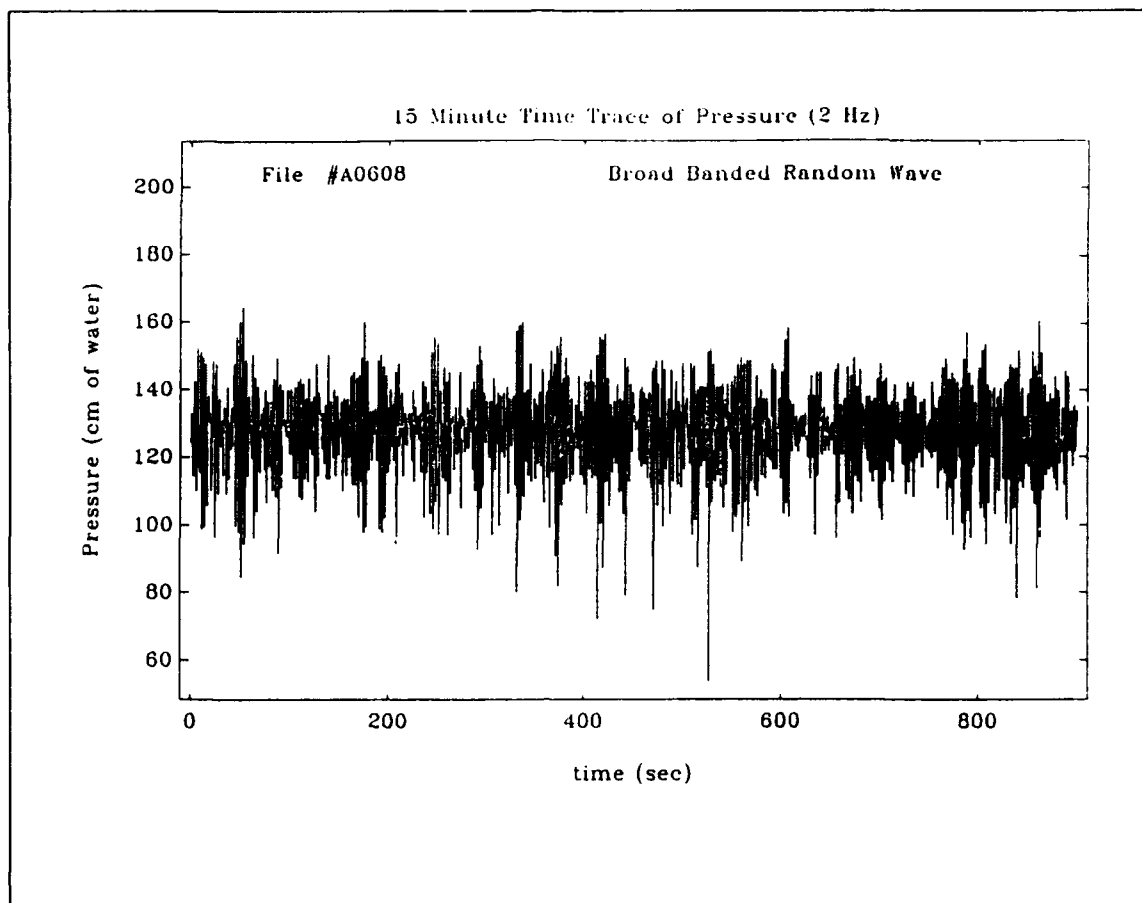
Figure 9-12. Time-trace-interpreted pressure data

The velocity time traces in Figure 9-11 and Figures I22-I96 show that the monochromatic waves (A1317A and A0817A) do indeed show equal velocities with each passing wave, and unequal onshore and offshore excursions of the amplitudes past zero suggest that the waves are not first-order linear. The narrow-band random waves (A0510A and A0711A) show definite wave groups of differing periods along the 15-min intervals. The broad-band random waves (A0608A, A0611A, A0812A, and A0814A) show some periods where groups of waves seem to occur, but these events are not as regularly occurring or as easy to identify as those for the narrow-band waves.

The pressure data, Figure 9-12 and Figures I97-I103, show the same trends as the velocity data for each type of wave even more clearly. They show that even the broad-band waves have a "groupiness" where some groups have longer periods than others. Average pressure data shows that the center of the instrument mounting was about 125 cm below the still-water level of the channel.

Identification of marginal data sets

The data sets judged to be unsatisfactory are listed in Table 9-6. Because there are two sets of data for each wave run data file, the complete data set should not necessarily be avoided. For example, if a particular set has many missing data bytes within the ACP data file, data obtained from the BASS sensors could be fully intact, which may be useful to some investigators. Table 9-6 lists the data sets that contain either marginal ACP data or marginal BASS data, where the information related to the BASS sensors includes all four BASS frames. An explanation is included with each listing.

Table 9-6 Marginal Data Sets		
Wave Run File Number	**Wave Type**	**Reason to Avoid File**
A0509A	Narrow Banded Random	Missing 95% ACP and 3% BASS records
A0512A	Narrow Banded Random	Missing 22% ACP records
A0515A	Narrow Banded Random	Missing 75% ACP records
A0517A	Narrow Banded Random	Missing 68% ACP records
A0609A	Broad Banded Random	Missing 53% ACP and 1.5% BASS records
A0618A	Broad Banded Random	Missing 15% ACP and 2.3% BASS records
A0710A	Narrow Banded Random	Missing 11% ACP and 7.5% BASS records
A0713A	Narrow Banded Random	Missing 88% ACP and 1% BASS records
A0715A	Narrow Banded Random	Missing 100% ACP and 1.3% BASS records
A0808A	Broad Banded Random	Missing 14% ACP and 9% BASS records
A0809A	Broad Banded Random	Missing 12.5% ACP and 1.2% BASS records
A0815A	Broad Banded Random	Missing 1% BASS records
A0816A	Monochromatic	Missing 11.5% ACP and 1% BASS records
A0908A	Broad Banded Random	Missing 15% ACP and 12% BASS records
A0914A	Broad Banded Random	Missing 15% ACP and 1.4% BASS records
A0915A	Broad Banded Random	Missing 11% ACP and 10% BASS records
A1209A	Broad Banded Random	Missing 99% ACP and 1% BASS records
A1211A	Monochromatic	Missing 14% ACP and 1% BASS records
		(Continued)

Table 9-6 (Concluded)

Wave Run File Number	Wave Type	Reason to Avoid File
A1213A	Monochromatic	Missing 75% ACP
A1217A	Broad Banded Random	Missing 9% ACP
A1307A	Broad Banded Random	Missing 14% ACP and 1% BASS records
A1309A	Monochromatic	Missing 13% ACP and 1.4% BASS records
A1310A	Broad Banded Random	Missing 14% ACP and 6% BASS records
A1311A	Monochromatic	Missing 45% ACP and 13% BASS records
A1313A	Broad Banded Random	Missing 26% ACP and 3% BASS records
A1315A	Broad Banded Random	Missing 13% ACP and 1% BASS records
A1317A	Monochromatic	Missing 14% ACP and 1% BASS records
A1408A	Broad Banded Random	Missing 14% ACP and 1% BASS records
A1411A	Broad Banded Random	Missing 11% ACP and 1% BASS records
A1413A	Broad Banded Random	Missing 87% ACP and 1% BASS records
A1415A	Broad Banded Random	Missing 52% ACP and 1.2% BASS records
A1416A	Broad Banded Random	Missing 13% ACP and 2.6% BASS records
A1417A	Broad Banded Random	Missing 13% ACP and 1% BASS records
A1508A	Narrow Banded Random	Missing 17% ACP and 1% BASS records
A1510A	Narrow Banded Random	Missing 17% ACP and 1% BASS records
A1511A	Narrow Banded Random	Missing 17% ACP and 13% BASS records
A1515A	Narrow Banded Random	Missing 78% ACP and 8% BASS records
A1516A	Narrow Banded Random	Missing 16% ACP and 9% BASS records
A1607B	Broad Banded Random	Missing 15% ACP and 4% BASS records
A1608A	Broad Banded Random	Missing 70% ACP and 3% BASS records
A1610A	Broad Banded Random	Missing 16% ACP and 1% BASS records
A1611A	Broad Banded Random	Missing 13% ACP and 1% BASS records
A1613A	Monochromatic	Missing 12% ACP and 4.5% BASS records
A1614A	Monochromatic	Missing 2% ACP and 2.6% BASS records
A1615A	Monochromatic	Missing 95% ACP and 1% BASS records
A1616A	Monochromatic	Missing 12% ACP and 1.3% BASS records

Summary

Review of experiments and results

In conclusion, there a few main points to be reiterated that allowed for the success of the OSU deployment during SUPERTANK. The successful configuration of ARMS, with inclusion of the never-before-deployed BASS velocimeter array, for the laboratory provided a remotely obtained and non-invasive set of measurements. The laboratory configuration allowed for nearly instantaneous monitoring, via the PC array, of data during sampling to maintain optimal gain setting for the ACP and to determine performance characteristics of the BASS array during its first deployment.

Second, the controlled laboratory conditions of the wave channel allowed for measurement of sediment resuspension and transport in monochromatic third-order waves and their spectral equivalents with broad and narrow spectral peaks of known width. Working in a wave channel also meant the waves were fully unidirectional, and the wave paddle was designed to accommodate and damp out beach, wall, or paddle reflections. Water samples within the concentration profiles could be obtained often and easily in the laboratory during wave runs, which improves the accuracy of the concentration profiles.

A preliminary analysis of vertical sediment fluxes measured during SUPERTANK shows that nonlinear waves produce a persistent sediment transport on the order of 10^{-2} mg/cm^2/sec. This transport is directed offshore because asymmetry in the nonlinear waves shows higher orbital velocity amplitudes in the offshore direction, and the wave periods were 3 and 4.5 sec, which would be classified as erosional waves. Further analysis of the vertical and horizontal transport fluxes can be found in O'Neil (1993).

Another preliminary analysis was performed to determine whether the profiles of suspended sediment are amenable to the available models. Because the data were obtained in a waves-only climate, and not the wave-current climate observed in nearly all field conditions, there are few models with which to compare. At this time, there are no known models derived from laboratory or field data which predict the sediment concentration with height above the bottom as observed at SUPERTANK.

Acknowledgements

Dibble of the O. H. Hinsdale Wave Research Laboratory at Oregon State University for their help and support.

References

American Public Health Association. (1989). *Standard methods for the examination of water and wastewater*. Amer. Public Health Assoc., New York.

Bedford, K. W. (1989). "In situ instrumentation for the measurement of entrainment, resuspension and related processes at dredged material placement sites," unpublished report, U.S. Army Engineer Waterways Experiment Station, Vicksburg, MS.

Bedford, K. W., Wai, O. W. H., and van Evra, R. E. III. (1987). "Sediment entrainment and deposition measurements in Long Island Sound," *J. Hydr. Engrg.* 113(10), 1325-42.

Bedford, K. W., Wai, O. W. H., van Evra, R. E., III, Velissariou, P., Lee, J., and Libicki, C. (1990). "The local near-bottom response of a dredged material placement site to wind and tide effects," unpublished report, U.S. Army Engineer Waterways Experiment Station, Vicksburg, MS.

Edo Corporation. (1981). "Instruction manual for the Model 563 3 MHz depth sounder," Rep. No. 13331, Salt Lake City, UT.

Libicki, C. (1986). "Acoustic sensing of the vertical and temporal structure of sediment transport in the benthic boundary layer," Ph.D. diss., Ohio State University, Columbus, OH.

Libicki, C., Bedford, K. W., and Lynch, J. (1989). "The interpretation and evaluation of a 3 MHz acoustic backscatter device for measuring benthic boundary layer sediment dynamics," *J. Acoust. Soc. Am.* 85(4), 1501-11.

O'Neil, S. (1993). "Laboratory benthic boundary layer data analysis and sediment transport at SUPERTANK," M.S. thesis, Ohio State University, Columbus, OH.

van Evra, R. E. III. (1983). "Coastal data acquisition and retrieval tower," M.S. thesis, Ohio State University, Columbus, OH.

van Evra, R. E. III, and Bedford, K. W. (1992). "ARMS: Acoustic Resuspension Measurement System instrumentation manual," unpublished report, U.S. Army Engineer Waterways Experiment Station, Vicksburg, MS.

Williams, A. J. (1990). "BASS instructions," Oceanographic Instrument Systems, Woods Hole, MA.

Wika. (1989). ST-420 pressure transducer data sheet, *No. 9734635,* Law-
renceville, GA.

10 Intermittent Near-Bed Sediment Suspension in the Offshore at SUPERTANK[1]

Introduction

Background

The processes of wave-seabed interaction are extremely complicated and exhibit nonlinear behavior due to many couplings amongst the flow properties and bed characteristics. An adequate understanding of the physical interactions between fluid and grains near the seabed is necessary to develop the capability to model, predict, and control coastal sediment transport and associated bathymetric change. The intermittent suspension of sand by waves is a significant process and the focus of this study.

Previous observations (Jaffe, Sternberg, and Sallenger 1985; Hanes 1990; Vincent, Hanes, and Bowen 1991) of sand suspended by waves indicate that fluctuations in suspended sediment concentration are significant. The phase of sediment entrainment and the characteristics of suspension events are related to the direction of time-averaged net cross-shore suspended transport. The importance of intermittent suspension to sediment flux can be demonstrated by considering the various temporal contributions to cross-shore transport of sediment. The time-averaged net cross-shore suspended sediment in wave-dominant regions consists of a fluctuating portion and a steady portion, i.e.,

$$\overline{UC} = \overline{U}\,\overline{C} + \overline{U'C'} \tag{10-1}$$

where

U = cross-shore component of instantaneous sediment velocity
C = instantaneous concentration of suspended sediment

---

[1]Written by Daniel M. Hanes, Tae Hwan Lee, and Eric D. Thosteson, University of Florida.

and the overbar and prime denote time average and instantaneous fluctuation from the average, respectively.

By assuming that suspended sand moves at approximately the same horizontal velocity as the water, temporal characteristics of the fluctuating portion of the transport can be examined through the application of the co-spectrum (Huntley and Hanes 1987), as shown schematically in Figure 10-1.
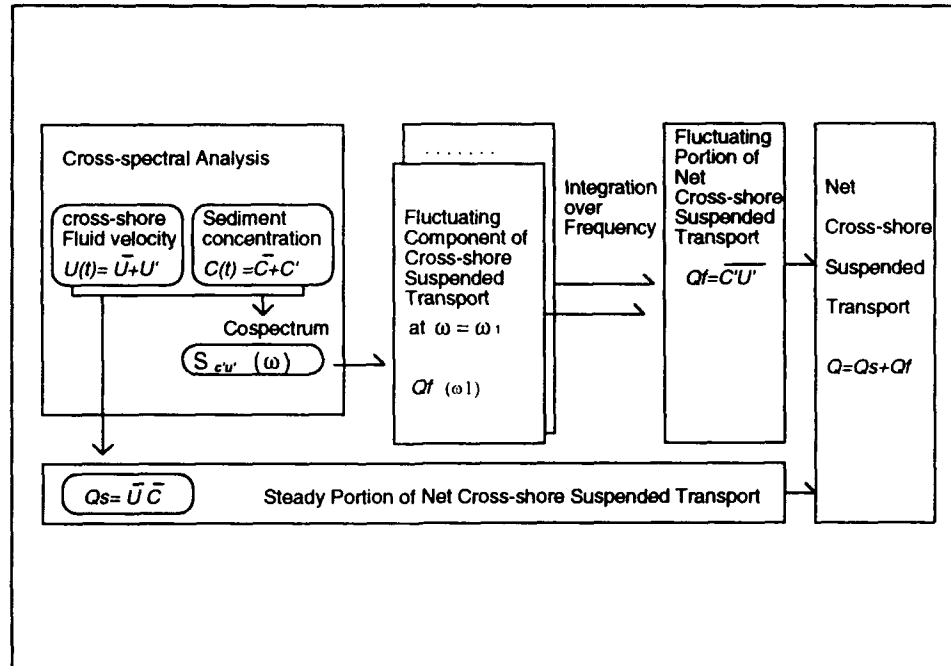
Figure 10-1. Summary of cross-shore suspended transport

Objectives

The purpose of the intermittent near-bed sediment suspension measurement at the SUPERTANK Laboratory Data Collection Project was to study small-scale sediment dynamics under controlled laboratory conditions at prototype scale. The fluid-sediment interaction which occurs in large-scale laboratory tests probably embodies much of the same physics as the small-scale fluid-sediment interaction in the field. Laboratory conditions provide a degree of control and reproducibility which is not possible in the field.

Emphasis is on measurement of the small-scale, short-time response of suspended sand to waves. Specific phenomena to be studied are the vertical and temporal structures of suspension events, the relation of suspension events to cross-shore sediment transport, and the reference concentration near the bed. The acquired data will be used to evaluate models of reference concentration as well as to quantify the significance of intermittent suspension to cross-shore transport of sand.

186

Scope

The following measurements and analyses are described in this chapter.

Measurements.

a. Time series of profiles of suspended sediment concentration by acoustic concentration profiler (ACP) with 4-Hz temporal and 1.5-cm spatial resolutions.

b. Time series of suspended sediment concentration at approximately 9 and 56 cm above the bed by optical backscatterance sensors (OBS) with 4-Hz temporal resolution.

c. Time series of pressure at approximately 150 cm above the bed with 4-Hz temporal resolution.

d. Time series of pore fluid pressure at approximately 15 cm below the bed with 4-Hz temporal resolution.

e. Time series of vertical and cross-shore components of fluid velocity at approximately 33 cm above the bed using an electromagnetic current meter (EMCM) with 4-Hz temporal resolution.

f. Video recording of ripple changes after wave runs.

Analyses.

a. Mean, minimum, maximum, and standard deviation of pressure, pore pressure, fluid velocities, and sediment concentration data from OBS sensors for each run.

b. Mean of suspended concentration profiles for each run.

c. Calculation of wave power spectrum with calibrated pressure data.

d. Ripple dimensions from the image data of underwater video camera.

The experiments were performed under a variety of forcing conditions, i.e., accretionary and erosive waves, and monochromatic, narrow-band random, and broad-band random waves. Conditions for the data runs are tabulated in Table 10-1, in which H is zero-moment spectral wave height.

Table 10-1
Wave Conditions for Data Runs

Wave Period sec	H_{mo} m	Bandwidth*	Total Run Time min	Run Number
	0.2	Mono BBR	20 20	54 53
3.0	0.4	Mono BBR	20 20	56 55
	0.6	Mono BBR	20 20	58 57
	0.7	BBR	20	38
	0.8	Mono NBR BBR	60 90 80	14 - 17, 60 1 - 7, 59 10 - 13, 18 - 20
	0.9	BBR	40	39, 40
	1.52	Mono	10	43
4.5	0.15	Mono	10	27
	0.8	Mono NBR BBR	40 155 135	33, 34 21 - 26 28 - 32
	0.9	BBR	55	41
5.0	0.7	BBR	60	36, 37, 42
6.0	0.4	Mono BBR	20 20	80 76
	0.8	BBR	20	35
7.0	0.4	Mono BBR	20 20	82 78
	0.5	Mono BBR	20 20	81 77
8.0	0.2	Mono	40	45, 46
		BBR	20	44
	0.4	Mono BBR	55 175	49 47, 48, 61 - 65
	0.5	BBR	95	66 - 68
	0.6	Mono BBR	20 55	51 50
	0.8	BBR	20	52
9.0	0.4	NBR	135	69 - 73
	0.5	NBR	75	74, 75
10.0	0.4	Mono BBR	55 20	83 79
SUBTOTAL			1300 min	81 data runs
Calibration			10.5	8, 9
TOTAL			1310.5 min	83 runs

* Mono: Monochromatic, NBR: Narrow-band random, BBR: Broad-band random

Experiment Apparatus

Instrument description

Acoustic concentration profiler (ACP). The Simrad Mesotech Model 810 is a transceiver that transmits and receives 5-MHz underwater sound. The sound pulse is generated every one-hundredth sec. Backscattered sound energy is detected at the sensor and sampled at 250 kHz. The time delay between transmission and reception of the pulse is proportional to the distance from the sensor to sediment particles. Backscattered intensity is related to the sediment concentration in the ensonified volume. Spatial resolution of the measurement is limited by the pulse length and sampling rate. Temporal resolution is related to the pulse repetition rate and to the number of profiles averaged to produce statistically meaningful data.

Optical backscatter sensor (OBS). The D & A Instrument Co. OBS-1 consists of a high-intensity infrared emitting diode (IRED), a detector (four photo diodes), and a linear, solid-state temperature transducer. The IRED produces a beam with half-power points at 50 deg (0.87 rad) in the axial plane of the sensor and at 50 deg (0.87 rad) in the radial plane. The detector integrates IR scattered between 140 and 160 deg (2.44 and 2.79 rad). The integrated intensity is linearly proportional to the sediment concentration in the vicinity of the sensor. This sensor measures the time series of sediment concentration at one level.

Electromagnetic current meter (EMCM). The Marsh-McBirney Model OEM521 current meter consists of an alternating current electromagnet within a 3.8-cm-diam ball and two pairs of electrodes. The water flowing past the ball interacts with the magnetic field generated by the magnet and produces a voltage that is proportional to the velocity of the water. The two pairs of electrodes detect the voltage and resolve the velocity vector into two components.

Pressure sensor. The Trans Metrics P21 pressure transducer is the bonded strain gauge type, where strain gauges detect strains caused by pressure. It measures absolute pressure.

Pore pressure sensor. The Druck miniature pore water pressure transducer type PDCR 81 is a wet-dry differential pressure gauge with a porous filter plate at the wet end to resist the effective stress of bed soil. The wet end is exposed to bed soil and the dry end is kept dry in the housing. Back pressure is established by compressing the dry air in an underwater housing with a miniature latex balloon, which is installed inside the housing and inflated by hydrostatic water pressure. The strain of the diaphragm caused by the difference in pressure between the ends is detected by strain gauges.

Underwater video camera. The Sony Hi-8 CCD V99 video camera is put underwater and aimed towards a reference grid on the wall of the channel to measure sand ripples. The video signal is sent through cable to a shore-based video recorder. Camera features are directly controlled with a shore-based computer.

Location

ACP. The x, y, and z coordinates of the sensor were 205.13 ft (62.52 m), 9.73 ft (2.97 m), and -10.91 ft (-3.32 m), respectively, in the SUPERTANK coordinate system (Chapter 1). All electronic components were installed in a 3.5-in.- (8.9-cm-) square, 8.2-in.- (20.8-cm-) long, gold anodized aluminum alloy housing. The unit was attached to a steel bracket which was in turn clamped on the wall-mounted vertical steel rod. DC power, a TTL-compatible trigger source, and analog output were connected through a single 6-pin underwater connector to the shore station.

OBS sensor. Two sensors were deployed. The x, y, and z coordinates of the sensor closer to the ACP were 205.12 ft (62.52 m), 9.72 ft (2.96 m), and -10.989 ft (-3.35 m), respectively. The x, y, and z coordinates of the sensor closer to the bottom were 205.10 ft (62.51 m), 9.70 ft (2.96 m), and -12.530 ft (-3.82 m), respectively. Sensor components are potted in glass-filled polycarbonate with optical-grade epoxy. The unit was attached to a steel clamp, which was connected to the wall-mounted vertical steel rod. Electronic connection to the underwater package was made through an underwater pie connector.

EMCM. The x, y, and z coordinates of its center were 205.11 ft (62.52 m), 9.82 ft (2.99 m), and -11.74 ft (-3.58 m), respectively. The unit was attached to a steel clamp which is connected to the wall-mounted vertical steel rod. It was adequately oriented such that the cross-shore and vertical components of flow velocity were measured. Electronic connection to the underwater package was made through a permanent connector.

Pressure sensor. The x, y, and z coordinates of its center were 205.13 ft (62.52 m), 11.39 ft (3.47 m), and -7.917 ft (-2.41 m), respectively, from August 12 to 16. This unit was built into the underwater package. The underwater package was installed to a wall-mounted bracket above the other instruments. The sensor was at one end of the package cylinder and in line with the ACP from 12 to 16 August, but it was approximately 1 ft offshore from the other instruments over 5 to 9 August.

Pore pressure sensor. The x, y, and z coordinates of the sensor were 205.13 ft (62.52 m), 9.75 ft (2.97 m), and -13.207 ft (-4.03 m), respectively. The sensor is housed in a Plexiglas pipe, which was attached to a wall-mounted clamp. The clamp and sensor were buried in bed soil such that the distance from the sensor to the bed surface was approximately 6 in. (15 cm).

Underwater video camera. The camera is encased in an underwater video housing. The housing was mounted to a long pole and attached to a cart above the water, which allowed it to be easily relocated and removed from the water when not in use.

Instrument characteristics

ACP. The maximum range is 2.6 m. The operating frequency is 5 MHz. Nominal beam width is 3.2 deg. The pulse length is selected to 20 μsec, and its repetition rate is 100 Hz. Power requirement is 24 V DC at 300 mA. The output frequency, voltage, and noise are 455 kHz, 1 V peak to peak, and 300 mV peak to peak at maximum, respectively. The time varying gain is set to 20 $\log(R\text{-}0.007)$ + 4.54$(R\text{-}0.007)$ +10 db, where R is range in meters. The analog output is demodulated and then digitized by a Data Translation DT2831 board. The digital range is 0 to 4,095.

OBS. The dynamic range for sand and turbidity are 100 to 100,000 mg/ℓ and 0.5 to 2,000 FTU, respectively. The nonlinearity for sand is 3.5 percent over 0 to 600,000 mg/ℓ. The power requirement is 9 to 30 V/57 mA. Output span is 0 to 3.5 V. The cutoff frequency of the output filter is 20 Hz. The RMS noise at 0 FTU is less than 100 μV. The analog output is digitized by an Onset Computer Tattletale 6. The digital range is 0 to 4,095.

EMCM. The full-scale range of water velocity components is -3 to +3 m/sec. Analog voltages are scaled from -4 to +4 V. Long-term zero drift is less than 2 cm/sec. Nonlinearity is 2 percent of reading. Absolute calibration error is 2 percent of reading. Supply current is 18 mA at 6 V DC. The analog output is digitized by the Onset Computer Tattletale 6. The digital range is 0 to 4,095.

Pressure sensor. Rated and proof pressures are 20,000 and 40,000 psi. The full-scale output is a nominal 5-V DC standard. Analog output is digitized by the Onset Computer Tattletale 6. The digital range is 0 to 4,095.

Pore pressure sensor. The operating pressure range is 5 psi. The nominal excitation range is 5 V at 6 mA. The output voltage at nominal excitation is 35 mV. The zero offset is -10 to +10 mV. The combined nonlinearity and hysteresis is -0.2 to +0.2 percent BSL. Analog output is digitized by the Onset Computer Tattletale 6. Digital measurement is made in one of five overlapping ranges each ranging from 0 to 4,095.

Underwater video camera. The format of the image signal is NTSC Hi-8 type. Temporal resolution is 30 frames per second.

Experiment Procedures

Sequence of events

Data were collected from the instrumentation using two independent computer systems because of the high speed of collection and the large quantity of data generated by the ACP. In a typical data run, the collection software on the AT computer was started 15 sec before data collection was to begin. The AT then signaled the second system, Onset Computer Tattletale Model 6 data logger, that collection was to begin. After this original synchronization, the two systems ran independent of one another. The data logger then turned power on to each of the slow instruments, which consisted of the EMCM, both OBS, the pressure sensor, and the pore pressure sensor. This allowed almost 15 sec for the instruments to warm up. During the warm-up period, headers to the data files were created which specified the starting and ending times of collection and the number of points to be sampled. After the warm-up period, data collection from the ACP began on the AT, and, simultaneously, data collection from the slow instrumentation began on the data logger. On both systems, data were collected and stored in memory until the end of the data run, at which point data were saved to disk.

Calibration and zero reference

The calibration facility of the ACP and OBS sensors consists of a cylinder and a circulation system, as seen in Figure 10-2. The cylinder is made of Plexiglas and has four jet holes on the wall at its top and a funnel at its bottom. The circulating system consists of a centrifugal pump, circulation tube, and four jets. The pump circulates a sand-water mixture to create as uniform a sand concentration in the cylinder as possible. The jets help make the concentration more uniform. The funnel prevents accumulation of sand at the bottom.

The total volume of water is measured. Then dry sand is weighed and added to water in an accumulative manner to create from low to high concentration while the pump circulates the mixture continuously.

The relationship between the backscattered acoustic intensity and the suspended sediment concentration is expressed by the following nonlinear equation

$$A \ C(z) = V(z)^2 \ \exp \left[\int_0^z k_1 + k_2 \ C(\zeta) \ d\zeta \right] \tag{10-2}$$
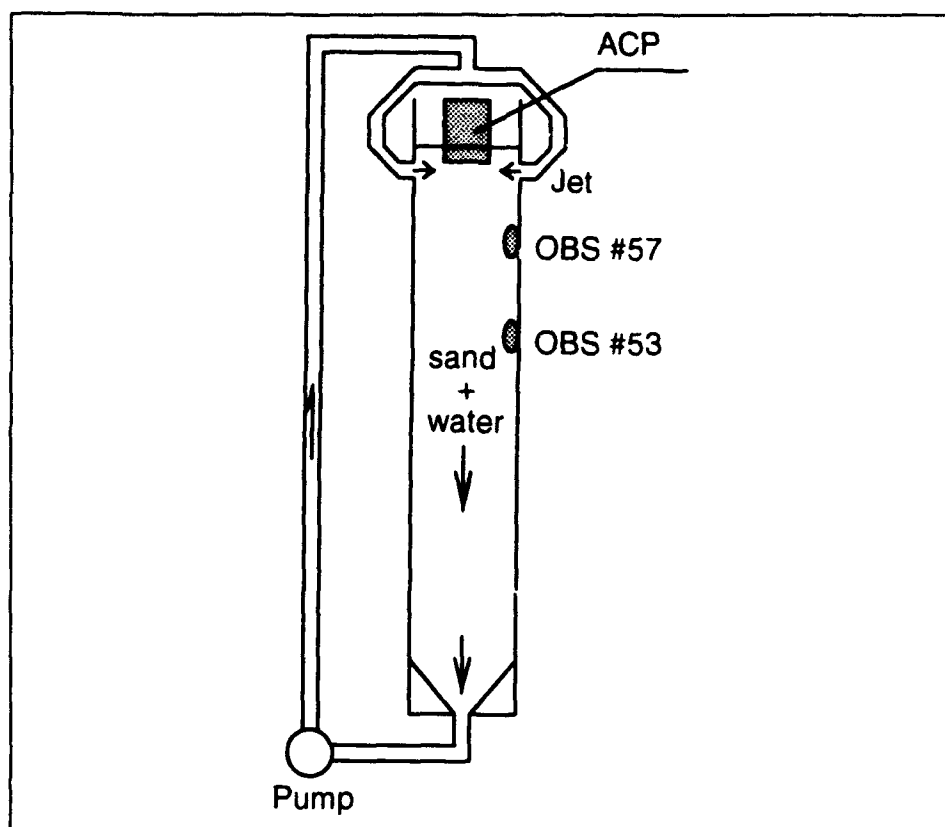
Figure 10-2. ACP calibration tank

where

A	=	overall system constant including backscatter coefficient for the suspended sediment
$C(z)$	=	suspended sediment concentration at distance z from the ACP
$V(z)$	=	backscattered intensity signal associated with the distance z from the ACP
k_1	=	attenuation coefficient associated with the absorption by water and wash load
k_2	=	attenuation coefficient associated with the scattering by suspended sediment particles

For uniform concentration, Equation 10-2 becomes the following simpler equation

$$A \, C = V(z)^2 \, \exp[(k_1 + k_2 C) \, z] \qquad (10\text{-}3)$$

The calibration constants, A, k_1, and k_2 are determined by taking the logarithm of Equation 10-3, solving for $V(z)$, and applying linear regression as follows:

$$\ln V(z) = G z + O \tag{10-4}$$

where $G = -\frac{1}{2}(k_1 + k_2 C)$ and $O = \frac{1}{2}\ln(A C)$. The coefficients k_1 and k_2 are found by linear regression of G and C. If $C(z_o)$, the concentration at $z = z_o$ in the near field, is known, then we need to know only k_1 and k_2 to invert the voltage-to-sediment concentration.

Equation 10-3 can be discretized

$$A C_I = V_I^2 \exp\sum_{i=1}^{i=I} \left\{\left[k_1 + \frac{1}{2} k_2 (C_{i-1} + C_i)\right] (z_i - z_{i-1})\right\} \tag{10-5}$$

If we divide Equation 10-5 by the following

$$A C_{I-1} = V_{I-1}^2 \exp\sum_{i=1}^{i=I-1} \left\{\left[k_1 + \frac{1}{2} k_2 (C_{i-1} + C_i)\right] (z_i - z_{i-1})\right\} \tag{10-6}$$

we obtain the implicit expression for C_I,

$$C_I = C_{I-1} \frac{V_I^2}{V_{I-1}^2} \exp\left\{\left[k_1 + \frac{1}{2} k_2 (C_{I-1} + C_I)\right] (z_I - z_{I-1})\right\} \tag{10-7}$$

The concentration C_I at $z = z_I$ is calculated by iteration with C_{I-1}, V_{I-1}, V_I, k_1, and k_2 given. V_{I-1} and V_I are raw data.

Simultaneous calibration of the ACP and the OBS in the recirculating calibration cylinder assured agreement in the sediment concentrations. Use of the sediment from the experiment minimized errors due to variable sediment characteristics.

The linear calibration formula is as follows:

$$Y = G X + Off \tag{10-8}$$

where G is the calibration gain constant, Off is the calibration offset constant, and X is the uncalibrated data value. This formula was applied to data from the pressure sensor, both OBS, the EMCM, and the pore pressure sensor with the gain and offset values shown in Table 10-2. After applying the calibration formula to the data, the resulting values for the OBS were adjusted by subtracting the background concentration. The background concentration was determined by averaging the OBS sensors return values during periods in which waves were not being generated. In this way, the sand suspension

events due only to wave activity could be isolated from the turbidity present even during periods of calm. In addition to determining the background concentration during these periods, the still-water level was determined using the mean return from the pressure sensor. Knowledge of the water level allowed accurate determination of wave energy spectra from the calibrated pressure signal, as described in the analysis portion of this chapter.

Calibration of the pressure sensor was accomplished by collecting data from the sensor at different gauge-measured pressures of compressed air. The EMCM was calibrated by the manufacturer prior to the experiment, so calibration constants were provided by the manufacturer.

To collect pore-pressure measurements with the maximum resolution the instrument was capable of providing, an interface was designed which allowed measurements to be made over five software selectable ranges. A low-resolution sample from the sensor was used to determine the appropriate range for high-resolution measurement. Each of the selectable ranges, as well as the low-resolution portion of the interface, were calibrated separately by varying hydrostatic pressure.

Sampling and time reference

As stated previously, two separate data acquisition systems were used for data collection. The first system consisted of a high-speed data acquisition card in a 386 AT computer. Data from the ACP were collected on this system at a maximum rate of 250 kHz. As many as 512 data points were collected at 250 kHz, these points making up a single profile. At this rate, each data point, or bin, in the profile represented the concentration over a vertical section 3 mm in height. It should be noted that, although the sampling rate allows a maximum resolution of about 3 mm per bin, the actual resolution is further limited by the pulse width of the ACP. Away from the bed, where high spatial resolution was not necessary, four adjacent bins were averaged reducing the maximum spatial resolution of the concentration to a vertical section 1.2 cm in height. This spatial averaging was performed in most of the data runs. Bins close to the bed were not spatially averaged. In addition to spatial averaging, each set of 25 consecutive profiles was averaged, finally yielding four profiles per second averaged in both time and space.

The first data acquisition system served as a master system, in that starting data collection on this system also simultaneously started acquisition on the second system. The second system was the Tattletale model 6 data logger sampling data from two OBS, one pressure sensor, one pore pressure sensor, and one EMCM, at 4 Hz.

**Table 10-2
Calibration Constants**

Instrument	Gain	Offset	Regression Coefficient	Number of Points
OBS 9 cm from the bed	5.1570 mg/l	-1125.7 mg/l	0.9845	20
OBS 56 cm from the bed	9.4681 mg/l	-2308.9 mg/l	0.9923	20
Pressure	0.0084 m of H_2O	-11.0216 m of H_2O	1.0000	6
Current (both components)	1.861×10^{-3} m/sec	-3.81 m/sec	-	-
Pore Pressure-low-gain	3.6×10^{-3} ft of H_2O	-1.3350 ft of H_2O	0.9999	84
Pore Pressure-range 1	7.302×10^{-4} ft of H_2O	-1.3232 ft of H_2O	0.9995	12
Pore Pressure-range 2	7.133×10^{-4} ft of H_2O	0.9117 ft of H_2O	1.0000	23
Pore Pressure-range 3	7.196×10^{-4} ft of H_2O	3.0889 ft of H_2O	1.0000	21
Pore Pressure-range 4	7.564×10^{-4} ft of H_2O	5.2803 ft of H_2O	1.0000	17
Pore Pressure-range 5	7.874×10^{-4} ft of H_2O	7.5625 ft of H_2O	0.9999	10

After initial synchronization between the two systems, each system sampled according to its own internal clock. Each of the internal clocks was set at the beginning of the day to the international time standard.

Preprocessing and filtering

Because the ACP used in this experiment was designed for field use, the return signal from it is amplitude modulated on a 455-kHz carrier. Such a modulated signal can be sent over long distances with only small losses in data quality. Because of this, low-pass filtering is necessary to separate the signal from the carrier. This filtering of the acoustic data was performed with a passive two-pole low-pass filter with a 100-kHz cut-off frequency. The OBS and pressure sensor contain low-pass filters with cut-off frequencies of 5 Hz to remove electronic noise and to make the measured data points representative of the time-averaged signal between samplings. The EMCM signal

is low-pass filtered through a two-pole filter with a cutoff of 5 Hz. The pore-pressure signal was not susceptible to electronic noise, and because it was desirable to have a rapid response on this instrument, this sensor remained unfiltered.

Data Analysis

Analysis and interpretation methods

To simplify analysis of the data, data from each run were stored in two separate files, one file containing acoustic profiler data and the other containing data from all of the additional instruments. Analysis of the data from all of the instruments was performed using the software package Matlab from Mathworks, Inc.

Statistical values, including the mean value, the standard deviation, the minimum value, and the maximum value, were computed for each of the slow instruments for each experimental run. Because some of the data runs included time intervals in which waves were not being generated, these statistical values were computed over only the time period during which waves were being generated. Variable names for these statistical values, as well as all other calibrated and uncalibrated data values for each of the slow instruments, are found in Table 10-3.

To determine the wave energy spectrum, a fast Fourier transform was applied to the calibrated pressure signal, and from this the pressure spectrum was determined. To correct for the attenuation of higher frequency pressure measurements with depth, the pressure response factor K_p was determined for each run (Dean and Dalrymple 1984)

$$K_p(z) = \frac{\cosh k (h + z)}{\cosh k h}$$ (10-9)

where

k = wave number for particular frequency
h = water depth
z = depth of pressure sensor

Wave frequencies greater than 1 Hz were filtered out from the pressure spectrum to remove instrument noise. Each discrete frequency component of the pressure spectrum was then multiplied by $1/K_p$ for that frequency to obtain the final wave energy spectrum.

The high-resolution pore pressure was then calibrated by examining the low-resolution return signal and then determining in which range the high-

Table 10-3
List of Variables from Slow Instrument Data File

Variable Name	Description
STIME	Starting time of data collection - string variable.
ETIME	Ending time of data collection - string variable.
PRESSURE	Calibrated regular pressure in m of fresh water.
MEANPRES	Mean regular pressure in m of fresh water.
STDPRES	Standard deviation of regular pressure in m of fresh water.
MAXPRES	Maximum regular pressure in m of fresh water.
MINPRES	Minimum regular pressure in m of fresh water.
SPEC	Pressure-corrected surface elevation spectrum from pressure data.
XAXIS	Frequency axis for surface elevation spectrum.
PPLOW	Calibrated low-gain channel of pore pressure sensor in m of fresh water.
MEANPPL	Mean low-gain pore pressure in m of fresh water.
STDPPL	Standard deviation of low-gain pore pressure in m of fresh water.
MAXPPL	Maximum low-gain pore pressure in m of fresh water.
MINPPL	Minimum low-gain pore pressure in m of fresh water.
PPHIGH	Calibrated high-gain channel of pore pressure sensor in m of fresh water.
MEANPPH	Mean high-gain pore pressure in m of fresh water.
STDPPH	Standard deviation of high-gain pore pressure in m of fresh water.
MAXPPH	Maximum high-gain pore pressure in m of fresh water.
MINPPH	Minimum high-gain pore pressure in m of fresh water.
OBS09	Calibrated OBS at 9 cm from bed in g/ℓ.
OFF09	Background conc. applied to OBS at 9 cm from bed in mg/ℓ.
MENOBS09	Mean of OBS at 9 cm from bed in g/ℓ.
STDOBS09	Standard deviation of OBS at 9 cm from bed in g/ℓ.

(Continued)

Table 10-3 (Concluded)

Variable Name	Description
MAXOBS09	Maximum of OBS at 9 cm from bed in g/ℓ.
MINOBS09	Minimum of OBS at 9 cm from bed in g/ℓ.
OBS56	Calibrated OBS at 56 cm from bed in g/ℓ.
OFF56	Background conc. applied to OBS at 56 cm from bed in mg/ℓ.
STDOBS56	Standard deviation of OBS at 56 cm from bed in g/ℓ.
MENOBS56	Mean of OBS at 56 cm from bed in g/ℓ.
MAXOBS56	Maximum of OBS at 56 cm from bed in g/ℓ.
MINOBS56	Minimum of OBS at 56 cm from bed in g/ℓ.
CURRENTU	Calibrated u direction current in m/sec.
MEANU	Mean u direction current in m/sec.
STDU	Standard deviation of u component current in m/sec.
MAXU	Maximum u component current in m/sec.
MINU	Minimum u component current in m/sec.
CURRENTW	Calibrated w component current in m/sec.
MEANW	Mean w component current in m/sec.
STDW	Standard deviation of w component current in m/sec.
MAXW	Maximum w component current in m/sec.
MINW	Minimum w component current in m/sec.
H	Water depth in m.
Z	Depth of pressure sensor in m.
INDEX	Run number.
BOTTOMBIN	Bottom bin number of mean signal.
PRECONC	Concentration profile inverted from mean signal in mg/ℓ.
BACKBOTTOM	Bottom bin number of background signal.
BACKCONC	Background conc. profile inverted from background signal in mg/ℓ.
MEANCONC	Preconc. subtracted by backconc. in mg/ℓ.

resolution data were collected. Once this was known, the appropriate calibration for that range was applied. Because the interface could possibly change ranges for even a single data point, this determination of the range was performed for each data point in the time series.

Data file format

During the course of the two weeks that data were collected, 83 files of both slow instrument data and ACP data were collected. Because several data collection periods often occupied a single official wave run, the naming convention for the data files differs slightly from the set standard. All data are stored in the binary file format used by the Matlab software package. One file in this format contains one or more variables. One data file contains each of the variables listed in Table 10-3.

Each variable starts with a fixed length 20-byte header that contains information describing certain attributes of the variable. For purposes of this report, the information in Table 10-4 is sufficient to describe the header and the additional information found in the data file.

Sample raw data

Figures 10-3 through 10-6 show the uncalibrated signals from the pressure sensor, pore pressure sensor, u channel of the EMCM, and OBS located 56 cm from the bed. The data are from about 2 min into run 12. Digital values from the data logger are plotted against the sample number. Since data were sampled at a rate of 4 Hz, each sample number represents a 0.25-sec time increment. Spikes in the high-gain pore pressure plot, Figure 10-4, result from the interface changing sampling ranges as described previously. Figure 10-7 shows the ripple pattern that has been digitized from the videotape after run 56.

Uncalibrated data from the ACP are shown in Figure 10-8. The vertical axis in this plot represents the digital value returned from sampling the return voltage from the ACP. The sediment concentration at some location on this axis is a function of the intensity of the return as well as the distance from the sensor head and the concentration above the point. The bottom left axis represents the distance from the sensor head, and the bottom right axis represents the elapsed time from profile to profile.

Sample interpreted data

Figures 10-9 through 10-12 display calibrated versions of the same data shown in the previous section, from run number 12, for the pressure sensor, pore pressure sensor, u channel of the EMCM, and OBS located 56 cm from the bed. Shown in Figure 10-13 is the ripple pattern shown in Figure 10-7

Byte numbers	Typical values (stored LSB to MSB)	Description
		Table 10-4
		Data File Format
1 to 4	100	If the integer 0 is stored in these four bytes, data are stored in a column-wise orientation (first column, then second column, etc.). If the integer 100 is stored in these four bytes, data are stored in a row-wise orientation (first row, then second row, etc.).
5 to 8	100	The integer stored in these four bytes represents the number of rows in the matrix.
9 to 12	8	The number of columns in the matrix.
13 to 16	0	Indicates that the matrix is of real numbers.
17 to 20	4	Length of the variable name plus one.
21 to 23	tat	ASCII codes of characters in variable name. Note that there will be one byte for each character in the variable name.
24	0	NUL character.
25 to (N-1)	DATA	Data in the matrix, stored sequentially as eight-byte floating point values.
N to (N + 3)	100	First four bytes of header for next variable.

with the best-fit straight line through the pattern subtracted from it. This detrending of the data minimizes effects of bottom slope and errors from the grid not being exactly horizontal.

Figure 10-14 shows mean concentration over the entire run against distance from the ACP. The furthest point from the ACP in the concentration profile is the concentration just above the bottom, where the bottom location has been determined from the most common instantaneous bottom location during the course of the run, whichever is closest to the ACP.

Summary of data characteristics

Table 10-5 shows an example listing of statistical data for run 12, consisting of the maximum, minimum, mean, and standard deviation for the pressure sensor, both OBS, both channels of the EMCM, and both the low- and high-gain channels of the pore pressure sensor. From the ripple measurements, the maximum, minimum, and standard deviation of the detrended data are listed.
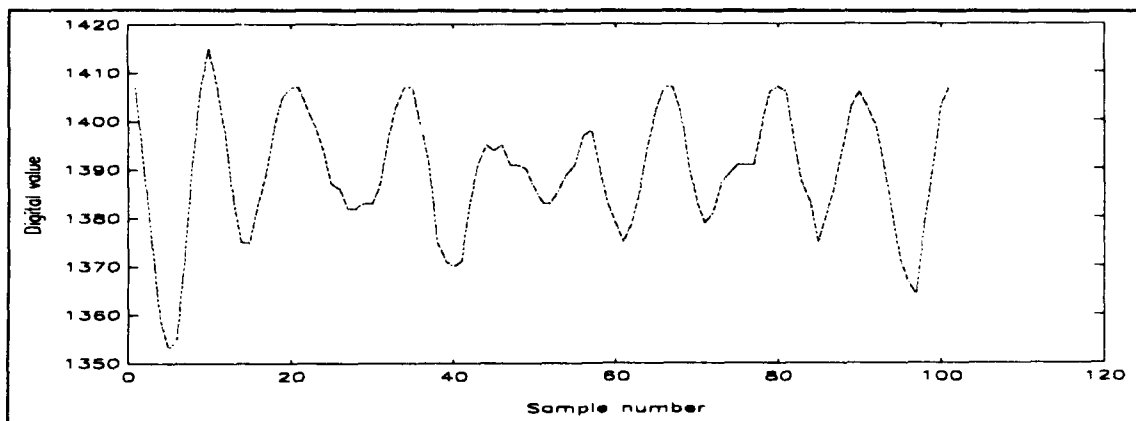
Figure 10-3. Uncalibrated pressure signal
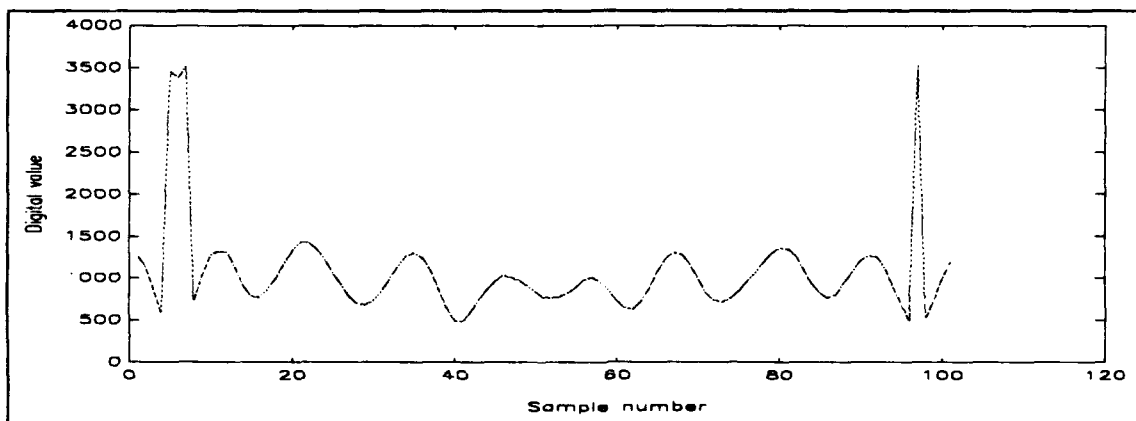
Figure 10-4. Uncalibrated high-gain pore pressure signal
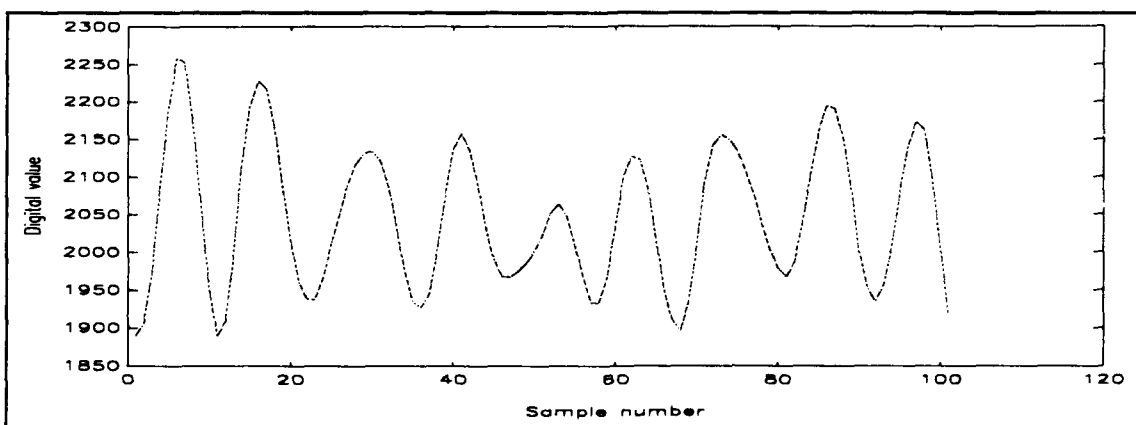
Figure 10-5. Uncalibrated u current velocity signal
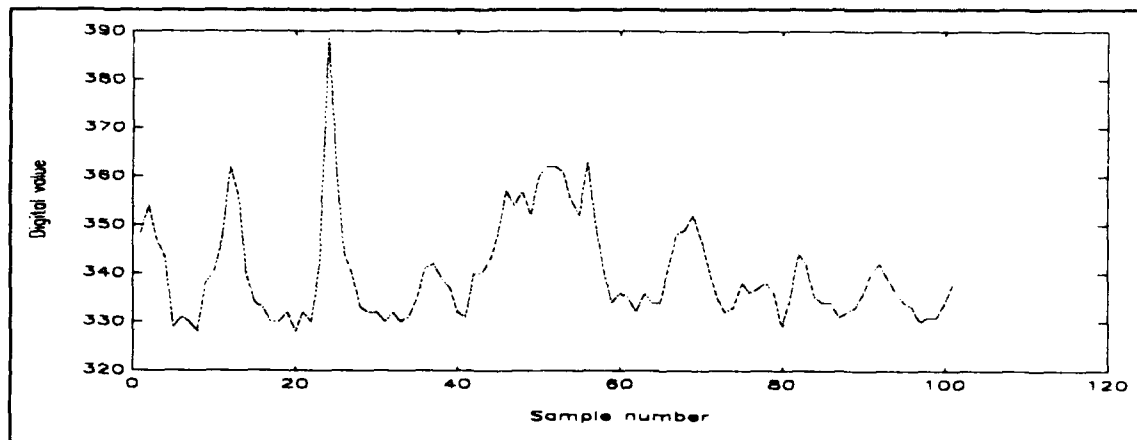
Figure 10-6. Uncalibrated OBS signal from 56 cm above the bed
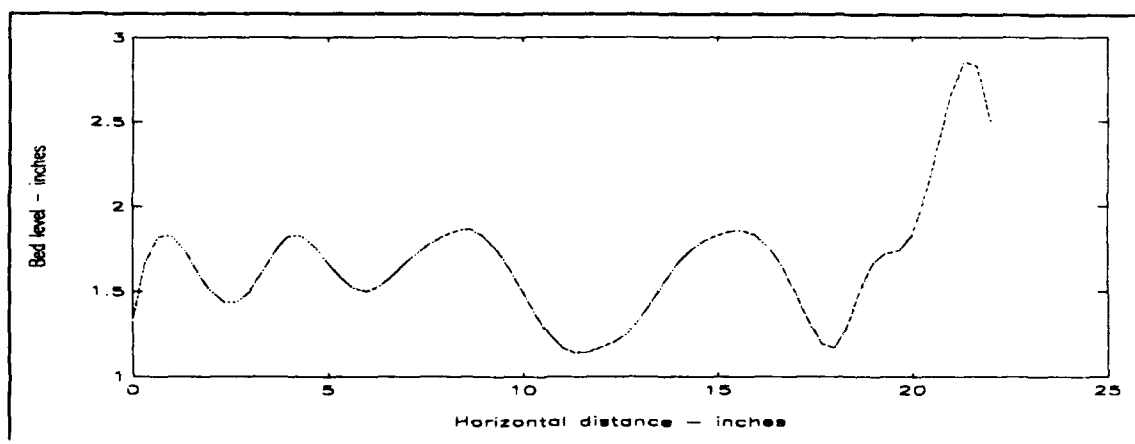
Figure 10-7. Observed ripple pattern

Several of the statistical values listed should be used with care due to peculiarities of the measurement systems. First, data calibrated from the pore pressure sensor contain spikes that one can easily identify, but cannot be as easily identified by a computer algorithm. The presence of these spikes in the data set can cause disagreement between the listed statistics and the statistics computed after their removal. Second, due to large particulate matter in the water, the signals from the OBS also contain spikes. The maximum value probably represents data collected from such an event. Also, because the background concentration has already been subtracted, the minimum value from the OBS sensors is not representative of the background. The background value subtracted from the signal is also given. Finally, what has been listed as the w-flow velocity component may contain some portion of the u-velocity component due to a slight rotation of the EMCM during deployment.
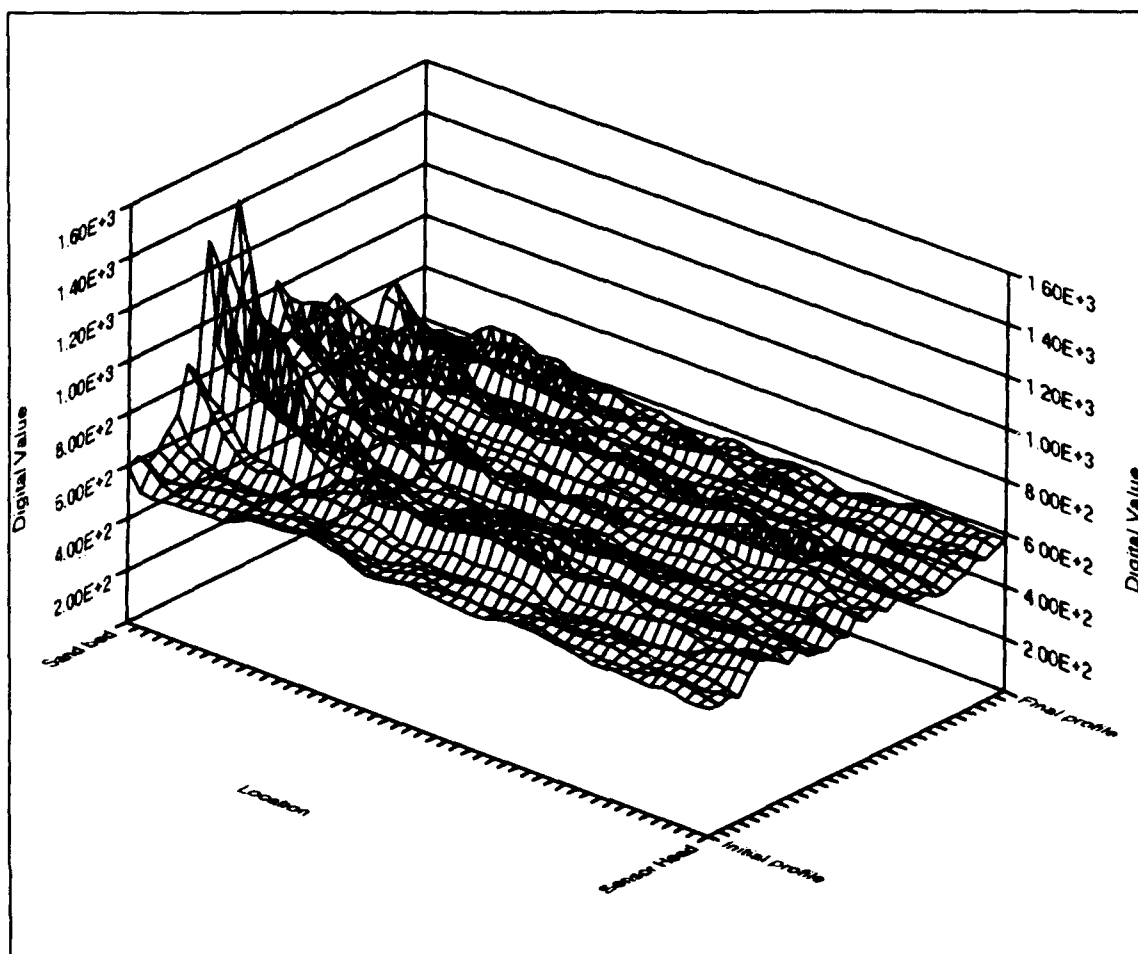
Figure 10-8. Time series of uncalibrated ACP profiles
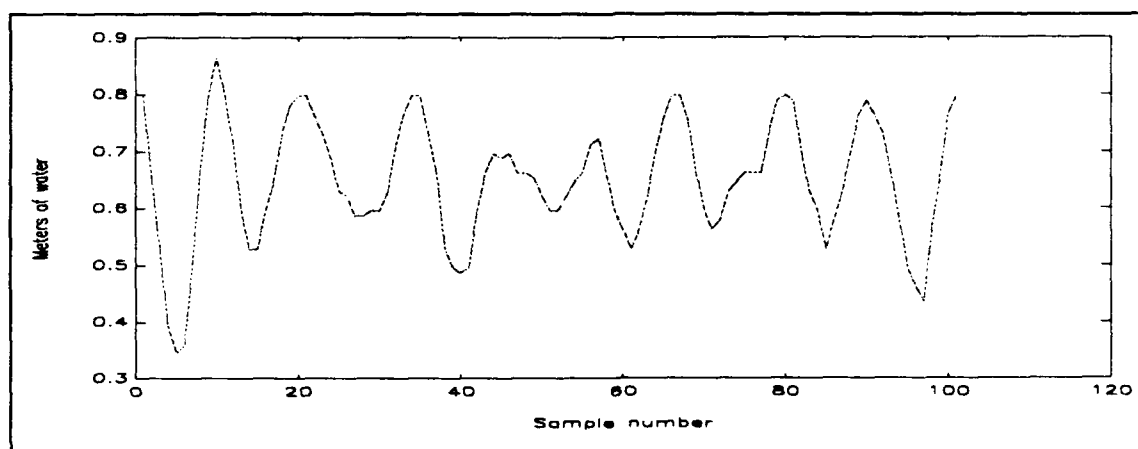
Figure 10-9. Calibrated pressure signal
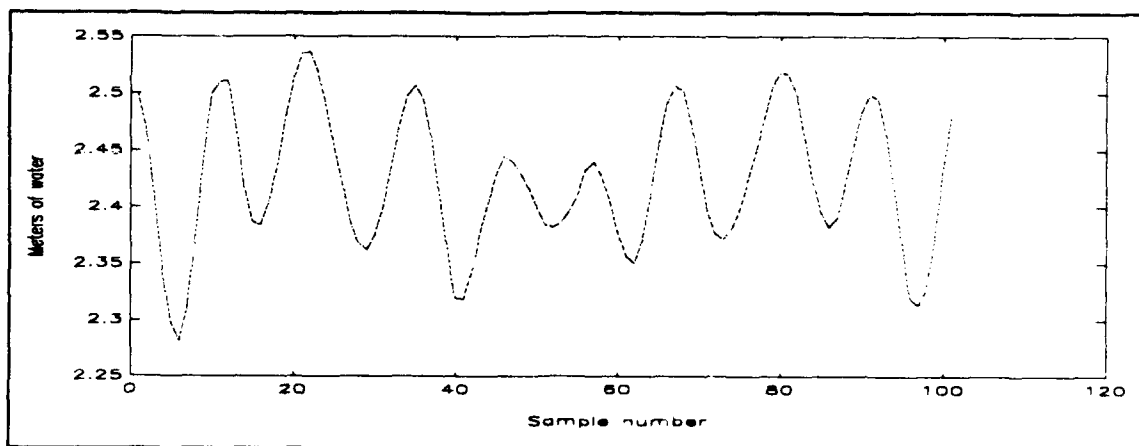
Figure 10-10. Calibrated high-gain pore pressure signal
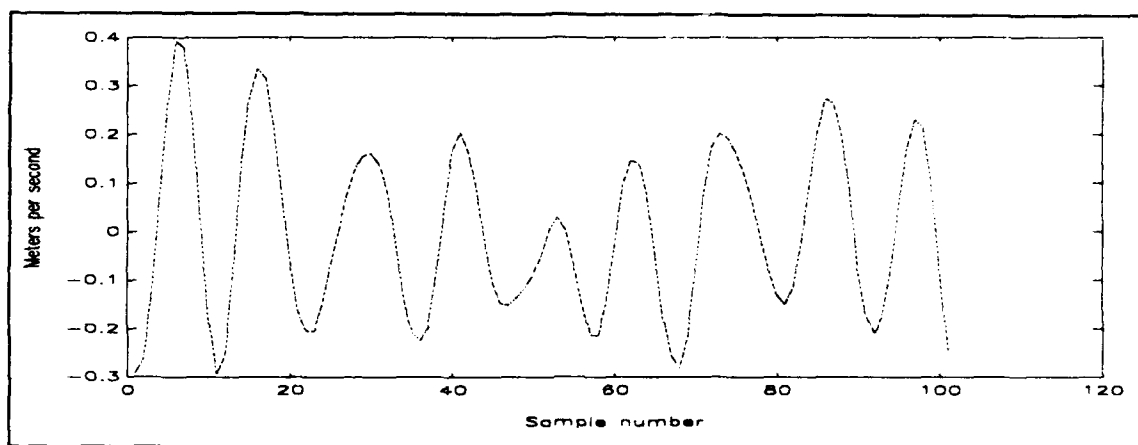
Figure 10-11. Calibrated U current velocity signal
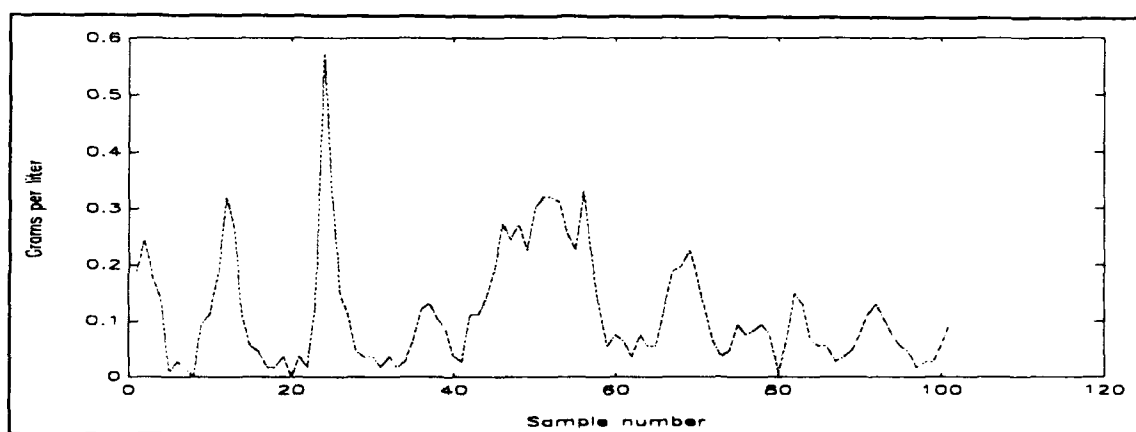
Figure 10-12. Calibrated OBS signal from 56 cm above the bed
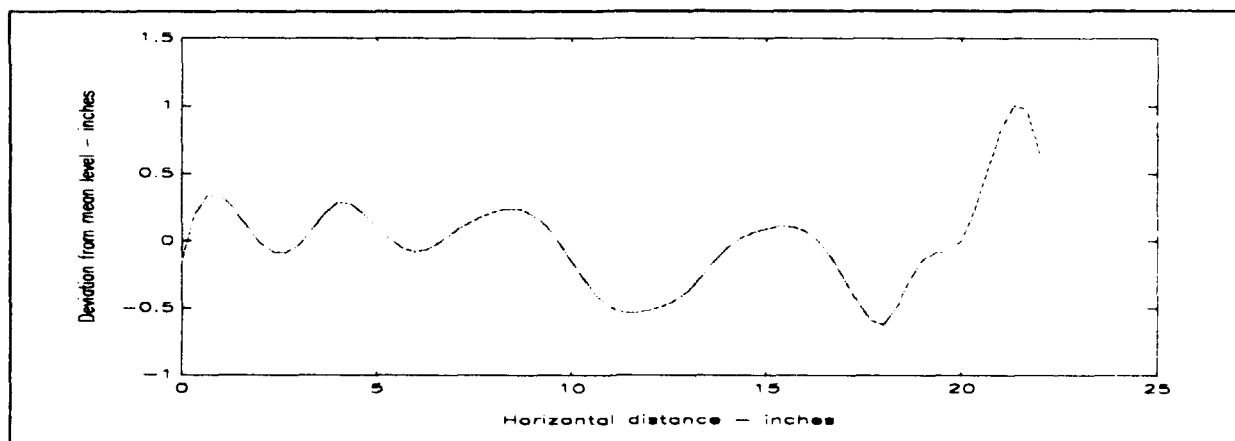
Figure 10-13. Detrended ripple pattern
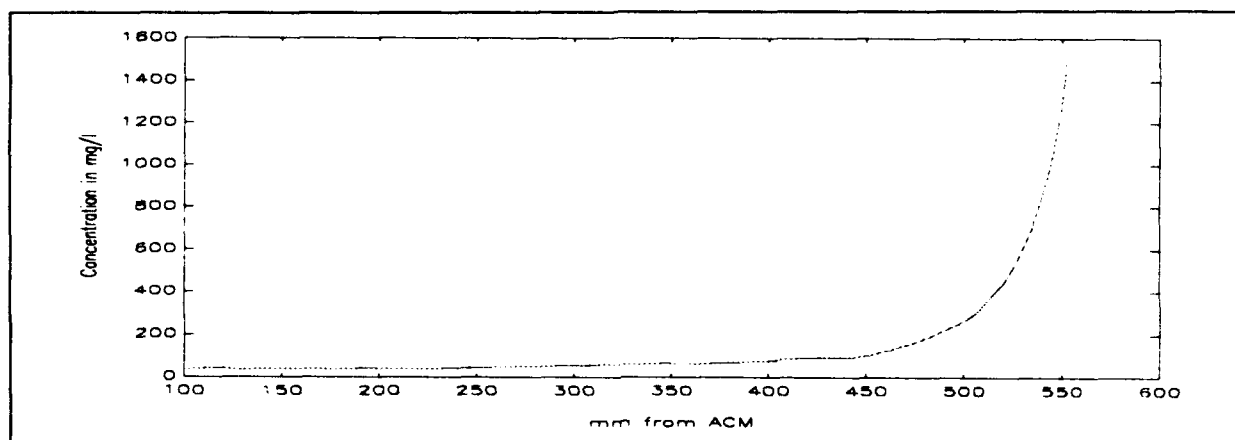
Figure 10-14. Calibrated ACP mean profile

The ACP data files have background concentration profiles and mean concentration profiles with and without subtraction of the background concentration as shown in Table 10-3. Some of the mean profiles without subtraction of the background show a bump which is caused by the partial reflection of the sonar beam from the OBS body. Some of the bumps were almost eliminated by subtracting the background from the mean concentration profile. The mean concentration profiles subtracted by the background are valid up to the smaller bottom bin number between those of the background and mean signal profiles.

Chapter 10 Intermittent Near-Bed Sediment Suspension

Table 10-5
Data Run Summary

Run number	12
SUPERTANK run title	A0611A
Starting date of wave run	08/06/91
Starting time of wave run	11:00:00
Starting time of data collection	10:59:50
Length of data collection	00:10:00
Wave energy spectral shape	BBR
Wave period - sec	3.0
Wave height - m	0.80
Water depth - ft	7.021
9 cm OBS background conc. - mg/l	861.1632
56 cm OBS background conc. - mg/l	798.0570
Pressure mean - m	0.648
Pressure standard deviation - m	0.116
Pressure maximum - m	0.999
Pressure minimum - m	0.243
Low-gain pore pressure mean - m	2.425
Low-gain pore pressure std deviation -m	0.068
Low-gain pore pressure maximum - m	2.649
Low-gain pore pressure minimum - m	2.144
High-gain pore pressure mean - m	2.424
High-gain pore pressure std deviation - m	0.075
High-gain pore pressure maximum - m	3.136
High-gain pore pressure minimum - m	1.688
	(Continued)

Table 10-5 (Concluded)	
9 cm OBS mean - g/ℓ	0.196
9 cm OBS standard deviation - g/ℓ	0.237
9 cm OBS maximum - g/ℓ	1.839
9 cm OBS minimum - g/ℓ	0.000
56 cm OBS mean - g/ℓ	0.044
56 cm OBS standard deviation - g/ℓ	0.052
56 cm OBS maximum - g/ℓ	1.580
56 cm OBS minimum - g/ℓ	0.000
u flow velocity mean - m/sec	0.033
u flow velocity standard deviation - m/sec	0.213
u flow velocity maximum - m/sec	0.891
u flow velocity minimum - m/sec	-0.535
w flow velocity mean - m/sec	0.014
w flow velocity standard deviation - m/sec	0.036
w flow velocity maximum - m/sec	0.146
w flow velocity minimum - m/sec	-0.121
Background concentration profile	Array of data
Mean concentration profile	Array of data, see Figure 10-14
Bed level deviation - standard deviation	Not measured
Bed level deviation - maximum	Not measured
Bed level deviation - minimum	Not measured

Identification of marginal data sets

Although problems did exist with some data sets, the majority of data collected are accurate and useful. During the first week, data from the OBS located 9 cm from the bed were corrupt, because the face of the sensor was partially blocked by the mounting apparatus. This problem only occurred

from runs 21 to 43, and, during this time, suspended sediment concentration data were still accurately collected from the other OBS and the ACP. Flow velocity data from the second week were inaccurate due to a malfunction of the EMCM. This malfunction occurred from runs 40 to 83. Velocity data could be derived from pressure sensor data or could be obtained from other investigators in the area.

Examination of the return signal from the ACP revealed the presence of the OBS in the path of the acoustic beam. Because the OBS were at fixed locations, acoustic signals were affected identically with each profile. the presence of the OBS in the profile is not significant, and the effect was eliminated from almost all the concentration profiles in the calibration as explained in the summary of data characteristics. This presence can be seen in the raw data from runs 1 to 62.

Summary

Review of experiments and results

The information provided in this chapter represents a fairly thorough description of the hydrodynamics and resulting sediment dynamics in a single location in the offshore region of the channel. The large fluctuation of measured values over short periods of time in this region suggests the timing of individual suspension events may be an important contribution to the resulting sediment transport. Variations in sediment concentration with height from the bed appear to be significant, and inspection of data from the OBS and the ACP verifies that these fluctuations can be measured with high spatial and temporal resolution. This knowledge will aid in describing the small-scale processes, which will in turn reveal the importance of these processes in modeling large-scale bathymetric changes. At times, other investigators simultaneously collected data with instrumentation positioned at the same location in the offshore region. Examination of additional data from these other investigators can further enhance the value of this data set.

Recommendations

Although this data set is fairly complete, its usefulness is limited due to several factors. The most obvious limiting factor was in the use of a laboratory channel. Because the waves were prototype scale, agreement with field measurements is probably close, but the ideal unidirectionality of the waves, the near ideal bathymetry, and other obvious discrepancies with an actual field site are sure to cause some differences. In March of 1992, a field experiment was conducted at Vilano Beach, FL, with the same instrumentation. The present analysis of the data from the field experiment should provide the necessary data to form a comparison between the lab and

field projects. Any additional research on the hydrodynamics near the seabed would increase the usefulness of data collected with this instrumentation.

Acknowledgments

References

Dean, R. G., and Dalrymple, R. A. (1984). *Water wave mechanics for engineers and scientists*. Prentice Hall, Englewood Cliffs, NJ.

Hanes, D. M. (1990). "The structure of events of intermittent suspension of sand due to shoaling waves." *The sea: ocean engineering science*. Wiley-Interscience, New York.

Huntley, D. A., and Hanes, D. M. (1987). "Direct measurement of suspended sediment transport." *Proc. of Coastal Sediment '87*. ASCE, New York, 723-37.

Jaffe, B. E., Sternberg, R. W., and Sallenger, A. H. (1985). "The role of suspended sediment in shore-normal beach profile changes." *Proc. of 19th Coastal Engrg. Conf.* ASCE, New York, 1983-96.

Vincent, C. E., Hanes, D. M., and Bowen, A. J. (1991). "Acoustic measurements of suspended sand on the shoreface and the control of concentration by bed roughness," *Marine Geology* 96, 1-18.

11 Laser Doppler Velocimetry and Sediment Concentration in the Bottom Boundary Layer at SUPERTANK[1]

Introduction

Background

Understanding of near-bed dynamics of wave boundary layers is central to sediment transport predictions in the nearshore region. Wave-induced motion at the bed produces a thin oscillatory boundary layer where shear is high and turbulence generation is vigorous. The bulk of the coarse suspended sediment stays close to the seabed, and the transport rate is determined primarily by the concentration and velocity profiles in the near-bed region. For these reasons, the velocity field, the concentration profile, and sediment flux constitute the essential variables of scientific interest in sediment transport study. Past measurements of the velocity structure and sediments in full-scale laboratory flows do not exist, although smaller-scale flows have been extensively examined in the laboratory.

This work is driven by the need for improved models of sediment transport. Modeling the dynamics of the turbulent bottom boundary layer in an environment of waves amounts to dealing with the turbulence closure problem and modeling the turbulent Reynolds stresses in some relation to the mean quantities. By tuning the closure parameters, observed and predicted velocity profiles can be made to agree (Grant and Madsen 1979; Trowbridge and Madsen 1984a,b; Davies 1988). In contrast, sediment transport modeling in the boundary layer has not been as successful for two major reasons. First, it

---

[1]Written by Yogesh C. Agrawal, Northwest Research Associates, Inc., Paul A. Hwang, Quest Integrated, Inc., and Joan Oltman-Shay, Northwest Research Associates, Inc.

Chapter 11 LDV in the Bottom Boundary Layer

is difficult to specify an appropriate boundary condition for sediment concentration or sediment flux at the bed. Second, data on near-bed velocity and sediment characteristics under full-scale random waves are inadequate and imprecise. The SUPERTANK Laboratory Data Collection Project afforded an opportunity to remedy this limitation.

Objectives

Objectives of this program were to measure the wave-driven velocity and sediment concentration profiles over the sand bed, and to derive the sediment flux rates from these measurements.

Scope

In this report, the results of co-located velocity and sediment concentration measurements are presented. By using a newly developed fiber-optic laser Doppler velocimeter (LDV), both the velocity field and the sand grain concentration profile in the near-bed region (from 1 to 16 cm above the bed) have been derived. Simultaneously, velocity data outside the bottom boundary layer were acquired by a fixed acoustic current meter BASS (Benthic Acoustic Stress Sensor) at 1.4 m above the bed. A pressure sensor was used to sense water surface displacement. At a later stage, an optical forward scatterometer (OFS) operated by Mr. Jeff Mather of Sea Tech Inc. was placed close to the LDV system to measure the sediment concentration independently. The experimental procedure and representative results from the data sets are presented in the following sections.

Experiment Apparatus

The suite of instruments, the LDV, pressure sensor, and BASS, along with the OFS in the last 2 weeks of the experiment, were attached to a traversing mechanism (the profiler, Figure 11-1a), secured on a bracket mounted on the inside wall of the wave channel (Figure 11-1b). The profiler outer structure was used to mount the BASS, a pressure sensor, and one OFS, so that these instruments were at fixed locations. The telescopic inside profiling member carried the LDV. The measurement station was located 1.5 m shoreward of Station 19, which is approximately 18.5 m downstream of the wavemaker. Water depth at this station was nominally 3 m.

212

(a)

(b)
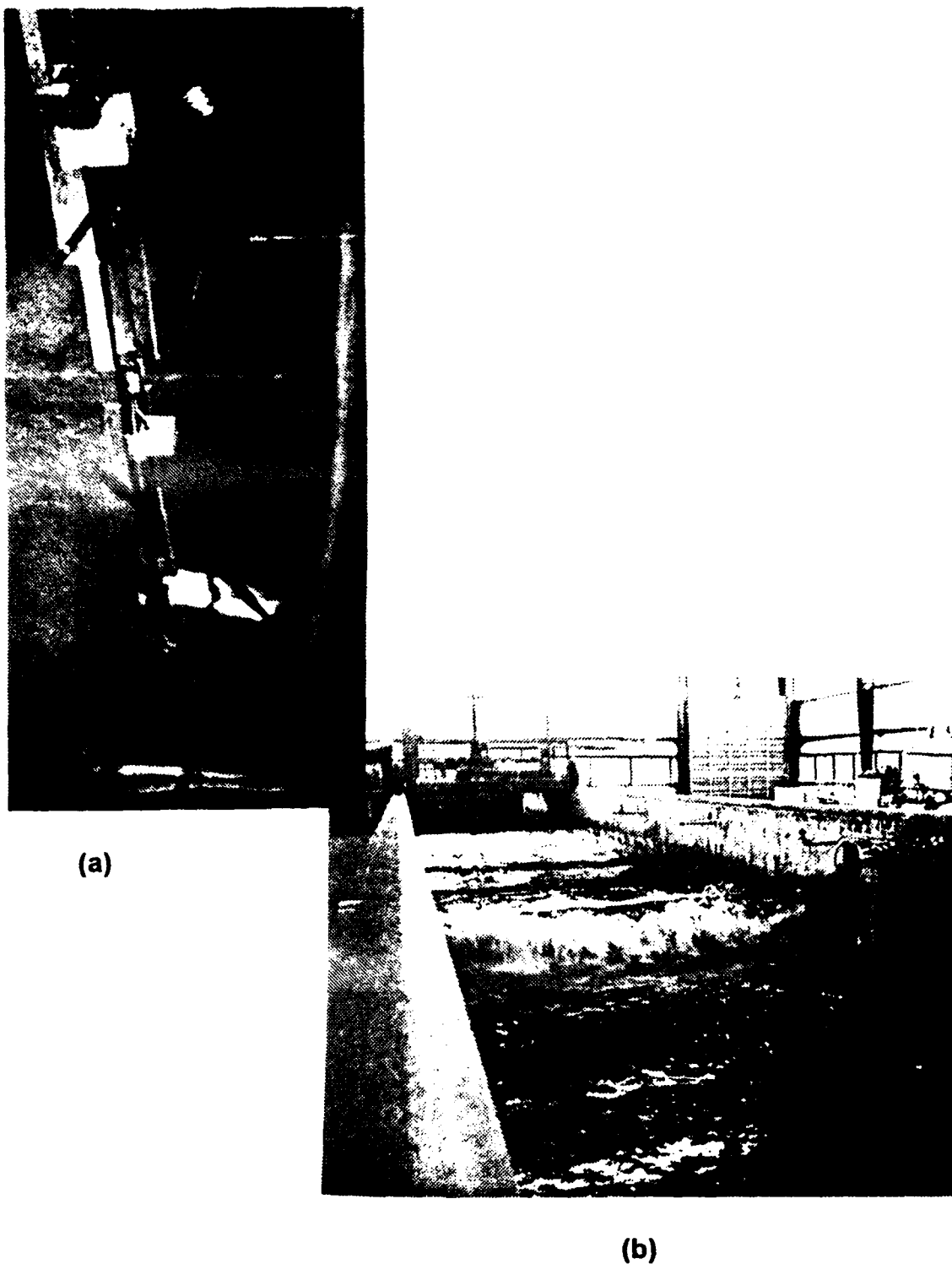
Figure 11-1. (a) The vertical profiler mechanism and mounting bracket and
(b) view of instrument system during data acquisition

Instruments

LDV. The LDV is a two-axis backscatter system developed under the Office of Naval Research sponsorship for ocean deployment. For the SUPERTANK deployment, the LDV measured the two horizontal velocity components of the flow field. In this report, the cross-channel velocity component is not discussed; only the longitudinal velocity component data are presented.

An LDV measures flow velocity by sensing the Doppler shift in light scattered by particles (Agrawal and Belting 1988). Figure 11-2a is a simple sketch showing the operating principle. The Doppler shift is fundamentally given by

$$f_D = (k_s - k_i) \frac{v}{2\pi}$$ (11-1)

where

f_D = Doppler frequency shift (Hz)
k_i = wave number vector of the incident beam (rad/cm)
k_s = wave number vector of the scattered light (rad/cm)
v = particle velocity (cm/sec)

If two laser beams are used to illuminate the particle (Figure 11-2b), the differential Doppler shift, derived from taking the difference of the two Doppler shift equations similar to Equation 11-1 is given by

$$f_D = (k_{i1} - k_{i2}) \frac{v}{2\pi}$$ (11-2)

where the subscripts 1 and 2 denote the two distinct incident laser beams. This is the differential mode of operation, in which the direction of observation does not enter into the measurement. The velocity component in the plane of the two laser beams and normal to their bisector is sensed. To measure two velocity components, it is sufficient to use three beams, one common and two others for the two orthogonal velocity components. A detecting optics arrangement consisting of imaging lenses and a pinhole senses the light scattered from the beam intersection region (the sensing volume). Light entering the pinhole is sensed by a photomultiplier. The optical signal is converted to electrical, with amplitudes proportional to the particle scattering intensity and frequency representing the Doppler shift. The former is a function of particle size, and the latter is linearly proportional to the particle velocity. To prevent signal crosstalk between the two velocity axes, the two velocity components are distinguished by shifting the individual laser beams into different frequency bands. This is accomplished by Bragg cells. In the present design, one velocity axis is put in a 1-MHz band with a ±300-kHz bandwidth, and the other in a 4-MHz band, also with a ±300-kHz bandwidth.

214
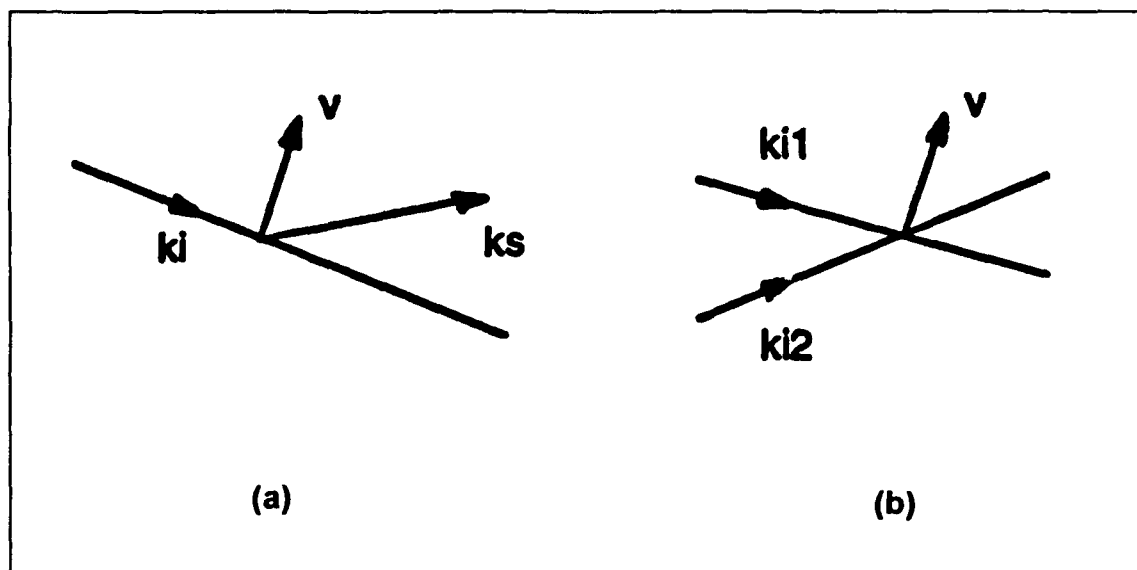
Figure 11-2. Principles of LDV operation: (a) single beam system and (b) two-beam system operated in differential mode

To implement the LDV for the present experiment, as for ocean research, several further issues needed to be addressed. First, the range of turbidity in the ocean can vary greatly. In the nearshore region, as also in the SUPERTANK project, sand or sediment suspension can produce large concentrations of suspended particle mass. Under these extreme conditions, laser beams penetrate only a short distance in water, attenuated by small particles and blocked by large particles or bubbles. To reduce attenuation, in-water paths are shortened. To minimize flow disturbance from the probe arising from the path shortening, the probe must be small, which is accomplished by using fiber-optic technology. A schematic of the present instrument is shown in Figure 11-3, where the laser source, beam-splitting optics, Bragg cells, optical fiber couplers, and the probe head are shown. The backscattered light is collimated by the same lens, and then focused to a multi-mode fiber tip. The multi-mode fiber brings this signal to the photomultiplier. The probe used in the SUPERTANK project was 3.18 cm in diameter and 20 cm long. The measurement point was 8.9 cm from the probe tip, approximately 3 diameters away.

As mentioned earlier, the amplitude of the scattered light is a function of the particle size. The scattering cross section is determined by two parameters, the refractive index and the dimensionless size parameter, $2\pi a/\lambda$, where a is the particle radius and λ is the optical wavelength. The refractive index is a function of scattering material, which is uniform for the SUPERTANK data because scattering is mainly from sand. For relatively large particles ($2\pi a/\lambda \gg 1$), the scattering cross section is approximately twice the geometric cross section of the particle (e.g., van de Hulst 1981). The LDV system was operating as a velocimeter sensitive to sand grains only by setting the detection threshold high. The consequences were two-fold: first the data rate
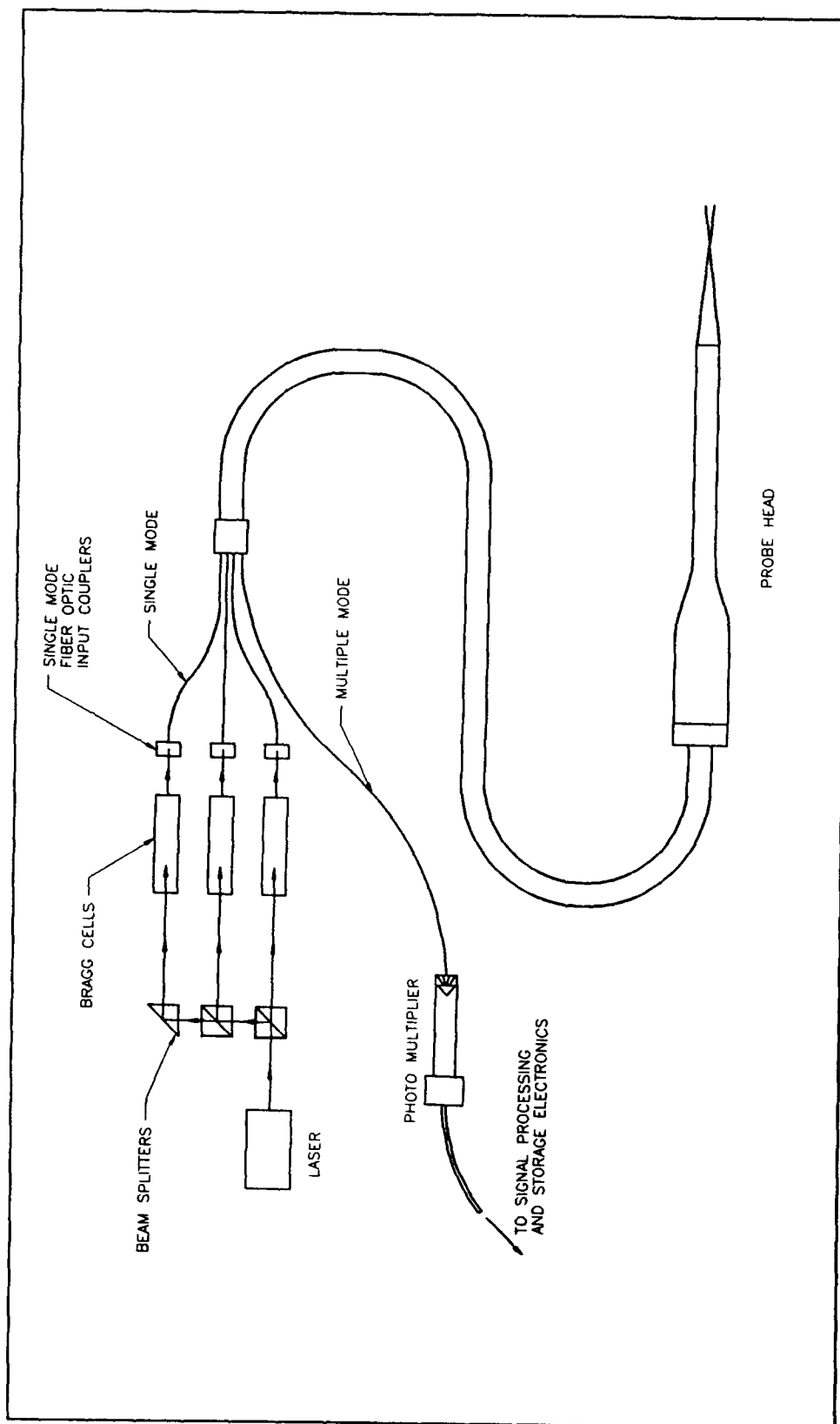
Figure 11-3. Schematic diagram of the fiber-optic LDV system

was low, but on the other hand, the number of velocity realizations per unit time represented the concentration of sand grains in the data. It is this latter result which makes it possible to derive estimates of sand grain concentration and flux in the SUPERTANK bottom boundary layer data. The number of valid velocity data accumulated over a fixed time is proportional to the sediment concentration and is denoted as n. The same data could also be used for flux estimation in the SUPERTANK project because uniform size sand was used. The LDV system can be modified to record the signal amplitude as a measure of grain size, for deployment in environments where the sediment composition is poorly sorted.

Pressure sensor. A pressure sensor was mounted on the fixed outside tube of the telescopic profiler for wave-height monitoring. The sensor consisted of a Sensym model ST2015G2 absolute pressure sensor. Amplifier electronics were modified to give a resolution of 0.2 cm of water. Bench tests showed that the short-term stability of the electronics was better than the resolution. Pressure data were sampled, digitized, and stored along with velocity data to ensure synchronization.

BASS current meter. The BASS current meter measures the difference in acoustic travel time between sound waves traveling with and against the flow. The instrument is fully described by Williams (1985), and only a brief discussion is presented here. The BASS sensor consists of four pairs of acoustic transducers. Each pair is aligned so that the members of a pair receive and transmit signals from and to each other only. The eight transducers are arranged in two sets of four. Each set is placed on a horizontal ring with sensors pointing at 45 deg relative to the horizontal plane. The spacing between the two rings is 10 cm so that the acoustic path is approximately 15 cm. In operation, one transducer in a pair fires a short pulse which is received by the other member of the pair a measured time later. Shortly thereafter, the former receiving transducer fires the pulse and the former transmitter detects it, again a measured time later. The difference in the two measured times is the time delay due to fluid velocity. Measurements from the four transducer pairs form an over-determined estimate of the three velocity components. As configured, the BASS obtains velocity with a spatial resolution of 15 cm, which implies that it is suitable for velocity measurements at sufficiently great distances from the seabed or boundaries. In the present experiment, the BASS was used to measure current velocity outside the boundary layer. The sample rate was set at 1 Hz. The velocity measurement was stored as a 12-bit word for each of the four axes.

OFS. A sediment concentration sensor system was added to the LDV-BASS-pressure package in the last 2 weeks of SUPERTANK. The system measured the light scattered by suspended material over a range of forward scattering angles. In this instrument, a laser diode-optics arrangement transmits a divergent beam of light along the sensor housing. Light scattered over a broad range of angles is sensed by a photo diode, molded in the integral package. Because forward scattering is far more intense than backscatter, this device is capable of sensing lower concentration limits. The present

experiment did not call for this capability, however. This measurement became available strictly on an opportunity basis. Two of these sensors were used: one attached to the profiler, sensing scattering approximately 16 cm above the LDV sample volume, and the other attached to the fixed member of the profiler, 122 cm above the bed.

Instrument calibration coefficients

LDV. As described in the previous section, the calibration factor is uniquely determined for a given geometric configuration of the transmitted beams. For the LDV as configured for SUPERTANK, the calibration factor was 1.6 kHz/cm/sec. The frequency resolution of the signal processor was 1.465 kHz/bin, i.e., 0.92 cm/sec per digitization step. The maximum measurable velocity was 128 bins, or 1.2 m/sec.

BASS. The calibration factor for the BASS depends on the change in transit time across the 15-cm path of the acoustic beams and gain settings in the electronics converting the delays to stored digitized bits. The manufacturer has specified a calibration factor for the BASS to be 0.0207 cm/sec per digitization step. The calibration factors were confirmed through tow-tank measurements at QUEST's 18-m facility.

Pressure sensor. The static calibration of the pressure sensor was performed by submerging the sensor in water at different depths. The resulting calibration factor was 0.028 cm per digitization step.

OFS. No calibration was performed for the OFS at the time of report preparation. The calibration for optical scattering devices depends upon the size spectra producing the scattering. For this reason, we apply an empirical calibration coefficient chosen to ensure that the LDV concentration measurements are continuously matched to OFS data.

Key instrument specifications and calibration coefficients are summarized in Table 11-1.

Experiment Procedures

Sequence of events. To obtain the vertical velocity distribution, the LDV sensor head must be positioned at a known distance from the sand bed. This is achieved as follows. The LDV sensor head is first positioned at a large distance (~ 50 cm) above the bed. Profiling down under computer control, the photomultiplier current (scattering intensity) is monitored. As the sensor head approaches the bed (from an earlier indication) the profiler moves the sensor head in progressively shorter segments. When the sensor head reaches the sand bed, intense scattering from the bed causes a sudden increase in the photomultiplier current; this is recognized by the software as the location of

Table 11-1
Operational Specification of the Instruments Used in This Study

Instrument	Elevation	Sample rate	Sample volume	Calibration Coefficient
LDV	1, 2, 3, 4, 8, and 16 cm	25 Hz	100 μm x 1 mm	0.92 cm/sec per digitization step
BASS	100 cm	1 Hz	15 cm	0.0207 cm/sec per digitization step
Pressure	50 cm	25 Hz	3 mm port	0.028 cm per digitization step
OFS1	16.6 cm above LDV	10 Hz	undefined	Not calibrated
OFS2	122 cm	10 Hz	undefined	Not calibrated

the bed. Using this point as a reference, the profiler is then backed up pre-programmed distances. The distances for this experiment were approximately log spaced: 1, 2, 3, 4, 8, and 16 cm. Velocity was sampled and recorded in 90-sec segments at each of these locations above the bed. At the end of a complete vertical profile, the profiler returned to the point nearest the bed, and the data-collection cycle started again. Data collection was begun for each run approximately three or four wave periods after start of the wavemaker.

Sampling and time reference. LDV velocity data were sampled at 25 Hz. The pressure sensor was interrogated synchronously with the LDV to maintain coincidence with velocity observations. For this purpose, the pressure sensor analog output was digitized by the multi-channel analog-to-digital board on the LDV.

BASS samples were synchronized with the LDV as follows. Approximately 2 msec prior to the moment that the LDV began logging velocity (and pressure) data, a "start" pulse was transmitted to the BASS electronics. The BASS would then log data for 90 sec, based on its own clock. The relative drift in the LDV and BASS clocks over the 90 sec, which would be the maximum synchronization error of the two records, was less than a millisecond. It follows that these data do not contain time references to the master clock maintained at the Oregon State University facility. The run numbers listed with the data (Table 11-2) give the necessary cross-reference.

Data storage. All velocity, pressure, and BASS data were stored on magnetic media and later saved as disks and tapes. These data are to remain as archival sets available to other investigators.

Experimental conditions. Successful operation of the complete instrument system in a coordinated fashion began only in the fifth week of SUPERTANK. Nevertheless, extensive data were obtained. The majority of the data were measured under monochromatic wave conditions of 3-, 4.5-,

Table 11-2
Experimental Conditions (in Chronological Order)

Run	Time[1]	Wave Type[2]	T, sec	H, m	Data Length[3]	BASS	OFS
A2809B	09:30	R	3	0.7	4x1		
A2811A	11:20	R	3	0.7	6x2		
S0311B	11:50	P	3	0.7	6x4		
S0314B	14:30	P	3	0.2	6x4	BASS903	OFS2 903
S0315A	15:30	P	3	0.6	6x4		OFS3 903
S0409B	09:55	P	3	0.7	6x4		
S0410A	10:55	P	3	0.4	6x4		
S0414A	14:10	P	3	0.8	6x1		
S0415A	15:00	F	3	0.8	1x15		WAVE1.905
S0508A	08:25	F	3	0.8	1x48	BASS905A	WAVE2.905
S0510A	10:06	F	4.5	0.7	1x24	BASS905C	WAVE3.905
S0511A	11:10	F	4.5	0.6	1x24	BASS905D	WAVE4.905
S0512A	12:10	F	4.5	0.7	1x6	BASS905E	WAVE5.905
S0514A	14:25	F	8	0.5	1x13		WAVE6.905
S0515A	15:15	F	8	0.5	1x24	BASS905F	WAVE7.905
S0516A	16:25	F	8	0.5	1x24	BASS905G	WAVE8.905
S0517A	17:55	F	8	0.5	1x48	BASS905H	WAVE9.905
S0609A	09:30	P	8	0.5	6x4	BASS906B	WAVE1.906
S0610A	10:55	P	8	0.5	6x4	BASS906C	
S0612A	12:25	P	8	0.5	6x4	BASS906D	WAVE2.906
S0614A	14:05	P	8	0.5	6x4	BASS906E	WAVE3.906
S0616A	16:35	P	8	0.5	6x4	BASS906F	WAVE4.906

[1] The listed time is the starting time of data collection, in the format of hh:mm. Data are encoded in the first three letters of the filename, for example, A28xx is August 28, (1991), S06xx is September 6, (1991), etc. The data length is given in the sixth column. Please see the note below.

[2] Wave type: see Table 11-3 footnote.

[3] Data length: in MxN segments, where M is the number of elevations per profile and N is the number of profiles. The data length of each segment (collected at one elevation) is 90 sec.

and 8-sec periods. Limited data were acquired with spectral waves under a single set of conditions (A28xx: T=3 sec, H=0.7 m). Table 11-3 is a matrix showing the combinations of period and wave height in the LDV data set. The pertinent information for each data segment, including the file names (for LDV, BASS, and OFS), starting time of data collection, wave type, wave

period (T), wave height (H), and data length (in 90-sec block, each block corresponding to data collected at one elevation) are listed in Table 11-2.

Table 11-3 Matrix Showing the Combination of Wave Period and Wave Height in the LDV Data Set			
	T = 3 sec	4.5 sec	8 sec
H = 0.2 m	P	-	P
0.4 m	-	-	P
0.5 m	-	-	PP
0.6 m	P	F	-
0.7 m	PR	F	P
0.8 m	P	-	-

F: Monochromatic waves, instruments at a fixed elevation (z = 4 cm).
P: Monochromatic waves, instruments in vertical profiling operation.
R: Random waves, instruments in vertical profiling operation.
-: No measurements.

Data Analysis

Methods

The quantities to be presented in this report are: phase-averaged velocities, phase-averaged turbulent intensities, and phase-averaged sediment concentration. These quantities are derived as follows.

Velocities. For monochromatic waves, which represent the bulk of the data obtained, velocities are decomposed as

$$u = U + <u> + u' \qquad (11\text{-}3)$$

where

u = measured velocity
U = mean drift velocity
$<u>$ = phase-averaged wave velocity
u' = turbulent velocity

The phase averages are constructed from concatenated time series from different profiles, e.g., for 8-sec waves, 11 cycles per profile, times four profiles per run (Run S0609) would produce a phase average over 44 waves. For this example, it follows that the error of the phase-averaged velocity would be

0.15 u'. For LDV data, pressure records are used to define the reference wave phase. Waves were divided into 10-deg (0.17-rad) slots for phase averaging. Phase averages are similarly calculated for BASS data.

Sediment concentration. The sediment concentration is obtained from the number of sand grains crossing the sample volume of the LDV which produce velocity realizations. The number of grains crossing the sample volume is directly proportional to the sand grain volumetric concentration. However, in order to obtain unbiased estimates of concentration as a function of height above bed, it is important to recognize that the number of realizations itself depends upon the concentration and the velocity. In other words, for a given concentration, the volume of fluid swept past the sample volume is proportional to the velocity of the fluid; therefore, the number of sand grains crossing will be proportional to the velocity. The concentration is corrected via normalization as:

$$n_c = \frac{n}{\sum |v_i|} \tag{11-4}$$

where

n_c = corrected number density
n = measured counts
v_i = velocity realizations

The magnitude is taken to ensure that the volume swept is always positive.

Sediment Flux. The flux of sand grains is also obtainable as follows.

The quantity $F \propto \sum_i \dfrac{|v_i|}{v_i}$ represents the directional transit of particles;

i.e., each velocity realization is associated with the transport of a sand grain in the direction represented by the sign of the velocity. Clearly, flux is measurable in this manner and is obtained from the present data. Absolute flux can be obtained by applying a multiplicative constant that includes sample volume cross-sectional area, effects arising from grains grazing the sample volume, and size of the grains. In SUPERTANK, sand grains were well sorted, so the vertical distribution of F represents the profile shape faithfully.

Sample time series

Figure 11-4 shows an example of the near-bottom velocity measured by the LDV under random waves (Run A2811A, Table 11-2). Under such strong wave agitation, there are sufficient sediment particles suspended to serve as the seeding for laser Doppler measurement. In this figure, the LDV-measured longitudinal velocity u is shown as circles, and the solid curve is the surface elevation. In comparison, the LDV velocity measurements under similar

monochromatic waves (Run S0315A, Table 11-2) are shown in Figure 11-5. In both cases, longitudinal velocity and surface elevation are generally in phase with each other, as expected. Note that although the data acquisition program samples the LDV output at a 25-Hz rate (the sample rate), the rate of sediment particles crossing the sensing volume (the data rate) was considerably lower, creating a significant amount of dropout; this is especially obvious at higher elevations. High data rates at wave peaks and troughs are evident in both Figures 11-4 and 11-5. In particular, near 10 sec in Figure 11-4, the data rate near zero crossings becomes very small, which is indicative of the rapid settling out of sand grains on scales smaller than the wave period. It is for this reason that spectral methods are not suitable for analysis. Instead, phase averaging is used as the major data analysis tool.
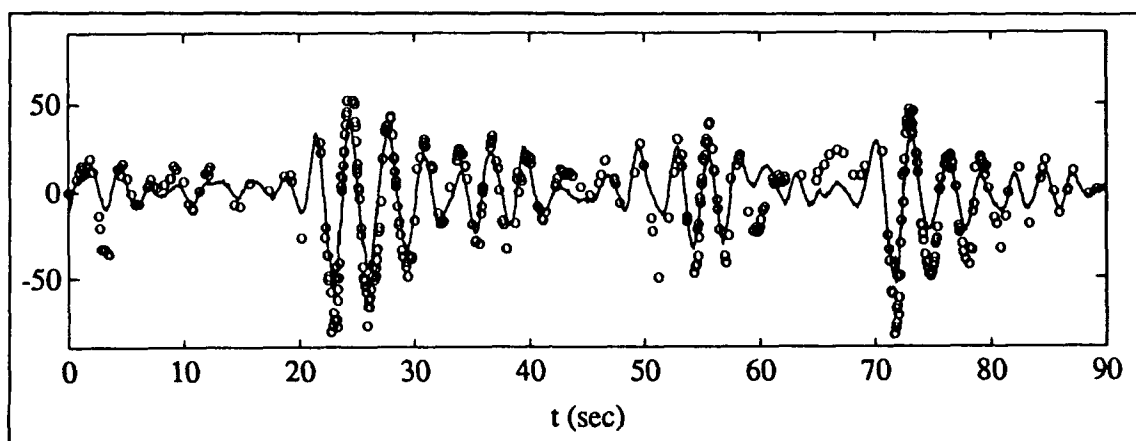
Figure 11-4. Time series of water surface elevation (solid curve, cm) and LDV-measured longitudinal velocity at 1 cm above the bed (circle, cm/sec); Run A2811A
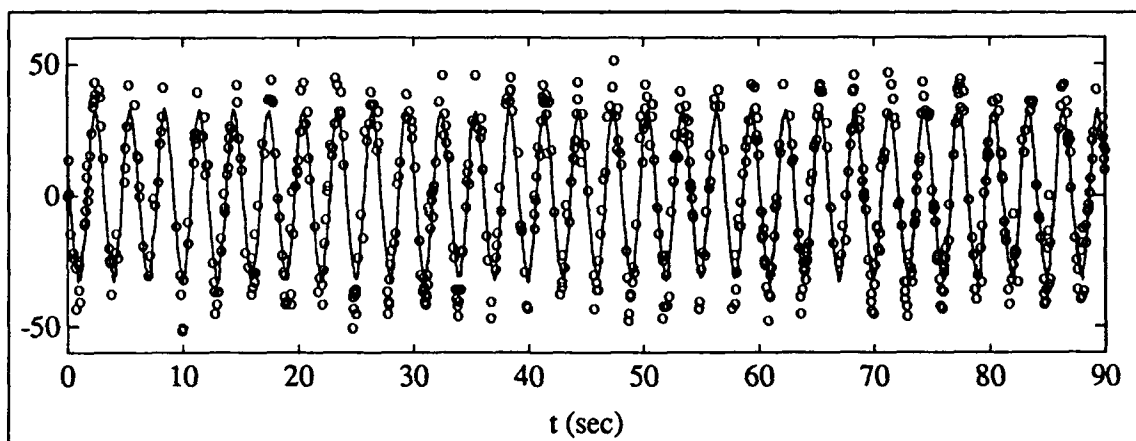
Figure 11-5. Time series of water surface elevation (solid curve, cm) and LDV-measured longitudinal velocity at 1 cm above the bed (circle, cm/sec); Run S0315A

Phase-averaged time series

The individual wave is defined by the zero-crossing points of the wave pressure signals, and the ensemble averaging uses 10-deg phase slots. Figure 11-6 shows an example of the computed phase-averaged surface elevation (solid curve), fluid velocity measured by LDV (symbol o), and other quantities to be discussed later. For these data the LDV sensing volume was 2 cm above the bed, the wave period was 8 sec, and the wave height was 0.5 m. For the construction of this figure, data segments from Runs S0609A, S0610A, S0612A, and S0614A, collected under the same wave conditions, are combined. The data length of each test segment is 90 sec and usually contains 11 complete wave cycles, therefore, the results shown in Figure 11-6 represent the ensemble average of 44 wave cycles. The measured LDV velocity is found to be in good agreement with linear wave theory prediction (dotted curve) except for a phase shift, which is presumably due to frictional effects.
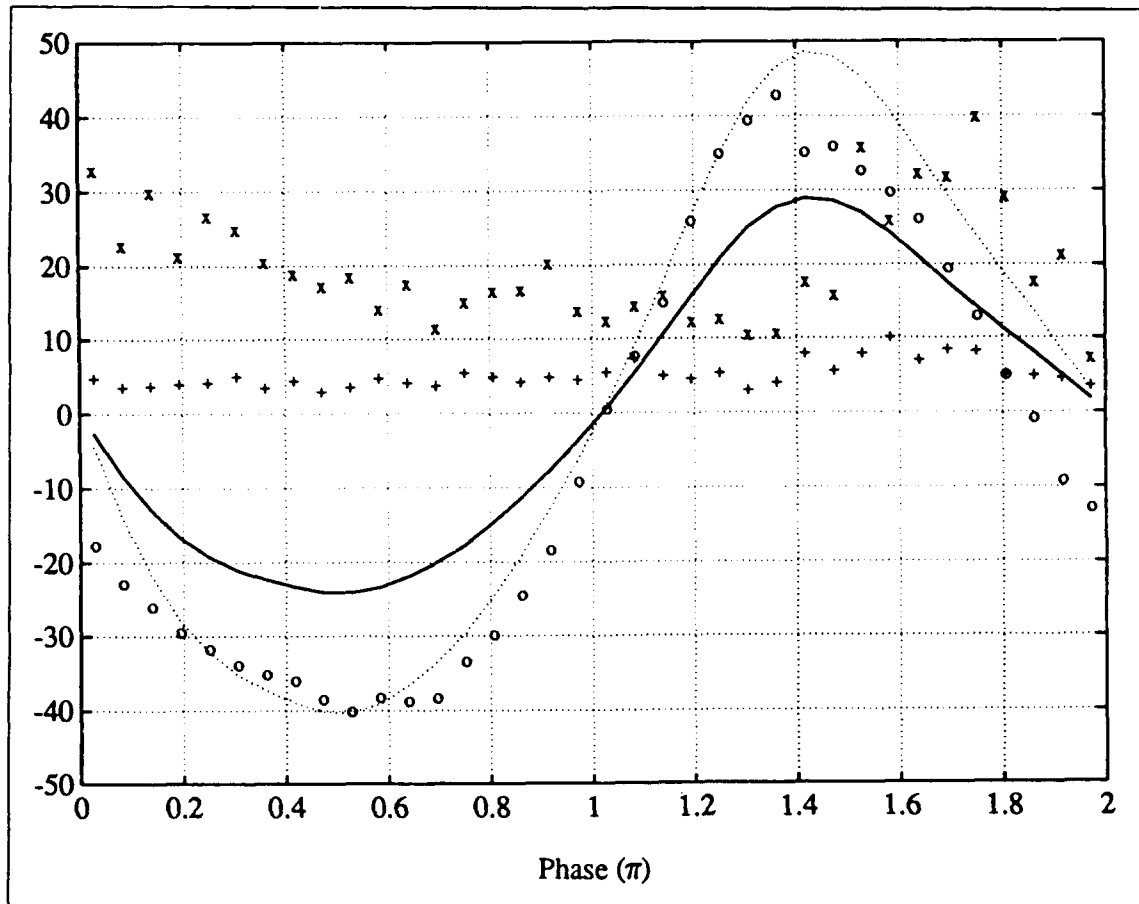
Figure 11-6. Example of phase-averaged surface elevation (solid), velocity (LDV - o, linear theory - dotted), rms turbulent intensity (+), and number of sand grains (x)

Turbulence intensity

Two sets of data are analyzed in some detail at this stage: (a) tests of
3-sec wave conditions with H = 0.2 (S0314B), 0.6 (S0315A), and 0.8 m
(S0414), and (b) tests of 8-sec wave conditions with H = 0.4 (S0410A), 0.5
(combined S0609A, S0610A, S0612A, S0614A), and 0.7 m (S0409B). An
example of the phase distribution of the root-mean-square (rms) turbulence
intensity u'_{rms} is shown as the symbol + in Figure 11-6. The distribution
appears to contain harmonics, suggesting the presence of nonlinear processes.

The vertical distribution of turbulence intensity averaged over the complete
wave cycle is presented in Figure 11-7a. The profiles under the 3-sec wave
conditions with wave height 0.2 (o, Run S0314B), 0.6 (x, Run S0315A), and
0.8 m (+, Run S0' ' *A) are shown with solid lines. The nearly constant but
low turbulence intensity of Run S0314B reflects ambient conditions in the
water column when wave motion is rather mild. With more vigorous
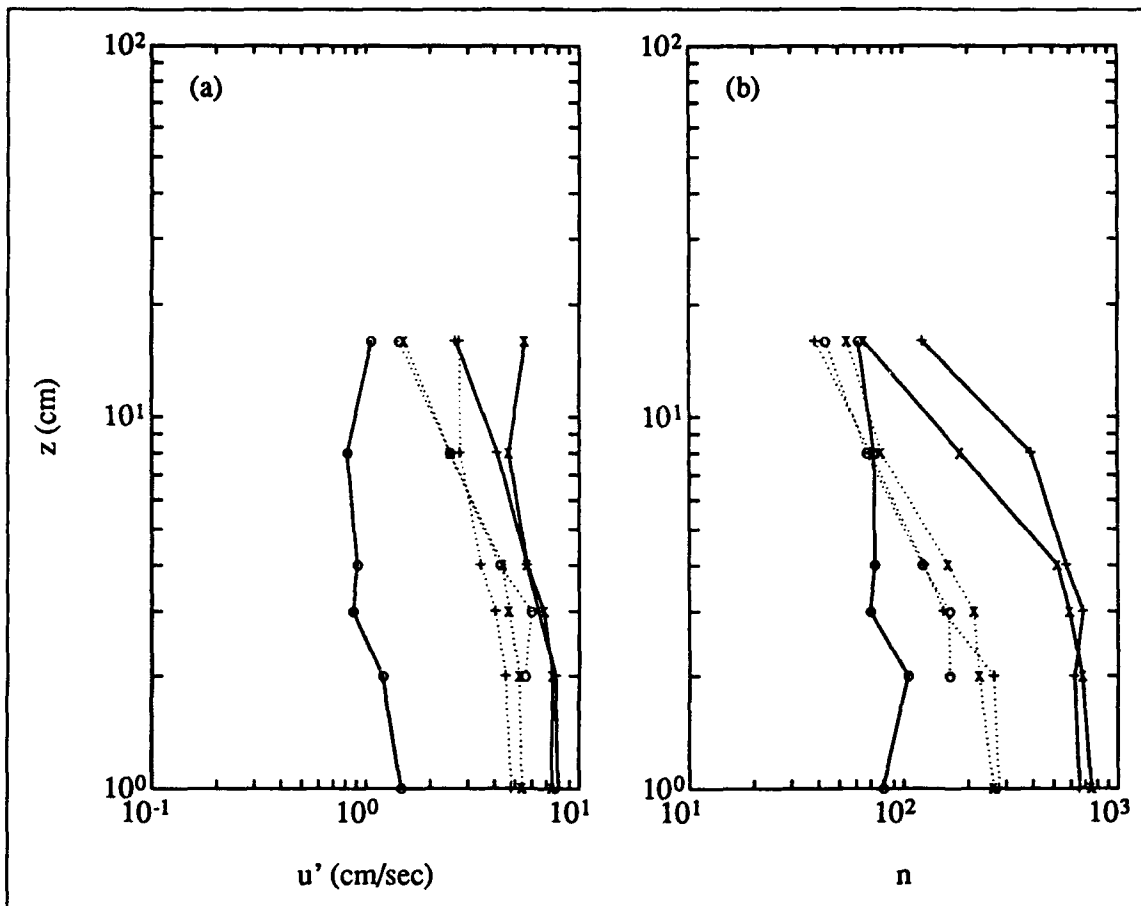
Figure 11-7. Vertical distribution of (a) turbulence intensity u'_{rms} (cm/sec) and (b) sediment
concentration, in the lowest 16 cm on water column

agitation (H = 0.6 and 0.8 m), the turbulence intensity increases. Similarly, the profiles under 8-sec waves with wave heights of 0.4 (o, Runs S0410A), 0.5 (x, Runs S0609A, S0610A, S0612A, S0614A), and 0.7 m (+, Run S0409B) are shown with dotted lines. There are some common features between these two sets of data. In the lower region, typically 2 to 3 cm above the bed, the rms turbulence intensity is approximately constant, suggesting the presence of a constant flux layer. Above this constant flux layer, the turbulence intensity decreases upward. Data at the highest elevation are sparse and hence have poor statistics so that they may be disregarded. The dimensionless turbulence intensity, normalized by the amplitude of the wave orbital velocity, ranges from 0.14 to 0.25 for the 3-sec wave conditions and 0.08 to 0.16 for the 8-sec wave conditions.

Sediment concentration

The number of sand grains passing through the sampling volume (Figure 11-6, symbol x) is directly proportional to the sediment concentration and velocity. The concentration level appears to display a periodic distribution with maxima near the points of flow reversal (corresponding to the zero-crossing points of the surface elevation or longitudinal velocity profile). Presumably, this is a consequence of the nature of turbulence generation in an oscillatory flow where the growth of instabilities at reversals is known to produce high turbulence intensity.

The vertical distribution of the sediment suspension is derived from the integration of sediment distribution over the complete wave cycle. Figure 11-7b shows profiles of sediment suspension under 3- and 8-sec wave conditions (the symbol notation is the same as Figure 11-7a). It is interesting to see that in the near-bed region (z < 3 cm, where z is the distance above the bed), the vertical sediment distribution is nearly uniform; above this region, the concentration can be modeled by a power-law decay. These features were also observed in the distribution of the turbulence intensity, as shown in Figure 11-7a. As noted, the profile of Run S0314B (T = 3 sec, H = 0.2 m) is distinctively different from the other runs. The turbulence intensity of this test is approximately 0.8 to 1.4 cm/sec with very weak vertical distribution (Figure 11-7a). The settling velocity of sand particles used in this experiment is 3.3 cm/sec (median diameter d_{50} = 0.25 mm, data supplied by Dr. Nicholas C. Kraus). Since a sufficiently large turbulence motion is essential to keep the sediment particles in suspension (e.g., Kennedy and Locher 1972; Raudkivi 1976; Yalin 1976), the low turbulence intensity of Run S0314B suggests that the measured particle concentration is probably not due to active wave agitation. For unidirectional steady flow, the sediment suspension profile is well represented by the Rouse equation

$$\frac{n}{n_a} = \exp\left(\int -\frac{w_f}{v_T} \, dz \right) \tag{11-5}$$

where

n = number density of grains at elevation z
n_a = the reference number density at a reference elevation
w_f = fall velocity of particles
ν_T = eddy viscosity

For example, if ν_T is constant, the distribution is exponential, and if ν_T increases linearly with z, the vertical profile follows a power-law. When using $\nu_T = \kappa\, u_* \, z$, where κ is the von Karman constant taken as 0.4 and u_* is the bottom friction velocity, the vertical distribution is represented by

$$\frac{n}{n_a} = \left(\frac{z}{z_a}\right)^r \tag{11-6}$$

where

z_a = a reference elevation (cm)
n_a = the reference concentration at z_a (cm^{-3})
$r = - w_f / u_* \, \kappa$

Typically, the smaller the magnitude of r (higher agitation or smaller particles), the more uniform the concentration distribution. Some initial insight can be gained by interpreting the present admittedly time-dependent cases in light of steady profiles. First, it is plausible to assume that u_* is proportional to u' so that the ratio r is proportional to w_f/ u'. The ratio r as computed from this formulation would be 4.1, 0.78, and 0.73 for the three 3-sec waves, and 1.08, 1.08, and 1.20 for the three 8-sec waves, arranged in the order of ascending wave amplitude. Using magnitudes of u' at the lowest levels, the magnitude of the exponent r would be expected to decrease, producing more nearly constant profiles, as turbulence intensity increases. The measured exponent r for the 3-sec cases (excluding Run S0314B) was approximately 1.5, and for the 8-sec cases it was approximately 1.0. The latter is in good agreement with the theoretical prediction. The former is off by a factor of two. The discrepancy may be caused by the steady model used or by the presence of relatively few non-sand particles producing measurements (see absence of a concentration gradient in Figure 11-7b, 3-sec, 0.2-m case). These bear further examination. In any case, it is evident that the present technique promises to produce non-invasive field estimates of sediment concentration C at a reference height above bed z_r.

Sediment flux in the boundary layer

Sediment flux profiles can be expected to begin at a magnitude of zero at the bed in the absence of bed load, or a non-zero magnitude when bed-load transport occurs. In the absence of bed load, the flux would reach a maximum in the boundary layer before decaying to zero outside it, where no suspended mass reaches. The active bed-load case will probably have a

similar profile, albeit starting at some non-zero rate at the bed. It is not obvious that the bed-load case would necessarily show a flux maximum in the boundary layer, it may simply monotonically decrease to zero.

Flux data are shown in Figure 11-8. The profiles show flux under 8-sec waves for increasing wave heights of 0.4, 0.5, and 0.7 m. Notably, the lowest elevations do not show zero transport rate, as was explained above. Furthermore, the scatter on the profiles might be considered large; this can be improved with longer time series and increased sensitivity of the system. The case of 0.5 m (symbol x) represents the average of 16 profiles, i.e., 24 min per elevation, and as such shows a smooth profile. Vertical integration of the profiles would produce the total transport rate.
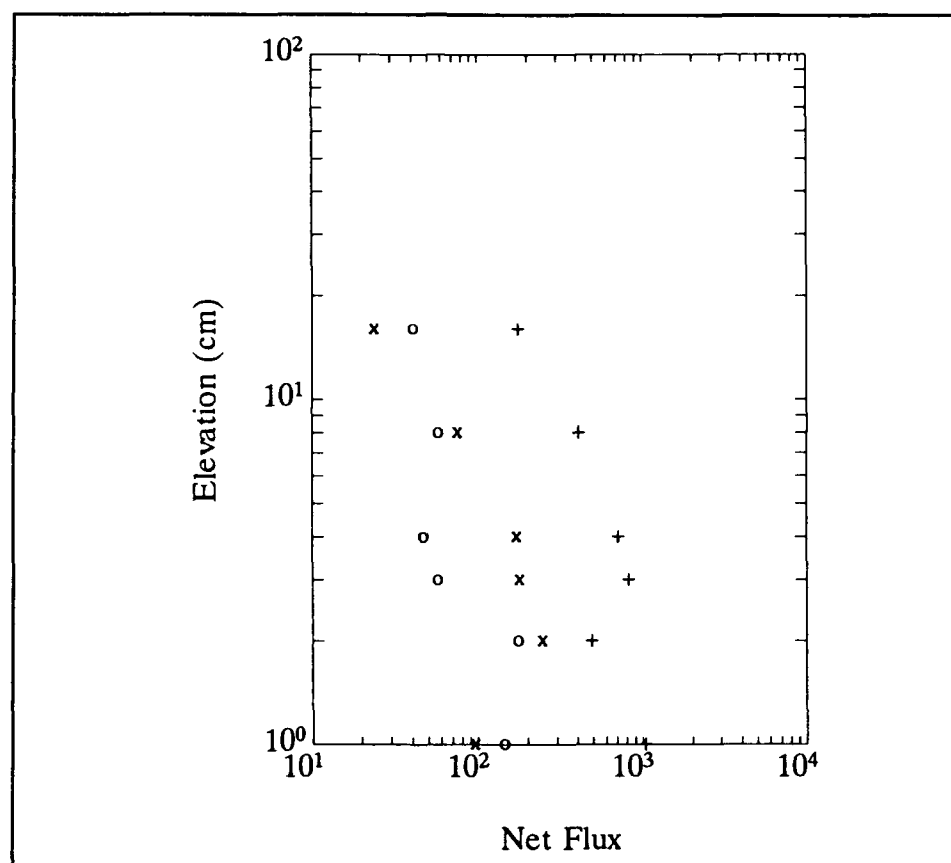
Figure 11-8. Vertical distribution of sediment flux for runs S0409B (+), S0410A (o), and the average of S0609A, S0610A, S0612A, and S0614A (x)

Comparison of LDV and BASS measurements

LDV measurements are compared with the BASS data. An example is shown in Figure 11-9. The wave period for these monochromatic waves is

228

8 sec with 0.5-m wave height. The dimensionless water depth kh (where k is wave number and h is water depth) is 0.424, approaching the shallow-water wave limit. Velocity amplitudes vary only slightly over the whole depth range of measurements (10 percent between surface and bottom based on linear wave theory, considerably less within the 16-cm extent covered by the measurements), as indicated from the two LDV measurements (symbol o) at $z = 2$ cm (Figure 11-9a) and $z = 16$ cm (Figure 11-9b). The LDV velocity realizations appear at unequal time spacing (in multiples of 40 msec), and the BASS (symbol x) was sampled at a constant 1-Hz rate. For reference, the surface elevation measured by the co-located pressure gauge is also plotted in each panel (solid curve). When the LDV data rate is high, the two instruments are in good agreement (Figure 11-9a). At $z = 16$ cm, when the data rate is low, the LDV velocity realization rate is low in the wave-crest region (Figure 11-9b).
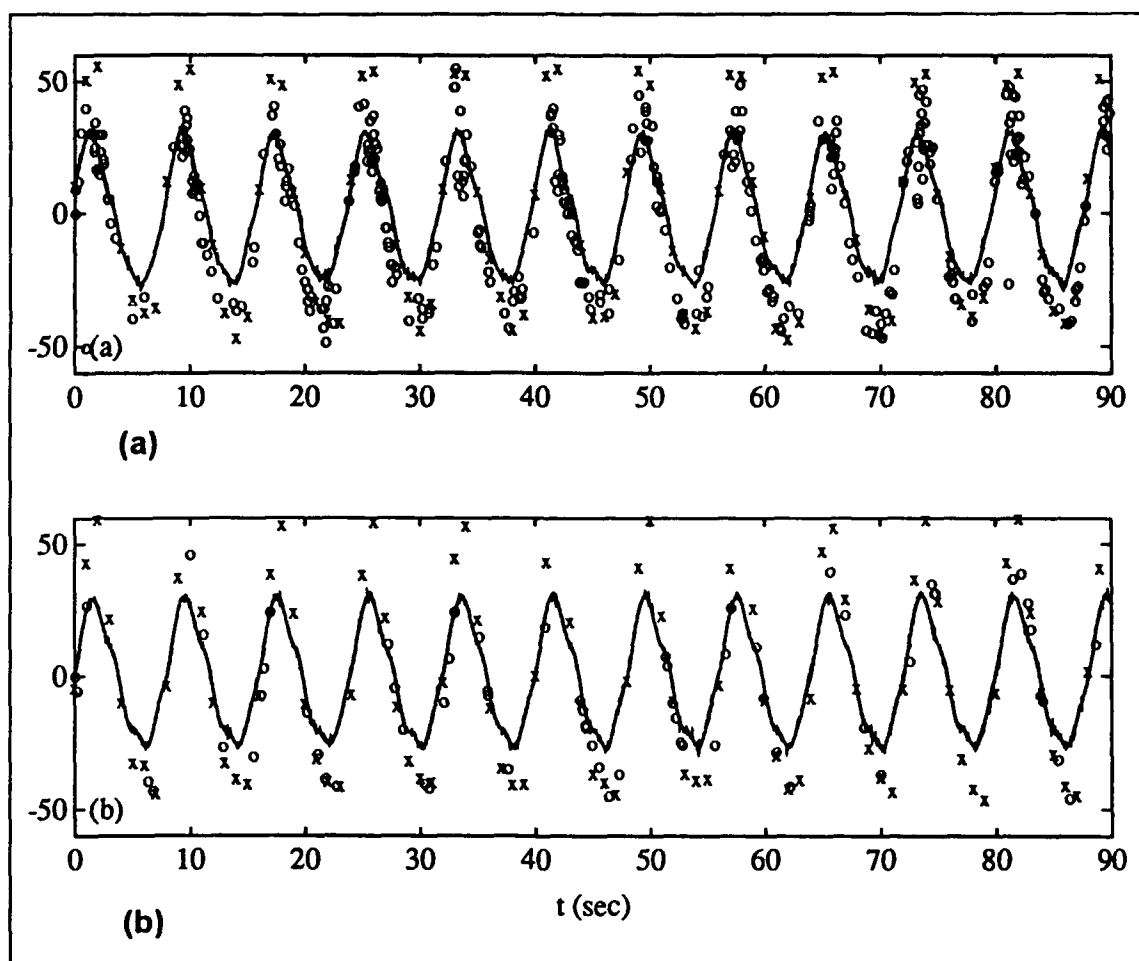
Figure 11-9. LDV (o) and BASS (x) measurements of fluid velocity, Run S0612A; surface elevation (solid line) given for reference; (a) $z = 2$ cm, (b) $z = 16$ cm

Comparison of LDV and OFS concentration estimates

The sediment concentration derived from LDV measurements is compared with the OFS results in Figure 11-10. As described earlier, the lowest OFS elevation is slightly above the highest LDV measurement station. Both instruments were carried on the traverse mechanism to provide simultaneous vertical profiles of the flow and sediment distribution. The OFS registers the optical scattering intensity from all suspended material. In order to extract the component that is contributed by the bottom sand, it was assumed that the uppermost measurement of the OFS (z = 32.6 cm) is derived from fine particles; this was treated as background noise and subtracted from the measured signals. The OFS and LDV data were then "matched" at the quasi-overlap region to produce the curve in Figure 11-10. The smooth continuation of the two measured profiles supports the contention that the data rate of the LDV is directly related to the sediment concentration.
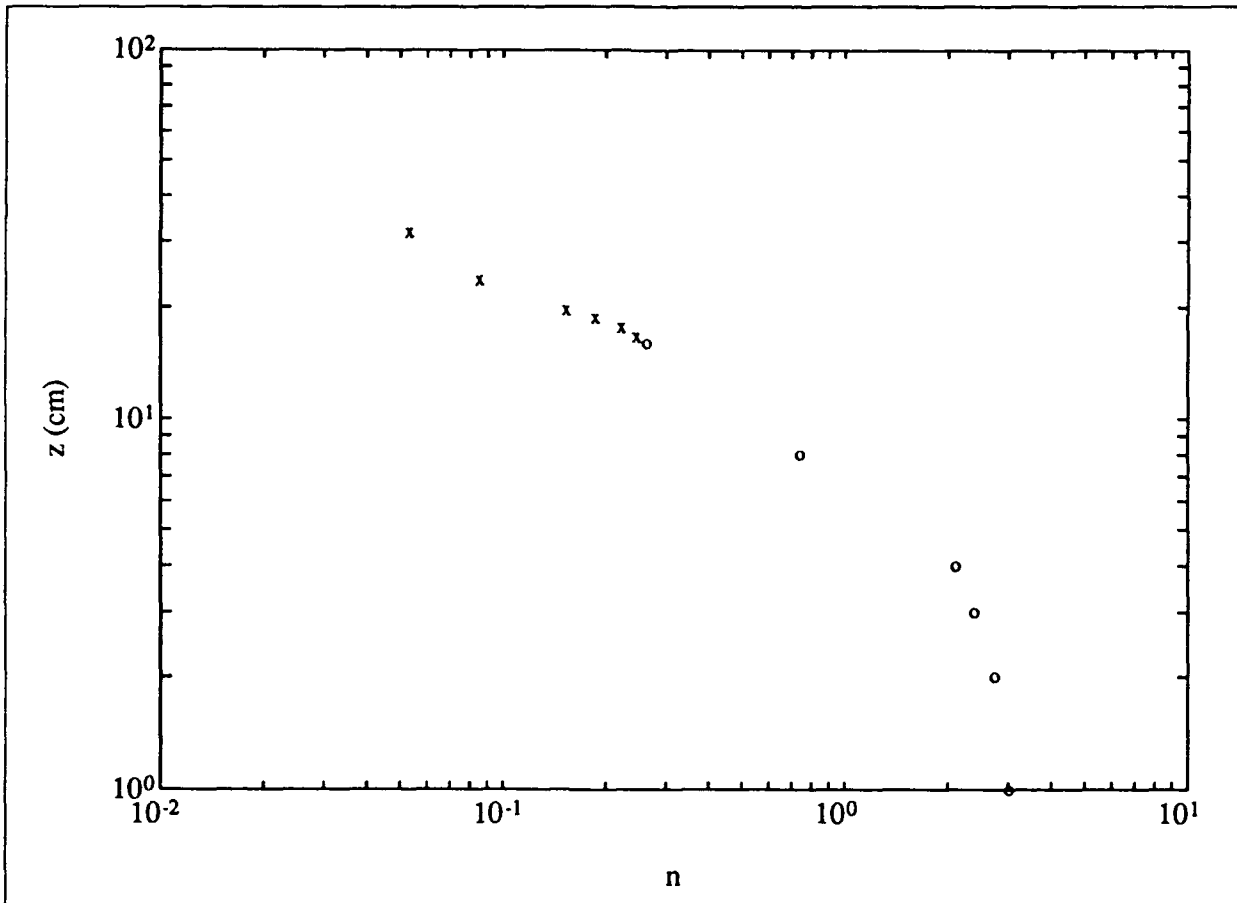
Figure 11-10. Sediment concentration profile produced from a composite of LDV (o) and OFS (x) data, Run S0315A

Summary

A system of four instruments was used for the observation of the bottom boundary layer: a two-axis backscatter fiber-optic LDV, a pressure sensor, a four-axis acoustic current meter BASS, and a light-scattering sensor OFS. They measured, respectively, velocity and sediment concentration in the near-bed region, wave height, velocity in the irrotational part of the wave motion 1.4 m above the bed, and sand-grain and suspended mass. The LDV was placed on a profiler to obtain vertical flow structure. The BASS was mounted at a fixed height above the bed. Of the two OFS used, one was mounted to the LDV sensor head and profiled with the LDV and the other was fixed at a height of 1.2 m above the bed.

Using conditional sampling techniques, the phase-averaged and turbulence properties such as the wave-induced velocity component and the longitudinal distributions of the rms turbulent intensities were obtained. These results allow the study of the distribution of turbulence in the water column.

In addition to the velocity measurement, the data rate of the LDV was proportional to the concentration of sediment in the water column as a result of the high threshold setting. This information is used to construct the concentration profile very close to the bed. The concentration and turbulence intensity profiles in the lowest few centimeters were found to be nearly uniform, indicating the presence of a constant-flux layer.

The data set is especially unusual in the sense that velocity and concentration profiles are truly "simultaneous" and measured by a single instrument -- the LDV. These data are the first measurements of sand grain flux in the boundary layer under full-scale conditions.

Recommendations

Results from the LDV measurements, as summarized above, represent the most promising database for the study of turbulence properties in the wave boundary layer and the detailed distribution of suspended sediment very close to the sediment-fluid interface. In the next stage of data analysis, it would be useful to compare turbulence results with the prevailing theoretical models of turbulence generation in the wave-induced bottom boundary layer, and to compare sediment concentration and flux results with sediment suspension models. The specification of absolute value of a reference concentration at the bed is thus within reach. Future work will require application of suitable factors and corrections to the concentration data presented here to reduce the present results to mass concentration.

Simultaneous measurement of concentration and particle motion has permitted deducing the flux of sediment in the boundary layer. These data are

highly valuable for the study of sediment transport. It is conceivable that a significant advance toward relating wave forcing and transport rates has been made. These data promise to improve the U.S. Army Corps of Engineers' capability in sediment transport predictions.

Acknowledgments

References

Agrawal, Y. C., and Belting, C. J. (1988). "Laser velocimetry for benthic sediment transport," *Deep-Sea Res.* 35, 1047-67.

Davies, A. M. (1988). "On formulating two-dimensional vertical integrated hydrodynamic numerical models with an enhanced representation of bed stress," *J. of Geophys. Res.* 93, 1241-63.

Grant, W. D., and Madsen, O. S. (1979). "Combined wave and current inter-action with a rough bottom," *J. of Geophys. Res.* 84, 1797-1808.

Kennedy, J. F., and Locher, F. A. (1972). "Sediment suspension by water waves," *Waves on beaches and resulting sediment transport*, R. E. Meyer, ed., Academic Press, New York, 249-95.

Raudkivi, A. J. (1976). *Loose boundary hydraulics*. 2nd ed., Pergamon Press, New York.

Trowbridge, J., and Madsen, O. (1984a). "Turbulent wave boundary layers; 1: Model formulation and first-order solution," *J. of Geophys. Res.* 89, 7989-97.

_____. (1984b) "Turbulent wave boundary layers; 2: Second-order theory and mass transport," *J. of Geophysical Res.* 89, 7999-8007.

van de Hulst, H. C. (1981). *Light scattering by small particles*. Dover, England.

Williams, A. J. (1985). "BASS, an acoustic current meter for benthic flow-field measurements," *Marine Geology* 66, 345-55.

Yalin, M. S. (1976). *Mechanics of sediment transport*. 2nd ed., Pergamon Press, New York.

12 Pore Pressure and Sediment Density Measurements at SUPERTANK[1]

Introduction

Background

Pore pressure and sediment density measurements were undertaken as part of the SUPERTANK Laboratory Data Collection Project to complement measurements of wave transformation and beach evolution. Pore pressure measurements may be used to test coupled models of wave interaction with permeable seabeds. Sediment density measurements may be used to relate mass flux to volume flux for models of cross-shore sediment transport.

The large-scale tests in the SUPERTANK project using prototype sands provided an opportunity to make in-place relative density measurements in the nearshore in a controlled environment. There may be significant variations in the relative density across the profile. On the berm and dune, relative density is anticipated to be lower than on the subaerial portions of the profile. This suggests that a volume of sand eroded from the berm or dune does not result in an equal volume of accretion on the subaerial profile. For a clean uniform sand, porosity can vary from approximately 0.29 to 0.5. This can lead to a 70-percent increase in volume from the most dense to the most loose state. This significant change in volume should be considered in beach profile and shoreline change modeling.

The degree of packing of a granular sediment can significantly influence both the volume occupied by the sediment and the strength of the sediment. Laboratory investigations have shown that stiffness and strength properties of a wide range of granular materials are similar if they have similar relative

---

densities. Two different clean, dry, un-cemented granular soils will have nearly the same modulus and friction angle if they are at the same relative density. As expected, as the packing becomes tighter, volume decreases and strength increases. A way to characterize the density of this packing is with the relative density D_r. Relative density is defined as,

$$D_r = \frac{\gamma_{d\,max}}{\gamma_d} \frac{\gamma_d - \gamma_{d\,min}}{\gamma_{d\,min} - \gamma_{d\,min}} \qquad (12\text{-}1)$$

where γ_d is the dry in-place unit weight of the soil, $\gamma_{d\,max}$ is the dry unit weight of the soil in its most dense condition, and $\gamma_{d\,min}$ is the dry unit weight of the soil in its loosest condition. Relative density can also be expressed in terms of either void ratio e or porosity n as the following,

$$D_r = \frac{e_{max} - e}{e_{max} - e_{min}} = \frac{n_{max} - n}{n_{max} - n_{min}} \frac{1 - n_{min}}{1 - n} \qquad (12\text{-}2)$$

in which e_{min} is the void ratio of the soil in its densest condition, e_{max} is the void ratio of the soil in its loosest condition, and e is the in-place void ratio. Void ratio is the volume of voids to volume of the solids and is a common parameter used in geotechnical engineering. In sediment transport, it is more common to use porosity n, which is the ratio of the volume of the voids to the total volume.

Wave-induced pore pressures may lead to a less stable soil matrix and enhance sediment erosion at the seabed. Cyclic loading of fine sands can lead to volume reduction. An accumulation of pore pressure can result if drainage occurs more slowly than the volume reduction rate. If pore pressure increases to equal the overburden pressure, then the sediment grain effective stress approaches zero and the sediment begins to behave like a liquid. Liquids are not capable of supporting significant shear stresses; thus, liquefied sediments will be more sensitive to shear-induced soil failures (Seed and Rahman 1978). This sensitivity is enhanced by both dynamic and mean excess pore water pressure.

Several models exist to predict wave-induced pore pressure in sediments. A potential pressure model is appropriate if the soil matrix is assumed to be rigid and the fluid incompressible (Reid and Kajura 1957). A linearly elastic model of the soil was developed by Biot (1941). This model has been applied to horizontal seabed models by many investigators (Yamamoto 1977, Madsen 1978, McDougal and Sollitt 1984). Some of these models have been validated with large-scale experiments (Yamamoto et al. 1978; Sollitt and McDougal 1984). However, large-scale laboratory studies of these models applied to sloping beaches are not reported in the literature. SUPERTANK provides the data sets for validation of pore pressure models applied to realistic, erodible beaches.

Objectives

The objectives of this component of the SUPERTANK project were to provide the following:

a. A fine, uniform beach sand.

b. Measurements of sediment density to quantify variations in bulk density in the nearshore region.

c. Measurements of wave-induced pore pressure in the nearshore.

Scope

This chapter describes the materials, equipment, procedures, and sample results associated with in situ sediment behavior. The discussion is ordered as follows:

a. Beach material.

b. Sediment density measurements.

c. Pore pressure measurements.

Experiment Apparatus

Beach material

The beach sand used in the SUPERTANK project was obtained from an aeolian deposit in Florence, OR. The material was procured from a dune sand enterprise, commercially identified as Leisure Acres, Incorporated. This material was selected because of its similarity to beach sand found along the central Oregon coast. The grain size distribution is that of a fine-grain, uniform quartz sand with a median grain size of 0.22 mm.

The material was front-end loaded from the dune base into 20-cu-yd (15.3-cu-m), belly dump trucks. The truck beds were covered with tarpaulins to prevent loss of material during transit. The truck-transport system appears in Figure 12-1. The material was deposited on the pavement next to the wave channel and placed in the channel with a front loading Bobcat, Model 753. The Bobcat, with a 0.25-cu-yd (0.19-cu-m) bucket, appears in Figure 12-2.
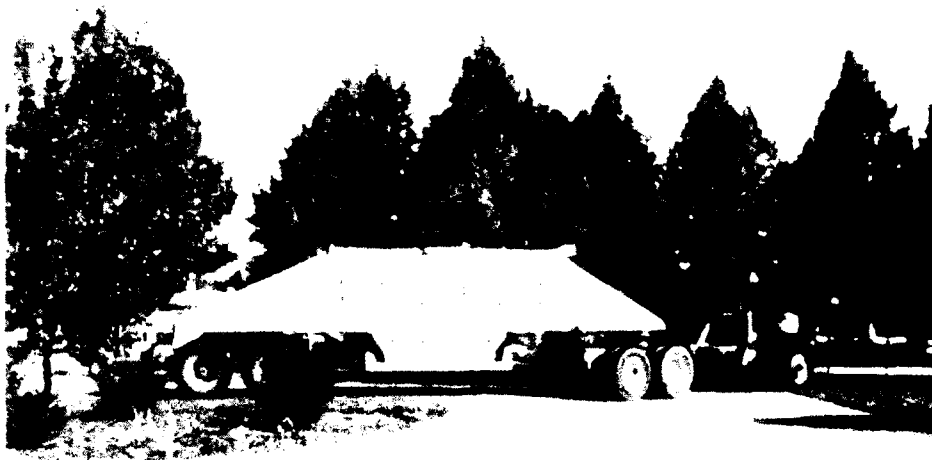
Figure 12-1. Truck used for sand transportation

Figure 12-2. Bobcat front end loader

The wave channel was filled with water during sand placement to minimize air entrapment and to selectively remove light organics from the material. A target beach profile was painted on the walls of the wave channel. Soundings were taken to establish the depth of the deposited material relative to the target profile. Water was drained from the channel and refilled, then waves were run to condition the beach. This process was repeated four times to clean the sand prior to instrument installation.

Approximately 700 cu yd (540 cu m) of sand were placed on the original beach. An additional 200 cu yd (150 cu m) were placed during the final phase of the project to simulate an offshore berm. Perforated drain pipe was placed through the base of the berm to facilitate filling and emptying of the wave channel. A photograph of the offshore berm is shown in Figure 12-3.

Dune erosion studies were conducted early in the project. Dunes were prepared to simulate many seasons of sand accumulation. To meet this requirement, the sand was placed in 1-ft (0.3-m) layers, dampened, and compacted with a gas-powered panel vibrator. The resulting dune face appears in Figure 12-4.

Sand-core densitometer

Instrument description. The American Society for Testing Materials has established Standard Tests D2049-64T for determining in-place relative density. The tests consist of determination of minimum and maximum density corresponding to the loosest and most dense states of the soil and determination of in-place density using Standard Test D1556 (sand cone test). The loosest state of the soil is achieved by slowly pouring the sand into a standard mold. The most dense state is achieved by placing the sand in the mold in five layers, applying a confining pressure corresponding to a load of at least 12 kg, and striking the mold 30 times with a rubber mallet. These two tests are repeated three times and extreme values are used.

In the sand cone test, a hemispherical hole 17 cm in diameter is excavated using a standard template. All sand removed from the hole is placed in plastic bags and sealed tightly. This hole is then filled with a standard sand; for these tests Ottawa sand was used. The weight of the Ottawa sand required to fill the hole is used to estimate the volume of the hole. Wet samples taken from the site are weighed and then oven-dried for 24 hr to determine the dry weight. A photograph of the sand core apparatus appears in Figure 12-5.

Location. The apparatus for determining in-place density is located onsite at the O.H. Hinsdale Wave Laboratory, Oregon State University (OSU), and equipment for determining minimum and maximum density is located at the Soil Mechanics Laboratory, OSU. Specific sample locations are noted in Table 12-1.

238

Figure 12-3. The offshore berm

Figure 12-4. The dune face during erosion tests

239

Figure 12-5. Sediment densitometer

Pore pressure gauges

Instrument Description. Ten pore pressure gauges were used during SUPERTANK. Each gauge is fabricated from a DRUCK precision pressure transducer and an environ ental enclosure fitted with a porous stone.

DRUCK model PDCR 10 total pressure transducers were used as sensors for pore pressure measurements. The sensing principle is a strain gauge bridge bonded to a silicon diaphragm. Each pressure transducer is approximately 2.25 in. (5.72 cm) long by 0.69 in. (1.75 cm) in diameter. A four-core shielded cable includes a ventilation tube for reference of total pressure to local atmospheric pressure.

Each pressure transducer was enclosed in a 1-in. (2.54-cm) aluminum pipe to protect the molded cable attachment from environmental abuse. Carborundum porous stone isolates the pressure transducer from the sand environment. The enclosure eliminates soil pressure from the measurement, providing a separate measurement of pore water pressure.

Location. Each pore pressure gauge and housing was hose clamped to a 1-in.- (2.54-cm-) diam aluminum rod, which was threaded into the stainless steel inserts in the walls of the wave channel. The sensor head was located approximately 1.5 ft (0.46 m) from the wall. A representative in-place gauge is shown in Figure 12-6.

240

Table 12-1
Relative Density Sample Descriptions

Date	Sample #	Description	Distance from Station-1 ft	Location
8 Aug 91	6	Post-Erosion test	6	dune
	2	with random waves	12	berm
	4		60	sub-aerial profile
	3		96	sub-aerial profile
	1		120	sub-aerial profile
	7		120	sub-aerial profile
21 Aug 91	4B	Pre-Dune erosion	6	dune
	3B	Test 1	12	dune
	5B		24	berm
	2B		32	sub-aerial profile
	1B		36	sub-aerial profile
22 Aug 91	1C	Post-Dune erosion	9	dune
	2C	Test 1	11	dune
	3C		14	berm
	4C		24	sub-aerial profile
	5C		28	sub-aerial profile
23 Aug 91	3D	Pre-Dune erosion	14	dune
	2D	Test 2	20	dune
	1D		24	berm
23 Aug 91	1E	Post-Dune erosion	12	dune
	2E	Test 2	13	dune
	3E		18	berm
	7E		20	berm
	4E		32	sub-aerial profile
	6E		36	sub-aerial profile
	5E		38	sub-aerial profile
26 Aug 91	1F	Post-Seawall Test 1	0	toe of seawall
	2F		14	upper-area profile
	3F		24	sub-aerial profile
	4F		36	sub-aerial profile

The ten pressure gauges were moved to various locations throughout the project. This allowed each instrument to be placed in the most useful position relative to the ongoing experiment. A summary of the pore pressure gauge locations during SUPERTANK is presented in Table 12-2.

Instrument characteristics. Each pore pressure gauge is powered by 10 V DC and operated over a total pressure range of 0 to 5 psi (0 to 34.5 kPa). The output of each instrument is very linear with no discernable drift in a 24-hr period. Sensitivity is approximately ± 3 mV, with outputs responding at approximately 1 V per 0.5 ft of head. The natural frequency is in the kHz range. Temperature effects are less than ± 0.5 percent of full scale for $0°$ to $50°C$.

Figure 12-6. Pore pressure gauge

Experiment Procedures

Sediment density measurements

Sequence of events. Determination of relative density requires determination of in-place density and minimum and maximum densities. Minimum and maximum densities were determined at the Soil Mechanics Laboratory for three dry samples taken randomly. In-place densities were measured when the channel was drained on 8, 21, 22, 23, and 26 August 1991.

Calibration and zero reference. Calibration for this test was repetition of the test five times with a variation of less than approximately 1 percent of the sample weight.

Sampling and time reference. Table 12-1 summarizes samples taken to determine relative density.

| Table 12-2 | | | | | |
| Pore Pressure Gauge Log | | | | | |

Channel No.	Gauge I.D.	Date-Time Station No.-Depth* or Comment			
17	A	8/5-0800 #2-6'	8/27-0700 removed	8/27-1800 #2-6'	9/7-0840 #12-10'
18	B	8/5-0800 #2-5'	8/26-0700 removed	9/7-0840 #13-8'	
19	C	8/5-0800 #4-6'	8/8-0700 #4-7'	9/2-0700 disconnected all day	9/7-0840 #13-9'
20	D	8/5-0800 #3-5' ------- 8/27-1800 #3-7'	8/7-1500 removed ------- 9/2-0700 disconnected	8/8-0700 #3-6' -------- 9/3-0800 #3-7'	8/27-0700 removed -------- 9/9-0830 disconnected
21	E	8/5-0800 #6-9'	8/29-0800 disconnected AM	8/29-1300 reconnected	9/9-0830 disconnected
22	F	8/5-0800 #6-8'	9/9-0830 disconnected		
23	G	8/5-0800 #7-9'	8/12-0900 zeroes off for runs A1208ZHY & A1209AHY	9/5-0830 disconnected until 1030	9/7-0840 #14-10'
24	H	8/5-0800 #9-10'	8/12-0900 zeroes off for runs A1208ZHY & A1209AHY		
25	J	8/5-0800 #11-11'	8/12-0900 zeroes off for runs A1208ZHY & A1209AHY		
26	K	8/5-0800 #13-12'	8/12-0900 zeroes off for runs A1208ZHY & A1209AHY	9/7-0840 #13-10'	

* Depth measured in ft from top of channel wall

Pore pressure measurements

Sequence of events. Pore pressure measurements were acquired simultaneously with wave profile and wave velocity measurements. The MTS-VAX data acquisition system, described in Chapter 13, was used for all three measurements. Each separate data run was initiated with the control signal to the wave generator. Length of run was predetermined and sampling was terminated approximately 1 min after the wave generator was shut down. The reader is referred to Chapter 1 for an expanded discussion of specific wave conditions.

Calibration and zero reference. Pore pressure gauges were calibrated weekly by filling or emptying the wave channel and recording the output signals from the instruments. The reference was a video record of a 0.1-ft-(3.0-cm-) division staff, painted on the side of the channel. The staff can be read to ±0.01 ft (± 0.3 cm). Calibrations for the nearshore gauges were contaminated by hydraulic gradients due to drainage of the beach. Post-SUPERTANK calibrations demonstrated that all instruments remained within a few percent of the gain-set calibration constants of 0.5 ft (0.15 m) of head per volt. Table 12-3 summarizes the post-SUPERTANK calibration constants.

Zero references for the pore pressure readings occur at the beginning of each run, before waves arrive at the beach. These zero references were augmented by 10-min time series of zeroes run at the beginning and ending of each day, after the first week of testing.

Sampling and time reference. The ten pore pressure gauges were sampled simultaneously at a rate of 16 Hz. The samples were synchronized with wave profile and velocity measurements through a common data acquisition system. All samples were synchronized with WWV radio broadcast time signals, as discussed in Chapter 13.

Pre-processing and filtering. All pore pressure gauges were differentially driven to avoid d-c drift. Each channel of data was analog filtered prior to digitizing. A 10-Hz, fifth-order Bessel filter was used to avoid aliasing problems in the digitally sampled data.

Table 12-3
Pore Pressure Gauge Calibration Constants

Channel No.	Gauge I.D.	Calibration Constant ft of head per volt
17	A	0.4984
18	B	0.4963
19	C	0.4985
20	D	0.4915
21	E	0.4762
22	F	0.5056
23	G	0.5010
24	H	0.4915
25	J	0.5018
26	K	0.5044

Data Analysis

Sediment density data

Sample raw data. The sample raw data for determination of in-place density consist of data for the wet samples, dry samples, volume of the hole, dry density, and water content. Sample data for 21 August 1991 are given in Table 12-4. W_{wet} is the weight of the wet samples, W_{jug} is the weight of the Ottawa sand and the container before it is poured into the hole, W_{jug} remaining is the weight of the Ottawa sand remaining in the jug after pouring the sand, W_{sand} is the weight of the Ottawa sand filling the hole, and W_{dry} is the weight of the samples after oven-drying. To obtain the volume of the hole V_{hole}, the W_{sand} filling the hole is divided by γ_o, which is the unit weight of the Ottawa sand. The unit weight dry is obtained by dividing W_{dry} by V_{hole}. The water content w is obtained by

$$w = \frac{W_{wet} - W_{dry}}{W_{dry}} \tag{12-3}$$

Sample interpreted data. The relative density D_r was calculated using Equation 12-1. Table 12-5 summarizes results for samples taken 21 August 1991.

Identification of marginal data sets. The sand cone test used to determine relative density requires the excavation of a small hole in the beach. In the offshore region, the sand was still saturated on 8 August and the hole was not stable. As a result, Samples 1A and 7A are considered marginal. The sand cone test also requires a level working surface. As a result, samples taken on or near the berm face may be subject to error. These samples included 3B, 4B, 5B, 2C, 4C, 1D, and 2D.

Pore pressure data

Analysis and interpretation methods. Pore pressure data were analyzed for statistical and spectral properties. Statistical parameters include the mean and standard deviation, computed in 256-sec blocks. Spectral properties were computed from the sine and cosine transform of a 512-sec time series. The longer time series is used to quantify a 2^5 ∙ ∙ seiche in the wave channel. Spectral density is computed as the sum ∙∙ ∙ne squares of the sine and cosine amplitudes divided by twice the frequency interval. Total energy is summed from the area under the spectral density curve. Zero-moment wave height is computed as four times the square root of the total energy.

Data file format. The file header for each run is contained in the first nine blocks of the file. Each block has the capacity to store up to 256 data points. Block 10 begins with the first 256 data points for Channel 1 of the 64-channel data acquisition system. Channels 1 through 16 correspond to the

Table 12-4
Sample Data Sheet for Sediment Density

#	Location	W_{wet} g	W_{pan} g	W_{pan} remaining g	W_{sand} filling the hole g	W_{dry} g	V_{hole} cm³	Unit Weight dry g/cm³	Water Content w W_{water}/W_s
1B	Station 4 off berm	2323	2320	730.5	1589.5	1858.3	1001.575	1.8554	0.2501
2B	Station 3 + 8' off berm	2182.6	2372.85	905.4	1467.45	1762.3	924.6692	1.9059	0.2385
3B	Station 2 top of berm	1368.85	2596.85	1076	1520.65	1343.8	958.1916	1.4024	0.0186
4B	Station 1 + 6' top of berm	1259.55	2544.05	1194.4	1349.65	1209.3	850.4411	1.4220	0.0416
5B	Station 3 berm	1203.85	2496.55	1057	1439.55	1047.3	717.2796	1.4601	0.1495

Unit Weight Ottawa Sand: 1.587 g/cm³.
Measurements conducted before running waves.

Table 12-5
Sample Results

#	Location	Distance from Station 1 ft	W_{wet} g	W_{av} g	V_{bag} cm³	Unit weight dry g/cm³	Water content w	Porosity GS = 2.66 n	Void ratio	Relative density D_r
4B	Station 1 + 6' top of berm	6	1259.55	1209.30	850.44	1.4220	0.0416	0.4654	0.870645	0.063312
3B	Station 2 top of berm	12	1368.85	1343.80	958.19	1.4024	0.0186	0.4728	0.8967	0.0035797
5B	Station 3 berm	24	1203.85	1047.30	717.28	1.4601	0.1495	0.4511	0.821794	0.1707346
2B	Station 3 + 8' off berm	32	2182.60	1762.30	924.67	1.9059	0.2385	0.2835	0.395689	0.9110562
1B	Station 4 off berm	36	2323.00	1858.30	1001.58	1.8554	0.2501	0.3025	0.433677	0.8565686

Measurements conducted before running waves.

16 resistance wave gauges, starting at Station 6, increasing with each station number offshore, and ending at Station 21. The pore pressure gauges start at Channel 17 and continue through Channel 26. The remaining channels are devoted to electromagnetic current meter measurements. Block 11 contains the first 256 data points for Channel 2. This format continues with buffer number one containing blocks 10 through 73, which are the first 256 data points for Channels 1 through 64. Buffer 2 contains the next 64 blocks, with data points 257 through 512 for Channels 1 through 64. This pattern repeats to the end of the data file.

Sample raw data. Time series samples from a pore pressure gauge and the co-located resistance wave gauge at Station 9 are shown in Figures 12-7 and 12-8. The time series are for the first 80 blocks or 21 min of Run A0618A. Wave conditions for the run were a TMA spectrum with a peak period of 3.0 sec and a zero-moment wave height of 0.6 m. The unscaled time series (Figures 12-7 and 12-8) identify the randomness of the measurements and the visual zero offset corresponding to wave setdown. Channel 24 is the pore pressure gauge, and Channel 4 is the wave gauge.

Sample interpreted data. Samples of the spectra from a co-located pore pressure and wave gauges are shown in Figures 12-9 and 12-10, respectively. Figures 12-9a and 12-10a represent the first 512 sec of a 2,400-sec record, and Figures 12-9b and 12-10b represent the last 512 sec. Figures 12-9 and 12-10 are expressed in units of ft^2/sec, with feet of water surface elevation for the wave profile and feet of head for the pressure data. All spectra were smoothed with a moving box-car filter, using 13 frequency intervals in the averaging process. Total energy beneath the spectral density curve E is noted in the upper right-hand corner of each figure.

Comparison of Figures 12-9 and 12-10 shows a considerable reduction in pressure head transmitted into the seabed. Energy is reduced by more than a factor of four, reducing the amplitudes by more than a factor of two. This behavior reflects pressure attenuation both in the water column and within the sediment.

Comparing the beginning and ending of each run (Figure 12-9, a to b, Figure 12-10, a to b), a small reduction in total energy is noted. The reduction is due to the effect of terminating the wave generator motion while continuing to sample waves. A small but noticeable increase in low-frequency energy occurs from the beginning to the end of the run. The seiching mode amplifies in time, and this is reflected in both records. Note that the seiching mode represents a greater fraction of the pressure energy density because higher frequency pressure components are attenuated in the water column and sand bed, leaving the low-frequency component as a more significant fraction of the distribution.

Summary of data characteristics. Tabular values of the mean and standard deviation of the two time series are presented in Table 12-6. Statistics are computed in 256-sec blocks. A reduction in both statistics at the end of

248
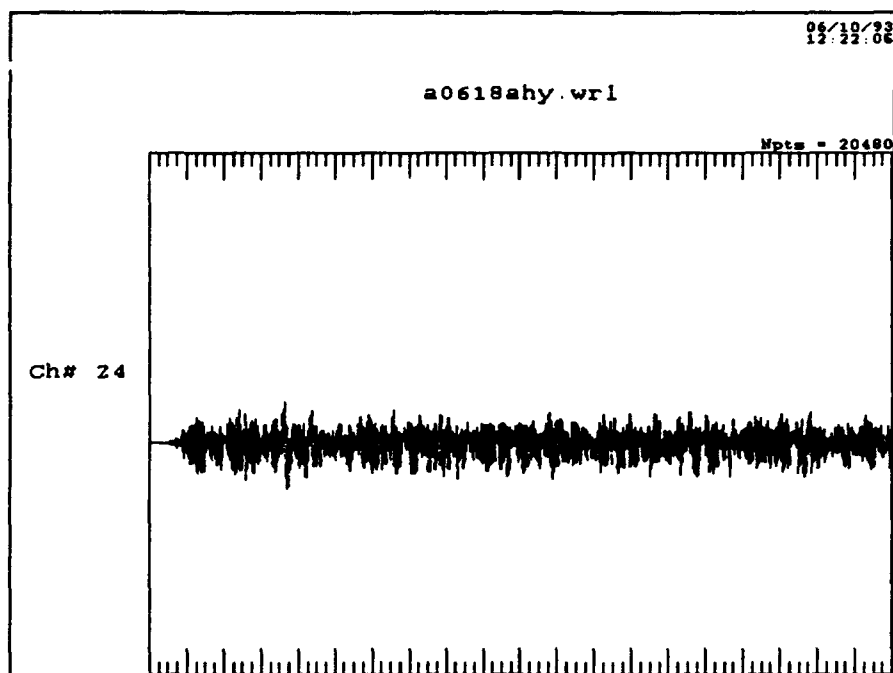
Figure 12-7. Time series of pore pressure gauge, Channel 24, Run A0618A
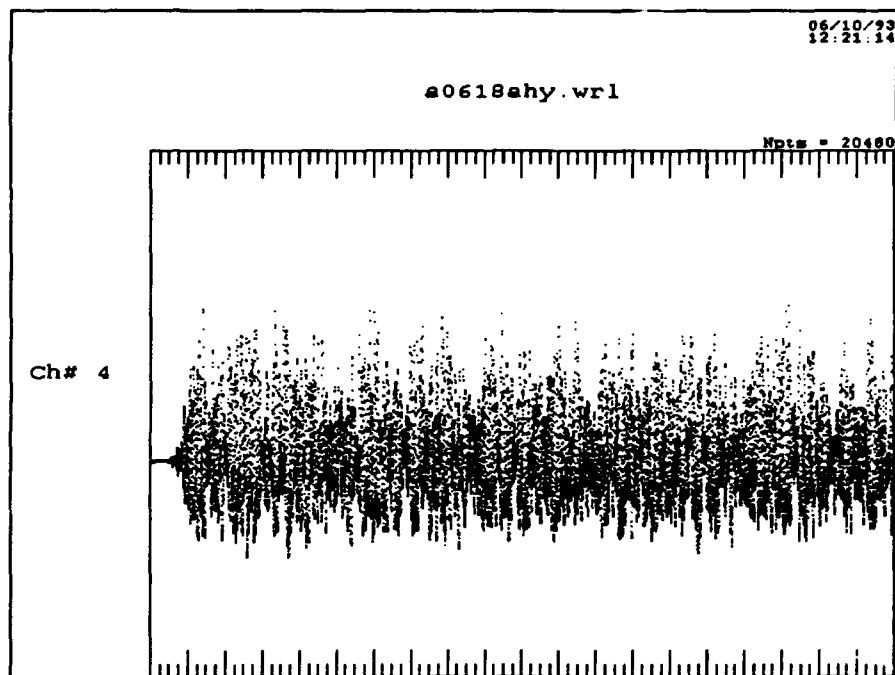
Figure 12-8. Time series of wave profile, Channel 4, Run A0618A
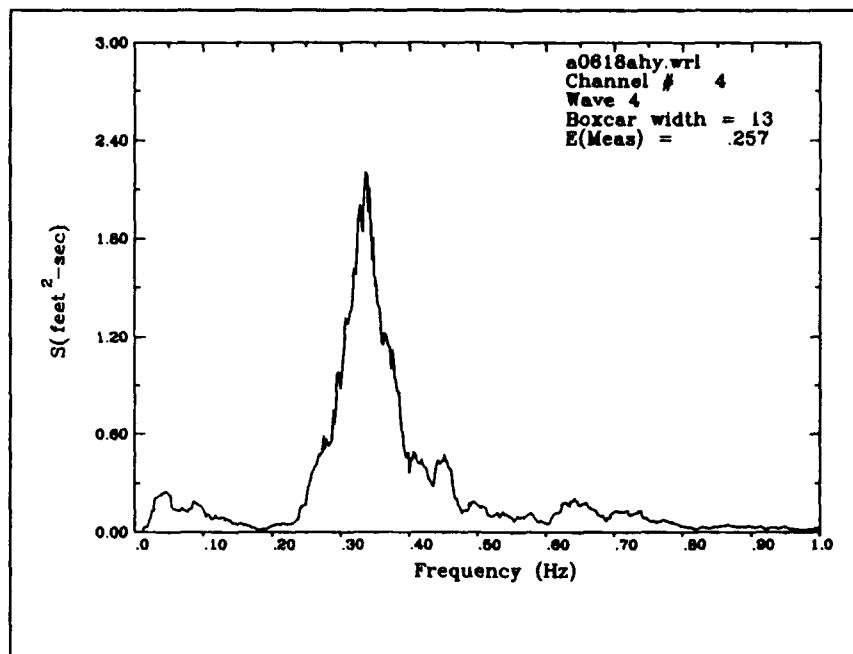
a. First 512 sec
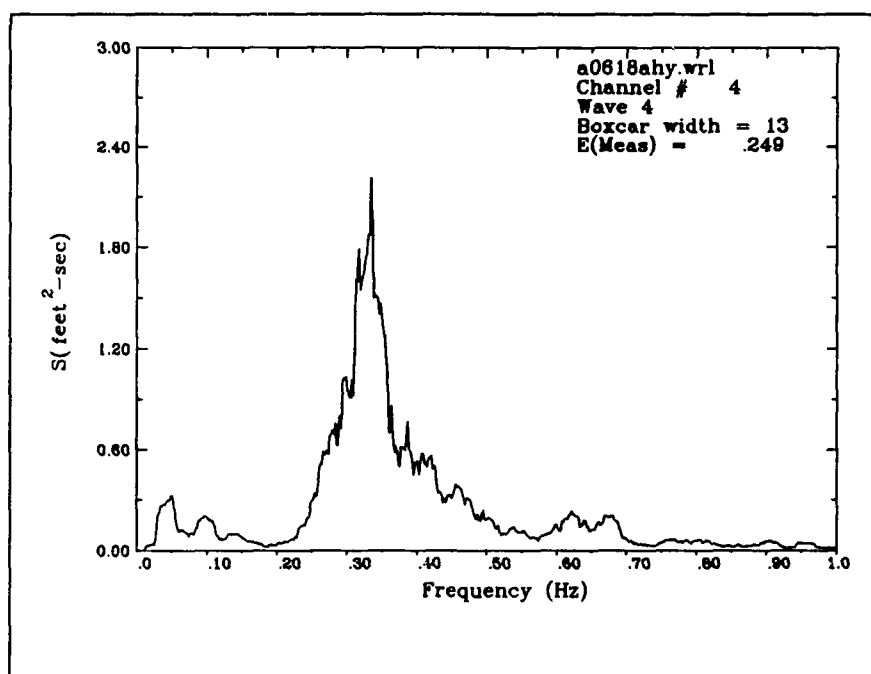
b. Last 512 sec

Figure 12-9. Spectral behavior of wave profile
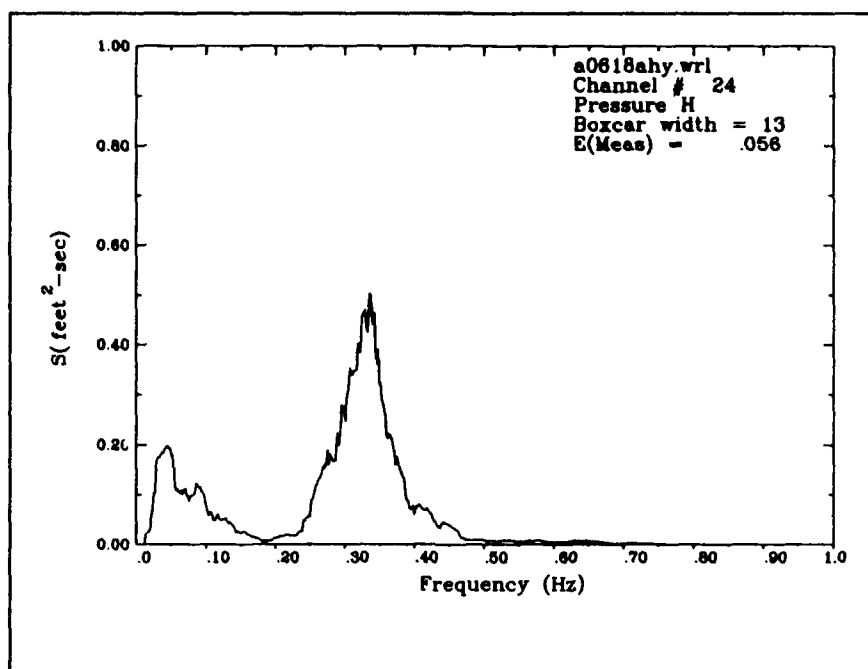
a. First 512 sec
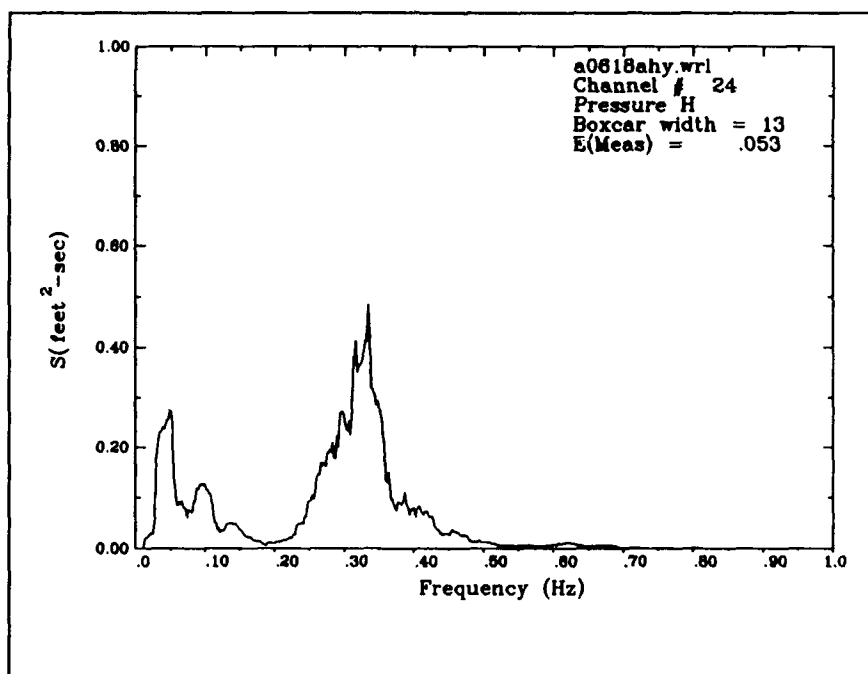
b. Last 512 sec

Figure 12-10. Spectral behavior of pore pressure

the record corresponds to terminating the wave generation signal while continuing to sample the waves. Squaring the standard deviation yields the variance, which is theoretically equal to the total energy under the spectral density curves. Note that tabulated standard deviations are within approximately 5 percent of the square root of the energy levels identified in Figures 12-9 and 12-10. Mean values reflect setdown of the water surface profile near the breaker zone. Mean values from the wave and pore pressure gauges are approximately equal because static pressures are not attenuated in the water column or the sediment.

Table 12-6 Statistics of Wave Profile 4 and Pore Pressure Head 24 File: A0618AHY.WRL			
Channel	256-sec block	Mean ft	Std deviation ft
4	1	-.592663	.473351
4	2	-.604135	.505336
4	3	-.591660	.477283
4	4	-.589063	.485818
4	5	-.589842	.489397
4	6	-.590401	.501392
4	7	-.604909	.504524
4	8	-.602705	.493688
4	9	-.596072	.494718
4	10	-.563763	.242535
24	1	-.570276	.222024
24	2	-.578107	.236154
24	3	-.568982	.220605
24	4	-.562733	.228357
24	5	-.565518	.221738
24	6	-.565460	.227875
24	7	-.577615	.234550
24	8	-.574427	.234908
24	9	-.567233	.224543
24	10	-.542446	.117655

Identification of marginal data sets. Pore pressure gauges which were disconnected or removed from service are noted in Table 12-2. No other marginal data sets are known at this time.

Summary

Sediment density and pore pressure were measured to complement the other SUPERTANK studies. Twenty-nine samples were acquired on seven different days to evaluate variations in sediment density. Pore pressure measurements were acquired at six to ten locations throughout the SUPERTANK project.

Sediment density varied considerably with location. Highly disturbed sites, such as those on top of the berm, experienced much higher porosities (0.46) as compared to regions onshore and offshore from the berm (0.29). These variations have significant implications in evaluation of mass flux from volume flux in sediment erosion computations.

Pore pressures are shown to decrease both with depth and frequency. Static pressures correlate well with observed mean water levels. The complete data set will provide a useful database for validating hydrodynamic models of wave-seabed interaction.

Acknowledgements

References

Biot, M. A. (1941). "General theory of three-dimensional consolidation," *J. Appl. Phys.* 12, 155-65.

Madsen, O. S. (1978). "Wave-induced pore pressures and effective stresses in a porous bed," *Geotechnique* 28, 377-93.

McDougal, W. G., and Sollitt, C. K. (1984). "Geotextile stabilization of seabeds: Theory," *Engnrg. Structures* 6, 211-16.

Reid, R. D., and Kajura, K. (1957). "On the damping of gravity waves over a permeable sea bed," *Trans. Am. Geophys. Un.* 38, 662-6.

Seed, H. B., and Rahman, M. S. (1978). "Wave-induced pore pressure in relation to ocean floor stability of cohesionless soils," *Marine Geotech.* 3, 123-50.

Sollitt, C. K., and McDougal, W. G. (1984). "Geotextile stabilization of sea-beds: Large scale experiments," *Engrg. Structures* 6, 217-22.

Yamamoto, T. (1977). "Wave-induced instability in seabed." *Proc. Coastal Sediments.* ASCE, New York, 898-913.

Yamamoto, T., Koning, H., Sellmeijer, H., and Van Hijum, E. (1978). "On the response of a poroelastic bed to water waves," *J. Fluid Mech.* 78, 193-206.

13 Wave Generation and Data Collection Systems at SUPERTANK[1]

Introduction

Background

Interaction of waves with an erodible boundary is a fluid phenomenon that must be examined at large Reynolds numbers to avoid distortion of dynamic phenomena due to viscous scale effects. This scale effect has been demonstrated previously in rubble slope stability tests (Sollitt and DeBok 1976). Predictive modeling of cross-shore hydrodynamics, sediment transport, and beach profile response to waves requires model validation through experiments conducted at prototype or near-prototype scale. A large, two-dimensional wave channel provides a controlled and repeatable environment for examining cross-shore processes in a cost-effective manner. Several large-scale laboratory studies of cross-shore beach profile change have been conducted, including the initial work of Saville (1956) and more recently Kajima et al. (1982), Vellinga (1986), and Dette and Uliczka (1987). However, these studies used wave channels with reflective seaward boundaries and did not utilize the full complement of contemporary instrumentation now available to monitor beach processes. The latter conditions were the primary motivation for performing the SUPERTANK Laboratory Data Collection Project at the O. H. Hinsdale Wave Research Laboratory (WRL), Oregon State University (OSU).

A major feature of the WRL is the large two-dimensional wave channel which is 342 ft (104.2 m) long, 12 ft (3.66 m) wide, and 15 ft (4.57 m) deep, appearing in Figure 13-1. A hydraulically driven, hinged-flap wave board generates random and monochromatic waves up to 5 ft (1.5 m) high. Direct digital controls were installed in 1991 which allow active absorption of

---

a. Wave generator end
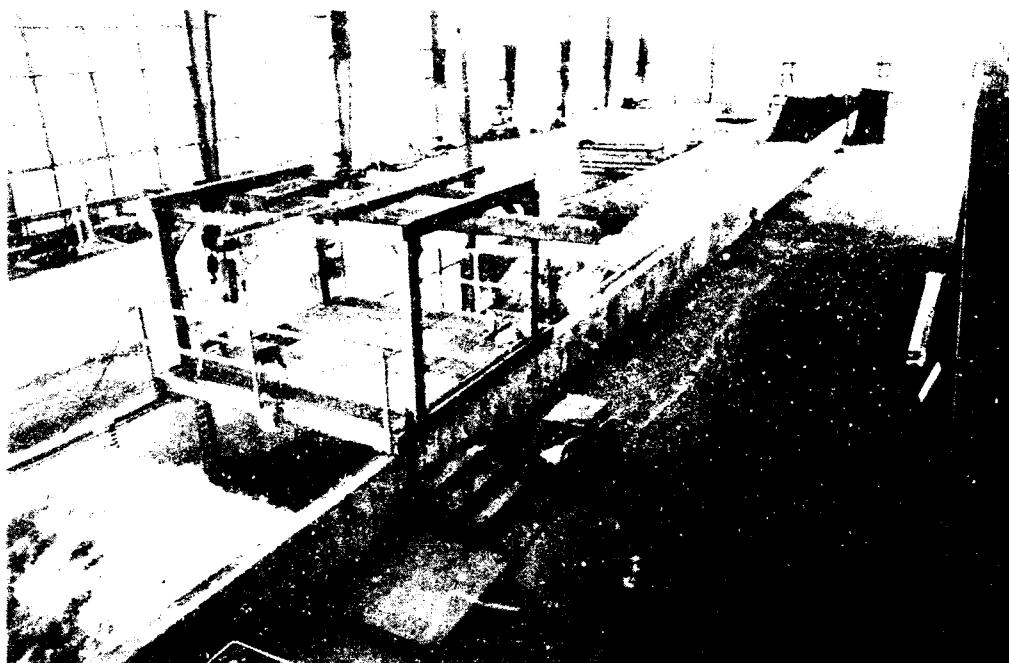
b. Beach end

Figure 13-1. O. H. Hinsdale Wave Research Laboratory two-dimensional wave channel

reflected waves. The SUPERTANK project was conducted in this facility. The wave channel is enclosed in a 37,500-ft² (3,480-m²) building. An elevated control room with an area of 1,875 ft² (174 m²) overlooks the wave channel, providing an environmental enclosure for the wave generator controller and digital data acquisition system.

Objectives

The WRL was selected for these experiments because of the large size of the two-dimensional wave channel and the ability to provide a range of monochromatic and random wave conditions with active reflected-wave absorption. Specific objectives included the following:

a. Provide a wave and sediment environment at prototype scale.

b. Provide computer software to reproduce simple periodic and random breaking waves in shallow-water wave environments.

c. Maximize absorption of beach-reflected waves at the wave board.

d. Digitally acquire 64 channels of wave profile, water particle velocity, and pore pressure measurements synchronously with co-existing personal computer- (PC-) driven data acquisition systems.

e. Facilitate beach profile surveys, offshore hydrodynamic measurements, and nearshore sediment concentration measurements with support carriages.

f. Provide a platform for other measurement systems deployed at SUPERTANK.

Scope

This chapter describes the equipment and procedures used to provide the wave and sediment environment for the SUPERTANK Laboratory Data Collection Project. The discussion is ordered as follows:

a. Two-dimensional wave channel.

b. Wave generator.

c. Data acquisition system.

d. Support facilities.

Equipment associated with each item is described and principles of operation are discussed. Data analysis is described in those chapters specifically identi-

fied with a particular type of measurement. A summary description of the pertinent WRL equipment concludes this chapter.

Experiment Apparatus

Instrument description

Two-dimensional wave channel. The two-dimensional wave channel provides a constant channel width of 12 ft (3.66 m) over a length of 342 ft (104.2 m). The test section is 15 ft (4.57 m) deep with 3.5 ft (1.1 m) of freeboard extending above the ground line. The wave generator is hinged at the bottom, 18 ft (5.49 m) from the south end of the channel, in an overall depth of 18 ft (5.49 m). The increased depth at the wave board provides a greater immersed surface area for increased wave generation capacity. The 18-ft (5.49-m) depth continues for 4 ft (1.22 m) in front of the wave board and then shoals to a depth of 15 ft (4.57 m) over a horizontal distance of 40 ft (12.2 m). The 15-ft (4.57-m) depth continues for 250 ft (76.2 m) and then rises vertically to a depth of 3 ft (0.91 m). The 3-ft (0.91-m) depth continues for the last 30 ft (9.1 m) of the wave channel. Plan and elevation views of the channel appear in Figure 13-2.

For SUPERTANK, a trapezoidal-shaped concrete sill was cast in place in front of the wave board to prevent transported sand from accreting near the wave board hinges and seals. The sill was 1 ft (0.3 m) wide at the crest, 1.7 ft (0.5 m) high, and had slopes at 50 deg (0.87 rad), fore and aft, as shown in Figure 13-3. The near edge of the sill was 4 ft (1.2 m) from the base of the wave board. Threaded inserts into the top of the sill allowed it to be removed with a hoist.

One-inch (2.54-cm), coarse threaded, stainless steel insert pairs were cast into the walls and floor of the wave channel, spaced at 12-ft (3.66-m) increments on center, horizontally. Insert pairs are separated by 8 in. (20.3 cm) horizontally, repeating at 1-ft (0.30-m) centers vertically on both interior wall surfaces of the channel. Insert pairs were also placed in the bottom of the channel, starting 2 ft (0.61 m) from the wall and continuing at 4-ft (1.22-m) spacings across the channel. The threaded inserts allow instrumentation and models to be attached to the walls and floor of the channel.

The inserts also serve as stations for the SUPERTANK project. The first row of inserts, at the beach end of the channel, occurs 1 ft (0.30-m) from the vertical face separating the 15-ft (4.57-m) and 3-ft (0.91-m) channel depths. This is referred to as Station 1. Station numbers increase by one for each column of inserts, separated by 12 ft (3.66 m) of longitudinal distance. The extreme station is station number 22, which is (22-1)12 + 1 = 253 ft (77.1 m) from the beach end of the 15-ft- (4.57-m-) deep section of the wave channel. Inserts are identified in Figure 13-2.
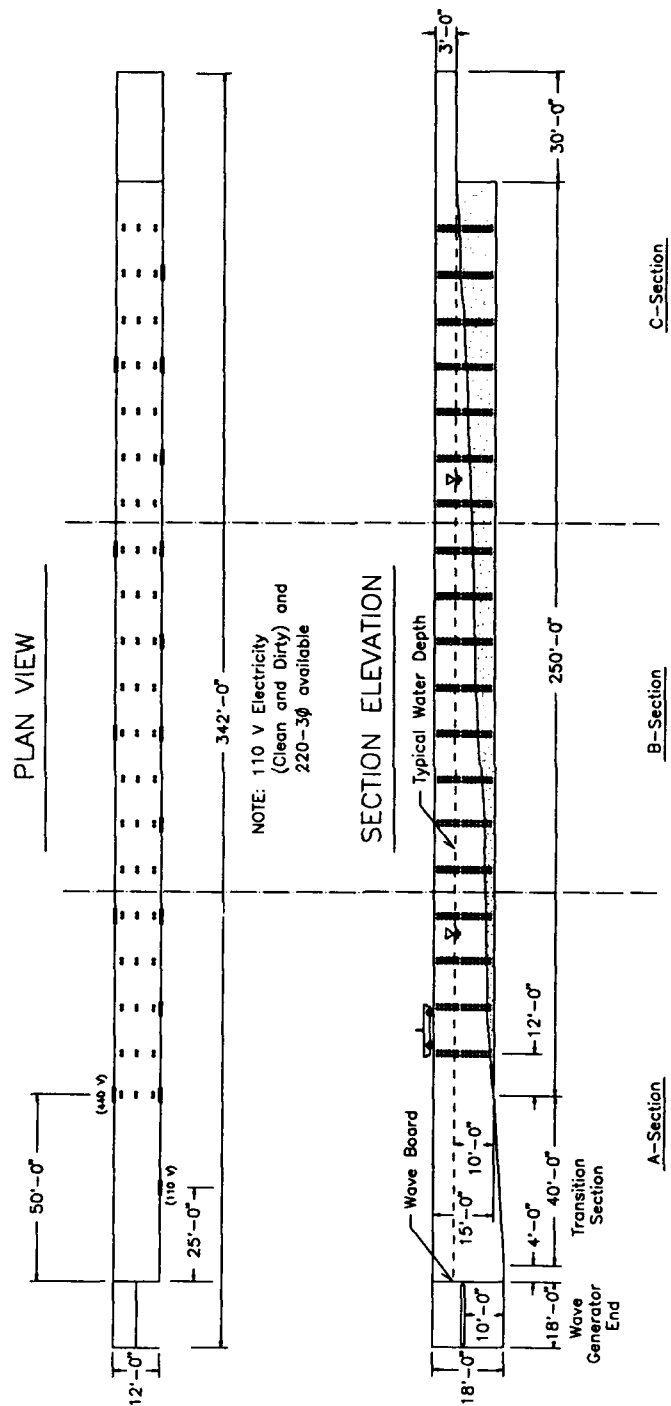
Figure 13-2. Plan and elevation views of the wave channel

Figure 13-3. Concrete sill in front of the wave board

Single-phase, 110-V power outlets are spaced at 25-ft centers along the exterior east wall of the channel. Additional 110-V outlets are available at 50-ft centers around the perimeter of the building. Three-phase, 440-V outlets are placed at 50-ft centers on the exterior west wall of the wave channel. Three-phase, 220-V power outlets are placed at 50-ft centers along the west wall of the WRL environmental enclosure.

The environmental enclosure is a 375-ft- (114-m-) long, 100-ft- (30.5-m-) wide, open-span steel building with an interior peak height of 35 ft (10.7 m) and eave heights of 28 ft (8.5 m). Vehicular doors, 16 ft (4.9 m) wide and 16 ft (4.9 m) tall, are placed in pairs, 40 ft (12.1 m) between the center lines, at the two ends of the building. The doors provide access for trucks and cranes to facilitate placement of the beach sand, as shown in Figure 13-4.

Fresh water for filling the wave channel is plumbed from a city fire main to the beach end of the wave channel, opposite the wave generator. A 5-in. (12.7-cm) PVC pipeline was routed along the exterior right wall of the chan-nel to provide a filling port 10 ft (3 m) in front of the wave board at the wave

260

Figure 13-4. Interior view of the beach end of the WRL building

generator end of the channel. The latter facilitated rapid water inflow without beach erosion. The filling port is shown in Figure 13-5. A sump for the drain pump is located 2 ft (0.6 m) in front of the wave board at the channel center line. Filling and emptying proceed at a rate of approximately 1 ft/hr (0.3 m/hr).

Interior lighting is provided by 56 metal halide lamps, 400 W each, suspended from the ceiling at 25-ft (7.6-m) centers longitudinally and 20-ft (6.1-m) centers laterally. Passive lighting is provided by a continuous band of 4-ft- (1.2-m-) high windows (3.5 ft (1.1 m) above the floor) around the perimeter of the building, 8-ft- (2.4-m-) deep translucent panels below the eaves and at the peaks of the end walls, and 1,700 ft² (160 m²) of 75-percent reflective glass on the west wall of the building. Passive lighting was sufficient for most video and still photography applications during daylight testing periods.

Wave generator. The wave generator is a servo-controlled, hydraulically driven hinged-flap wave board. The wave board is a 5,000-lb (2,270-kg) aluminum weldment that is hinged at the base of the channel in an overall

Figure 13-5. The filling port

depth of 18 ft (5.49 m). The board is a flat aluminum plate on the seaward side with webbed reinforcement welded to the back side of the structure. A hydraulic actuator is attached to the back side of the wave board via a clevis at an elevation of 10 ft (3.9 m) above the bottom of the channel. The actuator is an 8-in.- (20.3-cm-) diam hydraulic ram with a stroke of ±30 in. (±76 cm) (Figure 13-6).

The wave board operates with water on one side. With no water on the back side, waves are generated only on the seaward side, requiring half the power of a wave generator with water on both sides. Polyethylene wiping seals attached to the vertical edges of the wave board slide along stainless steel cladding on the sides of the concrete wave channel. A pivoting knife-edge seal minimizes seepage at the bottom of the wave board. The total leakage rate for 15 ft (4.6 m) of head on the wave board is in the range of 5 to 10 gal/min (0.3 to 0.6 ℓ/sec). A sump pump returns this water to the seaward side of the board.

Fifteen feet of head provide a hydrostatic pressure force of approximately 84,000 lb (374,000 N) on the wave board. This head is overcome by applying nitrogen gas pressure to the back face of the hydraulic ram. The ram places the hydrostatic force in equilibrium with a gas spring, requiring no additional power from the hydraulic power supply. Oil hydraulic pressure is applied to a piston ring at the center of the ram, isolated from the ambient pressure by fore and aft ring seals set in the walls of the ram cylinder. Oil

262
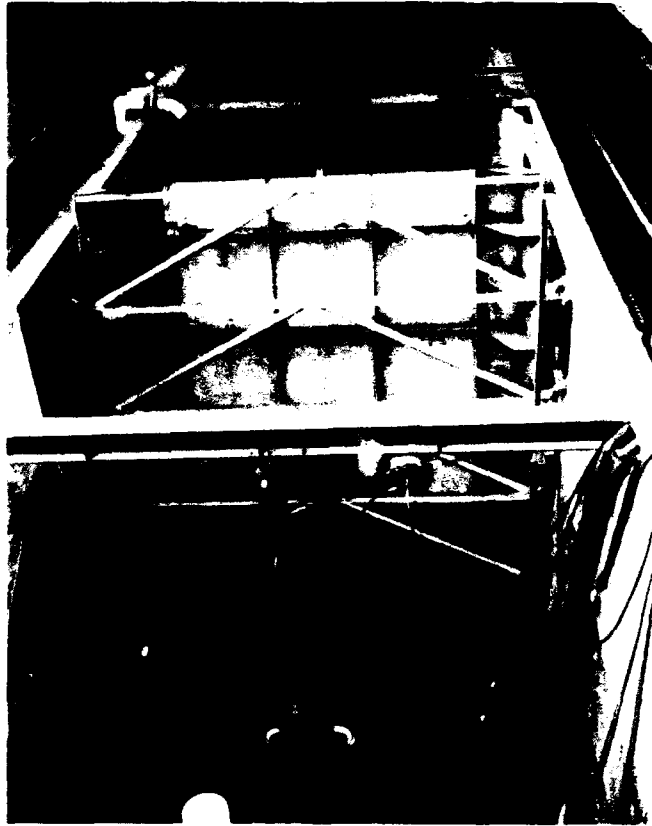
Figure 13-6. Back side of the wave board

hydraulic pressure on the back side of the piston ring pushes the ram and the attached wave board forward. Oil hydraulic pressure on the front side of the piston ring pushes the ram and the attached wave board back. A servo-valve on top of the cylinder gates the oil flow from one side of the piston ring to the other to control the wave board motion.

The hydraulic actuator is powered by a 76-gal/min (4.8-ℓ/sec), 3,000-psi (21,000-kPa) positive displacement pump. The pump is driven by a 150-hp (112-kW) a-c electric motor. The hydraulic power supply is water cooled and located in a covered enclosure adjacent to the actuator, as shown in Figure 13-7.

Direct digital control of the wave generator is provided by a two-loop feedback system. The primary loop computes the error between the wave board displacement, measured by a linearly variable displacement transducer, and the computed displacement, calculated from linear-wavemaker theory (Hudspeth and Chen 1981). This error is minimized by changing the input displacement of the wave board. The secondary loop computes the error
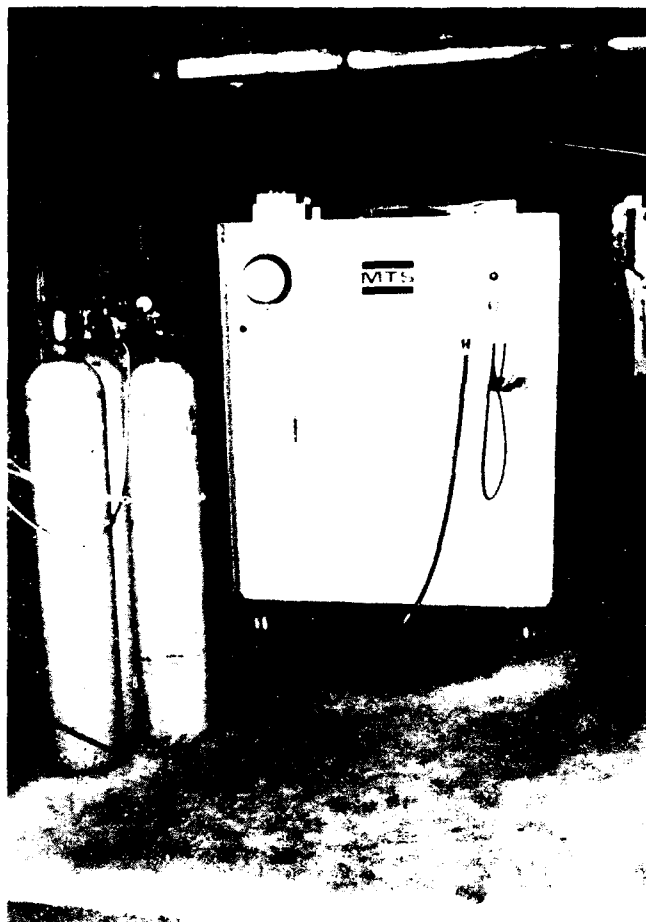
Figure 13-7. MTS hydraulic power supply

between the water surface profile, measured by an electro-resistive wave
gauge at the center of the wave board, and the computed profile, calculated
from linear wavemaker theory. This error is minimized by changing the
velocity of the wave board. Any reflections returning to the wave board from
the beach or other structure are canceled via this secondary loop. The trans-
fer function between wave board velocity and the wave profile is dependent on
water depth and wave frequency. For random waves, the peak spectral fre-
quency is used to quantify the transfer function. Thus, reflected wave absorp-
tion for random waves is most effective for frequencies close to the peak,
where most of the wave energy is concentrated.

Direct digital wave board control is provided by a Digital Corporation
VAX 3400 server, appearing in Figure 13-8, which downloads the command
displacement and velocity signals to a local transputer. The transputer com-
pares the measured and computed signals and transmits a corrected displace-
ment and velocity signal to the wave board, modifying the pressure drop
across and flow through the control valve. The wave board control signal is
updated at a rate of 20 Hz or higher The wave board, power supply, direct

264
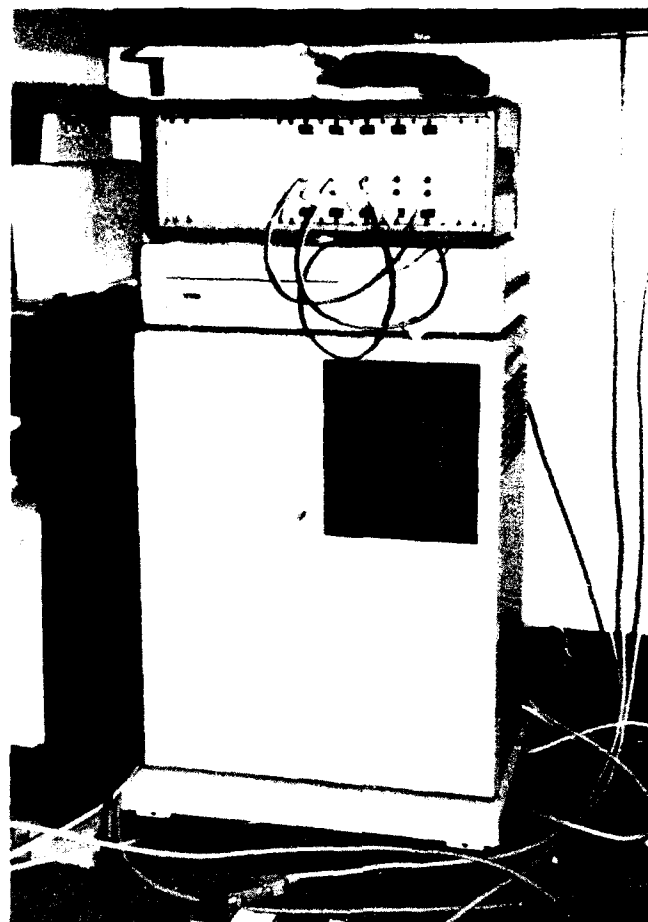
Figure 13-8. The VAX 3400 server

digital control system, and software are products of the MTS Systems Corporation, Minneapolis, MN.

The wave board controller is located in a 25-ft (7.6-m) by 75-ft (22.9-m) elevated control room approximately 200 ft (60 m) from the wave board. The computer floor of the control room is approximately 14 ft (4.3 m) above the pavement around the wave channel. The west wall of the control room is approximately 25 ft (7.6 m) from the center line of the wave channel. The control room includes a 240-ft^2 (22-m^2) computer room for the VAX server and optical interface, a 1,000-ft^2 (93-m^2) room for wave board control and data acquisition, and a 625-ft^2 (58-m^2) room shared by principal investigators. Ethernet connections are provided throughout the control room. The roof of the control room is frequently used for video and photographic observations. Exterior and interior photos of the control room appear in Figure 13-9.

Digital data acquisition system. Analog signals from the wave profilers, electromagnetic current meters, and pore pressure transducers are conditioned to a 0- to 10-V DC dynamic range. Each signal is low-pass filtered through a
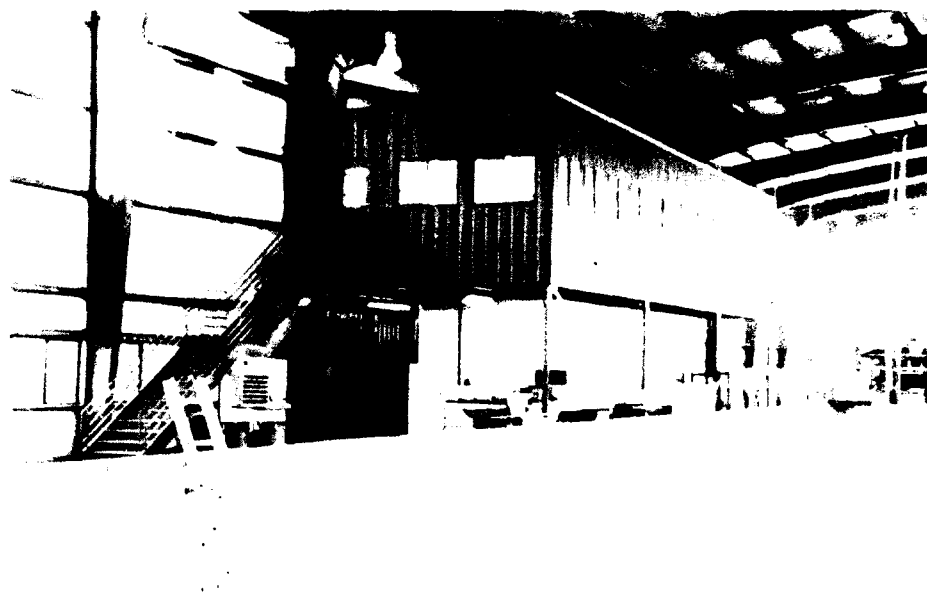
a. Exterior

b. Interior

Figure 13-9. Views of the elevated control room

fifth-order, 10-Hz, Bessel filter at the input to the 64-channel data acquisition system. Analog signals are digitized at 16 Hz, optically encoded, and transmitted to the VAX 3400 server. Digitized records are serially recorded in 256 time unit blocks to random access memory (RAM) and transferred to an 800-MB hard drive.

The data acquisition console (DAC) is a product of MTS Systems Corporation, Minneapolis, MN. It is based on the Series 499 control console design, applied to a variety of engineering applications. The DAC is shared by the directional wave generator, the spiral wave generator, and the two-dimensional channel wave generator. It is optically connected to remote stations, adjacent to the wave generator selected for a specific test series. Photographs of the console appear in Figure 13-10. The DAC is comprised of three modules.

The first module is a Model 499.45 analog-to-digital (A/D) module. It is an intelligent, transputer-based module that provides channel scanning and A/D conversion of up to 16 analog input channels. The board uses a scan table RAM to specify the channels to be included in a scan and the order in which they are to be converted. Four of these modules exist in the WRL system.

A second module is a Model 499.47 anti-aliasing filter, which is a 16-channel, non-programmable low-pass filter. Each of the 16 channels can be independently configured to support up to fifth-order Butterworth, Chebychev, Linear-Phase Elliptic, or Bessel responses. The filters are configured for their type and cut-off frequency by resistor networks contained in dual in-line package headers that are installed on the module circuit board. The filter module is designed primarily for anti-aliasing purposes in a digital signal processing application. The filters are also used to reduce unwanted high-frequency noise. Four of these units exist in the WRL system.

A third module is a Model 499.65 optical link, which provides the necessary optical communications links between the VAX computer system, servo boards, and data acquisition console. Two of these modules exist in the WRL system. The optical/electrical interface appears on top of the VAX server cabinet in Figure 13-8.

Five other PC-based digital data acquisition systems were used to acquire data in the foreshore and offshore. These systems were synchronized with each other and the MTS data acquisition system using Atomic Standard Time established in Fort Collins, CO, and broadcast as a radio signal (call letters WWV). A 10-MHz radio receiver (RD-10) and digital signal processing card (CTS-10) by Coordinated Time Link were used to decode the WWV time signal, update the board clock, and then update the computer system clock. This provided an accurate, reliable, and traceable common time base for all data acquisition systems associated with the SUPERTANK project. The clock interpreter and a local digital time readout are shown in Figure 13-11.
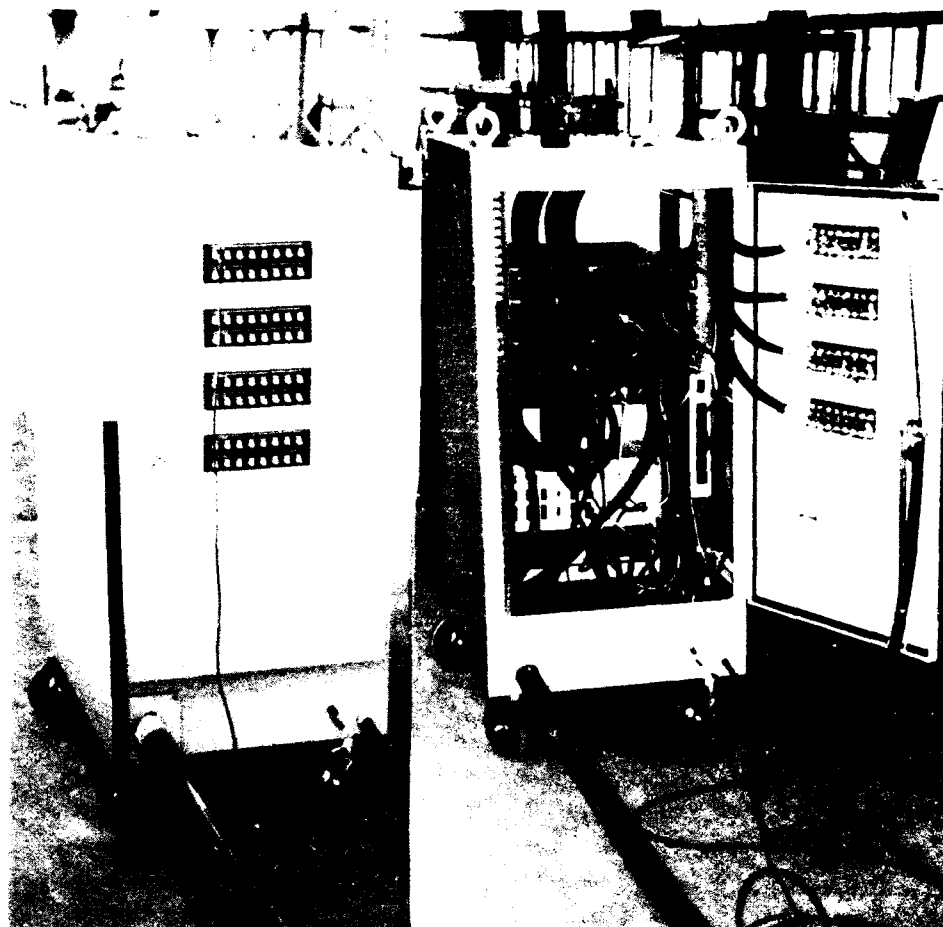
a. Closed console   b. Open console

Figure 13-10. The MTS data acquisition console

Support facilities. Video documentation of all test runs was provided by locating a camera on the roof of the elevated control room and panning the beach area. The camera shutter plane was located at $x = 167.5$ ft (51.1 m), $y = 32.5$ ft (9.9 m), and $z = 28.9$ ft (8.8 m) in the SUPERTANK coordinate system. The coordinate system origin was located at the top of the right inside wall of the wave channel, above the vertical rise in the channel bottom from 15 ft (4.57 m) to 3 ft (0.91 m). A Panasonic WV-D 5100 color video camera was used to acquire analog videos in the ½-in. VHS format. A photograph of the camera appears in Figure 13-12. Offshore underwater videos of bed forms were acquired for several intermediate runs. A camera and light were cantilevered from the wall inserts at Station 19. The submersible camera is a Deep Sea Power and Light model SC-2000 with a wide-angle lens. A photograph of the camera, light, and 3.0-in. (7.6-cm) grid appears in Figure 13-13.

An elevated platform was provided for video measurements of wave runup on the beach. This video platform is shown in Figure 13-14.

268
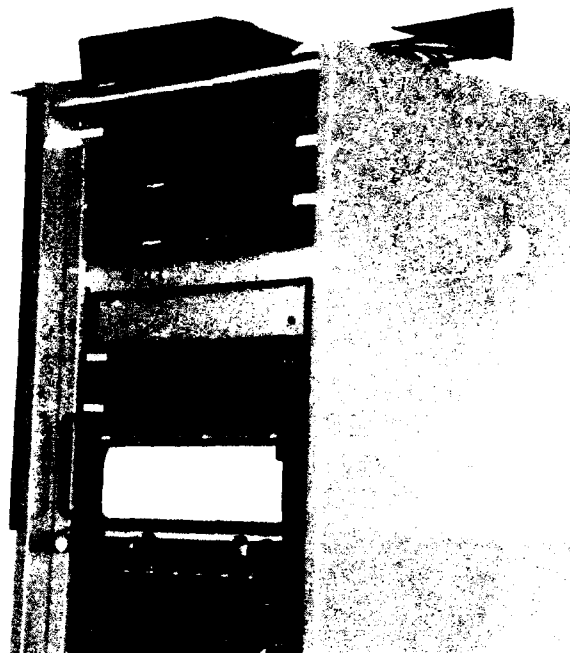
Figure 13-11. WWV time code interpreter and local readout

Figure 13-12. Panasonic video camera
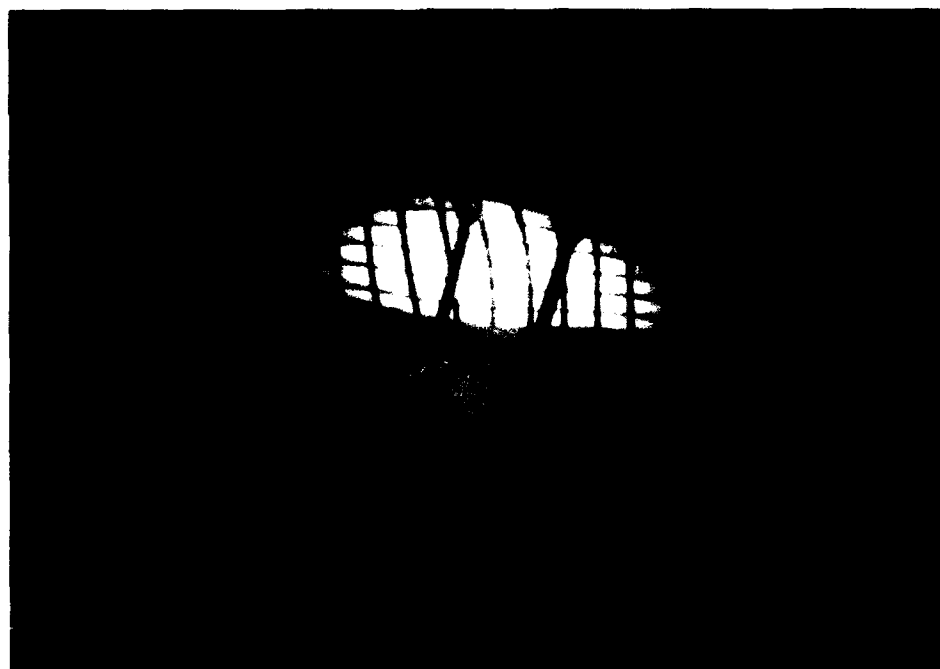
Figure 13-13. Underwater camera, light, and grid panel

Figure 13-14. Runup video platform

Local workstations were established for several investigative teams participating at SUPERTANK. Each station included a bench area to support instrumentation signal conditioners, data acquisition equipment, WWV antennae, and power. Photographs of the local workstations appear in Figures 13-15 through 13-18.

Summary

The O. H. Hinsdale Wave Research Laboratory at Oregon State University provided the modeling environment for the SUPERTANK Laboratory Data Collection Project. The major features of this environment included:

a. A two-dimensional wave channel, 342 ft (104.2 m) long, 12 ft (3.66 m) wide, and 15 ft (4.57 m) deep.

b. A hinged-flap, servo-hydraulic, direct digital control wave generator with active reflected-wave cancellation.

c. A 64-channel digital data acquisition system with optical communications links for wave profile, water particle velocity, and pore pressure measurements.

d. Software for control of the wave generator and data acquisition system.

e. A WWV time code interpreter and readout system for synchronous control of all data acquisition systems.

f. Surface video and bed form video documentation of the tests.

g. Workstation areas with power and WWV antennae connections for all supporting measurement groups.

Acknowledgements

271

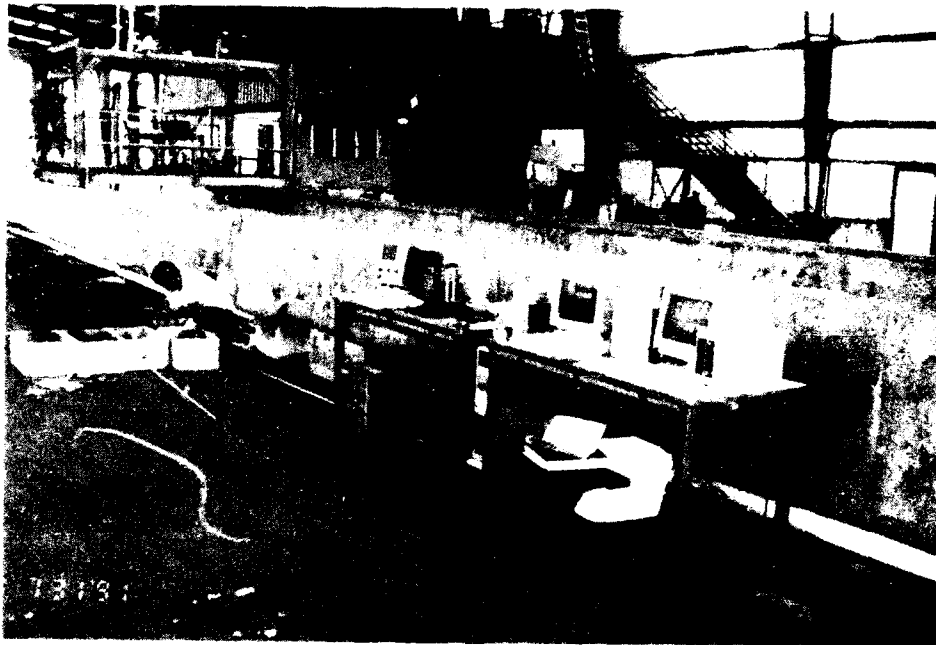Figure 13-15. Offshore acoustical measurement systems

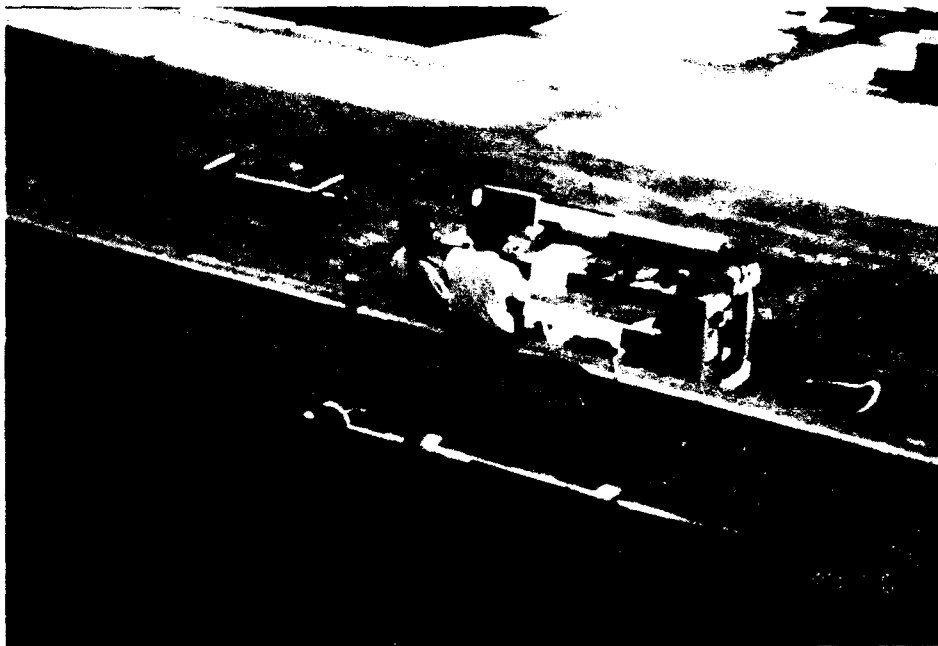
Figure 13-16. The Ohio State University workstation

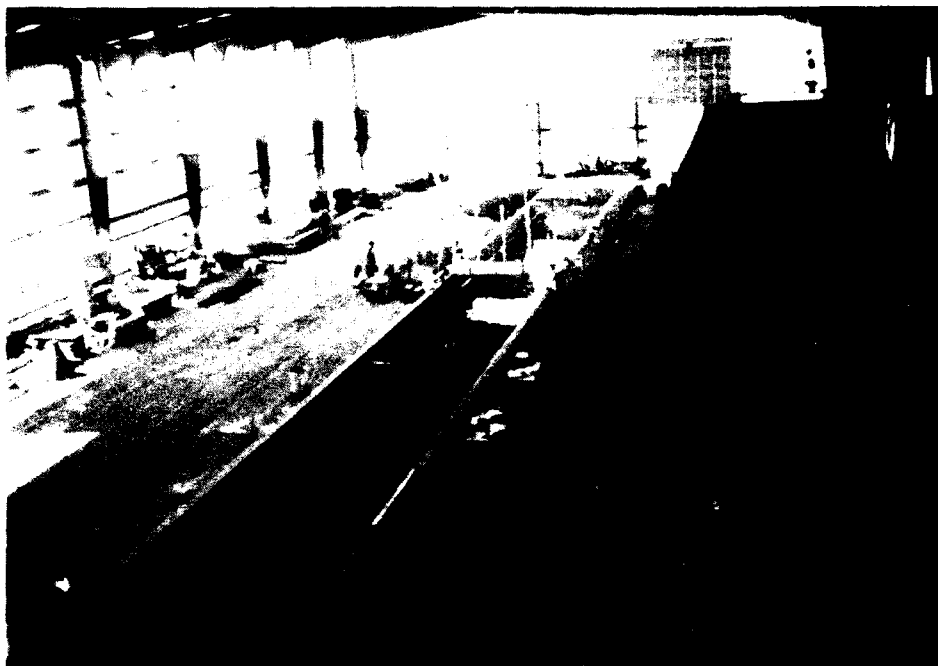Figure 13-17. The offshore laser-Doppler workstation

Figure 13-18. The onshore wave runup measurement station

References

Dette, H. H., and Uliczka, K. (1987). "Prototype investigation on time-dependent dune recession and beach erosion." *Proc. Coastal Sediments '87.* ASCE, New York, 1430-44.

Hudspeth, R. T., and Chen, M-C. (1981). "Design curves for hinged wavemakers: theory," *J. of the Hydraulics Div.* 197(HY5), 533-52.

Kajima, R., Shimizu, T., Maruyama, K., and Saito, S. (1982). "Experiments on beach profile change with a large wave flume." *Proc. 18th Coastal Engrg. Conf.* ASCE, New York, 1385-404.

Saville, T. (1956). "Scale effects in two-dimensional beach studies." *Trans. 7th General Meeting.* IAHR, A3.1-10.

Sollitt, C. K., and DeBok, D. H. (1976). "Large-scale model tests of placed stone breakwaters." *Proc. 15th Coastal Engrg. Conf.* ASCE, New York, 2572-88.

Vellinga, P. (1986). "Beach and dune erosion during storm surges," Delft Hydraulics Comm. No. 372, Delft Hydraulics Laboratory, Delft, The Netherlands.

1. AGENCY USE ONLY (Leave blank)	2. REPORT DATE January 1994	3. REPORT TYPE AND DATES COVERED Final report

4. TITLE AND SUBTITLE

SUPERTANK Laboratory Data Collection Project;
Volume I: Main Text

5. FUNDING NUMBERS

6. AUTHOR(S)

Nicholas C. Kraus, Jane McKee Smith

7. PERFORMING ORGANIZATION NAME(S) AND ADDRESS(ES)

U.S. Army Engineer Waterways Experiment Station
Coastal Engineering Research Center
3909 Halls Ferry Road, Vicksburg, MS 39180-6199

8. PERFORMING ORGANIZATION REPORT NUMBER

Technical Report
CERC-94-3

9. SPONSORING/MONITORING AGENCY NAME(S) AND ADDRESS(ES)

US Army Corps of Engineers, Washington, DC 20314-1000

10. SPONSORING/MONITORING AGENCY REPORT NUMBER

12a. DISTRIBUTION/AVAILABILITY STATEMENT

Approved for public release; distribution is unlimited.

12b. DISTRIBUTION CODE

13. ABSTRACT (Maximum 200 words)

This report provides information and data documenting a coastal processes project called the SUPERTANK Data Collection Project performed at the O.H. Hinsdale Wave Research Laboratory, Oregon State University, over the period 29 July to 20 September 1991. The objectives of the project were to (a) collect data to verify and improve existing macro-scale beach profile change numerical simulation models, (b) collect data to develop advanced hydrodynamic, cross-shore sand transport, and meso-scale beach profile change numerical simulation models, (c) collect data to quantify performance of sandbars constructed offshore as a beneficial use of dredged material, (d) test and compare sediment-sensing acoustic instruments in a controllred, field-scale environment in support of dredging research, and (e) collect data to improve understanding of micro-scale fluid and sand motion. SUPERTANK was conducted as a multidisciplinary and multi-institutional cooperative effort in which the investigators shared instrumentation and expertise.

14. SUBJECT TERMS

See reverse

15. NUMBER OF PAGES
285

16. PRICE CODE

17. SECURITY CLASSIFICATION OF REPORT UNCLASSIFIED	18. SECURITY CLASSIFICATION OF THIS PAGE UNCLASSIFIED	19. SECURITY CLASSIFICATION OF ABSTRACT	20. LIMITATION OF ABSTRACT

14. (Concluded).

Beach profile change   Swash
Cross-shore sediment transport Undertow
Laboratory measurements   Wave height transformation
Runup